`

Experimental investigations on temperature-dependent mechanical properties of artificially frozen sandy clay soils

Nader Girgis

A Thesis

In

The Department

Of

Building, Civil, and Environmental Engineering

Presented in Partial Fulfillment of the Requirements

For the Degree of

Master of Applied Science (Civil Engineering) at

Concordia University

Montréal, Québec, Canada

August 2019

© Nader Girgis, 2019

`

CONCORDIA UNIVERSITY

School of Graduate Studies

This is to certify that the thesis prepared

By: **Nader Girgis**

Entitled: **Experimental investigations on temperature-dependent mechanical properties of artificially frozen sandy clay soils**

and submitted in partial fulfillment of the requirements for the degree of

Master of Applied Science (Civil Engineering)

complies with the regulations of the University and meets the accepted standards with respect to originality and quality.

Signed by the final Examining Committee:

Chair and Examiner

Dr. Adel M. Hanna

Examiner

Dr. Ayhan Ince

Examiner

Dr. Attila Michael Zsaki

Supervisor

Dr. Biao Li

Supervisor

Dr. Benoît Courcelles

\

Approved by: _____
Chair of the Department or Graduate Program Director

Date: _____2019 _____
Dean of Faculty

`

ABSTRACT

Long term records indicate that on-going global warming has resulted in the thawing of some permafrost regions, which led to extensive geological disasters including slumps and ground settlements that were causing damage to infrastructures. An accurate characterization of the temperature-dependent mechanical properties of frozen clay soils is critical for predicting and preventing geological disasters in cold regions. This thesis presents the experimental investigations on measuring mechanical properties of two artificial frozen clay soils (kaolinite-sand and bentonite-sand) at different temperatures. A practical approach for preparing artificial frozen clay soils samples is proposed. The reason for using artificial frozen clay is to enable control and repeatability. The approaches of split cylinder test and double punch test are applied to measure the tensile strength. Uniaxial compressive tests are used to measure the uniaxial compressive strength, Young's modulus, Poisson's ratio, and stress relaxation characteristics. The tests are conducted at different deformation rates in a temperature-controlled cold room.

The results show that the double punch test approach is more effective in measuring the tensile strength of artificially frozen clay soil when compared with the split cylinder approach. The effects of temperature and deformation rates on the sample's tensile and compressive strengths are significant. Low temperature and a high deformation rate tend to generate brittle failure with post-peak softening behavior. A temperature close to the frozen fringe and a low deformation rate results in a diffuse failure associated with strain hardening. The temperature-dependent mechanical property relationships for the frozen kaolinite-sand and frozen bentonite-sand are modeled using a power-law function which covers a broad temperature range from -15°C to 0°C. The parameters for the modeling function are highly dependent on the applied deformation rates. Since the artificial frozen clay soils have pre-determined mineralogical composition, stress history, water content, and pore fluid salinity, these experimental results can be used as a considerable data resource for theoretical modeling the failure behavior of frozen clay soils.

Keywords: Artificially frozen clay soil, double punch test, tensile strength, temperature-dependent properties, strain rate effect, uniaxial compressive behavior.

`

ACKNOWLEDGMENT

First and foremost, I would like to express my thanks and appreciation to my supervisor Dr. Biao Li, for all of his support, encouragement, and motivation. His consistent guidance and help made this research an exciting journey. I want to thank him for providing me with the funding and materials needed and his time.

I express my sincere appreciation to my supervisor Dr. Benoît Courcelles for his valuable advice and for allowing me to perform experiments at Polytechnique Montréal; in addition to, providing financial support from his budget for the experimental setup.

My sincere gratitude to Dr. Adel Hanna for providing me with technical support and laboratory equipment. I would also like to thank Concordia's Foundation Engineering Lab group for being helpful and a source of motivation.

Special thanks to Dr. Hua Ge and Dr. Liangzhu Wang for providing access to the Building Envelope Performance Laboratory (BEPL) at Concordia University. They made available the facility of the environmental chamber with enthusiasm.

Grateful thanks go to Mr. Samuel Chénier and Mr. Éric Turgeon for their technical support in the Geotechnical Laboratory at Polytechnique Montréal.

I would also thank the examination committee members Dr. Adel Hanna, Dr. Attila Zsaki, Dr.Ayhan Ince, Dr. Biao Li, and Dr. Benoît Courcelles, for spending their valuable time on this thesis.

Finally, my heartfelt thanks to my wife, Nancy Baskhairon, and my children, David, Daniel, and Chantal, for their love, support, and patience during the research period; and my parents for their endless encouragement and support throughout the thesis.

`

TABLE OF CONTENTS

`

`

LIST OF FIGURES

`

LIST OF TABLES

`

LIST OF SYMBOLS, ABBREVIATIONS, AND NOMENCLATURE

A	An empirical parameter depends on strain rate in a dimension of stress
a	The punch radius in mm
B	A constant depends on the temperature in a dimension of stress x time
b	The sample radius in mm
D	The diameter of the sample in mm
d	The depth of the soil beam sample in mm.
E	Young's modulus in MPa
Et	The tangent Young's modulus in MPa
K	A constant equal 1.0 for soil, and 1.2 for concrete, and rock
L	The thickness of the sample in mm
m	An empirical parameter depends on strain rate (dimensionless)
n	A constant depends on the temperature (dimensionless)
P	The applied load at failure in N
S	The span length of beam sample in mm
T_f	The freezing point for the clay–water system in °C
T_{sn}	The temperature of spontaneous nucleation for the clay–water system in °C
W	The width of the soil beam sample in mm
α	An angle equal to $\frac{\pi}{2}-\frac{\phi}{2}$ in degree
$\Delta\varepsilon l$	The change in the lateral strain (dimensionless)
$\Delta\varepsilon$v	The change in the axial strain (dimensionless)

$\Delta\sigma c$	The change in applied stress in MPa
$\dot{\varepsilon}$	The strain rate in S^{-1}
θ	The negative temperature in °C
θ_o	A reference temperature is taken as -1.0 °C
σc	The uniaxial compressive stress in MPa
σ_T	The tensile strength in MPa
υ	Poisson's ratio (dimensionless)
ϕ	Internal friction angle in degree

`

Chapter 1

INTRODUCTION

1.1 Background

The permafrost region, which underlies a large portion of Canada, is divided into zones of continuous and discontinuous permafrost (Figure 1.1). Long term records shown in Figure 1.2 indicate that on-going global warming has resulted in thawing portions of the permafrost area, which leads to extensive geological disasters such as slumps (Wang et al., 2016) or ground settlements causing damage to infrastructures (Andersland and Ladanyi, 2013). In cold regions, clay soils have been given special attention due to their high chances of inducing frost heaving and thawing settlement. A thorough understanding of the mechanical responses of frozen clay soils in a warming environment is critical for proposing countermeasures for preventing natural disasters. As the technique of artificially frozen ground engineering is quite popular in soft grounds geotechnical projects, the physical properties of frozen clay soils demand considerable attentions (Hu et al., 2013).

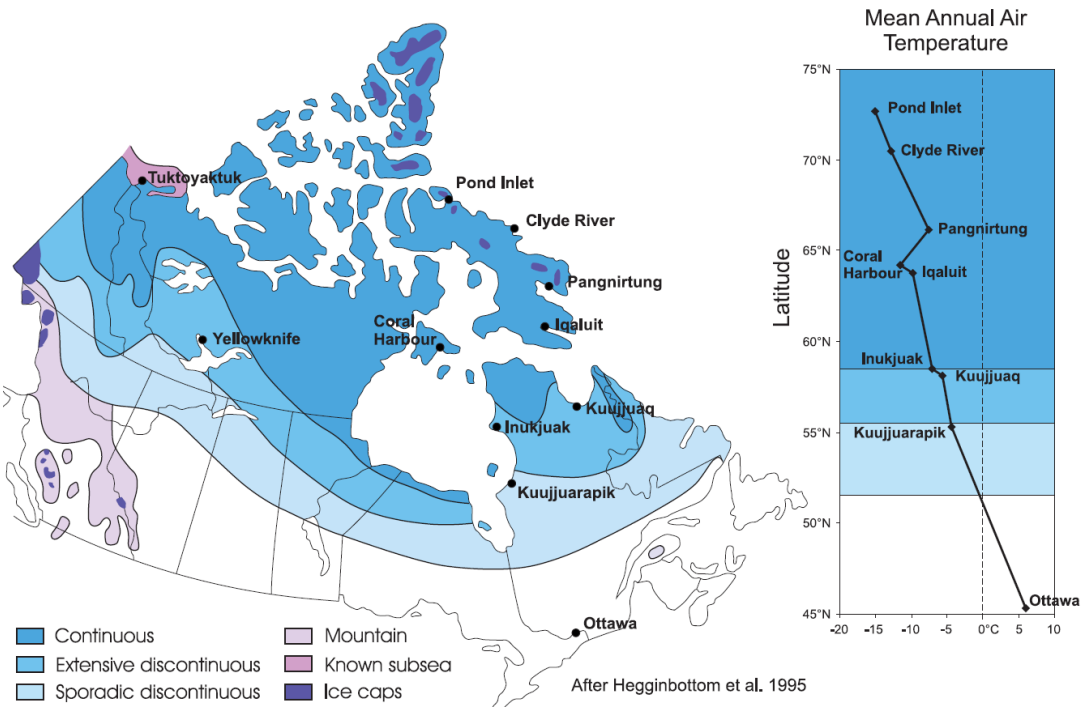

Figure 1. 1 Permafrost and mean annual air temperature distributions across Canada (Sladen, 2011).

Figure 1. 2 Picture showing the impact of thawing permafrost on nature slopes and infrastructures, after Sladen (2011) and Wang (2016).

`

A clay soil experiencing freezing and thawing may have dramatically different mechanical properties depending on its clay mineralogy compositions and thermal state (Leroueil et al., 1991; Hivon and Sego, 1995). Compared to some other soils such as sand and silt, clay soil has complicated physical mechanisms for the freezing and thawing processes. Clay soil can have significant variations in clay types, clay fractions, and micro-structures (Konrad and Morgenstern, 1981). Upon freezing, clay soil will have an increase in soil strengths and has a high possibility of generating ice lens; upon thawing, clay soil is expected to have a strength degradation accompanied by thawing induced consolidation (Nixon and Morgenstren, 1974). Early studies have demonstrated the importance of conducting laboratory tests when investigating the mechanical responses of frozen clay soils at elevated temperatures (Zhou et al., 2015). Some early trials were made to obtain undisturbed naturally frozen samples using special techniques for sampling, transporting, and preparing for laboratory tests (Johnston, 1963; Baker, 1976; Lee, 2002). A thorough understanding of the compressive and tensile mechanical behaviors of frozen soil requires a large number of specimens with similar compositions and micro-structures. Therefore, the artificial soils are very beneficial, because they permit control and repeatability, particularly for clay soils which have large variations in clay mineralogy, fraction, and structure. The sophisticated procedures and difficulties in obtaining in-situ frozen clay soils strongly hindered the theoretical development in the frozen soil behavior, so the artificially frozen soil is the preferable choice for the researchers. A thorough understanding of the mechanical responses of frozen clay soils should focus both on the tensile and compressive behaviors.

The tensile strength is a very important property for frozen soils, and it governs the design in many geotechnical problems to avoid tensile failure. For example, the curved or circular frozen wall is a perfect solution to overcome the relatively low tensile strength of frozen soils compared to the compressive strength. Most of the previous research used the uniaxial tensile test to measure the tensile strength of the frozen soil because it is the most accurate and reliable testing method (Haynes and Karalius, 1977). The difficulties with this test are to eliminate the bending and torsion stresses induced by the eccentric of loading and the complicated procedure of preparing the test samples. These Problems with the uniaxial loading method lead researches to use the most common indirect testing method, the Brazilian test, also known as the splitting test (Shloido, 1968). Bragg and Andersland (1981) observed that there is no tensile failure at low loading rate and warm

temperatures. Zhou et al. (2015) replaced the bearing tools by small strips, but the results did not show any increase in tensile strength with the increase in loading rate. The splitting test can be considered as an impropriate testing method for warm frozen soils at low loading rates due to the ductile behavior of the samples.

The beam bending tests are also used in measuring the tensile strength of the frozen soil, but the rotation of supporting and loading rollers affect the span length, thereby it needs a correction to eliminate the effect of rotation (Mujika, 2006). Azmatch et al., (2011) observed that at the frozen fringe range, the tensile strength decreased with an increase in loading rate, contrary to the results from beam bending tests by Yamamoto and Springman (2017), and the results of the uniaxial tensile tests that were done by Haynes (1978). The double punch test is proposed as an alternative for other indirect tests to measure the tensile strength of the frozen soil (Zhongyan et al., 1995)

The compressive strength of frozen soil is also an essential mechanical property for the determination of the failure envelope of frozen soil. Many studies carried out laboratory tests to measure the uniaxial compressive strength of frozen soils. Most of the research investigated the uniaxial compressive strength at temperatures lower than the frozen fringe range. A limited number of researches focused on warm soil such as Xu et al. (2017) who studied the uniaxial compressive strength at -2°C, so more investigations are needed to study the uniaxial compressive strength of warm frozen soils.

The relaxation test is a good alternative to the traditional creep test because it can be performed under a constant and independently of a material flow effect. Savigny and Morgenstern (1986) investigated the creep of undisturbed ice-rich clay soil using a triaxial test. The deformations were found to be due to shear stresses, consolidation, and viscoplastic deformations of ice and soil structures. The flow law for polycrystalline ice was applied, and the results showed that minimum strain rates of ice for the soil in the high-stress range are faster than the low-stress range, so almost all samples failed.

In summary, there are limited laboratory studies on measuring the tensile and compressive mechanical properties of frozen clay soils at varying temperatures due to samples' availability and

`

complicated preparation procedures. It is important to propose suitable approaches for frozen clay soil preparation and efficient measurement of the tensile and compressive properties.

1.2 Objectives

The main objective of this research is to propose effective approaches for preparing frozen clay soil samples and measuring their mechanical properties to better understand the tensile and compressive behaviors at different temperatures. The following objectives are then established:

1) To propose a simple and accurate practical approach for preparing artificially frozen saturated clay soils with a specific density and relatively high strength.
2) To examine suitability of the splitting disk testing method to investigate the tensile strength of frozen clay soils at warm temperatures and low loading rates, in addition to focusing on double punch test as an alternative method, and finally study the various parameters affecting the tensile strength such as temperature, loading rate, pore fluid salinity, and clay mineralogy.
3) To investigate the uniaxial compressive strength and the elastic deformation parameters of artificial frozen clay soils at different temperatures, also the impact of strain rate, clay mineral, and test setup on the uniaxial compressive strength was studied.
4) To study the stress relaxation test and frozen soil behavior at different temperatures, loading rates, stress levels, and clay minerals.

1.3 Organization of the thesis

This thesis is organized into six chapters. Chapter 1 gives a general overview of the entire study, including background, objectives of this research, and finally, the structure of the thesis.

Chapter 2 contains a review of the available literature relevant to the study of the temperature-dependent mechanical properties of the frozen soil and the various parameters affecting their values. The existing methods for the preparation of frozen soil samples are also presented to find a convenient method to prepare frozen sandy clay samples free of ice lenses. The review also includes the common indirect tension tests performed for determining the tensile strength of the frozen soil. The suitability of these testing methods for measuring the tensile strength of the frozen soil at different temperatures and the drawbacks and limitations of each

testing method is provided as well. Finally, both the uniaxial compressive strength and the uniaxial compression relaxation stress tests are discussed.

Chapter 3 includes the properties of materials used based on chemical and physical analysis, and mix design and USCS classification of both kaolinite-sand and bentonite-sand mixtures are also presented. The procedure of sample preparation is discussed in detail, including the special setup which is designed to consolidate six samples at a time. Lastly, the testing strategy of the frozen samples is described in the sample preparation test plan, including weight, water content, and density measurements before and after mixing, consolidation, and freezing processes.

Chapter 4 covers the test setup, measuring devices, and procedures used for the indirect tension tests. It presents the results obtained from all indirect tensile tests in tables, plots, and pictures. The effect of the temperature, loading rate, salinity, clay mineral, and type of indirect tensile test on the strength and deformation behavior of frozen sandy clay soils are analyzed and discussed along with few comparisons made within a group and with different tested groups.

Chapter 5 describes the test setup, measuring devices, and procedure of the uniaxial compressive strength test. This chapter is mainly divided into two parts. The first part includes the results of the uniaxial compressive strength tests in tables, plots, and pictures. Besides, studying the influence of the temperature, loading rate, clay mineral, and test setup on the compressive strength and deformation behavior of frozen sandy clay soils. The elastic deformation parameters, Young's modulus, and Poisson's ratio of the frozen samples are also calculated and discussed. The second part presents the results obtained from the uniaxial compression stress relaxation test. The effects of the temperature, loading rate, clay mineral, and stress level are analyzed.

Chapter 6 presents a summary of the findings, overall conclusions obtained from the current investigations, and recommendations for future research works.

`

Chapter 2

LITERATURE REVIEW

2.1 A general overview of frozen soil composition

Frozen soil can be defined as soil at a temperature less than or equal to the freezing point of water 0 °C (32°F) regardless of the temperature of the air and the ice content. The physical and mechanical properties of frozen soil are strongly affected by the decrease in temperature below the freezing point. When free water freezes and transforms into ice, the soil becomes a four-phase material consisting of solid particles, ice, water, and gas instead of the three-phase system in the unfrozen state as shown in Figure 2.1.

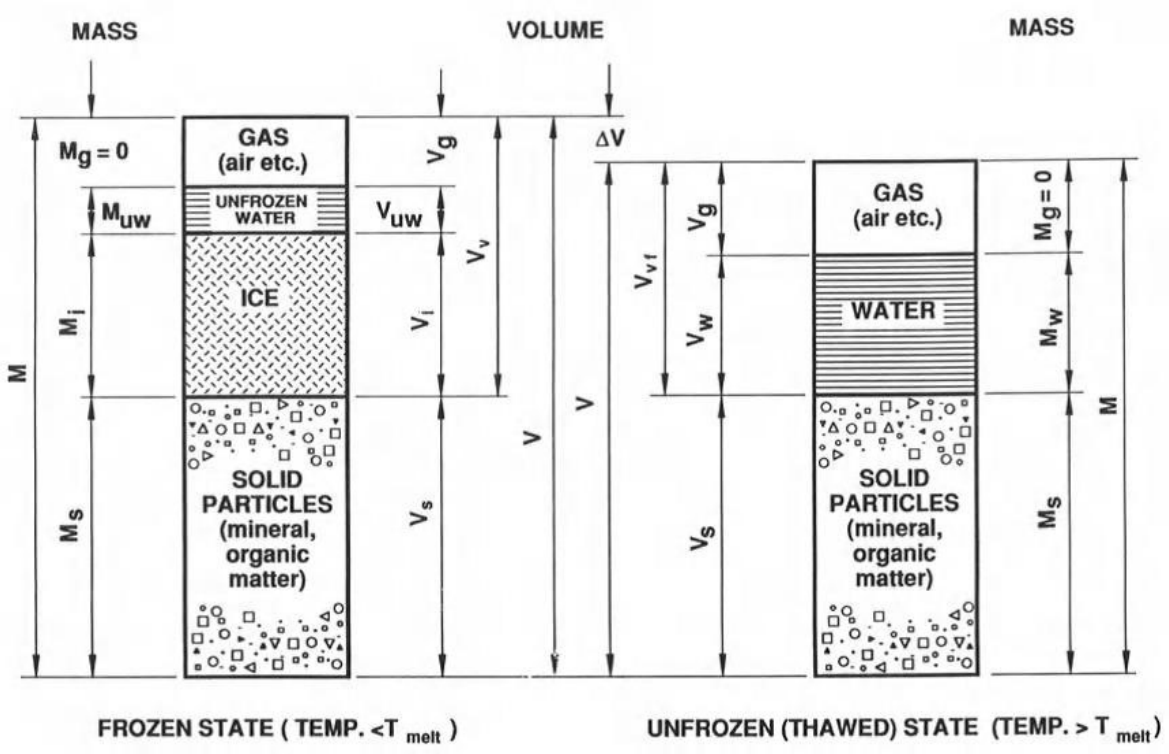

Figure 2. 1 Mass-volume relationships for frozen and unfrozen soil (Andersland and Ladanyi, 2013).

`

The properties of solid particles influence the freezing temperature of the soil. For fine-grained cohesionless soil, the freezing temperature was found to be close to zero, while cohesive soil with the small specific surface area has a freezing point lower than the freezing point of pure water as shown in Figure 2.2 (Kozlowski, 2009).

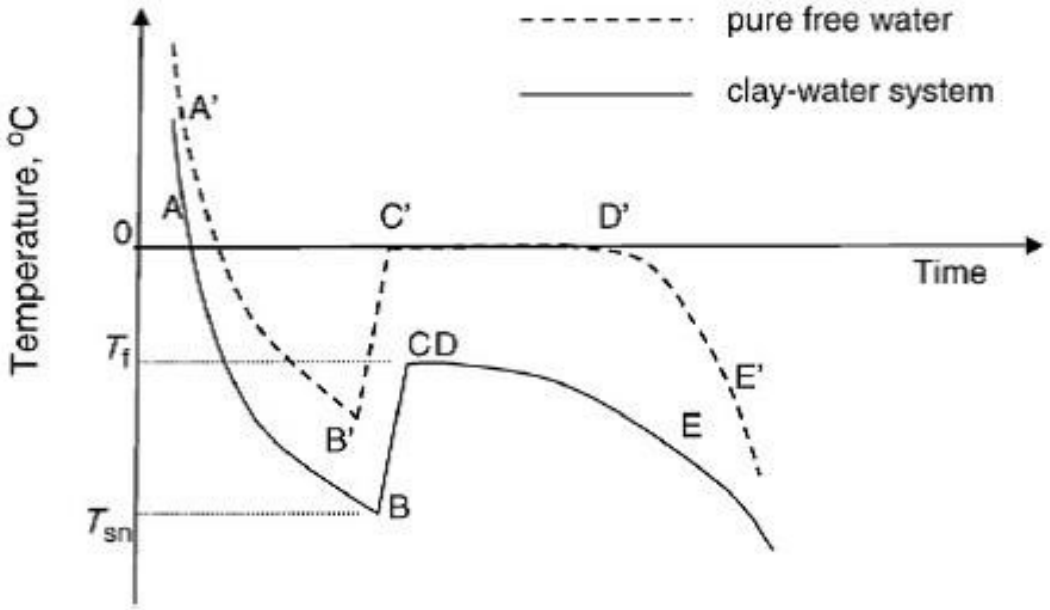

Figure 2. 2 Cooling curves for pure water and the clay–water system (Kozlowski, 2009).

T_f is the freezing point for the clay–water system; T_{sn} is the temperature of spontaneous nucleation for the clay– water system.

The type of soil also determines the content of the unfrozen water, because the amount of unfrozen water depends mainly on mineralogy, specific surface area, and surface chemistry of the soil. Thus, the behavior of the frozen soil is strongly affected by soil types and the content of the unfrozen water (Dillon and Andersland, 1966; Anderson and Morgenstern, 1973).

The ice formation starts when the temperature of pure water decreases below 0 °C which is known as supercooling (see Figure 2.2), and the ice acts as a cementing agent bonds the soil particles with bonded water together, thus soil strengths become much higher, and it can be considered as an impervious surface which prevents water from seepage (Kozlowski, 2009). The unfrozen water exists as a thin film coating that binds soil particles with ice and/or other soil

particles together, so it requires a very low temperature to be frozen. In recent years, several investigations have been concentrated on studying the unfrozen water-ice phase and how to evaluate the content of unfrozen water, and it is mainly dependent on external factors like applied pressure, and internal factors like temperature, soil mineralogy, the surface area of particles, and salinity of the water. Eventually, both of the void ratio and the saturation degree were found to affect the volume change of frozen soil. For example, a frozen compacted clay with a high void ratio was largely shrunk at lower saturation degrees, and then it started to expand at the saturation degrees more than 90% (Anderson and Morgenstern, 1973).

2.2 Factors affecting the strength of frozen soil

2.2.1 Tensile strength

The tensile strength increases significantly with freezing due to the formation of ice cements soil particles and bonded water together. As the temperature decreases, both the content and the strength of ice increases leading to considerable growth in the tensile strength and the brittleness of frozen soil. Furthermore, the tensile strength of frozen soil is sensitive to other factors such as the loading rates and the salinity. The tensile strength usually increases with the increase in the loading rate up to a specific rate, and beyond this rate, the influence of the loading rate becomes insignificant, while the low loading rates decrease the tensile strength, increase ductility, and may dominate the mode of failure of frozen soil. At the frozen fringe range, more investigations are required particularly for the effect of loading rate. Finally, the frozen soil salinity is associated with the reduction in the ice content, thereby decreasing the tensile strength (Andersland and Ladanyi, 2013).

Temperature

The tensile strength of frozen soil primarily depends on the ice quantity (the content of ice) and quality (ice tensile strength at different temperatures); therefore, the effect of temperature on the tensile strength and soil behavior was studied by many researchers. Haynes and Karalius (1977) conducted a series of tensile strength tests on frozen silt under a wide range of temperature from -56.7 to - 0.1 °C using uniaxial tension test. The tensile strength increased five times when the temperature dropped from 0 °C to -10 °C due to the quick growth in ice content and strength, while the rate of the increase in the tensile strength becomes smaller below - 10 °C.

`

The following equation was expressed to evaluate the peak tensile strength of frozen soil σ_T as a function of temperature as:

$$\sigma_T = A(\theta / \theta_o)^m \tag{2.1}$$

where θ is the negative temperature in °C, θ_o is a reference temperature taken as - 1.0 °C, and A (dimension of stress) and m (dimensionless) are empirical parameters depend on strain rates.

Yuanlin and Carbee (1987) investigated the tensile strength of frozen silt using a direct tension test. The results confirmed that the tensile strength increased with the decrease in temperature, and the tensile strength increased more rapidly at a temperature below - 0.5 °C. Akagawa and Nishisato (2009) studied the tensile strength of frozen silt samples in the frozen fringe temperature range from - 1.6 to 0 °C using an OFFENSEND apparatus. The results of the uniaxial tension test showed a noticeable growth in tensile strength compared to unfrozen soil, as shown in Figure 2.3.

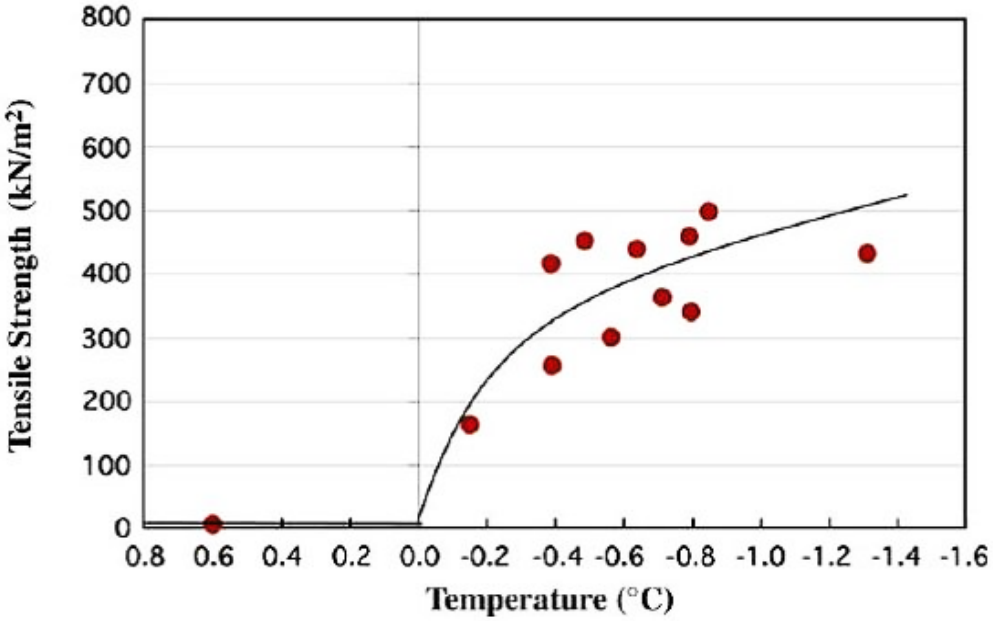

Figure 2. 3 Tensile strength of frozen silt against soil temperature (Akagawa and Nishisato, 2009).

`

Zhou et al. (2015) focused on the tensile strength of frozen clay and silty clay samples in the frozen fringe temperature range from - 2 to 0 °C. The results showed a quick increase in the tensile strength with the decreasing temperature. The ice content of the sample accounted for about 85 % of the tensile strength, while the increase in the ice strength contributed 10 % of the total tensile strength, and the contribution of cementation between particles surface and ice–water mixture was about 5 %.

Loading Rate

Haynes (1978) investigated the effect of strain rate on the tensile strength over a range from 5 x 10^{-4} s^{-1} to 10^{-1} s^{-1} and temperature varying from - 0.1 to - 56.7 °C and the equation obtained was:

$$\sigma_T = B(\dot{\varepsilon} \qquad (2.2)$$

where σ_T is the peak tensile strength in MPa, $\dot{\varepsilon}$ is the strain rate in S^{-1}, and the constants B and n are constants depend on temperature.

The results showed that the tensile strength was sensitive to low strain rates at a temperature above - 6 °C, and viscoelastic behavior was carried out at temperatures above – 4 °C and strain rate below 10^{-3} s^{-1}, while an absolutely brittle behavior occurred at temperatures below – 34 °C and strain rates above 10^{-1} s^{-1}.

Bragg and Andersland (1981) performed splitting tests to study the influence of loading rate on the tensile strength of frozen sand at a temperature of - 6.0 °C and a strain rate range from 2 x10^{-3} s^{-1} to 10^{-1} s^{-1}. The tensile strength was found to be slightly affected by loading rates in the range from 1.3 to 6.5 mm/min, as shown in Figure 2.4, and no tensile failure took place at lower loading rate.

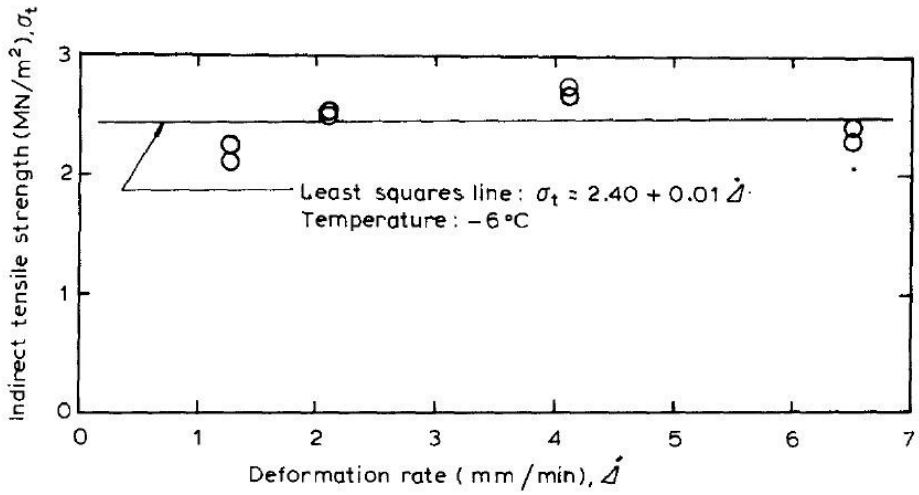

Figure 2. 4 Indirect tensile strength of frozen sand against the deformation rate (Bragg and Andersland, 1981).

Yuanlin and Carbee (1987) observed that the loading rate affected both tensile strength and the behavior at the failure of frozen silt at a temperature of - 5 °C. By decreasing the strain rate below 10^{-2} s^{-1}, the tensile strength decreased significantly, and ductile failure carried out as well. For strain rates higher than 10^{-2} s^{-1}, the tensile strength became less sensitive to loading rate, and a slight decrease in tensile strength was observed with increasing strain rate in Figure 2.5, while the failure mode changed to brittle failure.

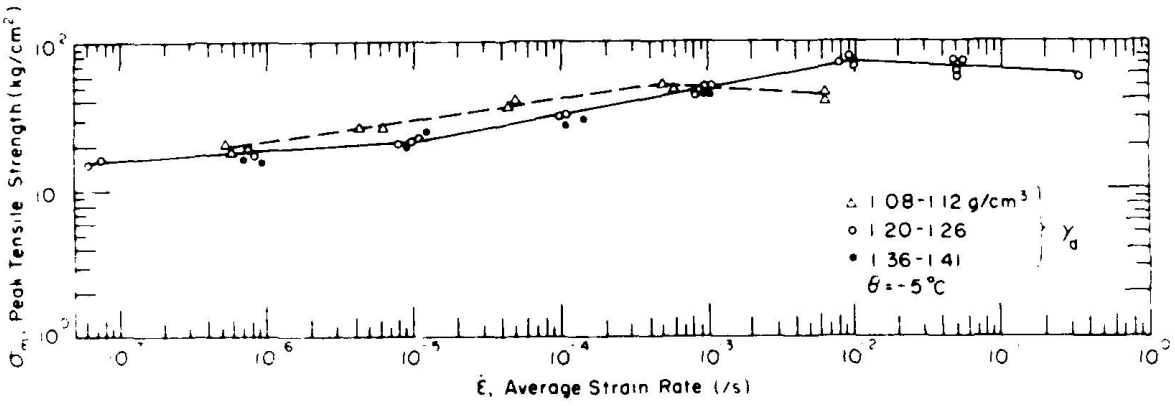

Figure 2. 5 Peak tensile strength of frozen silt against the average strain rate (Yuanlin and Carbee, 1987).

`

Akagawa and Nishisato (2009) found a different behavior of frozen silt at the frozen fringe with loading rates of 0.34 mm/min and 2.31 mm/min. The tensile strength decreased with an increase in loading rate, as shown in Figure 2.6. Azmatch et al. (2011) confirmed the previous observation when the tensile strength of frozen silt was investigated with the four-point bending test at loading rates from 0.08 to 8.0 mm/min at a temperature of - 0.7 °C as shown in Figure 2.6.

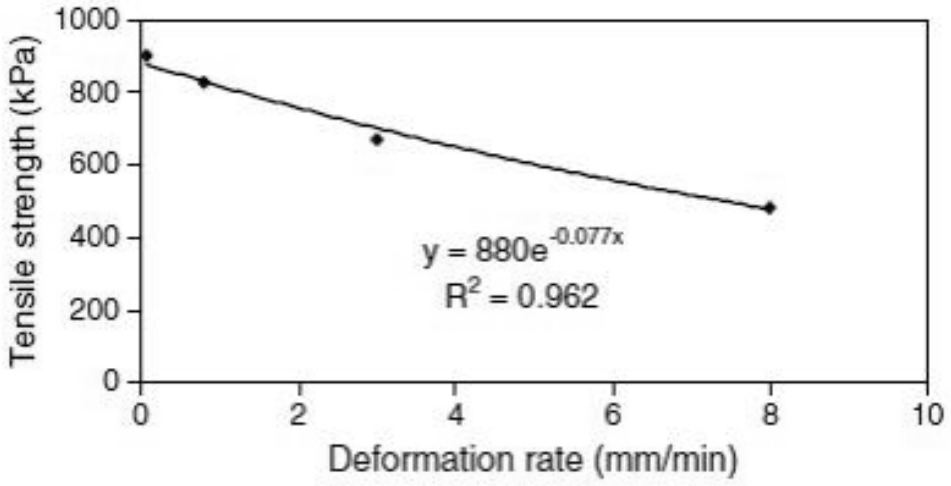

Figure 2. 6 Tensile strength against deformation rate for frozen silt (Azmatch et al., 2011).

Zhou et al. (2015) concluded that the tensile strength of both clay and silty clay soils are independent of the splitting rate at the frozen fringe under loading rates of 1.0, 2.0, and 4.0 mm/min as shown in Figure 2.7.

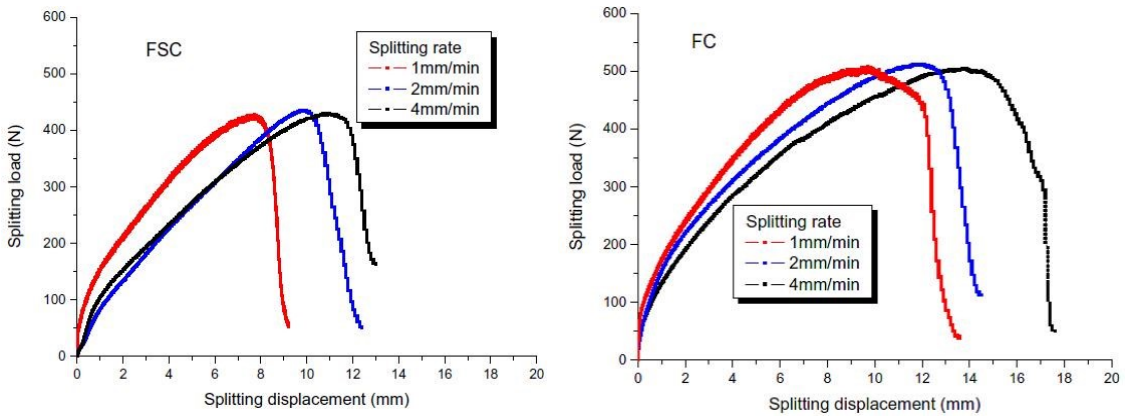

Figure 2. 7 Splitting load versus splitting displacement for clay and silty clay soil (Zhou et al., 2015).

Salinity

Soil salinity strongly affects the mechanical properties of frozen soil. It is therefore very important to investigate the effect of salinity on the strength of frozen soil, especially where the presence of salt is naturally occurring. Generally, the strength of frozen soil depends mostly on the ice content. Patterson and Smith (1985) concluded that the ice content in saline soil is a function of both salt content and temperature. By increasing the salinity, the volumetric ice content is reduced, and the unfrozen water increases.

Hivoni and Sego (1995) confirmed that the increase in salinity led to a decrease in the ice content, causing a reduction in soil strength. For fine-grained soil at low salinity, the ice binds the soil particles with its bonded water continuously, but ice layers became discontinuous with the increase in salinity due to the growth in thickness of the adsorbed water film. The contribution of ice decreased due to weak bonding and frozen soil strength, became mainly dependent on cohesion and friction contribution.

Bing and Ma (2011) found that the initial freezing temperature of saline soil reduced with the presence of the salt regardless of its type. The difference in the freezing point decreases when salt content decreases and water content increases for clay soil. Moreover, the effect of different anions on the freezing point was found to be $Cl^- > CO3^{2-} > SO4^{2-}$, while for different cations was $K^+ > Na^+ > Ca^{2+}$.

`

2.2.2 Compressive strength

The compressive strength increases remarkably by freezing compared with the tensile strength. Frozen soil compressive strength depends mainly on ice content, the strength of the ice, and unfrozen water content; therefore, it is a function of temperature. It is found to be sensitive to other factors like loading rate, salinity, and water content. The compressive strength and brittleness of frozen soil usually increase with a drop in temperature and the increase in loading rate.

Temperature

Haynes and Karalius (1977) conducted a series of uniaxial compression and tension tests to determine the strength of frozen silt at a temperature varying from -56.7 to 0 °C and loading rates 4.23 cm/sec and 0.0423 cm/sec. The results revealed that the ratio of compressive strength to tensile strength increases with the drop in temperature.

Loading Rate

Bragg and Andersland (1981) found that the compressive strength of frozen sand is inversely proportional to temperature and directly proportional to loading rate below 10^{-5} s^{-1}, while it became insensitive to strain rate at strain rate higher than 10^{-5} s^{-1}. The compressive strength was found to be more sensitive to strain rate at a temperature of - 2 °C.

Li et al. (2001) investigated the sensitivity of compressive strength to strain rate for frozen silty sand. The results showed that the compressive strength increases with decreasing temperature. The compressive strength was less sensitive to strain rates below 10^{-4} s^{-1}, and it became more sensitive in the strain rate range of 10^{-4} s^{-1} to 10^{-3} s^{-1}, while the compressive strength was extremely sensitive to strain rate above 10^{-3} s^{-1}.

Xu et al. (2017) studied the influence of temperature and strain rate on compressive strength of frozen loess at temperatures of - 2 °C, - 4 °C, - 5 °C, and - 7 °C and under strain rates of 10^{-2} s^{-1}, 10^{-3} s^{-1}, 10^{-4} s^{-1}, 10^{-5} s^{-1}, and 5×10^{-5} s^{-1}. The behavior of frozen soil was divided into three stages. Firstly, a linear stress-strain relationship with slope increased where the rise in strain rate up to yield point. In the second phase, the stress increased nonlinearly with the increase in strain up to the peak value. Finally, the softening stage was observed.

`

2.3 Laboratory tests on frozen soils

2.3.1 Frozen soil sample preparation

The frozen soil may be divided into two different categories according to the freezing condition; natural and artificially frozen soil. As a soil freezes in situ condition at temperatures close to the melting point, ice lenses start to form due to moisture migration. These ice lenses affect the physical and mechanical properties of frozen soil, so the naturally frozen soil usually is not appropriate for laboratory investigations. Furthermore, it is not easy to retrieve in situ undisturbed frozen soil samples due to the difficulty of conserving the frozen soil in its original state throughout the cutting process. In addition to ice lenses that make the specimen vulnerable to be broken during the coring, the preparation is very expensive due to transportation and machining costs when compared to artificially frozen samples.

Early trials were done by Johnston (1963) to get undisturbed naturally frozen sample using a core barrel, but the large water content which usually exceeds the soil liquid limit resulted in thawing the soil in contact with the core. Baker (1976) replaced the undisturbed specimen by an undisturbed block cut from the site. This undisturbed block was protected from thawing and thermal disturbance during transportation, storage, and machining in the laboratory. The appropriate cutting and machining procedures were followed based on soil type, size, and shape of the sample. The suitable ambient temperature for machining was found to be -5 °C ± 1 because the machining in higher temperatures caused thawing sample while cutting in lower temperatures led to cracking the sample surface; thus, it is required to change the temperature of the samples during machining. Some soil disturbances may have occurred due to temperature fluctuation for machining. Lee et al. (2002) used another technique to mitigate the negative effects of the core barrel sampling on fine-grained frozen soil by cooling the drill bit using liquid nitrogen, but the core bit jammed due to the stopping of coolant flow and the aggregating of soil around the bit. The specimen was then cut using a regular core barrel, and then a water-jet was used to cut the sample using a high steam pressure to reduce the disturbances of the core barrel.

Artificially frozen soil samples are mainly used in frozen soil investigations, and various techniques are proposed to prepare frozen samples depending on the purpose of the investigation. Zhou et al. (2015) mixed natural soil with water to reach the target water content and compacted

`

to obtain the required density before freezing, and then the mixture was frozen at a very low temperature. Akagawa and Nishisato (2009) prepared a slurry by adding water content twice the liquid limit to the soil, and then the slurry was consolidated to reach the required consistency before freezing.

2.3.2 Tensile strength measurements

In the absence of standardized testing methods for measuring the tensile strength of frozen soil, various testing methods and setups have been used to predict the tensile strength and to recreate the appropriate freezing conditions. The tests which have been performed to measure the tensile strength may be divided into two main categories are:

i. The direct testing method,
ii. The indirect testing method.

The direct method is also known as uniaxial tension test still seems to be the most trustworthy method to measure the tensile strength of soil, and the majority of tensile strength investigations were done using the uniaxial tension testing method. The difficulties associated with performing the test resulted in the development of several indirect methods, such as the Brazilian test and the beam bending test, which will be discussed in this section.

2.3.2.1 Direct tension test (uniaxial tension test)

The direct tension test is the simplest method to obtain the tensile strength of frozen soil samples. The results obtained from the uniaxial tension test are the most reliable and appropriate for both ductile and brittle samples because they are not based on any assumptions. The direct tensile strength can be defined as the maximum tensile stress can be carried by the sample, so it can be calculated easily by dividing the tensile force at the failure by the cross-sectional area.

An early work was done by Haynes (1978) to investigate the tensile strength of frozen saturated silt in the laboratory using the direct method at temperatures of - 0.1, - 1.7, - 5.6, - 9.4, - 17.8, - 34.4, and - 56.7 °C and loading rate of 0.0423 cm/sec and 4.23 cm/sec. The failure occurred close to the end caps for more than half of samples as shown in Figure 2.8 due to stress concentrations near the gripping and eccentricity; thus, new tests were performed to obtain satisfactory results.

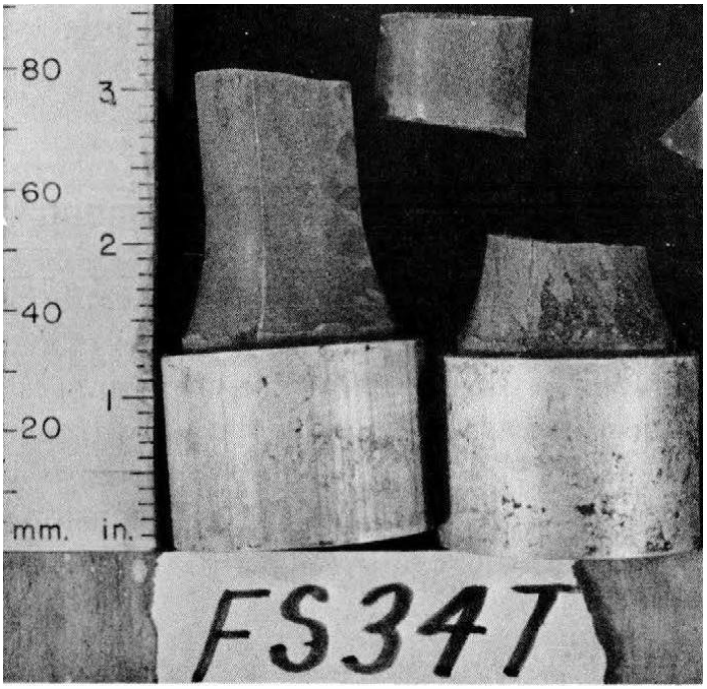

Figure 2. 8 Failure plane of tensile test for frozen silt samples (Haynes, 1978).

Jessberger (1981) performed several investigations focusing on the disadvantages of the uniaxial tension test to eliminate or mitigate their effects. Various devices were proposed to replace the traditional tension test, as shown in Figure 2.9. Akagawa and Nishisato (2009) chose one of these devices named "OFFENSEND" to investigate the tensile strength of frozen silt in the frozen fringe range between of - 1.31 to +0.6 °C and deformation rates of 0.88 and 0.34 mm/min.

The traditional uniaxial tension method was used by Christ and Kim (2009) to study the effect of temperature and moisture content on the tensile strength of frozen silt at - 20, - 15, - 10, - 5 and - 2 °C and loading speed of 1.0 mm/min.

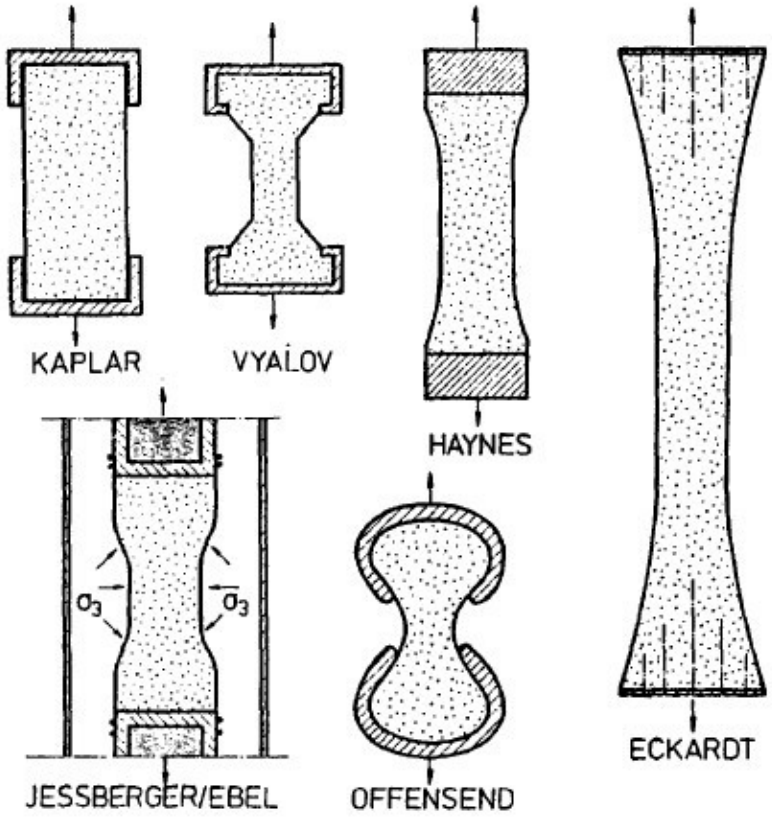

Figure 2. 9 Schematic representation of several laboratory devices of direct tension test for frozen soil (Jessberger, 1981).

2.3.2.2 Indirect tensile strength tests

Although the uniaxial tension test is the most effective method to determine the tensile strength, it is difficult to eliminate the bending and torsion stresses that are induced by the eccentricity of loading. A specific tensile testing machine is required to perform the test in addition to a complicated procedure for preparing the test samples, which makes it an expensive test. These drawbacks to the direct testing method increased the need to find other testing methods for determining the tensile strength of frozen soil. A new indirect testing method was developed by Carneiro (1943) and Akazawa (1943) separately to calculate the indirect tensile strength of concrete. The test involved splitting a cylindrical sample along its diametric plane, and is known as the Brazilian test, or splitting test. Another testing method was presented by Chen in 1970 to measure the indirect tensile strength by compressing a cylindrical sample concentrically with cylindrical steel punches at the top and bottom surfaces. Both of these testing methods need a

`

simple cylindrical sample with a small volume and a compression machine, whereas the beam bending test has been standardized by ASTM since 1970 to determine the tensile strength by applying concentrated loads on a simply-supported sample beam.

Splitting Tension Test (Brazilian Test)

The splitting tension test is the most common indirect test to determine the tensile strength of brittle materials such as concrete, rock, and frozen soil. This method is much easier and cheaper than the uniaxial tension test, so it is suitable for routine testing in the field. During the test, compressive stress is applied uniformly along a diametric plane of the sample through two opposite loading strips until failure occurs. The test sample assumed to be isotropic, homogeneous, and obey Hook's law up to the failure. The contact stresses induced in the sample at the loading areas due to friction between sample and loading parts supposed to be zero. Colback (1966) applied the modified Griffith failure to study the fracture of samples of the Brazilian test, and the results confirmed that the center of the disk is the point of maximum tensile stress at which failure should take place. Shloido (1968) correlated tensile strength results obtained from both the direct tension test and Brazilian test on frozen sand, sandy loam, loam, and clay in a temperature range from -10 to - 1 °C. The value of the correlation coefficient was found to be 1.0, and the variation coefficient of tensile strength results obtained with uniaxial tension test is twice that for the splitting test. In summary, the splitting tension test can be used to determine the tensile strength of frozen soil.

Bragg and Andersland (1981) studied the tensile strength of frozen sand using splitting tension testing method on disk samples of diameter 101.6 mm at - 6 °C and loading rates range from 1.2 to 6 mm/min. The results showed that the tensile strength was slightly affected by the loading rate in the range from 1.3 to 6.5 mm/min, and the tensile failure did not take place at low loading rate. This research indicates that the splitting test is impropriate testing method for warm frozen soils due to the ductile behavior of the samples.

Yue et al. (2003) concluded that the tensile strength of rock and concrete obtained by the splitting test is significantly affected by the homogeneity of material because the failure plane is predetermined, and the equation of splitting tensile strength test becomes inaccurate by increasing the length/diameter ratio.

`

The splitting tensile strength testing method for rock has been standardized by ASTM D3967 (2016). Equation 2.3 of tensile strength was derived based on the assumptions that tensile failure occurs at the point center of the disk where the maximum tensile stresses and line load is applied due to a very narrow strip loading.

$$\sigma_T = 2p / \pi LD \tag{2.3}$$

where σ_T is the tensile strength in MPa, P is the applied load at failure N, D is the diameter of the sample in mm, and L is the thickness of the sample in mm.

Yu et al. (2009) introduced a modified testing method of Brazilian test to improve the contact condition between sample and loading tools to reduce the stresses induced at the loading area. Two bearing blocks with arc-shaped of diameter equal to specimen diameter and 20° arc angle were used to determine the tensile strength of the rock. Zhou et al. (2015) carried out splitting tension tests on frozen clay and silty clay samples in a temperature range of - 5 to - 0.1 °C and loading rates of 1.0, 2.0 and 4.0 mm/min to investigate the effect of temperature, loading rate, and moisture content on tensile strength. The results showed no change in tensile strength values at the different loading rates (see Figure 2.7).

Double Punch Test

The double punch test is a testing method used in the determination of the tensile strength of concrete, soil, and rocks. This test is not a common testing method for frozen soil, although it is easier than other tests and samples fail at lower applied loads compared to other methods. The main theory and failure modes of this test are primarily based on the bearing capacity of tested materials (Chen and Drucker, 1969). This testing method was introduced to calculate the indirect tensile strength of concrete (Chen, 1969), soil (Fangand Chen, 1971), and rock (Dismuke and Chen, 1972). This method was developed to replace the splitting test mainly in the case of heterogeneous or anisotropic materials because the tensile strength observed in a double-punch test is an average strength over many cracked diametric planes, instead of one predetermined failure plane in the splitting test. In this test, a cylindrical sample is compressed concentrically and vertically through two cylindrical steel punches on the top and bottom surfaces of the sample. As a result of the uniform distribution of compressive stress, the outer segment of the sample divides vertically by

diametric cracks at the weakest planes due to the induced tensile stresses. The tensile strength can be calculated from the following equation:

$$\sigma_T = \frac{P}{\pi\left(KbL - a^2\right)} \tag{2.4}$$

where σ_T is the tensile strength in MPa, P is the punch load at failure on specimen in N, b is the sample radius in mm, a is the punch radius in mm, L is the specimen thickness in mm, and K is a constant equal to 1.0 for soil, and 1.2 for concrete, and rock. This equation was valid for b/a ≤ 5 or H/2a ≤ 5, and it was derived based on two assumptions; the tested material follows the perfect plasticity theory, and a Mohr-Coulomb failure surface is straight lines in compressive stress and parabolic in tensile stress (see Figure 2.10 and 2.11).

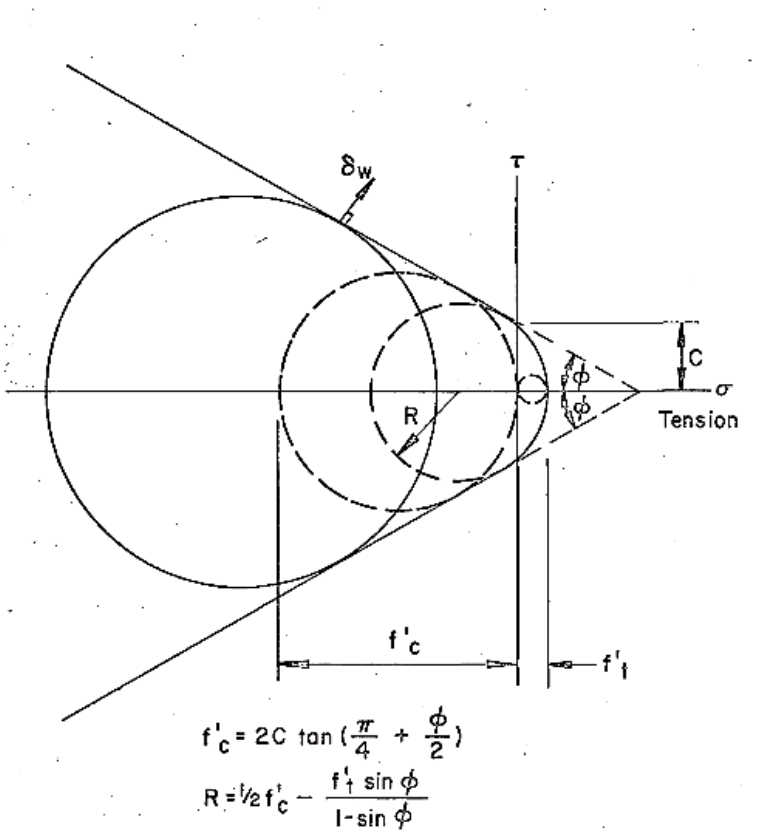

Figure 2. 10 Graphical representation of modified Mohr-Coulomb criterion (Chen, 1969).

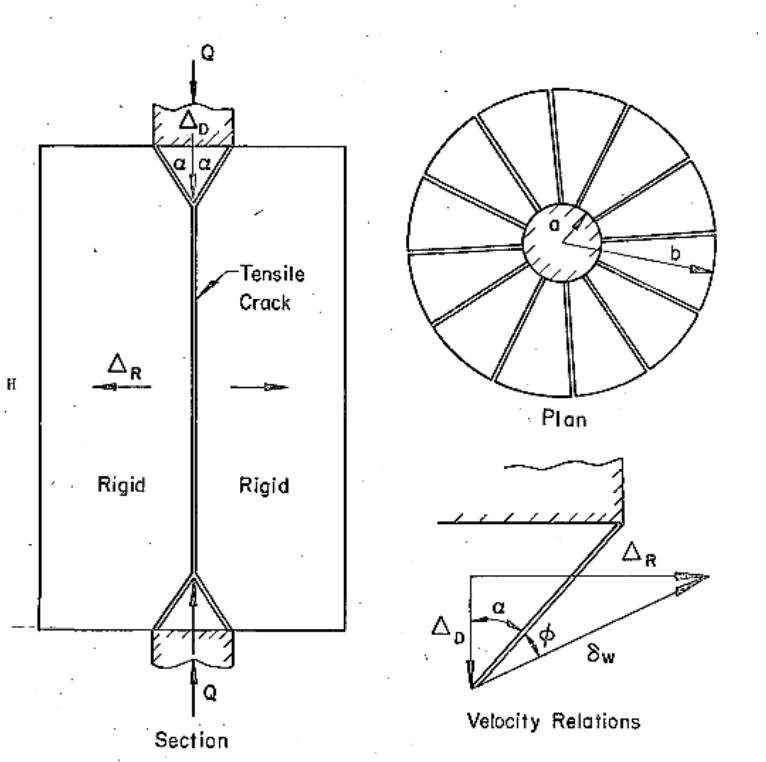

Figure 2. 11 Schematic representation of the failure mechanism of a double punch test (Chen, 1969).

Chen and Yuan (1980) investigated the tensile strength of concrete more precisely using the finite element method. Concrete is an elastic-plastic strain hardening material. The calculated indirect tensile strength was found to be 75 % of the tensile strength calculated by Equation 2.4.

Bortolotti (1988) expressed an equation to obtain the tensile strength of concrete, assuming that concrete failure follows the modified Coulomb failure criteria:

$$\sigma_T = \frac{P}{\pi(bL - a^2 \cot\alpha)} \tag{2.5}$$

where σ_T is the tensile strength in MPa, P is the applied load at failure on the specimen in N, a is the punch radius in mm, b is the sample radius in mm, L is the specimen thickness in mm, and $\alpha = \frac{\pi}{2} - \frac{\phi}{2}$ with internal friction angle ϕ.

`

Molinset et al. (2008) carried out double punch tests to study the tensile strength of fibered reinforced concrete as an alternative to bending tests. The coefficient of variation for the tensile strength results obtained from double punch tests was lower compared with beam tests. Iravanian and Bilsel (2016) performed both double punch and uniaxial compression tests to predict the Mohr-Coulomb failure envelope for a sand-bentonite-cement mixture.

Sarfarazi and Schubert (2017) presented an experimental and numerical study to determine the tensile strength of concrete using both direct and indirect tests. The results obtained from the double punch tests were very close to direct test results. Several advantages of the double punch test were indicated, such as small sample size, easy preparation, and low capacity compression device needed to perform the test.

Beam Bending Tests (Three-Point and Four-Point bending test)

The main idea of the beam bending tests is to apply concentrated loads at the midpoint or the third points of a simply-supported sample beam, causing failure under a pure bending moment. In the three-point test, the stress concentrates at a narrow region under the center, so it is suitable for testing a homogeneous material. The stress concentration in the four-point test is distributed over a larger area at the lower surface of the sample span; thus, it is used in measuring the flexural strength of nonhomogeneous material. In the three-point bending test, the sample beam is placed on the two rollers supports close to the ends of its span. The load is applied constantly by another roller at the midpoint above a pre-notched crack. The four-point bending test is performed using the same device, but the load is applied by two rollers at the third-points of the sample beam.

The beam bending test has been standardized by ASTM D78 (2016) and ASTM D790 (2007) to determine the tensile strength using the following equation:

$$\sigma_T = \frac{PS}{\mathrm{Wd}^2} \tag{2.6}$$

Where σ_T is the tensile strength in MPa; P is the load at failure in N; S is span length in mm; W is the width of the beam sample in mm; d is the depth of the beam sample in mm.

Coviello et al. (2005) investigated the tensile strength of soft rocks using both uniaxial tension and beam bending testing methods. The results showed that the three-point bending test is

an inappropriate testing method to determine the tensile strength of soft rocks, while the four-point bending test seemed to be independent on specimen geometry and slenderness. The results of the beam bending tests were found to overestimate or underestimate the uniaxial tensile strength for different soft rocks.

Mujika (2006) observed that the length of sample span decreases in both three-point and four-point beam-bending tests as a result of the rotation of the supporting rollers during the loading process, while the rotation of loading rollers increases the load span in four-point bending; therefore, a correction should be considered to eliminate the effect of rotation. This error was found to be dependent on the thickness of the sample and the radius of rollers, and its influence is much greater in four-point bending than in the three-point bending test. Thusyanthan et al. (2007) investigated the tensile strength of kaolin clay using a four-point bending test at a constant vertical deformation rate of 0.23 mm/min. A brittle tensile failure was observed at the lower fiber of the clay beam due to cracks initiation by stretching where total negative stress exists.

Azmatch et al. (2010) performed four-point bending tests to study the tensile strength of frozen Devon silt using square beam samples with dimensions of 304.8 mm x 76.2 mm x 76.2 mm in a temperature range from -9.5 to -0.7 ºC and deformation rates from 0.8 to 8.0 mm/min. The results showed that the tensile strength is dependent on the temperature, the deformation rate, and the unfrozen water content. The elastic modulus was found to be inversely proportional to the temperature and the deformation rate. Azmatch et al. (2011) conducted another series of four-point bending tests using the same samples and loading rates to study the tensile strength of frozen Devon silt at a temperature range of - 1.5 to 0 °C. The results confirmed the same dependency of tensile strength on the temperature and the unfrozen water content, but the tensile strength increased by increasing the deformation rate contrary to the results found in the previous investigation at - 5.4 °C.

Yamamoto and Springman (2017) carried out both beam bending tests under uniform vertical displacement rates of 0.1 and 1.0 mm/min at a temperature between - 3.1 °C and - 0.6 °C to study the tensile strength and the fracturing method of the frozen soil. The results showed a brittle failure at lower temperatures, whereas ductile failure was observed when the temperature rose close to zero degrees.

`

2.4 Uniaxial compression test

Many investigations have studied the uniaxial compressive strength of frozen soil because it is an essential mechanical property for engineering designs and constructions. The uniaxial compressive strength is determined by applying axial load on the frozen sample continuously at a constant strain rate up to failure. The compressive strength of the sample is calculated by dividing the maximum load at the failure by the average cross-sectional area. The test samples are usually cylinders of height/diameter ratio from 2.0 to 3.0. The Young's modulus of frozen soil can be determined easily by calculating the slope of the stress-strain curve, and Poisson's ratio can be determined from the radial-axial strain curve.

Haynes and Karalius (1977) conducted a series of uniaxial compression to determine the compressive strength of frozen silt at a temperature varying from - 56.7 to 0 °C at loading rates 4.23 cm/sec and 0.0423 cm/sec. Bragg and Andersland (1981) performed uniaxial compression tests on frozen sand at varying temperatures of - 15 °C, - 10 °C, - 6 °C, and - 2 °C under strain range of 5.69×10^{-7} s^{-1} to 1.78×10^{-3} s^{-1} to investigate the effect of temperature, strain rate, and sample size on frozen sand compressive strength. Li et al. (2001) carried out a series of uniaxial compression tests on frozen silty sand to investigate the sensitivity of compressive strength to temperature, and water content. The tests were performed at temperatures of - 20 °C, - 15 °C, - 10 °C, and - 5 °C and under a series of strain rates from 1.15×10^{-2} s^{-1} to 9.90×10^{-6} s^{-1}. Xu et al. (2017) investigated the compressive strength of frozen loess at temperatures of - 2 °C, - 4 °C, - 5 °C, and - 7 °C and under the strain rates of 10^{-2} s^{-1}, 10^{-3} s^{-1}, 10^{-4} s^{-1}, 10^{-5} s^{-1}, and 5×10^{-5} s^{-1}.

2.5 Relaxation test

When a load is applied to a frozen soil sample, an immediate deformation (primary creep) occurs followed by a time-dependent deformation (secondary creep) due to the transformation of elastic into inelastic strain, then a creep accelerates (tertiary creep) up to failure. Generally, in creep tests, the sample is subjected to step constant uniaxial loading at the same temperature and conditions, then the creep curves are plotted to show the change in the strain with time and the creep rate-time relationship is determined. Savigny and Morgenstern (1986) investigated the creep of undisturbed ice-rich clay soil using a triaxial test. The deformations were found to be due to shear stresses, consolidation, and viscoplastic deformations of ice and soil structures. The flow

law for polycrystalline ice was applied, and the results showed that minimum strain rates of ice for the soil in the high-stress range are faster than the low-stress range, so almost all samples failed.

The relaxation test is an alternative to the traditional creep test, in which the change in stress is monitored versus time under a constant strain and temperature, so it is known as the inverse of a creep test. The creep parameters can be determined based on the stress-time relationship and independently of a material flow effect. Lade (2009) investigated the creep and stress relaxation of sand using a triaxial testing method, and the results of both tests are shown in Figure 2.12. The results showed that the effect of strain rate is negligible for crushed sand, unlike for clays, and the behavior of tested sands is not viscous, whereas clays behave like a typical viscous material.

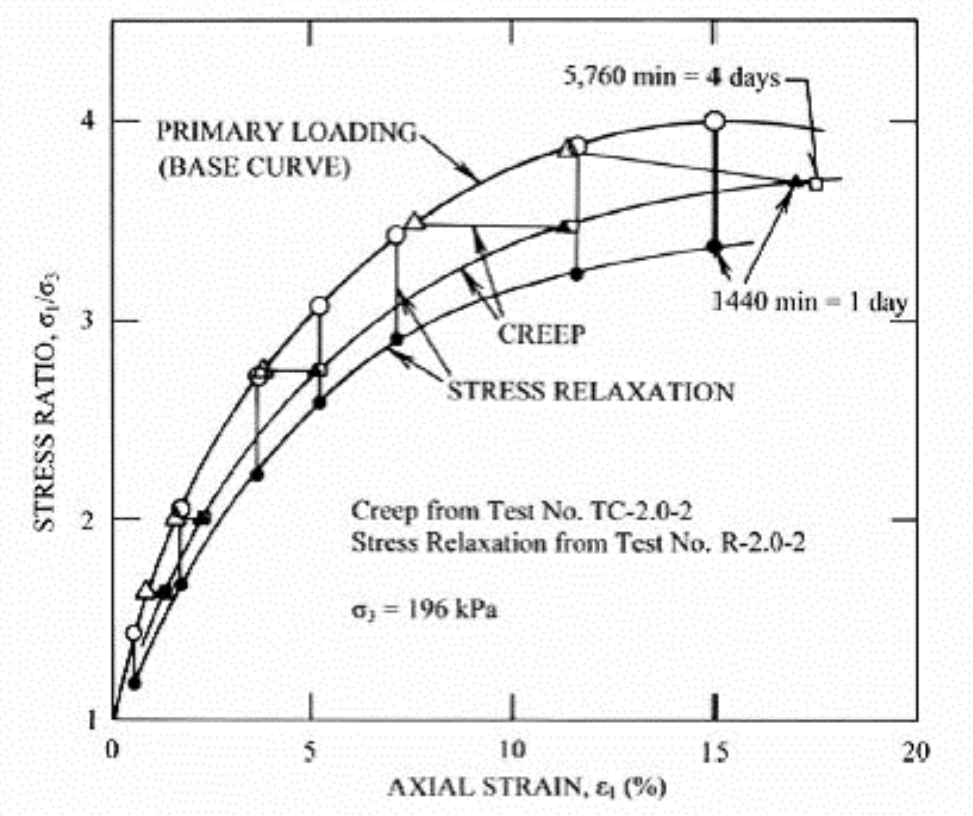

Figure 2. 12 Curves showing creep and stress relaxation results for sand (Lade, 2009).

`

2.6 Summary

The study of previous investigations can be summarized as the following:

- The strength of soil increases with freezing due to the ice formation that binds soil particles together. The strength and behavior of frozen soil depend on several factors such as mineralogy, temperature, loading rate, and salinity of the soil. Many investigations were conducted to study the effect of these factors on frozen soil, but limited studies focused on warm frozen soil strengths.
- Most of the tensile strength studies were carried out using the uniaxial tension test in spite of the difficulties associated with the testing method such as sample preparation and stress concentrations at the ends of the sample. The splitting tension test, the Brazilian test, is the most common alternative tension test, although it seems not appropriate for testing the frozen soil at frozen fringe temperatures.
- Recently, beam bending tests have been performed to investigate the tensile strength of frozen soil despite the changing in sample span length during the test and overestimated values for the tensile strength. Therefore, there is a need for appropriate indirect tension tests to assess the tensile strength of the frozen soil more accurately. The double-punch testing method is widely used to study the tensile strength of both isotropic and anisotropic materials like concrete, soil, and rock because the measured tensile strength is an average strength obtained on different planes of weakness. In addition to the small sample size and low compression stresses required to fail the sample compared with other tensile strength tests.
- The uniaxial compressive strength investigations carried out at temperatures lower than the - 2 °C are limited compared to those were done at temperatures below - 2 °C.
- The majority of creep investigations focused on the creep of frozen soil at low temperatures using a triaxial testing method under constant stress. The relaxation creep test still needs more studies.

`

Chapter 3

A PRACTICAL APPROACH FOR PREPARING ARTIFICIALLY FROZEN CLAY SOIL SAMPLES

This chapter describes a simple approach for preparing artificially frozen clay soil samples using a controlled procedure to replicate the natural frozen soil. This chapter presents the properties of the materials used and the sample preparation procedure, including mixing, vacuum, consolidation, and freezing to obtain a sample of given water content and density.

This chapter aims to introduce an appropriate method for preparing a homogeneous, full saturation, ice lenses free, and consolidated fine-grained artificially frozen soil sample, through a simple and easy procedure. An acceptance criterion is also proposed for each step of sample preparation after defining all the sources of variation, finding measurable solutions, testing, and comparing the results. Finally, a sample preparation report is developed for this approach to be followed during preparation.

This approach is limited to prepare a saturated cohesive soil. The consolidation is applied to simulate the field conditions and to reach a high tensile strength and suitable consistency for cutting as well. Eventually, the soil sample is cut before freezing to avoid melting or cracking.

3.1 Material properties

The materials used in this research are Silica sand 7030, English China clay kaolinite, Bentonite Western 325M, and Saline water. The properties of each material are experimentally determined, as mentioned in this section.

3.1.1 Silica sand 7030

Silica sand of 30% retained on 70 mesh (212 Microns) was used in this study. The particle size distribution of the silica sand based on the results obtained from the sieve analysis test performed according to ASTM C136 (2014) is shown in Figure 3.1. From the grading curve, the sand used in this research is poorly graded sand ‘SP’ according to the Unified Soil Classification System (USCS) with a uniformity coefficient, Cu of 2.10 and coefficient of gradation, Cc of 1.21. The specific gravity of the silica sand was 2.65 in accordance

with ASTM C128 (2015), and the chemical analysis results are shown in Table 3.1 as per the technical data (see Appendix B).

Table 3. 1 Chemical analysis of silica sand 7030

Mineral Oxides	Silicon Dioxide (SiO2)	Iron Oxide (Fe_2O_3)	Aluminum Oxide (Al2O3)	Calcium Oxide (CaO)	Titanium Dioxide (TiO2)	Magnesium Oxide (MgO)	Potassium Oxide (K2O)	Loss on Ignition
Weight (%)	99.17	0.06	0.27	0.21	0.03	0.03	0.06	0.23

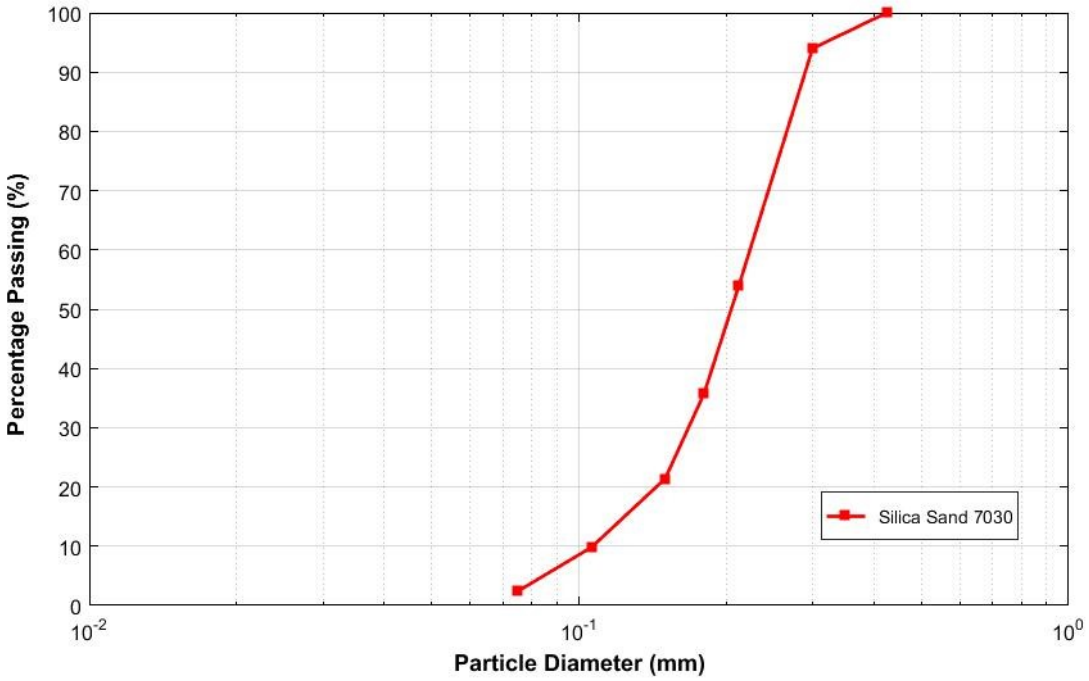

Figure 3. 1 Particle size distribution of silica sand 7030.

`

3.1.2 China clay kaolinite

A pure Standard Porcelain Kaolinite of 100% Kaolin according to the material data sheets was used. The particle size distribution of Kaolinite clay was determined from the hydrometer test according to ASTM D422 (2007) (see Figure 3.2), and the specific gravity of kaolinite was 2.62 as per the test performed in accordance with ASTM D854 (2014), while Atterberg limit test results are recorded in Table 3.2 as per ASTM D4318 (2017).

Table 3. 2 Atterberg limits data for China clay kaolinite

Atterberg limit	China Clay Kaolinite
Liquid limit (%)	61
Plastic Limit (%)	32
Plasticity index (%)	29

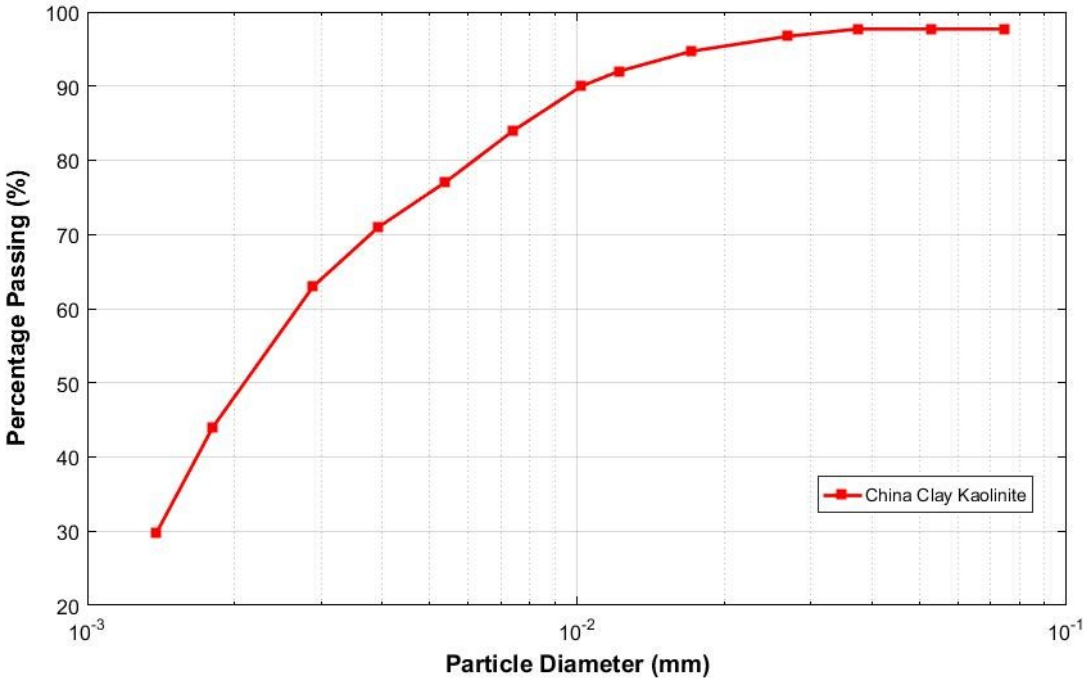

Figure 3. 2 Particle size distribution of China clay kaolinite.

`

3.1.3 Bentonite western 325M

The bentonite utilized in this research was a pure Bentonite composed of 100% smectite group minerals. The particle size distribution of bentonite clay shown in Figure 3.3 was determined according to ASTM D422 (2007), while the specific gravity of bentonite was 2.61 as per ASTM D854 (2014), and results obtained from Atterberg limit test are given in Table 3.3 in accordance with ASTM D4318 (2017).

Table 3. 3 Atterberg limits data for bentonite western 325M

Atterberg limit	Bentonite Western
Liquid limit (%)	235
Plastic Limit (%)	62
Plasticity index (%)	173

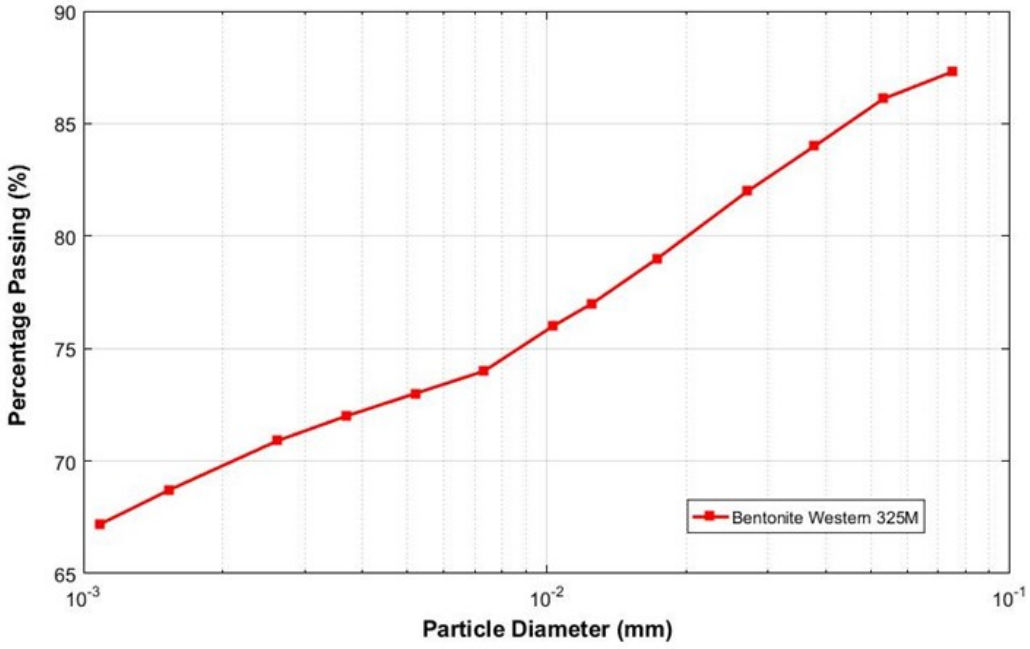

Figure 3. 3 Particle size distribution of bentonite western.

`

3.1.4 Saline water

The mixing water used in this research was saline water composed of distilled water and pure Chloride Sodium salt with a chemical composition shown in Table 3.4 (according to the product label). Three different concentrations were used in sample preparation are 0, 1.0, 3.0 g/L.

Table 3. 4 Actual lot analysis of sodium chloride

Assay	100.1%
Barium	Pass Test
Bromide	<0.01%
Calcium	<0.002%
Chlorate and Nitrate	<0.003%
Heavy Metals	<5.0 PPM
Identification	Pass Test
Insoluble Matter	<0.001%
Iodide	<0.002%
Iron	<2.0 PPM
Magnesium	<0.001%
PH 5% Solution @ 25 DEG C	5.8
Phosphate	<5.0 PPM
Potassium	<0.005%
Sulfate	<0.004 %

3.2 Mixtures description

3.2.1 Mixture selection and classification

All soil mixtures used in this research were artificially saturated kaolinite - sand and bentonite - sand soil. The kaolinite – sand mixture was classified as off-white, inorganic sandy clay of low to medium plasticity, frozen, no visible segregation, well-bonded soil ‘CL, Nbn’. Where the first part ‘CL’ described the soil mixture according to Unified Soil Classification System (USCS) independently of the frozen state, and the second part ‘Nbn’ identified the mixture characteristics after freezing based on visual examination of the bonding and ice condition in accordance with ASTM D4083 (2016). On the other hand, the bentonite–the sand mixture was classified as grey, inorganic sandy clay of high plasticity, frozen, no visible segregation, well-bonded soil ‘CH, Nbn’.

`

3.2.2 Mixtures ratio and saline content

The samples mixtures were divided mainly into two groups depending on clay mineral, and each group contained three kinds of mixtures according to the salinity of mixing water. All mixtures consisted of 50 % sand and 50 % clay of the total dry weight. Also, the percentage of saline water used in mixing was constant for all mixtures and equal to 120 % of its liquid limit to ensure that the mixtures are fully saturated, and the concentration of saline water prepared in the laboratory using NaCl were 0, 1, and 3 g/L as shown in Table 3.5.

Table 3. 5 Composition and identification of soil mixtures used

Mixture Name		Dry Sand (%)	Dry Kaolinite (%)	Dry Bentonite (%)	Saline water (%)	Salinity (g/L)
Group	Sub-Group					
K	0S	50*	**50***	0	**35***	0
	1S	50*	**50***	0	**35***	1
	3S	50*	**50***	0	**35***	3
B	0S	50*	0	**50***	115*	**0**
	1S	50*	0	**50***	115*	**1**
	3S	50*	0	**50***	115*	**3**

* The Percentage calculated per total weight of the dry mixture.

3.2.3 Mixtures properties

Particle size distribution curves of both sand-bentonite and sand-kaolinite mixtures were shown in Figure 3.4, and the specific gravity values of both mixtures were 2.65 and 2.63, respectively. Also, the results of Atterberg limit tests were recorded in Table 3.6 in accordance with ASTM D4318 (2017).

Table 3. 6 Atterberg limits data for soil mixtures used

Atterberg limit	Kaolinite - Sand	Bentonite - Sand
Liquid limit (%)	30	97
Plastic Limit (%)	20	34
Plasticity index (%)	10	63

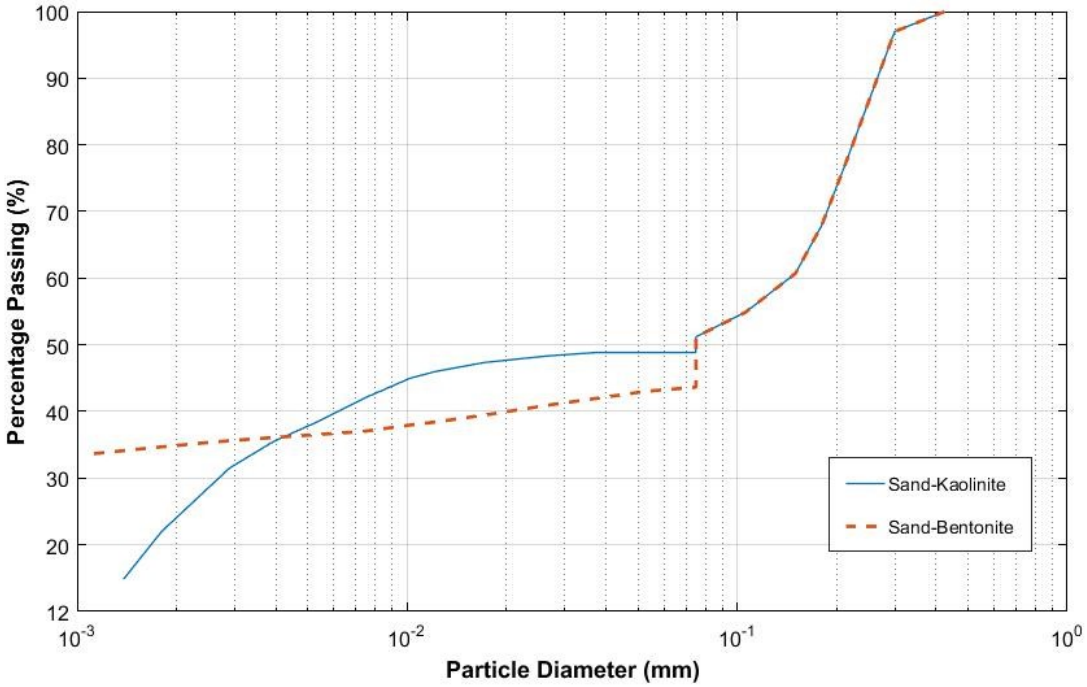

Figure 3. 4 Particle size distribution of soil mixtures used.

3.3 Sample preparation

3.3.1 Sample identification and tracking

The sample naming system consists of clay mineral name ‘K for kaolinite and B for bentonite’ followed by the salinity concentration of the mixing water used ‘0S, 1S, and 3S’, and finally the serial number of sample ‘1, 2, etc.’ e.g. ‘K1S1’ refers to the first kaolinite sample of water salinity 1 g/L. On the other hand, the naming system for uniaxial compression strength (UCS) test cylinders consists of the letter ‘C’ for cylinder followed by the first letter of clay mineral of mixture name ‘K for kaolinite and B for bentonite’ and the lastly the serial number of the cylinder. The salinity of samples does not mention in UCS naming system, because of all samples of salinity 1 g/L. For example, CB2 refers to the second bentonite-sand sample of salinity 1 g/L for the UCS test.

`

3.3.2 Materials storage

Sand, kaolinite, and bentonite are very finely-grained and highly hygroscopic materials; thus the bags of materials were stacked on a wooden plank and completely covered by an impermeable plastic sheet to protect the materials against moisture. Since the bag was opened, it was re-bagged in a heavy-duty bag and the mouth appropriately sealed. Furthermore, the moisture content of materials was routinely determined every month, according to ASTM D2216 (2010) to ensure precise batching of mixture ingredients.

3.3.3 Mixing technique

The mixing process is essential because the physical and mechanical properties of specimens mainly depend on the homogeneity of the mixture. Therefore, both the type and time of mixing were carefully determined to ensure proper mixing. The mixing in this research was done using a domestic stand mixer with stainless-steel bowl of 5L. The mixing was carried out in two steps as follows:

i. Dry mixing by combining clay mineral and sand in mixing bowl, then the mixture was blended well at low speed using wire whisk tool until a homogeneous mixture of uniform color was obtained.
ii. Wet mixing by adding an amount of saline water equal to 120 % of the mixture liquid limit, then the flat paddle is used for mixing, as shown in Figure 3.5.

(a) kaolinite-sand (b) bentonite mixture

Figure 3. 5 Dry and wet mixing for (a) kaolinite-sand and (b) bentonite-sand mixtures.

`

3.3.4 Consolidation cell assembly

A two-part Aluminum mold with an easy-close clamp of inner diameter 50 mm was used. This mold was fixed on the base flange with a pedestal and PVC ring, and then a clamping flange was installed at the top of the mold. Subsequently, both the mold and the flanges were held together by two stainless steel posts to ensure the verticality and stability of the assembly. After mold assembly, both the saturated porous stone and filter paper were placed on the pedestal of the base flange, and then the mold was filled with mixed soil in layers. For each layer, a small tamping rod was used to fill the mold properly to avoid the formation of air pockets, then saturated filter paper and porous plate are placed at the top of the soil. Eventually, the mold containing the soil mixture is submerged in a stainless-steel beaker filled with water with the same salinity of mixing water to keep the sample saturated, and loading block is placed on the top porous plate as shown in Figure 3.6 and 3.7.

Figure 3. 6 The consolidation cell.

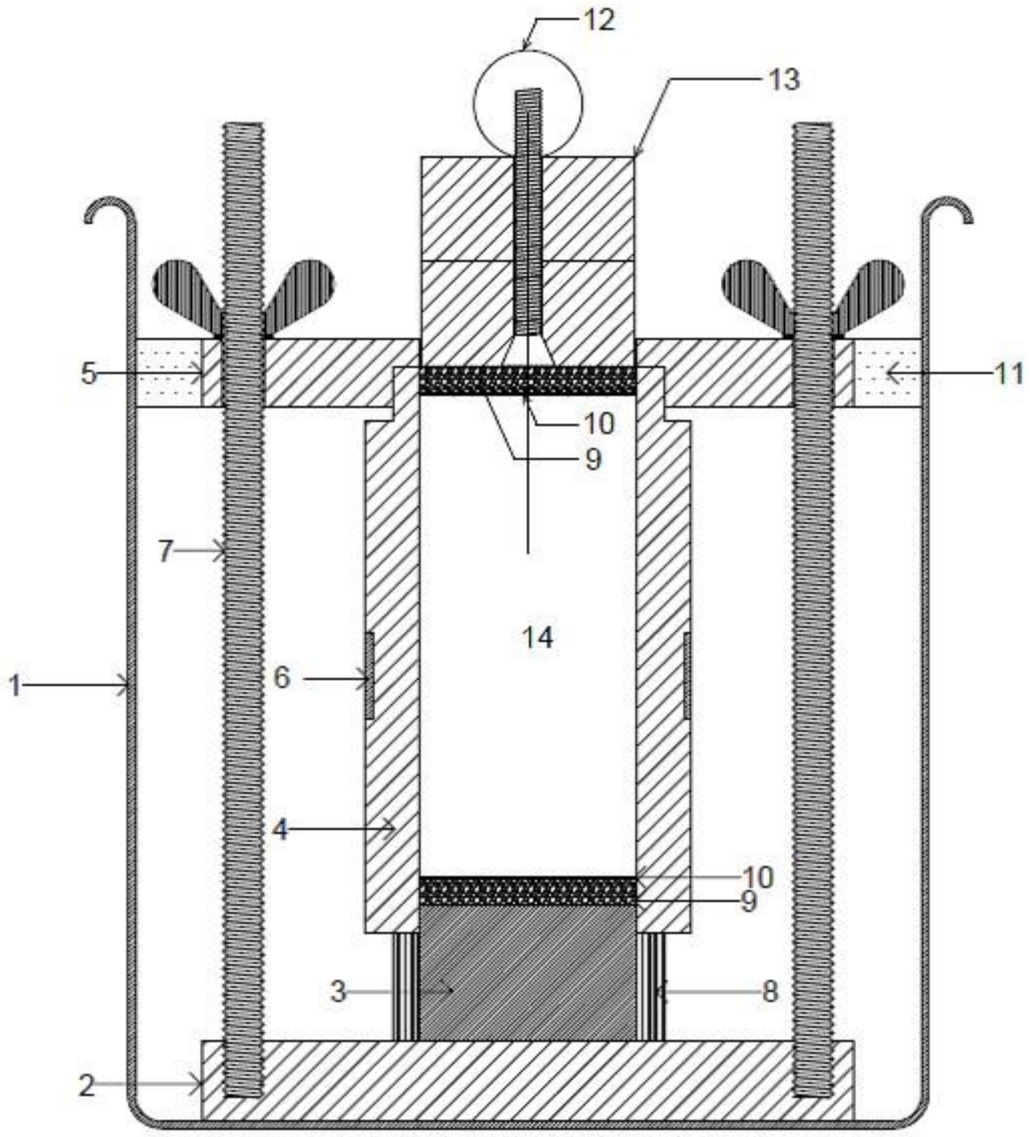

Figure 3. 7 Schematic representation of the consolidation cell.

1. Stainless steel beaker
2. Bottom aluminum flange
3. Stainless steel Pedestal
4. Aluminum Mold
5.Top clamping flange
6. easy-close clamp
7. Stainless steel post
8. PVC ring
9. Porous plate
10. Filter paper
11. Rubber spacer
12. Brass ball
13. Bearing disks
14. Sample

`

3.3.5 Vacuum application

The vacuum set-up used in this research consisted of a vacuum pump connected a vacuum chamber via a vacuum hose, as shown in Figure 3.8. The consolidation cell was placed into the vacuum chamber after removing the bearing block and fixing the top porous plate to prevent the escape of soil during the de-airing, then a vacuum pressure was applied for one hour to the top of the beaker to ensure that the water in the cell was de-aired.

Figure 3. 8 Vacuum set-up.

`

3.3.6 Consolidation under constant load

The consolidation of soil samples in this research is suggested to simulate the overburden pressure in the field before freezing, to achieve this purpose a consolidation setup was designed, calibrated, and validated to consolidate six samples concurrently to reduce sample preparation time in the laboratory. Also, the top and bottom filter papers and porous plates allow double drainage consolidation in addition to the side drainage to accelerate the soil consolidation. After de-airing, the beaker was placed on a brass ring between four steel angles, and then the loading block was put on the upper porous plate. Finally, the loading frame was placed to consolidate the soil cylinders under the constant pressure of 60 kPa. After positioning, the dial gauge was connected to the upper beam of loading fame at mid-span to measure the vertical displacement, as shown in Figure 3.9.

Figure 3. 9 The consolidation set-up.

`

3.3.7 Consolidation set-up

The consolidation setup consisted of the following:

i. Wood frame: was designed to receive up to three consolidation cells on its top surface. It provided with three brass rings surrounded by four galvanized steel angles to ensure that the surface under the consolidation cell is perfectly horizontal and accurately centering under the dial gauges. The frame rested on eight levelers to adjust the horizontality of the top surface, as shown in Figure 3.10.

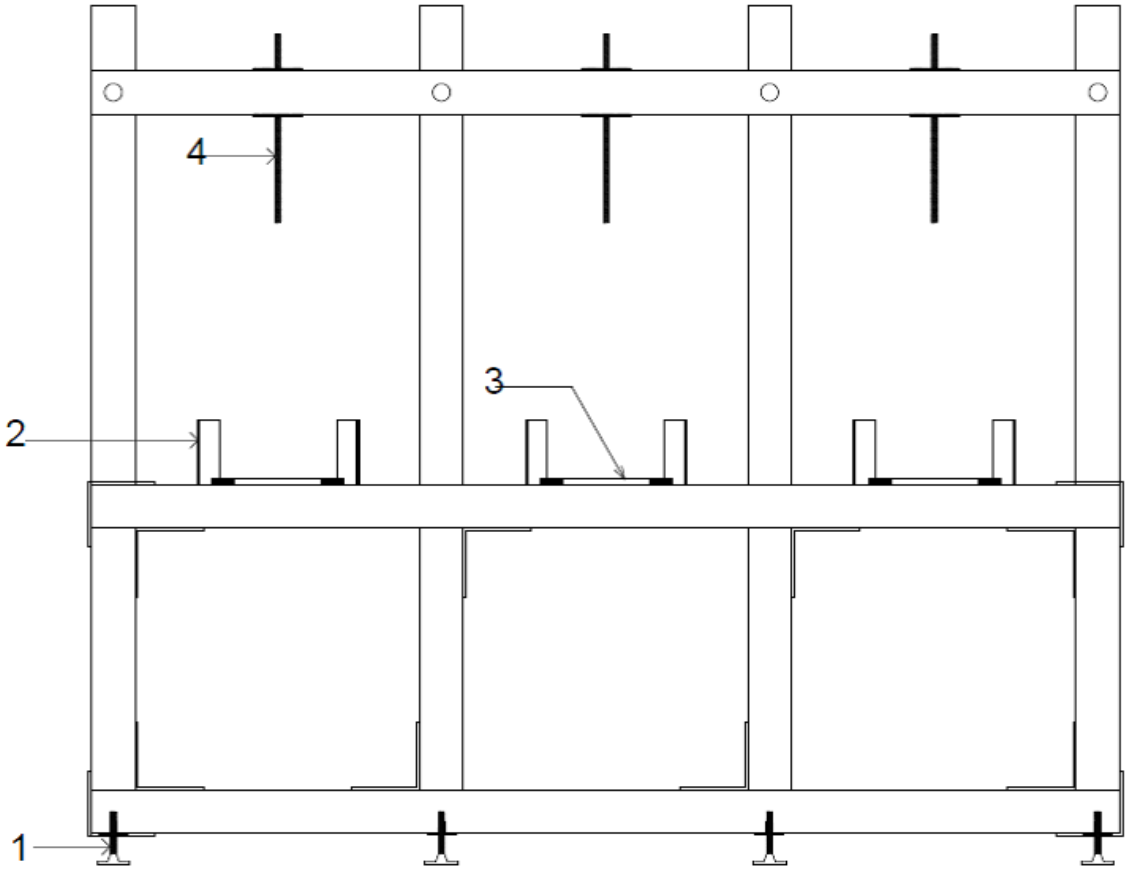

Figure 3. 10 Schematic representation of the wood frame.

1. Leveler 2. Galvanised steel Angles 3. Brass ring 4. Threaded rod

ii. Consolidation cell: as mentioned before in section 3.3.4.

`

iii. Load frame: was designed to be appropriate for use with the closed wooden frame. This load frame is composed of two vertical threaded rods, lower box section beam to carry 9.07 kg (20 Lb) disk weight at mid-span, and upper box section beam was holed precisely at mid-span to seat the frame on a brass ball of bearing block to ensure the vertically of the loads as shown in Figure 3.11.

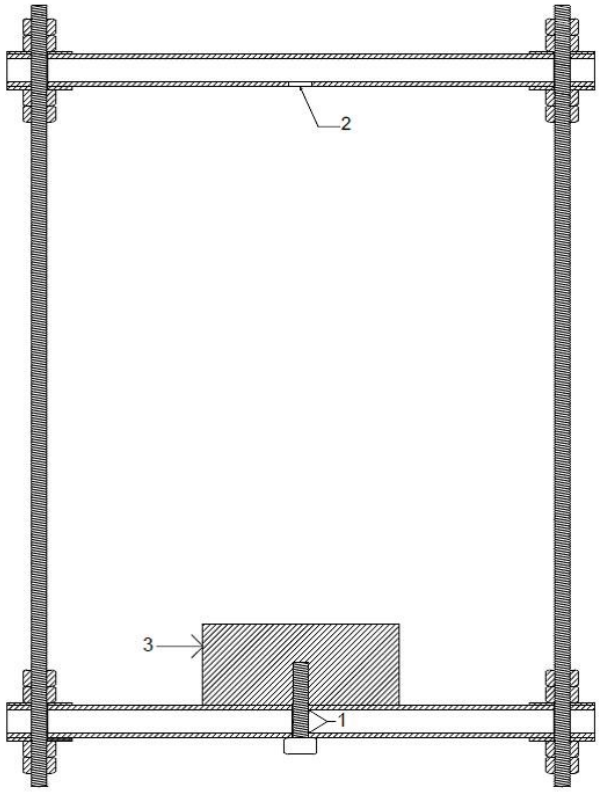

Figure 3. 11 Schematic representation of the load frame.

1. Mid-span hole to attach weights 2. Mid-span hole for ball seating 3. 20 Lb disk weight

iv. High-quality dial gauge: a high-quality gauge with accurate, repeatable readings manufactured by Humboldt Mfg. Co. This dial has a sensitivity of 0.01 mm and a range of 25.4 mm. It is furnished with a holed lug back to be fixed vertically in the wooden frame using a threaded bar.

`

3.3.7.1 Consolidation setup calibration and validation

The consolidation setup was calibrated and validated before releasing for use in this research. The setup was calibrated by placing one consolidation cell in motorized automatic consolidation frame manufactured by VJ Tech Ltd under a pressure of 60 kPa as shown in Figure 3.12, while the other two consolidation cell was consolidated using the consolidation setup. The readings of the consolidation taken by both setups were very close, as shown in Figure 3.13. Furthermore, the variations in values of water content, unit weight, and absolute weight for the three samples after consolidation were very small, so no correction is required for the consolidation setup. Also, the consolidation setup was validated by consolidating a consolidated sample according to ASTM D2435 (2011) using the motorized automatic consolidation system. From the results of the consolidation test, the maximum past stress was found to be 60 kPa as designed (see Figure 3.14).

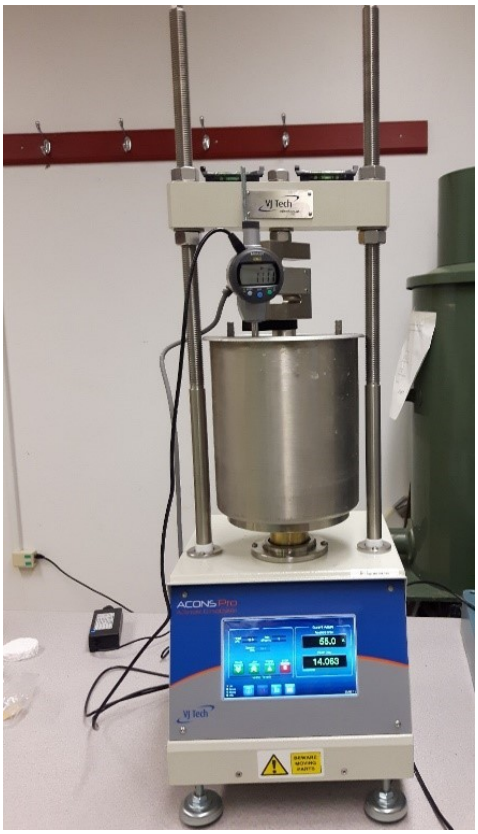

Figure 3. 12 Consolidation cell calibration.

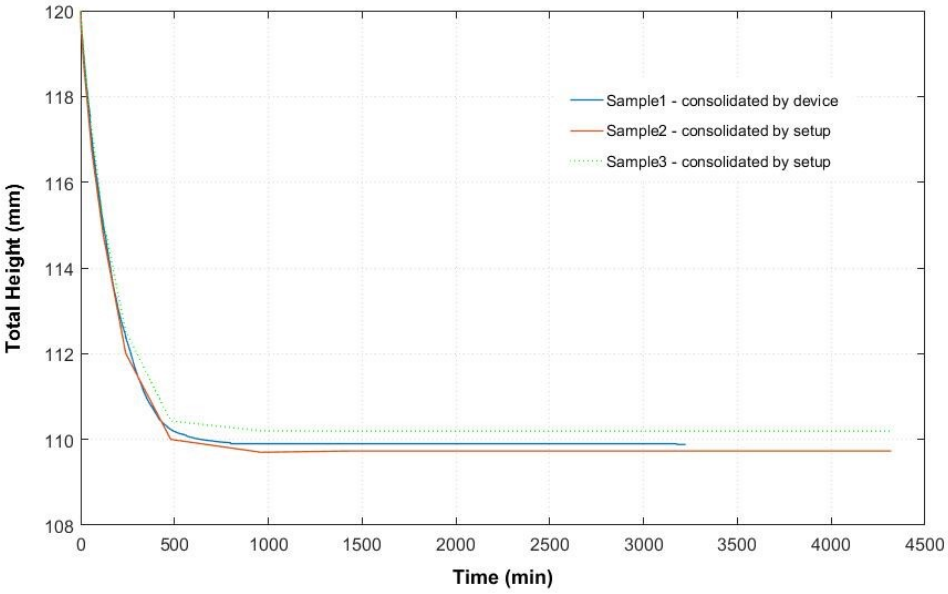

Figure 3. 13 Total height-time curve of kaolinite- sand samples consolidated by device and set-up.

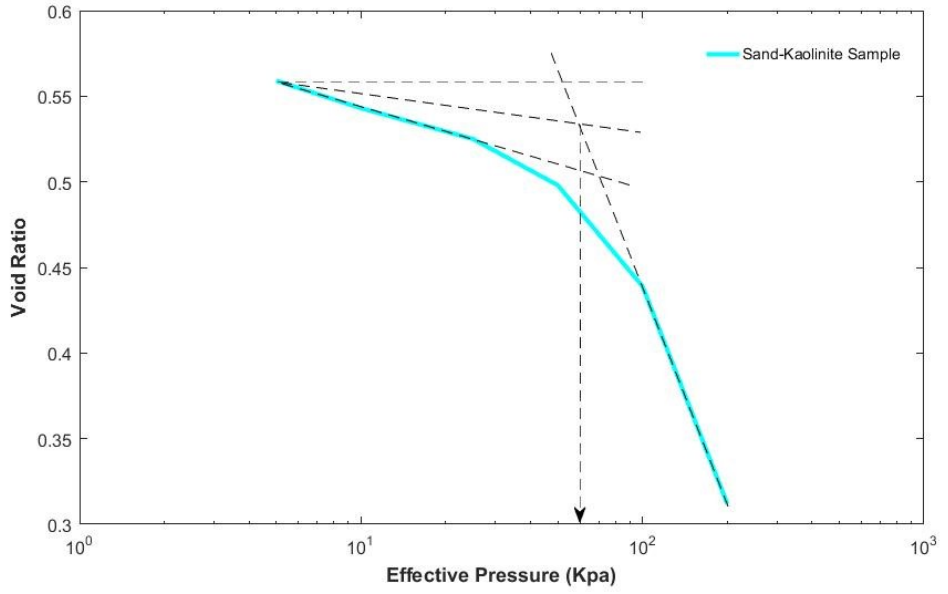

Figure 3. 14 Chart showing the pre-consolidation pressure of the consolidated kaolinite-sand sample.

`

3.3.7.2 Record of vertical displacement

The vertical displacements were recorded against time until the change in vertical displacement is less than 0.1mm/day. The vertical displacement was measured with a readability of 0.01 mm at time intervals of 1, 2, 4, 8, 15, and 30 minutes and 1, 2, 4, 8, 16, and 24 hours, then once per day. Eventually, the heights of the soil cylinder were plotted against the elapsed time, as shown in Figure 3.13.

3.3.7.3 Consolidation mold disassembly and sample cutting

After consolidation, the consolidation cell was carefully taken out of the beaker, then both of base plate and the clamping flanges are removed by loosening threaded rods' nuts. Finally, the mold is transferred to the ejecting setup. The cutting of samples is done before freezing to avoid any cracks that may be created due to increased brittleness of frozen samples. The ejecting and cutting process of soil cylinder was done just after consolidation. The cutting process contains five steps are: i) cutting the top 4mm of the cylinder, ii) ejecting and cutting the first sample of 50 mm, iii) cutting 4mm of the cylinder, iv) ejecting and cutting the second sample of 50 mm, and v) remove the remaining part from the bottom of the cylinder, respectively (see Figure 3.15).

(a) (b) (c) (d)

Figure 3. 15 Pictures of (a) cutting the first sample, (b) top and middle water content samples, (c) cutting the second sample, and (d) the bottom water content sample.

`

3.3.8 Molding, packing, and freezing

3.3.8.1 Freezing mold

The freezing mold was designed to allow easy and quick assembly/disassembly. Two different heights of freezing mold were used, both of them composed of a pipe of 50.8 mm (2 inches) inner diameter, bottom cap, and top cap, as shown in Figure 3.16. The first mold of 58 mm long was designed for tensile strength tests samples, while the other mold of 115 mm height was used for uniaxial compression test samples. The pipe end was beveled to avoid damaging of the sample during the pipe installation, and the pipe was split from one side to ensure easy extracting of the sample from the mold after freezing. All caps contained two small holes to escape air during the cap installation, and then the holes were coved with tape, as shown in Figure 3.17. Eventually, the caps were lubricated before the installation to make disassembly of mold easier after freezing.

(a) (b)

Figure 3. 16 Freezing molds for (a) tensile strength and (b) uniaxial compressive strength tests samples.

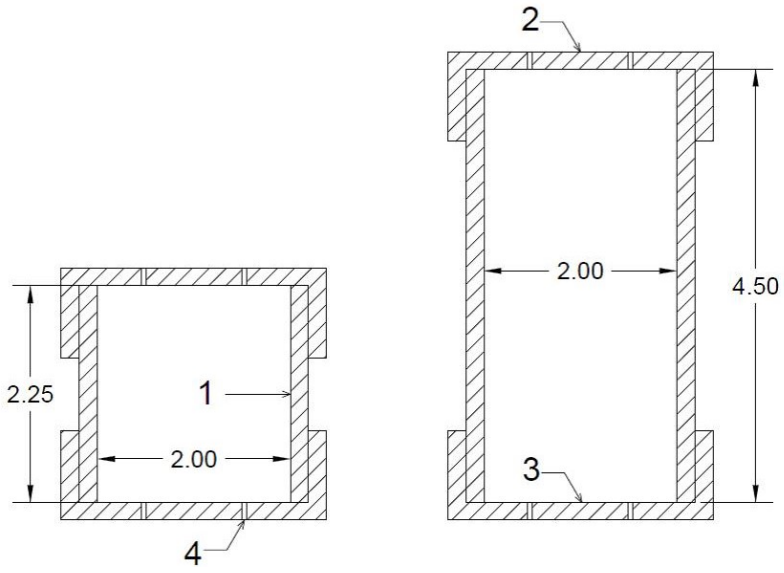

Figure 3. 17 Schematic representation of the assembled freezing molds.

1. ABS Pipe 2. Upper cap 3. Lower cap 4. Small holes

(All dimensions in inches)

3.3.8.2 Packing and freezing

After sample cutting, the sample was placed in the mold, then the top and bottom caps were installed. The cap holes were covered by adhesive tape, and an identification label was staked on the top of the freezing mold. The freezing mold was preserved into a multi-ply bag, and the packed sample was rapidly frozen and stored at - 40 °C to avoid the ice lenses formation (see Figure 3.18).

Figure 3. 18 Samples freezing and storage into a top opening freezer at - 40 °C.

`

3.3.9 Delivery and storage at external testing laboratories

The samples were transferred from the Foundation Engineering Laboratory at Concordia University to Building Envelope Performance Laboratory (BEPL) at Concordia University or to the Geotechnical Laboratory (GL) of Polytechnique using a portable freezer with a temperature range from 10 °C to - 22 °C and a resolution of 1 °C (see Figure 3.19) according to the following procedure:

1. The freezer is connected to AC source until it cools to the temperature lower than the minimum temperature required by 5 °C.
2. Samples are placed in the freezer, and the door is closed properly using the clamp.
3. The freezer is transferred to BEPL at Concordia University directly, or it is transported to Polytechnique Montreal by a van, and the freezer's DC connector is plugged into the DC source of the van until reaching the Geotechnical Laboratory at Polytechnique Montréal.
4. The freezer is connected again to an AC source at the lowest required temperature at least one day before testing.
5. After completing the tests at the lowest temperature, the temperature is changed to the next higher temperature for 24 hours or more before testing.
6. The previous step is repeated until all samples in freezer ae tested, then
7. The freezer is turned back to Foundation Engineering Laboratory, and the steps from 1 to 6 are repeated.

`

Figure 3. 19 The Portable freezer used for transferring and storage.

3.4 Sample preparation test plan

3.4.1 Mixing testing

Mix design

Before starting the mixing process, the sample mix design is reviewed, and the weights of the materials are corrected according to the moisture content, calculated monthly, absorbed by materials. The actual weights are determined with 0.01 g precision scale and recorded in the sample preparation report (See Appendix B - Item 1.1). The weight is acceptable when the difference in weight is less than or equal to ± 0.05 gm due to the sensitivity of the scale.

`

Water content after mixing

After mixing, the water content was calculated for mixture by taking three samples from the three molds in addition to two samples from the mixing bowl to monitor the variation in the same batch. The average of the five reading is calculated to observe the variation from batch to batch. The measurements are recorded in the sample preparation report, as shown in Appendix B - Item 1.2. The mixture is acceptable when the range of reading is less than 3 %, and the average water content is equal to the target water content ± 2 %. Figure 3.20 shows the variation in the target water content of sand-bentonite samples after mixing.

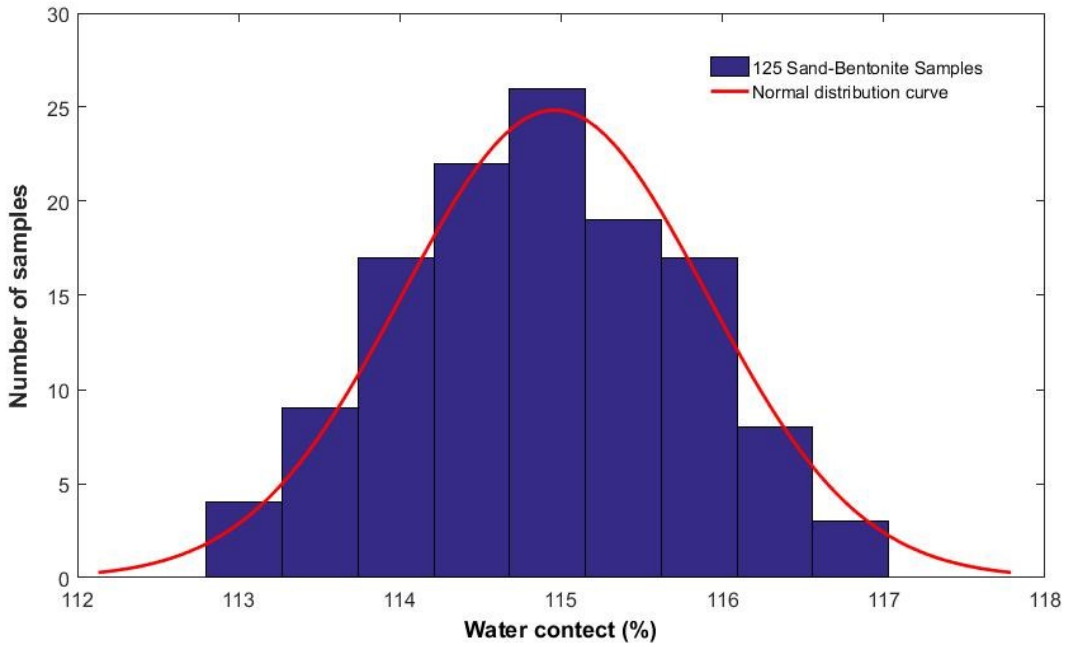

Figure 3. 20 Histogram and normal distribution curve for the water content of bentonite - sand samples after mixing.

`

3.4.2 Consolidation testing

Water content after consolidation

Since the mixture was consolidated, three water content samples are taken from each consolidation cell, as mentioned in section 3.3.6.4. The water content of the three samples are determined and recorded in the sample preparation report, as shown in Appendix B - Item 2.1 to ensure a uniform consolidation occurs. From the laboratory trials, the sample shows an excellent uniformity when the range of readings is less than 3 % for each cylinder, and the variation in average water content is less than 2 % compared with the average water content of the trials. Figure 3.21 shows the water content of sand-kaolinite samples after consolidation.

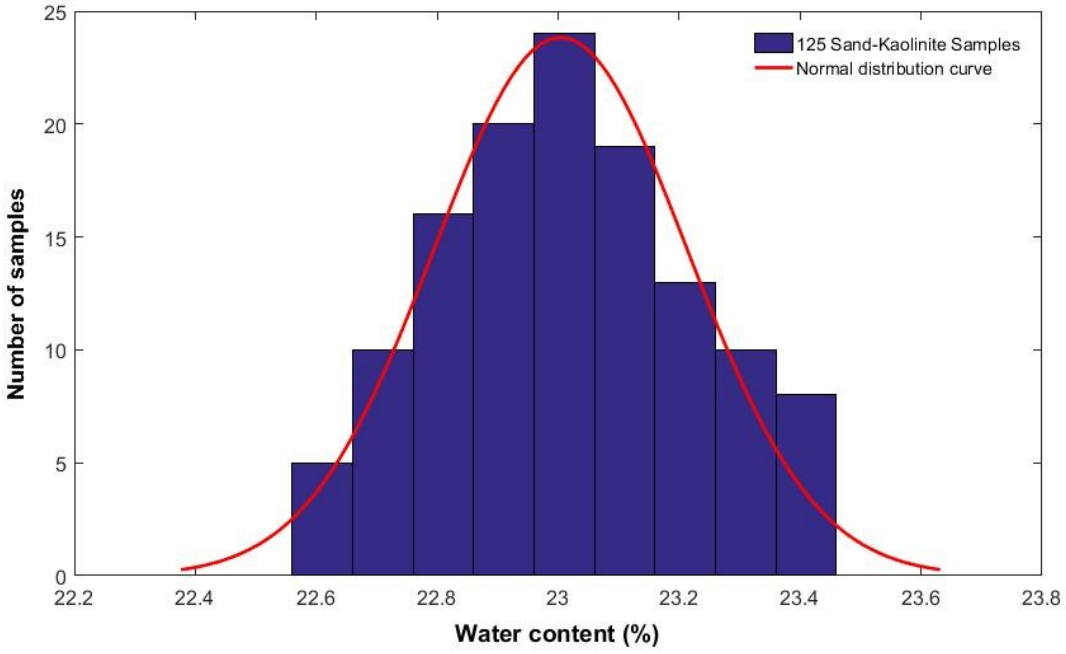

Figure 3. 21 Histogram and normal distribution curve for the water content of kaolinite-sand samples after consolidation

`

Density after consolidation

The diameter, height, and weight of each sample are measured and recorded in the sample preparation report, as shown in Appendix B - Item 2.2. The moist density of the mixture is calculated to ensure that the sample is consolidated properly and the target density is achieved. The allowed variation in moist density is ± 2 % due to the accuracy of measuring, and Figure 3.22 shows that the variation in moist density of more than 75 % of samples is less than 1 %.

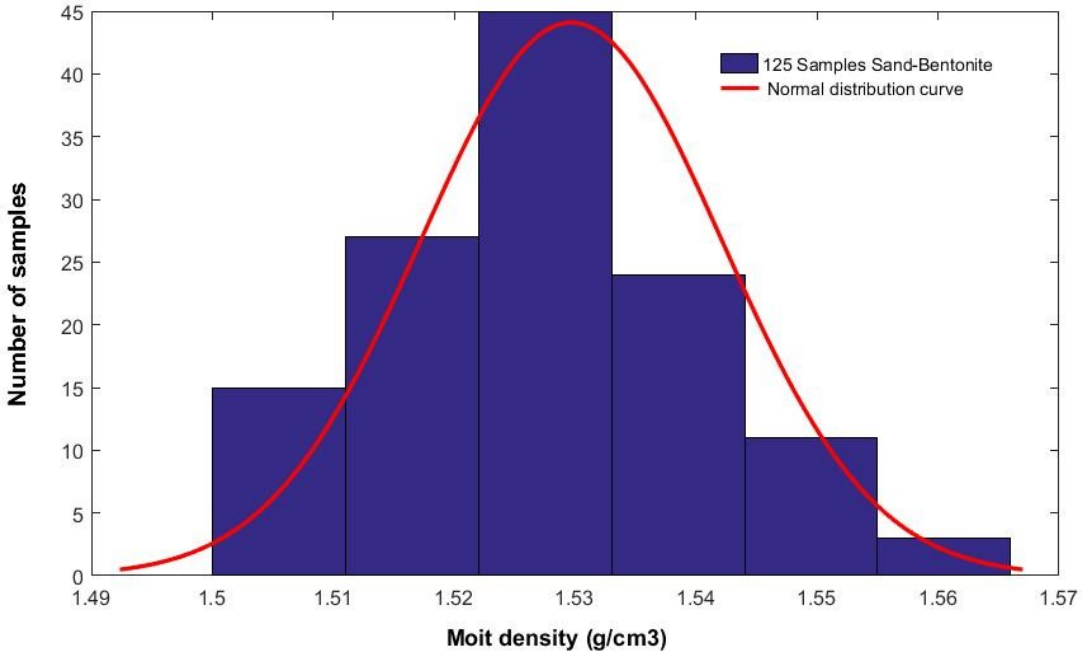

Figure 3. 22 Histogram and normal distribution curve for the moist density of bentonite - sand samples after consolidation.

Consolidation reading

The readings of displacement versus time were recorded in the sample preparation report (Appendix B - Item 2.3), and the relation between the total heights of mixture cylinder versus time is plotted and compared to the initial consolidation chart (see Figure 3.13).

`

3.4.3 Freezing testing

Each sample is visually inspected after freezing to ensure that the surface is free of damages and ice lenses, then the absolute weight of each sample is determined after freezing (Appendix B - Item 3.1) to calculate the weight loss due to surface evaporation and/or sublimation during freezing. The sample is accepted when weight loss is less than 2 grams. The weight loss of sand-bentonite samples is shown in Figure 3.23.

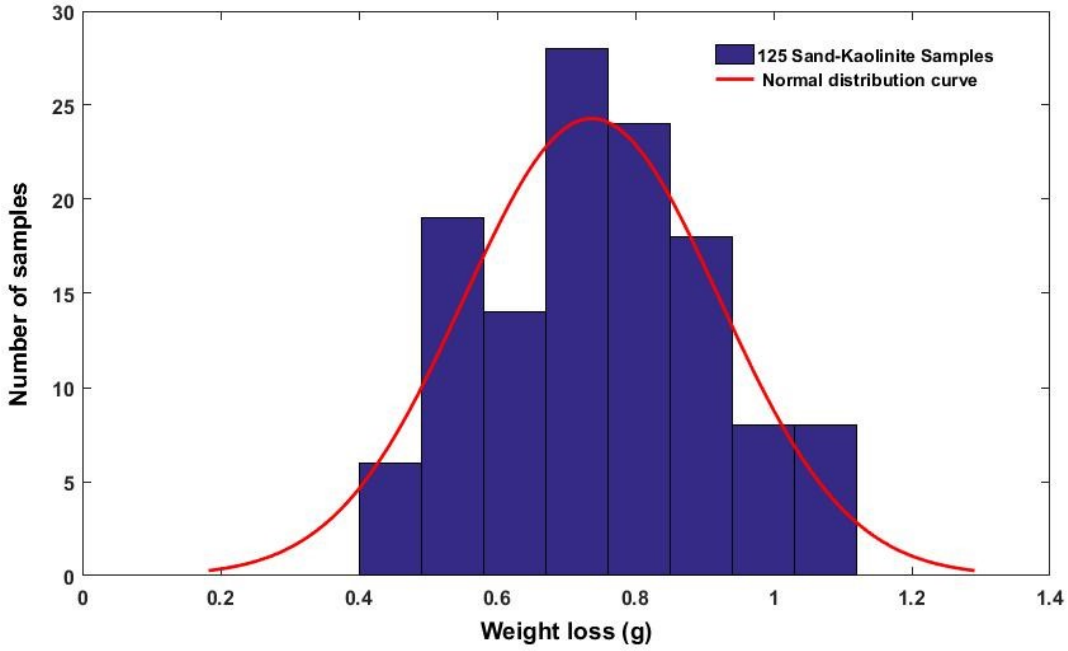

Figure 3. 23 Histogram and normal distribution curve for the weight loss of kaolinite-sand samples after freezing.

`

3.5 Summary

- To produce a homogenous and saturated clay samples, the soil should be mixed for enough time after adding an amount of water higher than its liquid limit. The appropriate time of mixing and water content can be calculated from the trail mixes.
- The consolidation process is essential to prepare a sample with specific unit weight, relatively high strengths, and low porosity.
- Cutting the soil sample before freezing is better to avoid any thawing for the surface at high temperatures or sample cracking due to cutting at low temperatures.
- The soil sample should be protected against evaporation and sublimation in a mold and well-sealed bag to prevent moisture loss.
- The sample should be frozen at very low temperatures to avoid ice lenses due to moisture migration.

`

Chapter 4

LABORATORY TESTS ON TEMPERATURE-DEPENDENT TENSILE STRENGTH

This chapter presents set-up, measuring devices, and procedure of tensile strength testing methods performed to investigate the temperature-dependent tensile strength for frozen sandy clay soils. A series of one hundred sixty-two indirect tensile strength tests performed on two types of frozen sandy clay, kaolinite-sand and bentonite-sand, soils. The samples of each type of frozen sandy clay soils are divided into twenty-seven groups of three samples to study the dependence of the tensile strength on the following factors (1) A temperature range from - 15 to 0 °C; (2) loading rates of 1, 3, and 9 mm/min; (3) salinities of 1,3, and 9 g/L; (4) different approaches of indirect tensile strength tests which are rod bar splitting test (RST), flat strip splitting test (FST), and double punch test (DPT). All those frozen soil samples used in the laboratory tests have a diameter of 50.8 mm (2 inches) and 50.8 mm (2 inches) in height, as mentioned in Chapter 3.

4.1 Tension tests set-up

All tensile strength tests carried out in the environmental chamber of the Building Envelope Performance Laboratory (BEPL) at Concordia University using the set-up shown in Figure 4.1, which is composed of the following:

1. Environmental chamber: a square hut with dimensions of 243.84 cm x 243.84 cm x 304.8 cm high is built with a structural insulated panel building system. It is provided with an advanced humidity and temperature conditioning unit (MAPX-6CWL from ESPEC) for precision control of temperatures from – 45 to 50 °C.
2. Wood frame: a rigid wooden frame made of lumber beams of sections 5.08 cm x 20.32 cm rested on eight levelers are used to carry the test setup.
3. Isolation container: a cooler with hard foam insulation is used after drilling the required holes to pass the loading frame levelers, columns, and platen through its walls. The cooler is provided with four bulbs connected with light intensity controller to maintain the temperature inside at +10 °C, a small fan to ensure a good circulation of warm air, and a

`

thermocouple connected to a data acquisition system to monitor the temperature inside the container.

4. ACONS Pro motorized loading frame manufactured by VJ tech: a loading frame using a stepper motor for loading with a maximum capacity of 15 kN, a resolution of 1 N, and an accuracy of 0.15 % for full range output. It can be controlled locally by the integrated 7 inches touchscreen or remotely from a PC.
5. Sub-frame: a special sub-frame is designed to perform the three indirect tensile strength tests using three different pairs of bearing tools. The sub-frame composed of a fixed base flange, four vertical smooth bars, and top flange with four oilite bushings to ensure smooth and vertical sliding on vertical bars. Two opposite vertical bars contain holes to pass the shaft of the horizontal LVDTs at the mid-height of the tested sample, and the two LVDTs are fixed using PVC fittings. The sub-frame provided with four pairs of loading tools made of stainless steel of grade 420. Three of them are used for the indirect tensile strength tests (see Figure 4.2), while the fourth is for the uniaxial compression test. The loading strip of the RST test is a rod of diameter 8 mm, and a flat strip of 3 mm width is used for the FST test, while the loading strip of the DPT test is a cylindrical punch with a diameter of a 12.7 mm.
6. Data acquisition and Pc: 34972A - Data Acquisition Unit of forty channels controlled remotely from Pc is used in data logging. An extra monitor, keyboard, and mouse are added to the Pc to allow control from inside the environmental chamber.
7. Removable holders: three pairs are designed to hold and place the samples in the appropriate position before beginning the test, as shown in Figure 4.2.

(a) (b)

Figure 4. 1 Set-up of tensile strength tests at BEPL Lab from (a) outside (b) internal

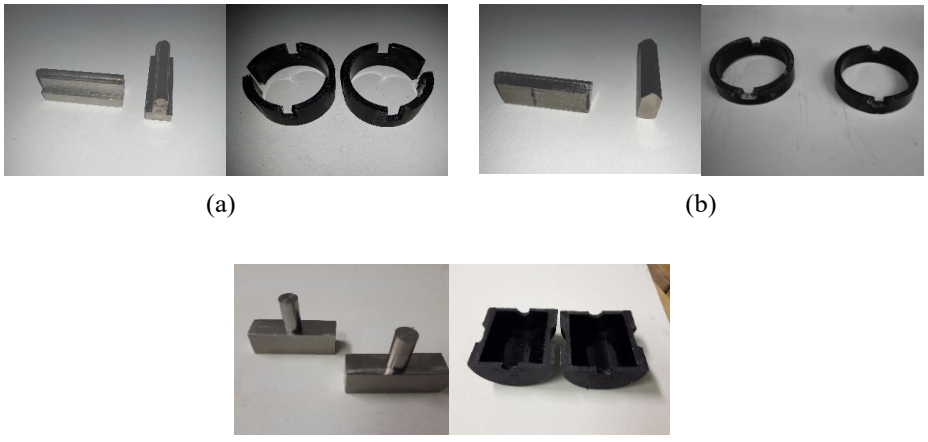

(a) (b)

(c)

Figure 4. 2 Holders for positioning the frozen samples before performing (a) RST, (b) FST, and (c) DPT tensile strength tests

`

4.2 Measuring devices

The axial displacement was measured via a high accuracy linear variable displacement transducer (LVDT) with a range of 50 mm produced by Omega, in addition to the platen measurements by ACONS Pro. The lateral deformations were obtained by two high accuracy LVDTs of range 50 mm manufactured by Solartron Metrology. All LVDTs were placed into PVC tubes, and both ends were appropriately insulated. Subsequently, they were placed in 31.1 mm PVC sleeve, and the gap between them was filled by a dense foam to ensure proper insulation. Eventually, the assembly was fixed on the subframe by a PVC tee fitting, as shown in Figure 4.3. All LVDTs were calibrated at a temperature ranging from - 20 °C to 20°C before starting the experimental work.

Two couples of thermocouples type T were used in measuring the temperature of the frozen soil sample and the ambient temperature. The first couple was adjusted to be in contact with the sample, while the second one was fixed close to the sample to measure the ambient temperature (see Figure 4.3). All thermocouples are calibrated by a resistance temperature detector (RTD).

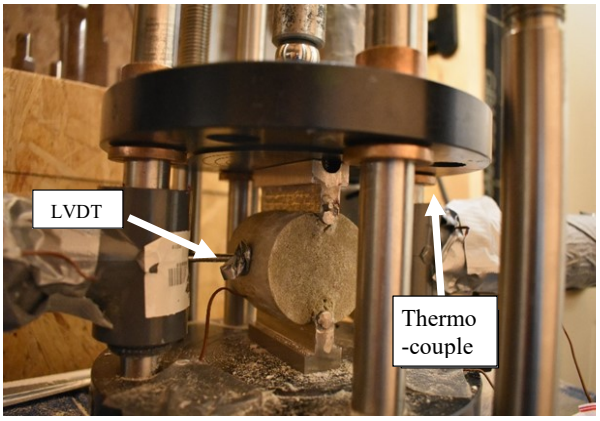

(a)

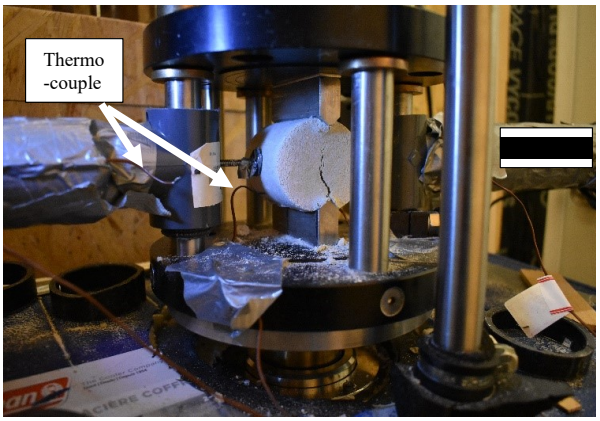

(b)

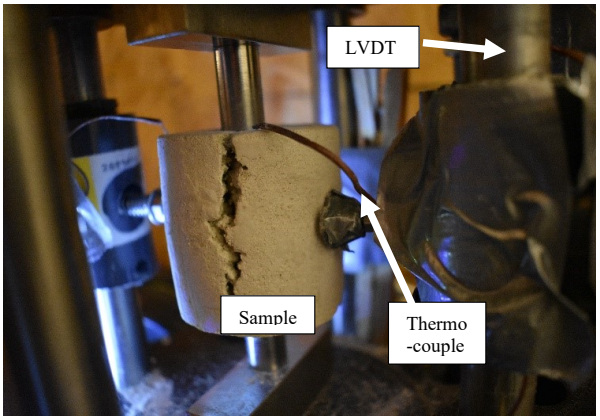

(c)

Figure 4. 3 Pictures showing the setup and measuring devices for (a) RST, (b) FST, (c) DPT

`

4.3 Indirect tension tests procedure

The indirect tensile tests are performed at BEPL laboratory using the following procedure:

i. The frozen soil samples are stored in the BEPL laboratory at the required temperature for a minimum of 24 hours.
ii. After removing the sample packing, the end surfaces of the sample are trimmed if needed, and the faces of the loading tools are cleaned properly to receive the sample.
iii. Test logging file is created including the test information (i.e., Name of the sample, the date, the test performed, the temperature, and the loading rate), then the loading rate is entered.
iv. The holders are installed on the sample surface before positioning the sample between loading strips of the sub-frame to ensure proper loading, then LVDTs and thermocouples are conducted to the sample. Eventually, a small engagement load of 5N is applied to ensure proper seating of the bearing plates and the holders are removed before loading.
v. After failure, the test is stopped, and the logging file is saved.

4.4 General results of indirect tensile strength tests

The tested fifty-four groups of tensile strength tests are divided into seven sets according to the temperature of the test to simplify the presentation of the results. Every set contains three groups of kaolinite-sand samples and another three of bentonite-sand samples with a salinity of 1 g/L for the pore fluid, to investigate the effect of different parameter on the tensile strength. These three groups are tested under the same experimental conditions but using three different testing methods to study the influence of the testing approach on the tensile strength values. Each group composed of three samples to be tested at different loading rates of 1, 3, and 9 mm/min to investigate the effect of loading rate on the tensile strength.

Twelve groups are added to the set of tests at -5°C with salinities of 0 and 3 g/L (see Table 4.3) to study the effect of salinity on tensile strength of frozen sandy clay soils at various loading rates and different testing approaches.

The results obtained from the tensile tests were vertical load, vertical displacement, horizontal displacement, and post-failure pictures. Tables 4.1 and 4.2 give the details of the groups tested at temperatures -15 and -1°C. Figures 4.4 to 4.19 show the axial load-axial displacement

`

curves, lateral displacement-axial displacement curves, and the post-failure pictures of tested groups the same temperatures. The details of the other groups are given in Tables form B 1 and B 5, while results of the tensile strength tests are shown in Figures B 1 and B 56.

Table 4. 1 Details of tested tensile strength groups at - 15 °C.

Group	Samples	Test	Salinity	Loading rate
K-01	K1S01-K1S03	RST	1 g/L	1, 3, and 9 mm/min
K-02	K1S04-K1S06	FST	1 g/L	1, 3, and 9 mm/min
K-03	K1S07-K1S09	DPT	1 g/L	1, 3, and 9 mm/min
B-01	B1S01-B1S03	RST	1 g/L	1, 3, and 9 mm/min
B-02	B1S04-B1S06	FST	1 g/L	1, 3, and 9 mm/min
B-03	B1S07-B1S09	DPT	1 g/L	1, 3, and 9 mm/min

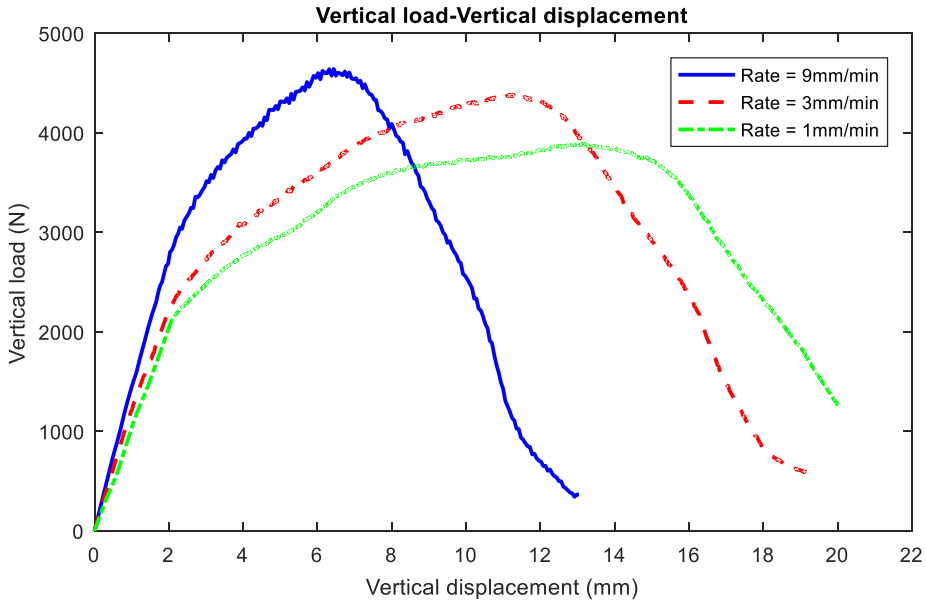

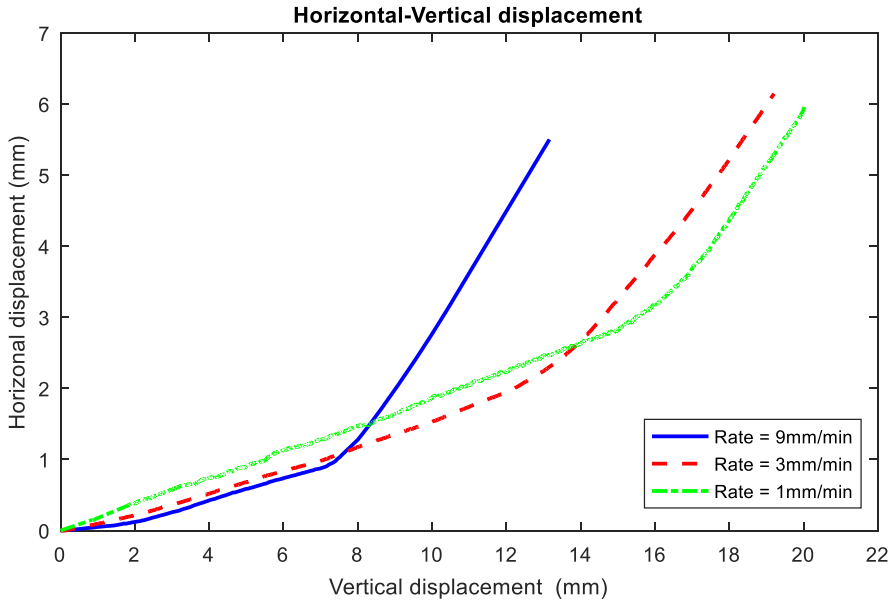

Figure 4. 4 Results of tensile strength tests performed on group K-01 (Loading approach= RST, T= - 15 °C, Salinity= 1 g/L).

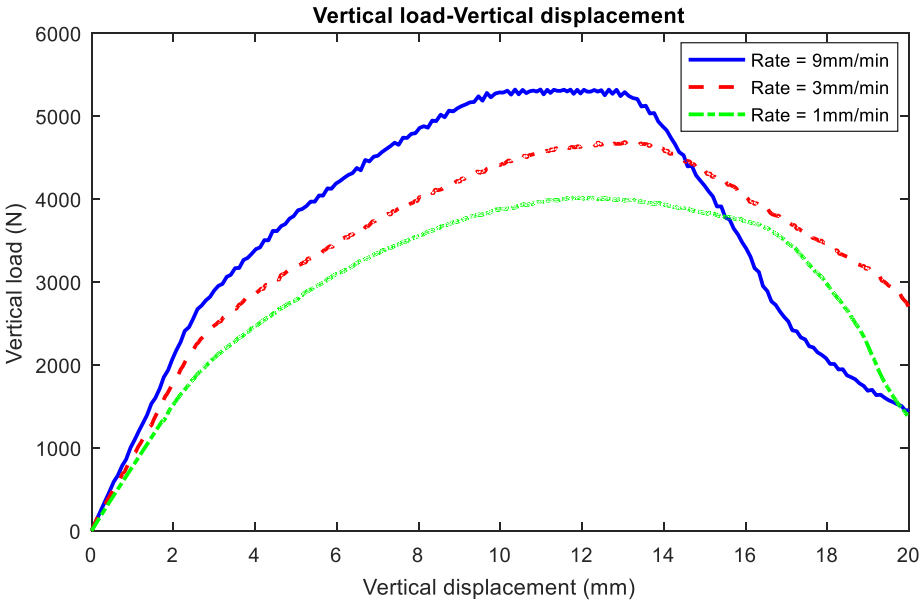

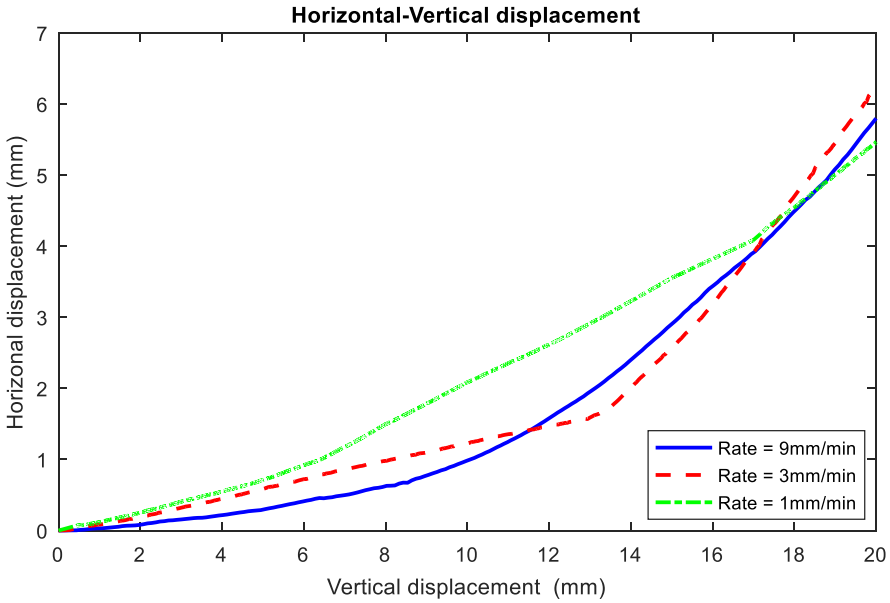

Figure 4. 5 Results of tensile strength tests performed on group K-02 (Loading approach= FST, T= - 15 °C, Salinity= 1 g/L).

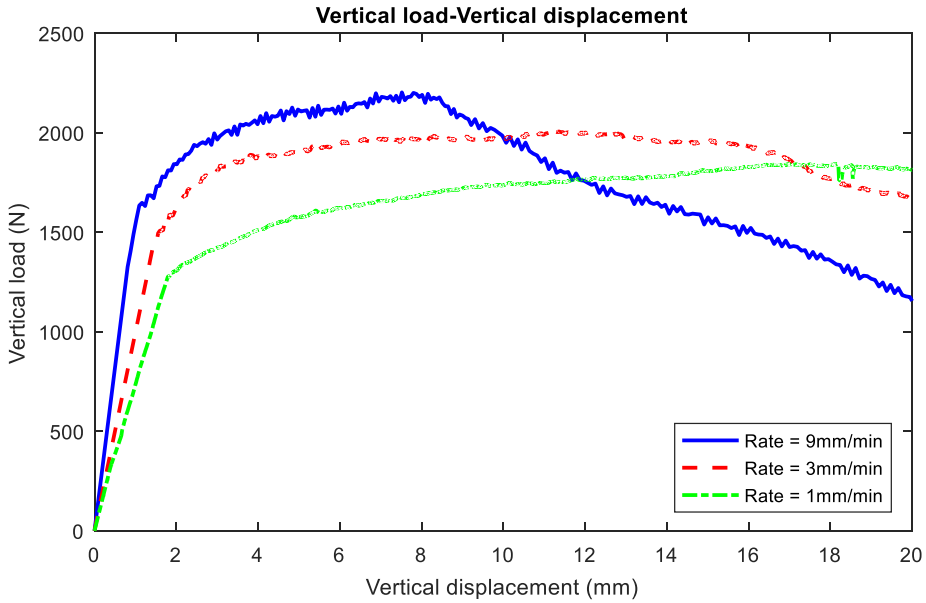

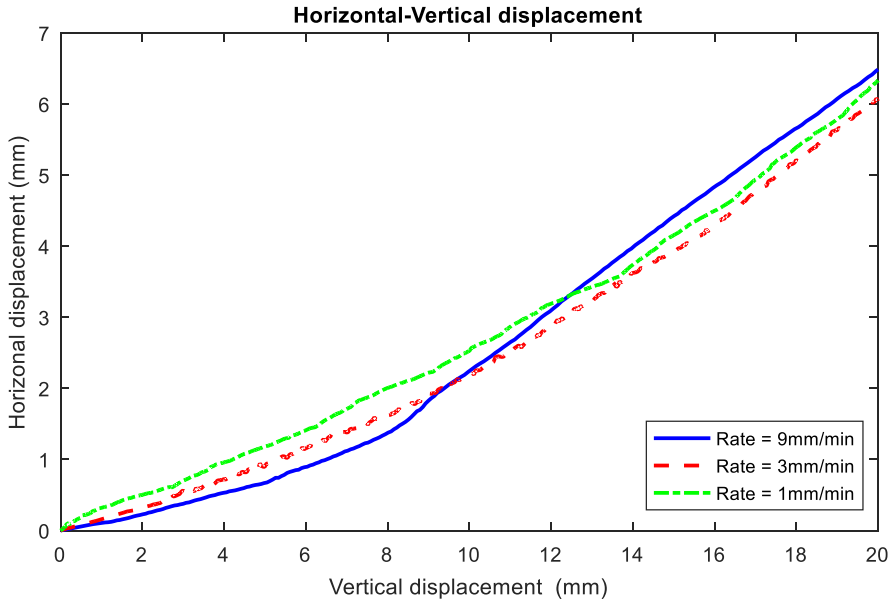

Figure 4. 6 Results of tensile strength tests performed on group K-03 (Loading approach= DPT, T= - 15 °C, Salinity= 1 g/L).

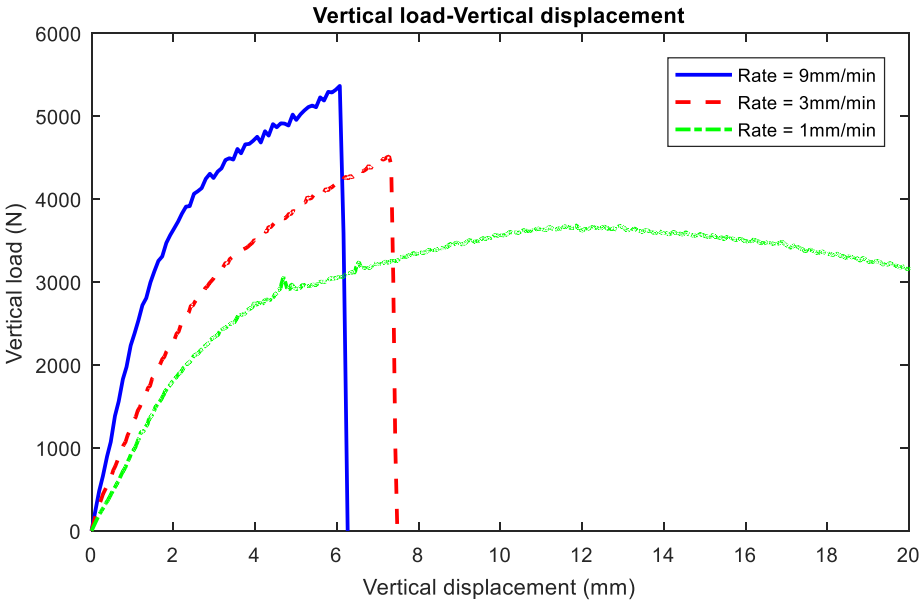

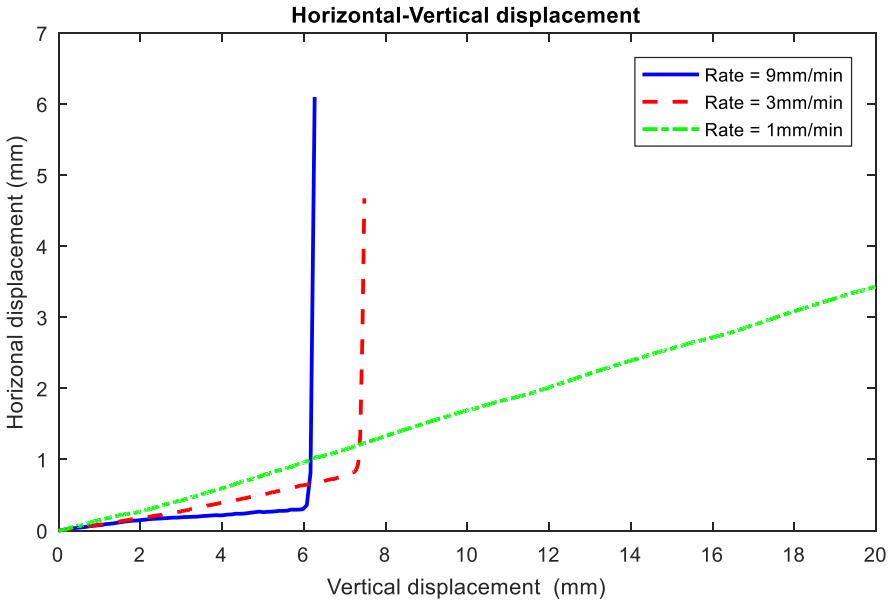

Figure 4. 7 Results of tensile strength tests performed on group B-01 (Loading approach= RST, T= - 15 °C, Salinity= 1 g/L).

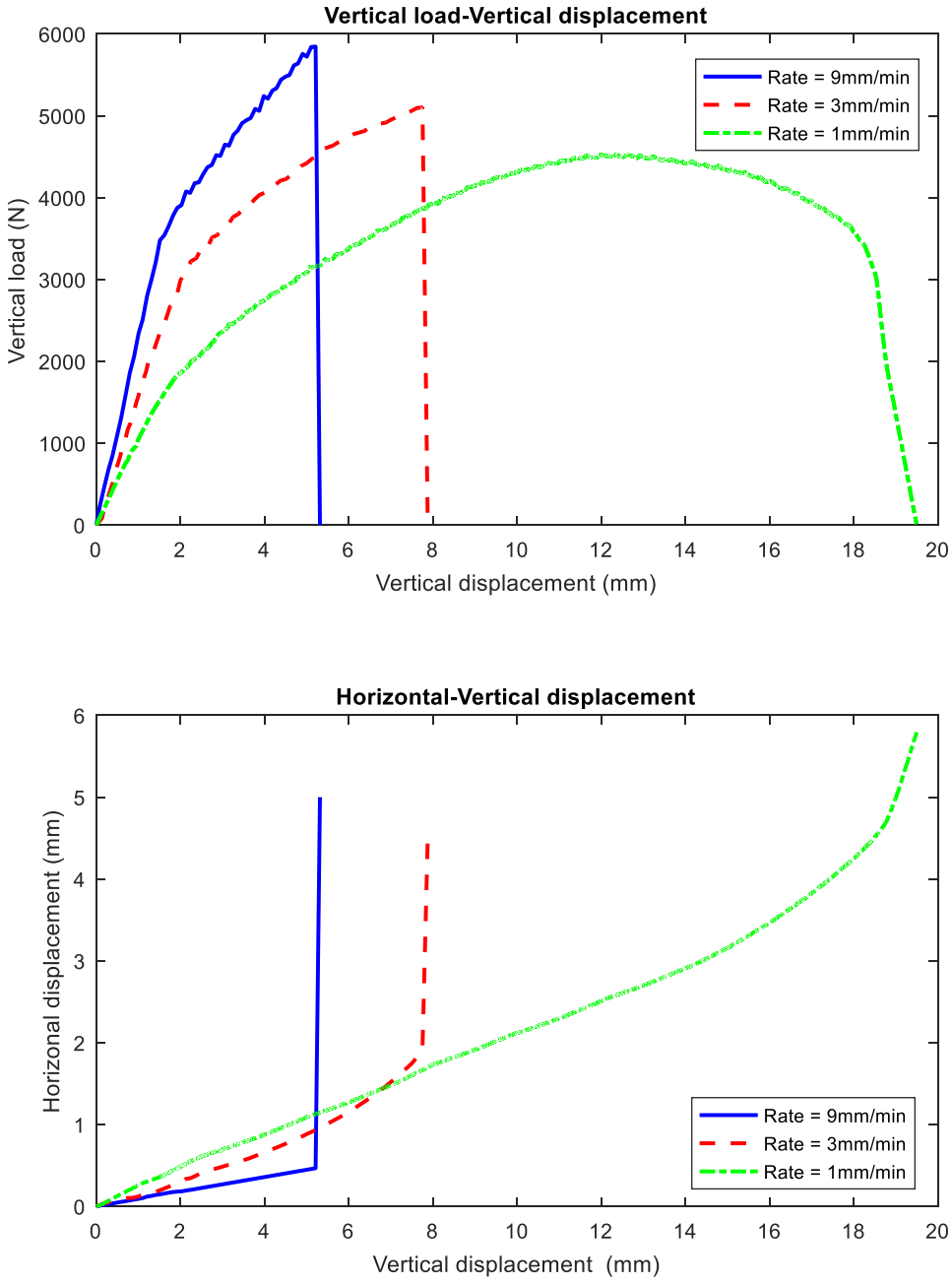

Figure 4. 8 Results of tensile strength tests performed on group B-02 (Loading approach= FST, T= - 15 °C, Salinity= 1 g/L).

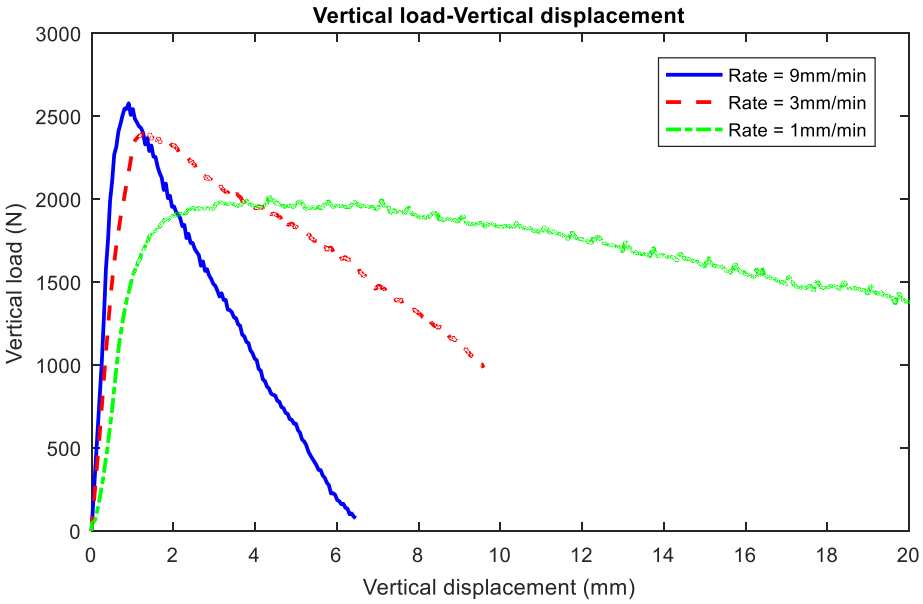

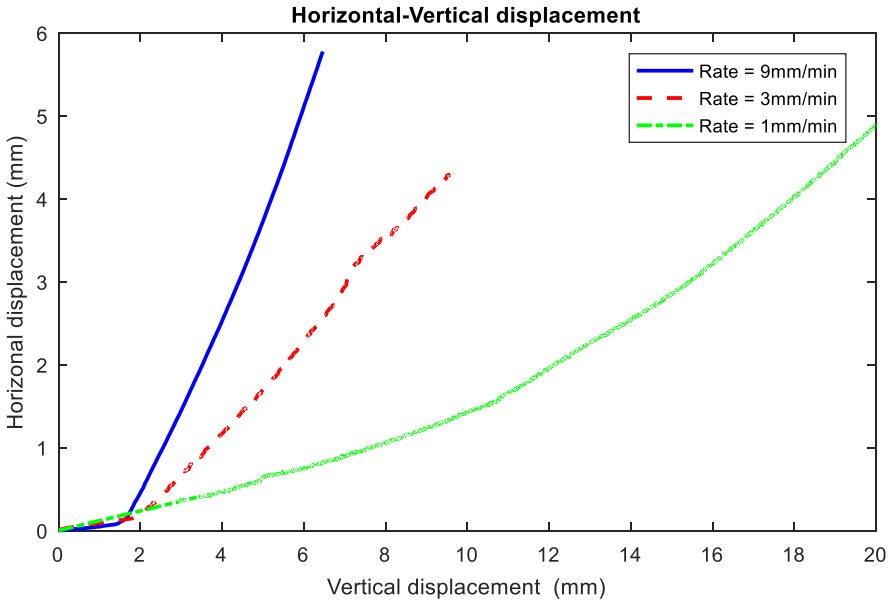

Figure 4. 9 Results of tensile strength tests performed on group B-03 (Loading approach= DPT, T= - 15 °C, Salinity= 1 g/L).

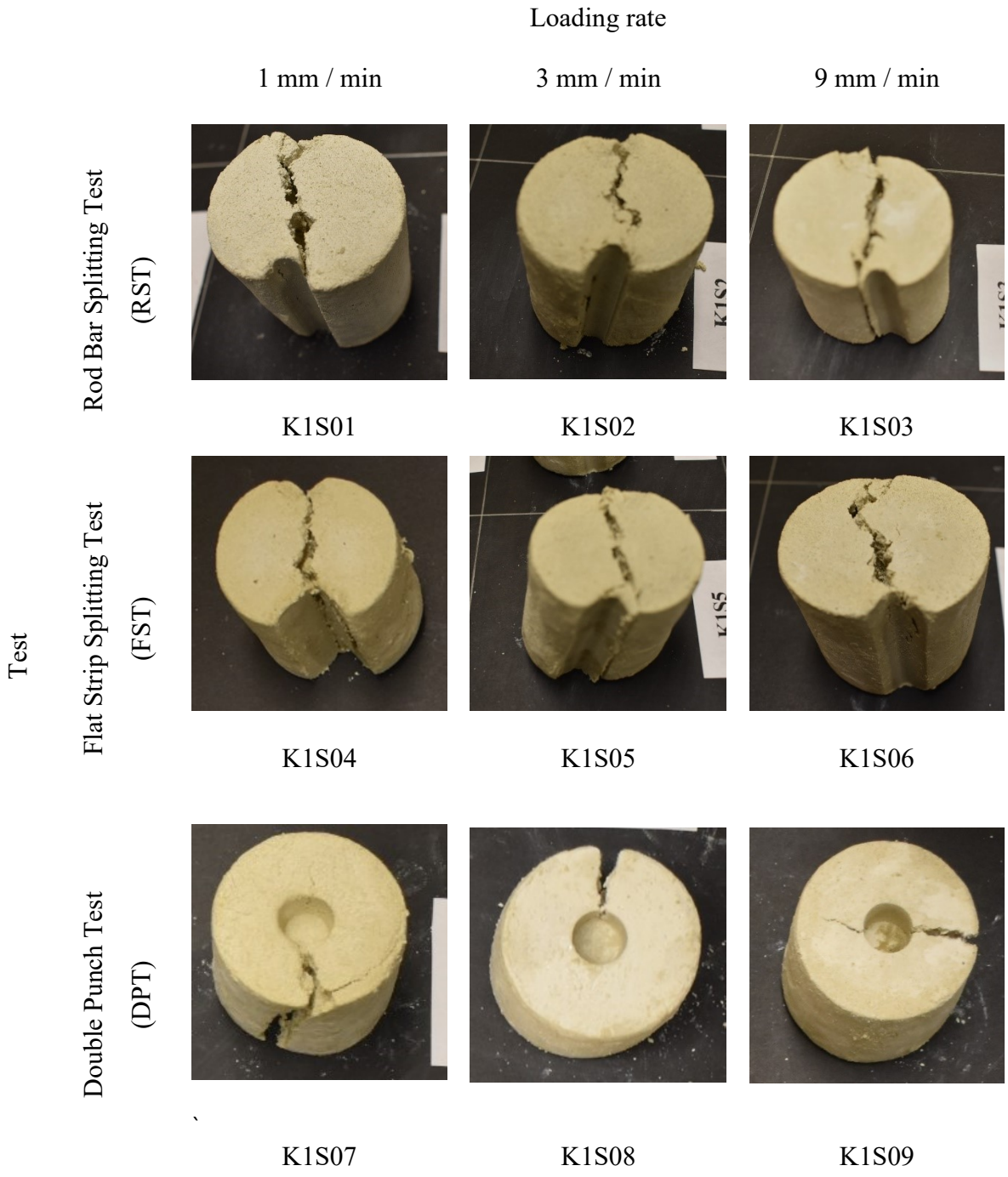

Figure 4. 10 Post-failure pictures of tested kaolinite-sand samples (T= - 15 °C, Salinity= 1 g/L).

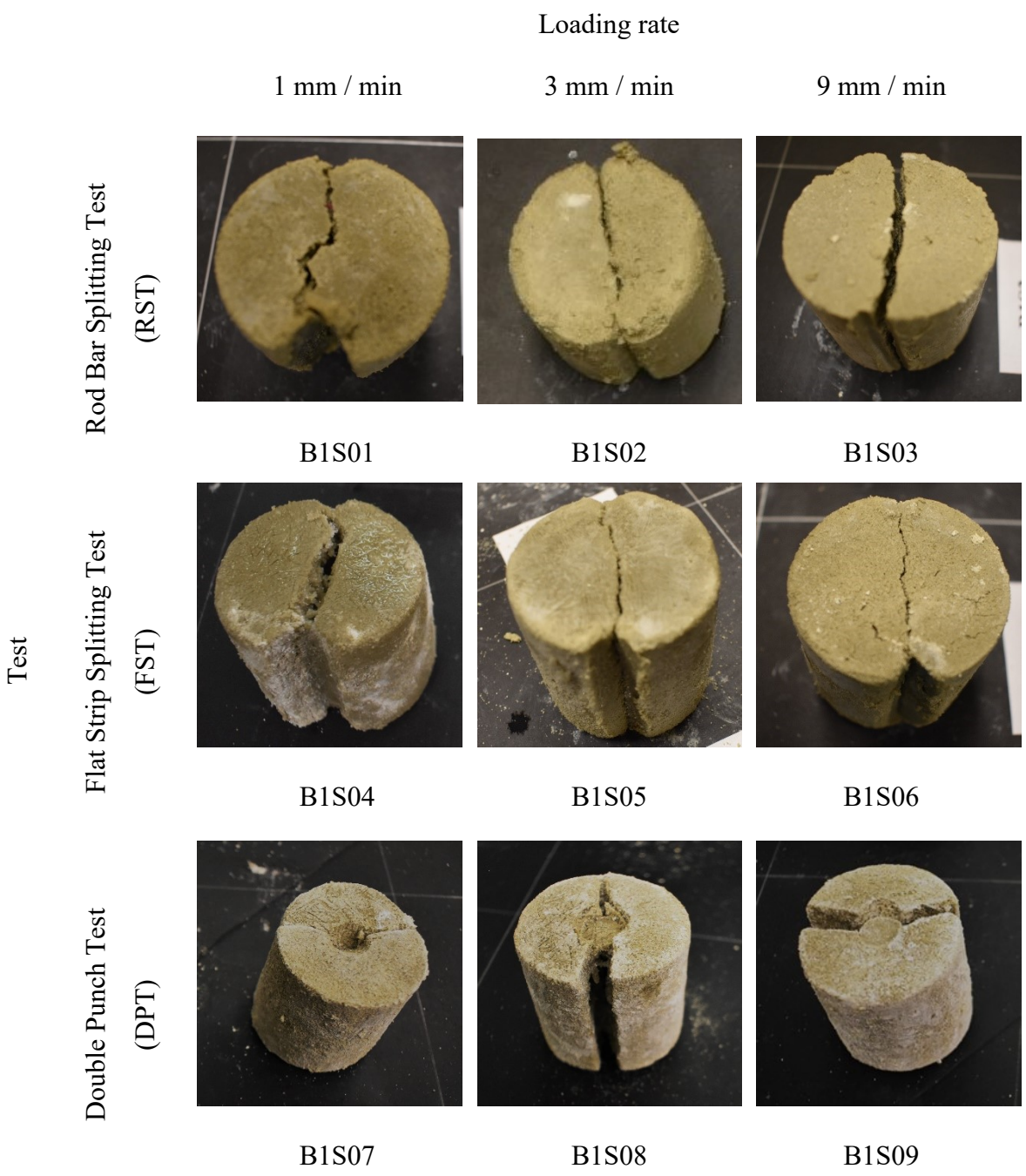

Figure 4. 11 Post-failure pictures of tested bentonite-sand samples (T= - 15 °C, Salinity= 1 g/L)

`

Table 4. 2 Details of the tested groups at -1°C.

Group	Samples	Test	Salinity	Loading rate
K-19	K1S37-K1S39	RST	1 g/L	1, 3, and 9 mm/min
K-20	K1S40-K1S42	FST	1 g/L	1, 3, and 9 mm/min
K-21	K1S43-K1S45	DPT	1 g/L	1, 3, and 9 mm/min
B-19	B1S37-B1S39	RST	1 g/L	1, 3, and 9 mm/min
B-20	B1S40-B1S42	FST	1 g/L	1, 3, and 9 mm/min
B-21	B1S43-B1S45	DPT	1 g/L	1, 3, and 9 mm/min

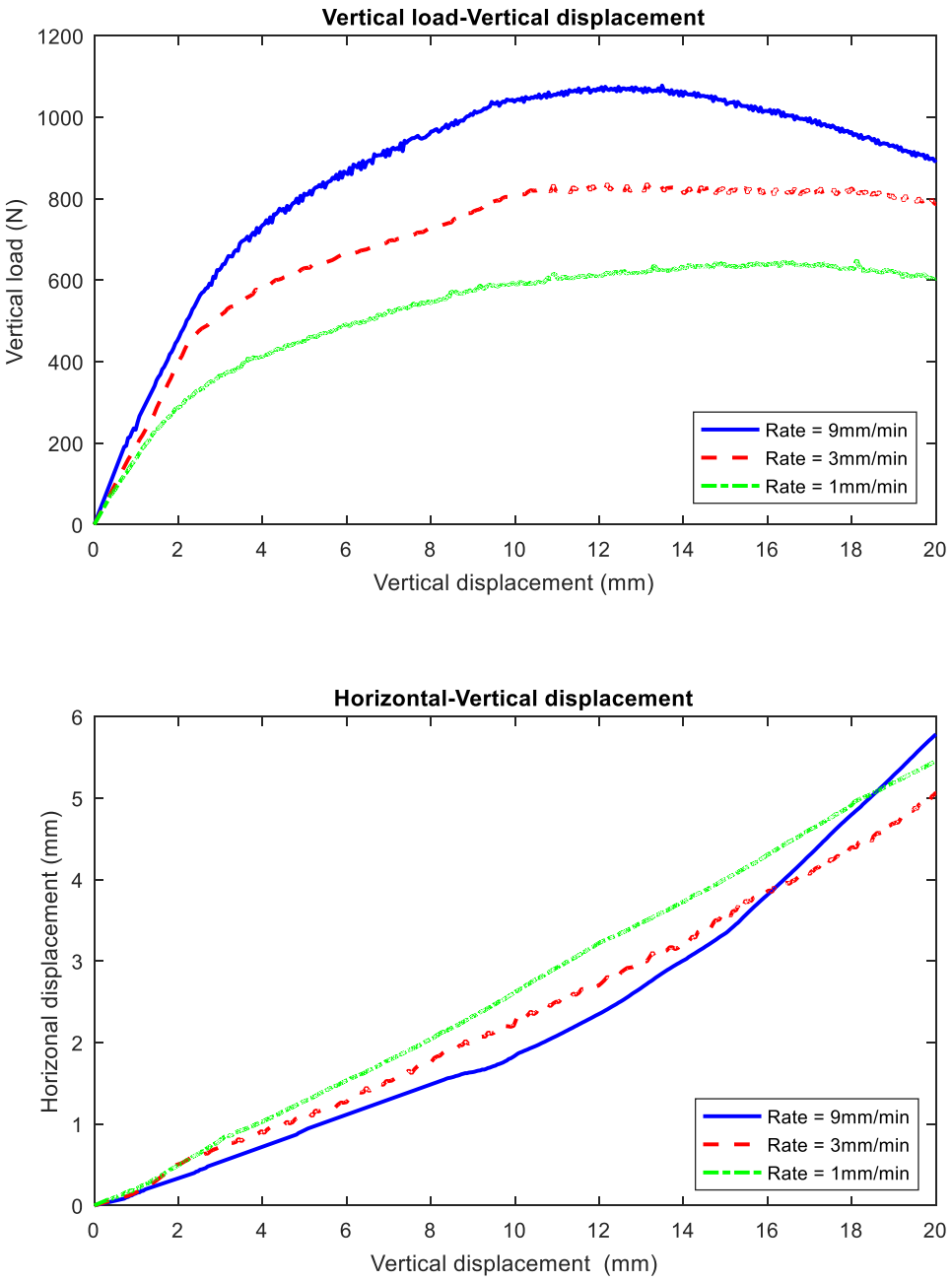

Figure 4. 12 Results of tensile strength tests performed on group K-19 (Loading approach= RST, T= - 1 °C, Salinity= 1 g/L).

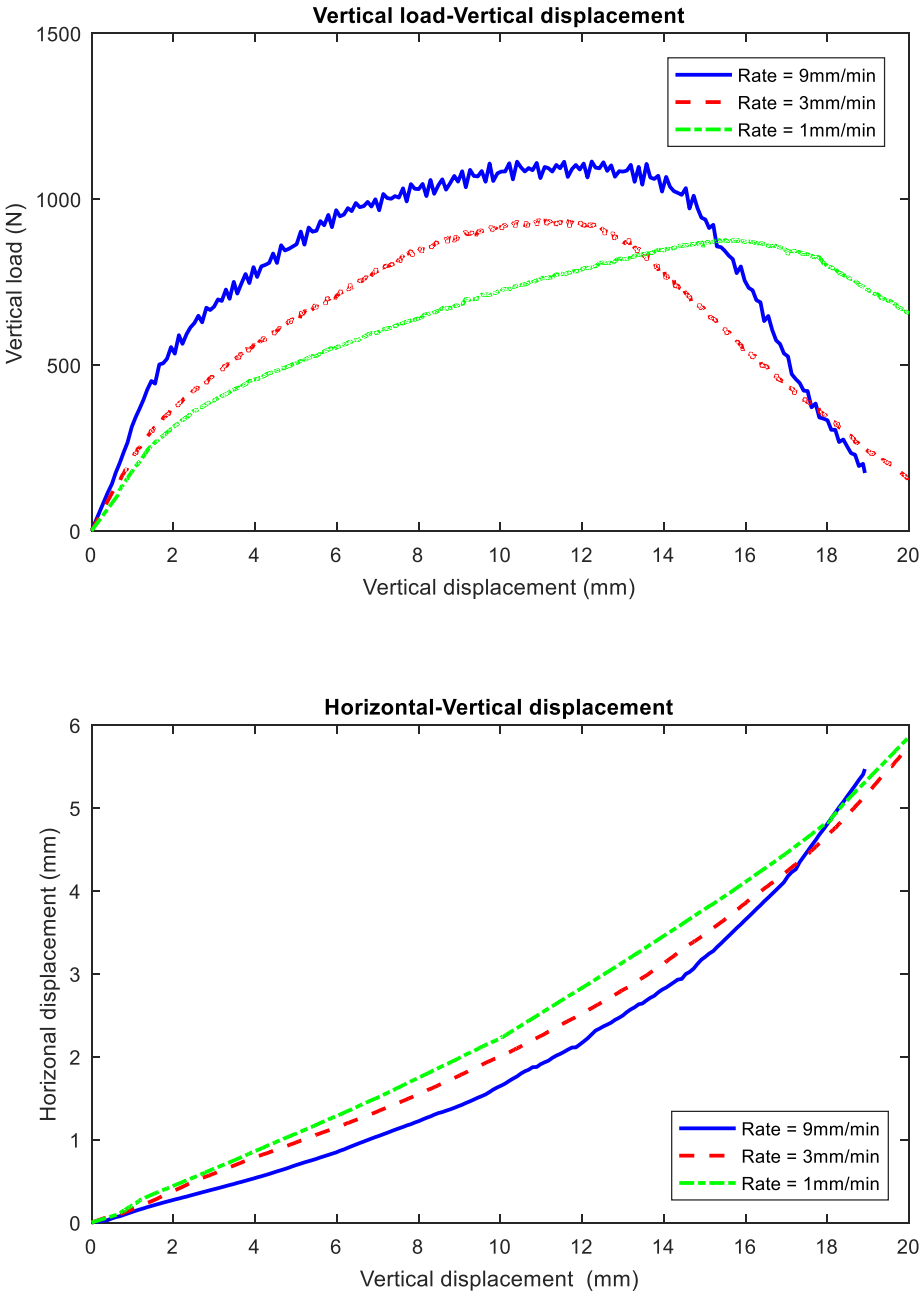

Figure 4. 13 Results of tensile strength tests performed on group K-20 (Loading approach= FST, T= - 1 °C, Salinity= 1 g/L).

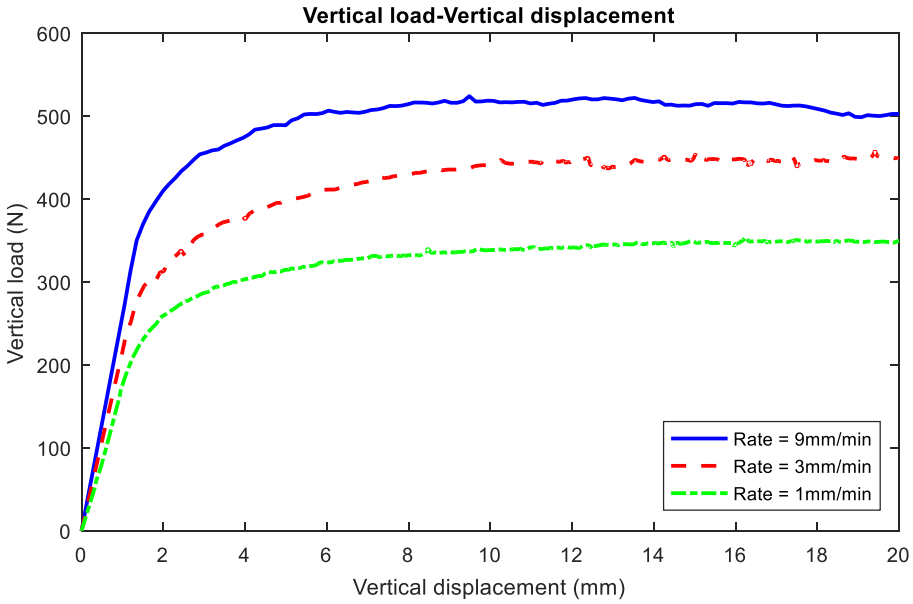

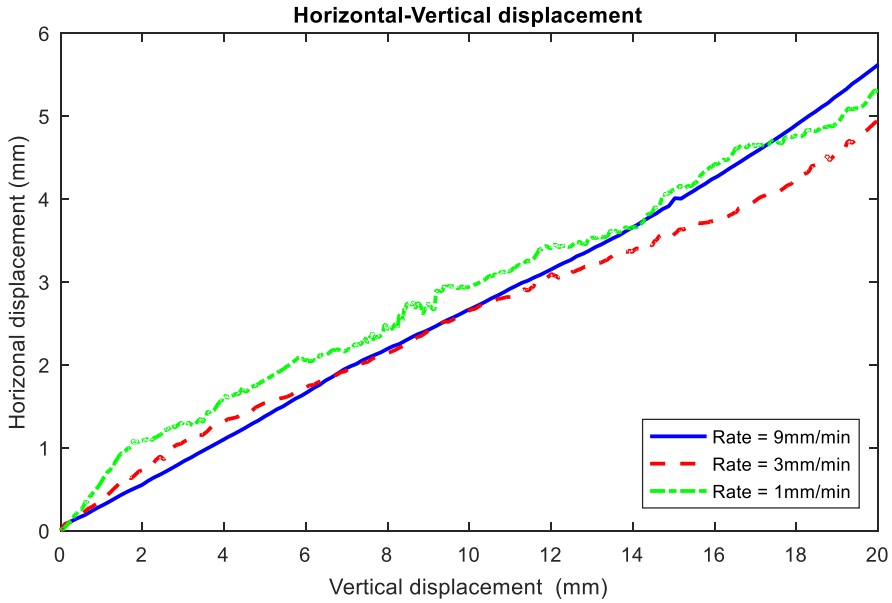

Figure 4. 14 Results of tensile strength tests performed on group K-21 (Loading approach= DPT, T= - 1 °C, Salinity= 1 g/L).

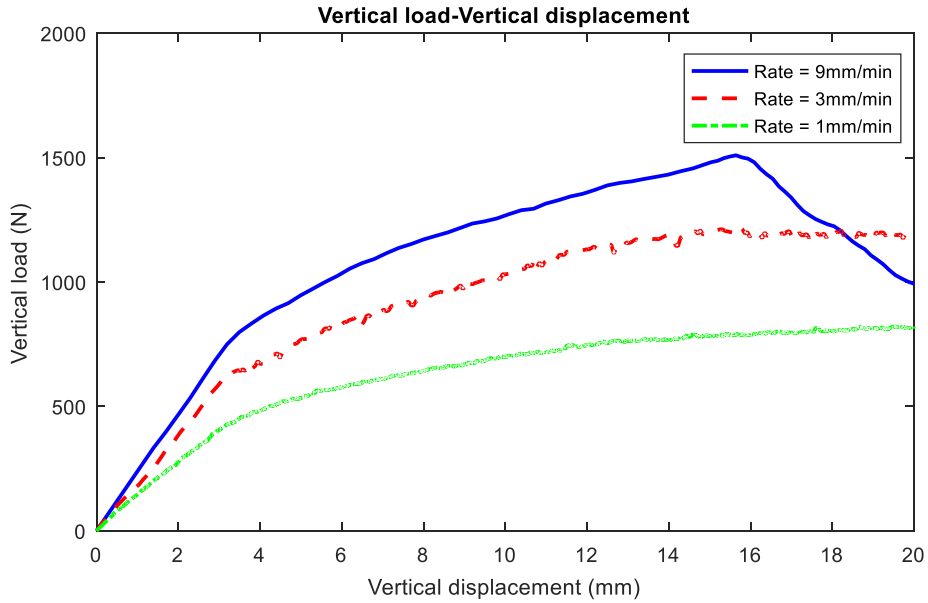

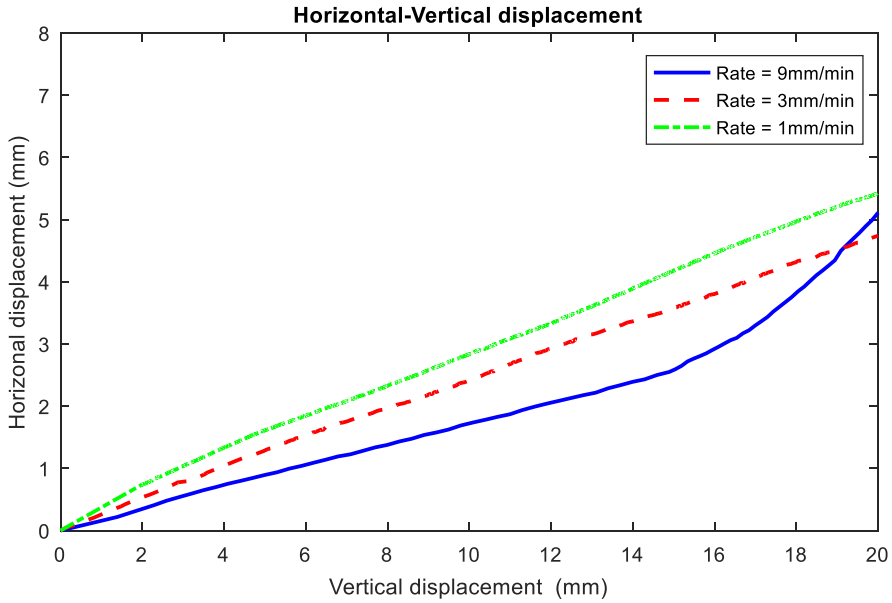

Figure 4. 15 Results of tensile strength tests performed on group B-19 (Loading approach= RST, T= - 1 °C, Salinity= 1 g/L).

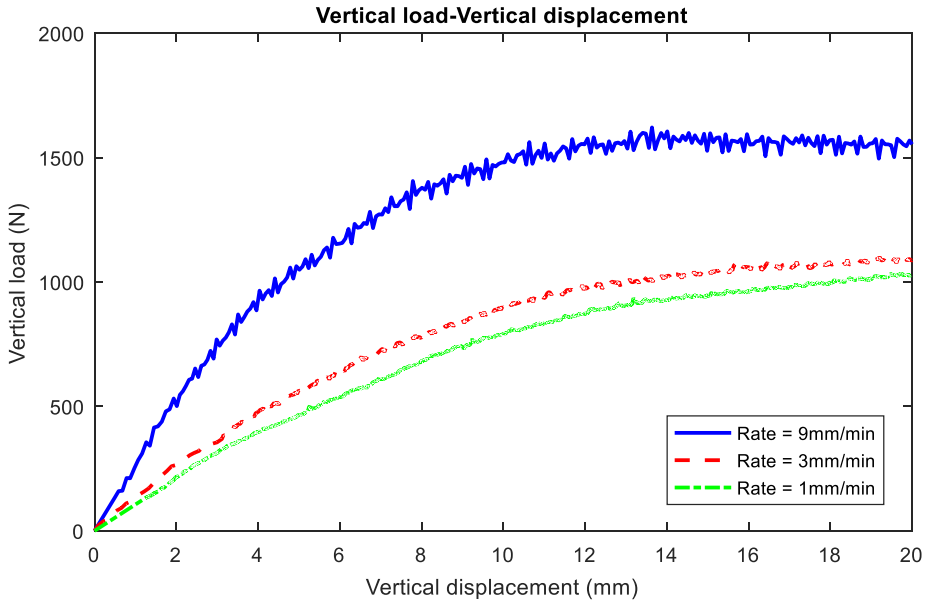

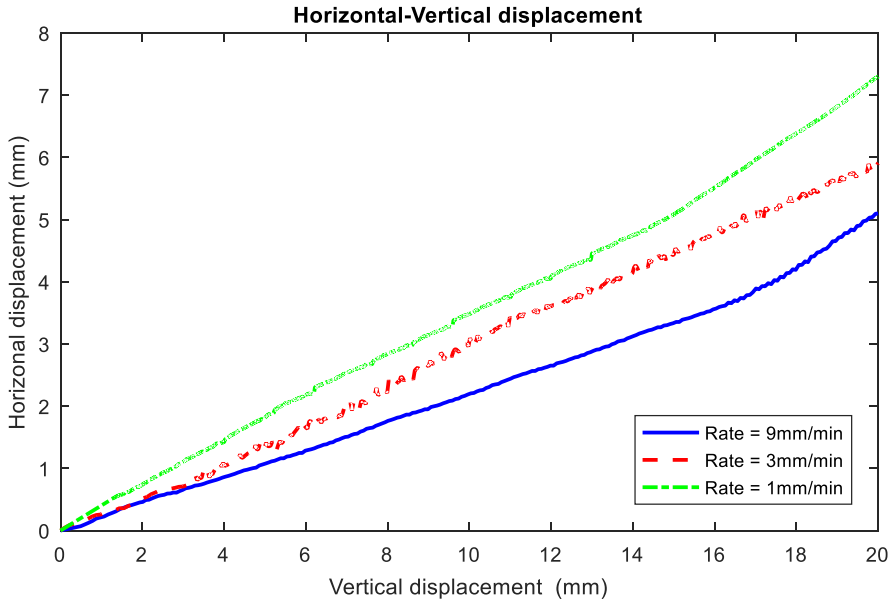

Figure 4. 16 Results of tensile strength tests performed on group B-20 (Loading approach= FST, T= - 1 °C, Salinity= 1 g/L).

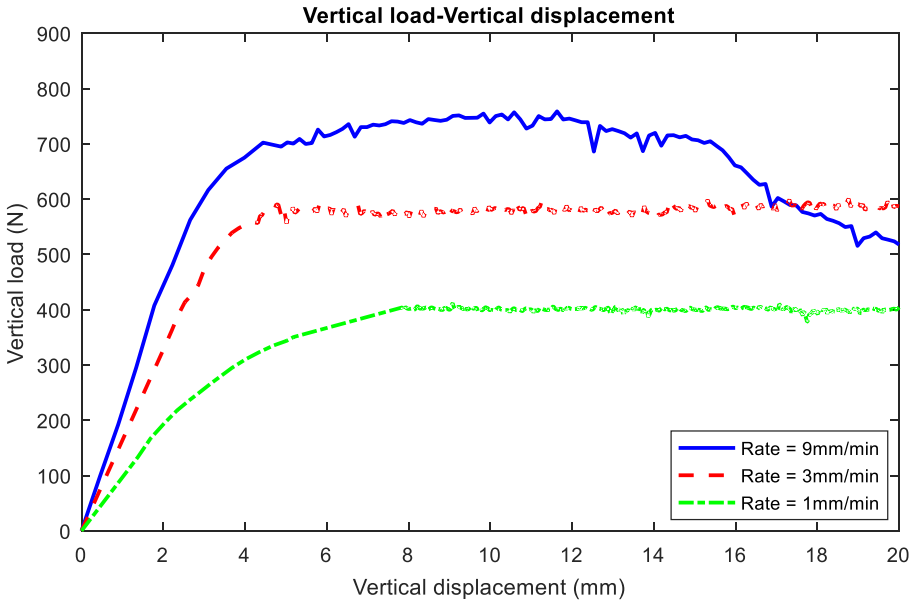

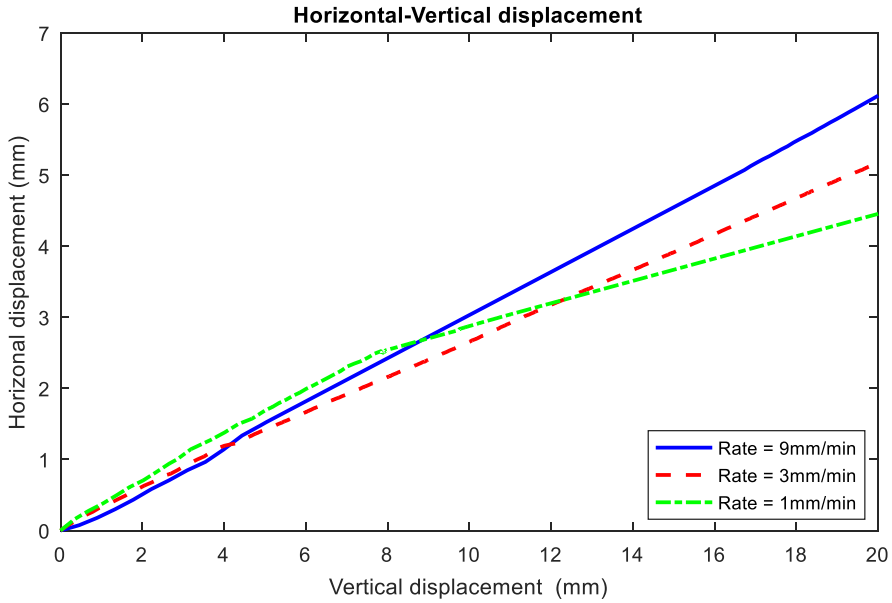

Figure 4. 17 Results of tensile strength tests performed on group B-21 (Loading approach= DPT, T= - 1 °C, Salinity= 1 g/L).

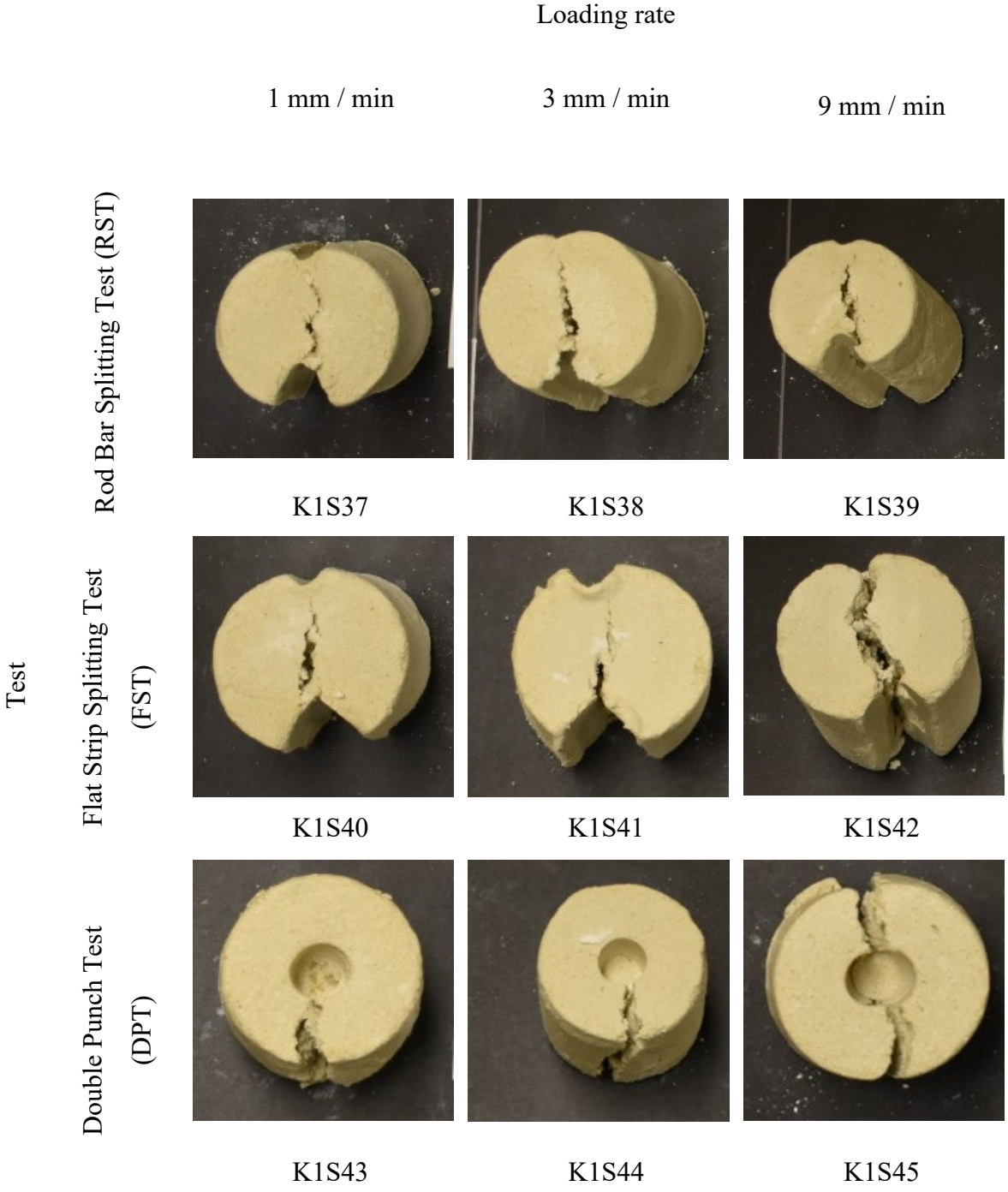

Figure 4. 18 Post-failure pictures of tested kaolinite-sand samples (T= - 1 °C, Salinity= 1 g/L).

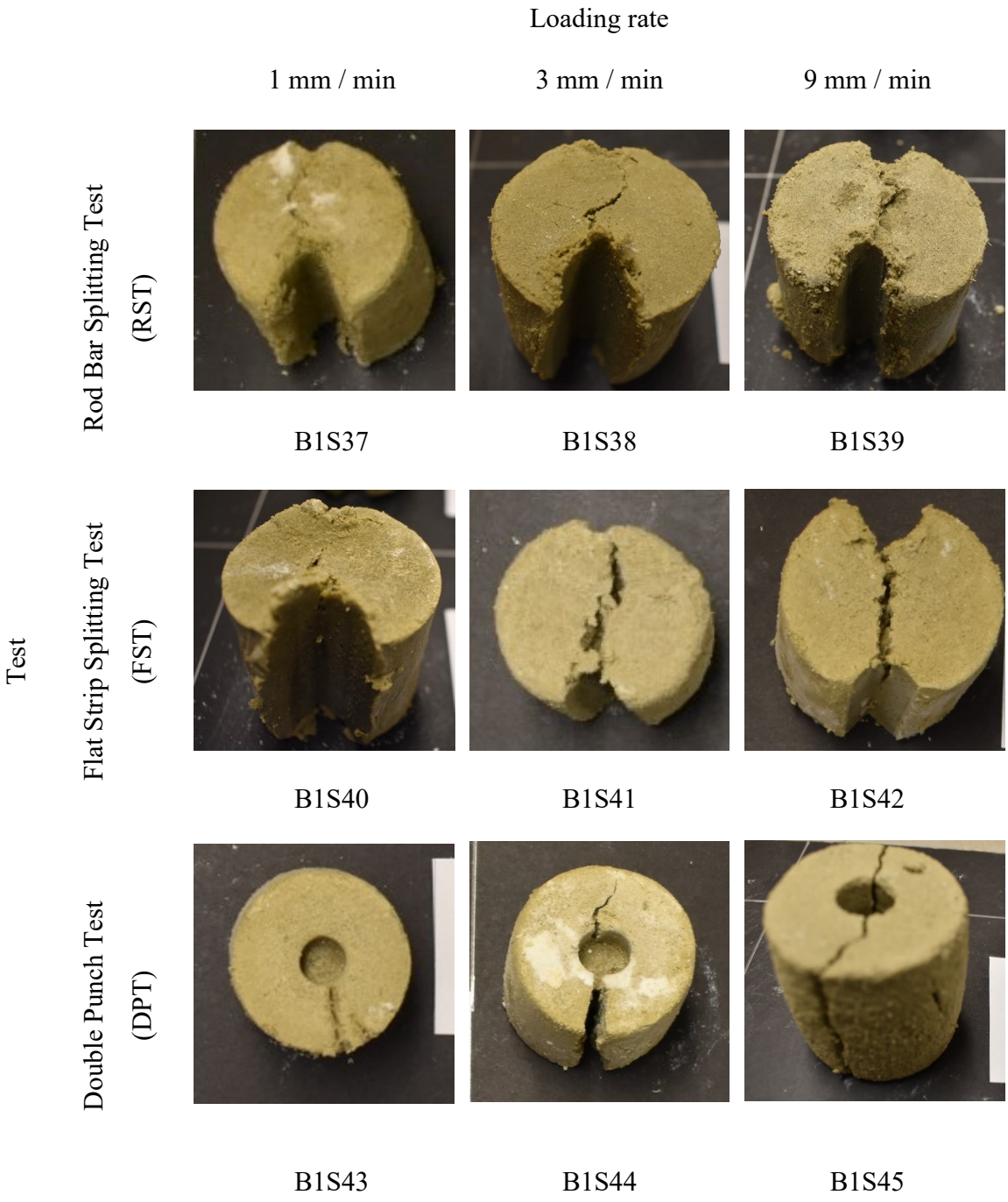

Figure 4. 19 Post-failure pictures of tested bentonite-sand samples (T= - 1 °C, Salinity= 1 g/L).

`

In this research, the tensile strength of each tested sample is calculated at two different load levels are:

i. the maximum elastic load corresponding to the end of the linear portion of the load-displacement curve and the corresponding tensile strength is called the yield tensile strength. It can be picked directly from the load-displacement curve, as shown in Figures from 4.20 to 4.22.
ii. the maximum applied load to determine the peak tensile strength. It may be clear like the peak tensile strength of group B-04 under 9 mm/min (see Figure 4.20), or it may need a verification from the horizontal deformation such as the tensile strength of the same group at a loading rate of 1mm/min as shown in Figure 4.22.

Both the yield and the peak tensile strengths are calculated using the same equation depending on the performed testing method. The tensile strength obtained from either rod or flat splitting tests is determined using Equation 2.3 given by (ASTM, 2007), whereas the Equation 2.4 introduced by Chen et al. (1970) is used in calculating the tensile strength from the double punch test. The values of the tensile strength of all tested samples are recorded in Table 4.3.

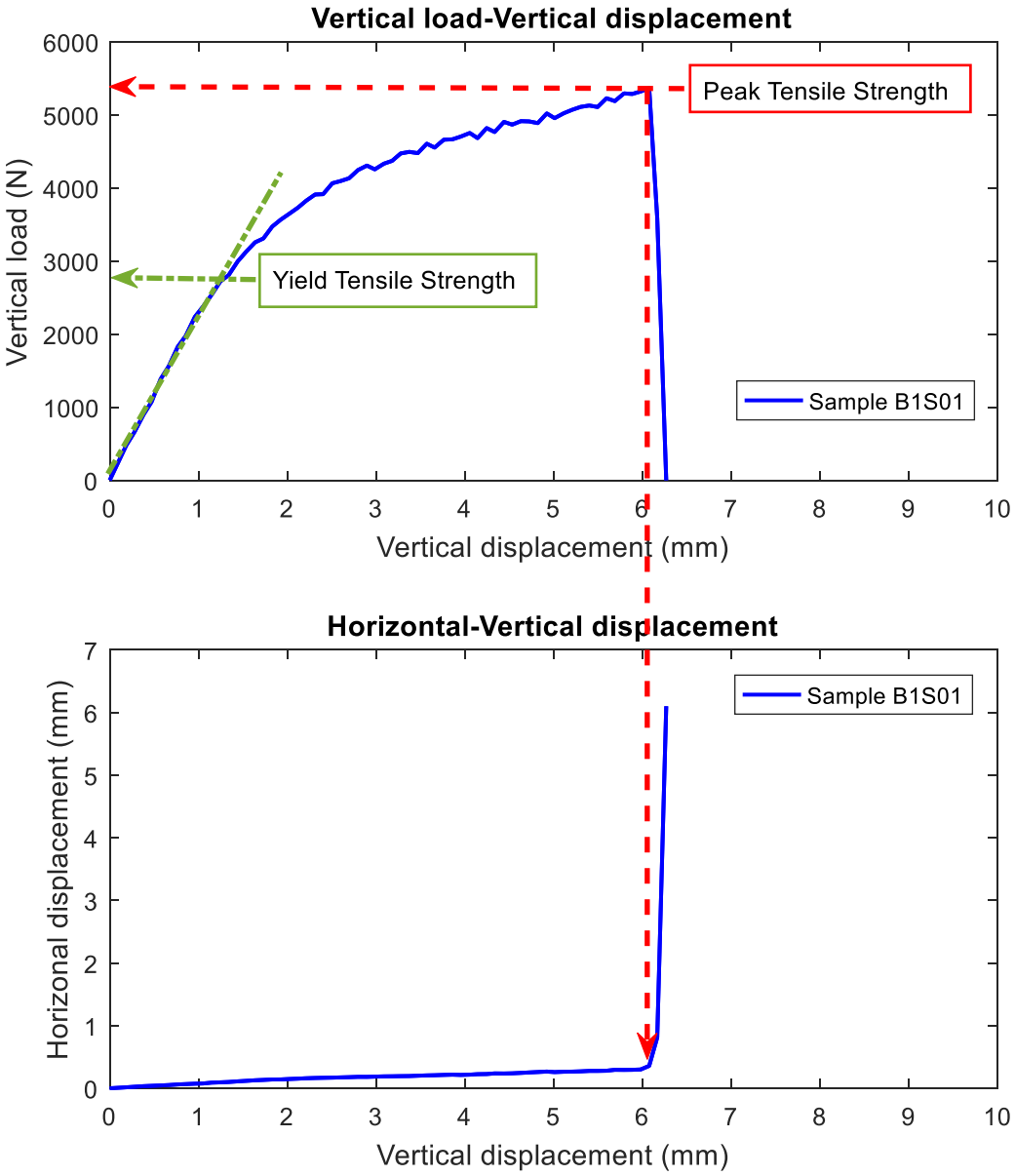

Figure 4. 20 Graph showing the yield and peak tensile strengths calculation for bentonite-sand samples (Loading approach= RST, T= - 15 °C, Loading rate= 9 mm/min, Salinity= 1 g/L).

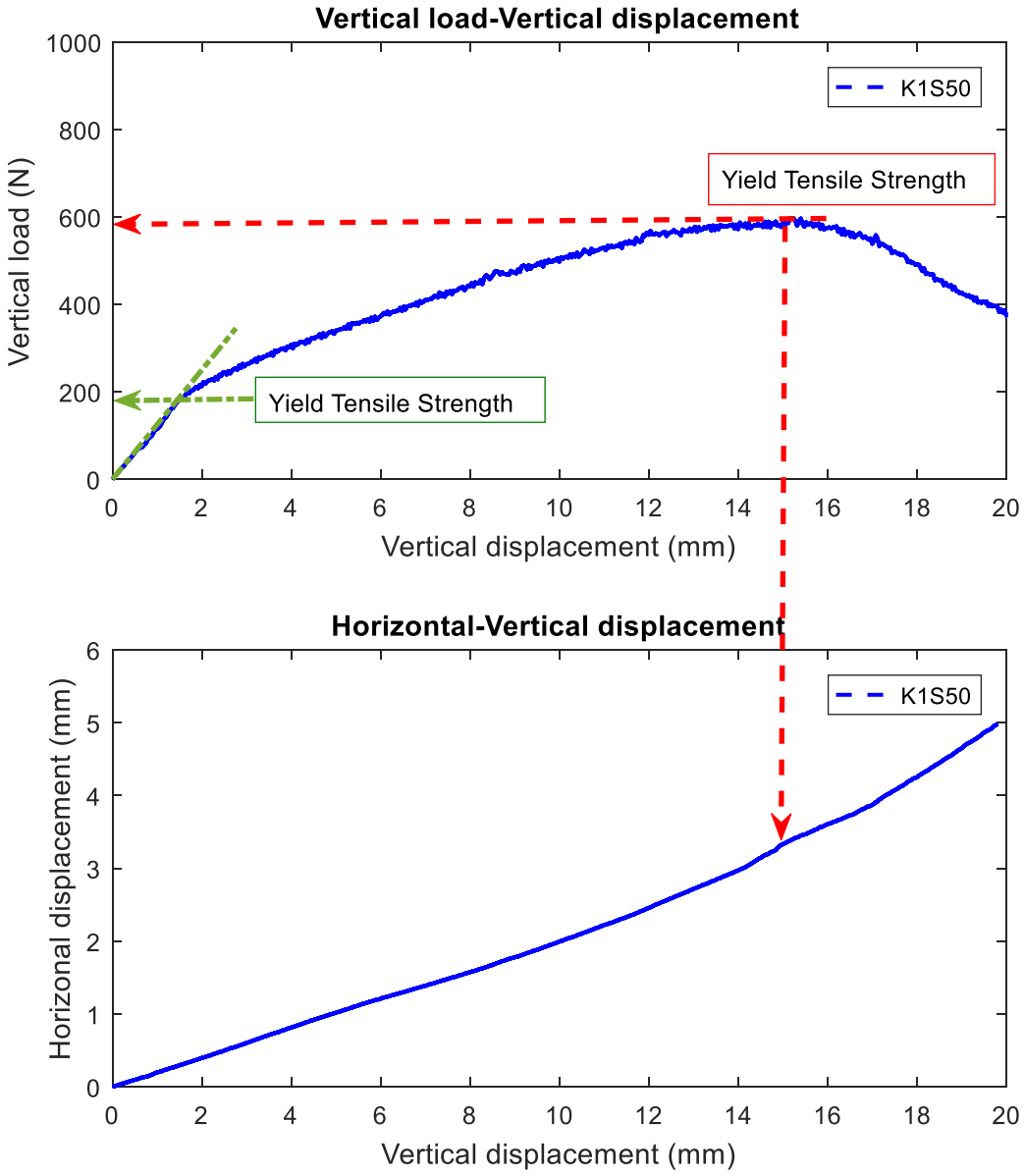

Figure 4. 21 Graph showing the yield and peak tensile strengths calculation for kaolinite-sand samples (Loading approach= FST, T= - 15 °C, Loading rate= 9 mm/min, Salinity= 1 g/L).

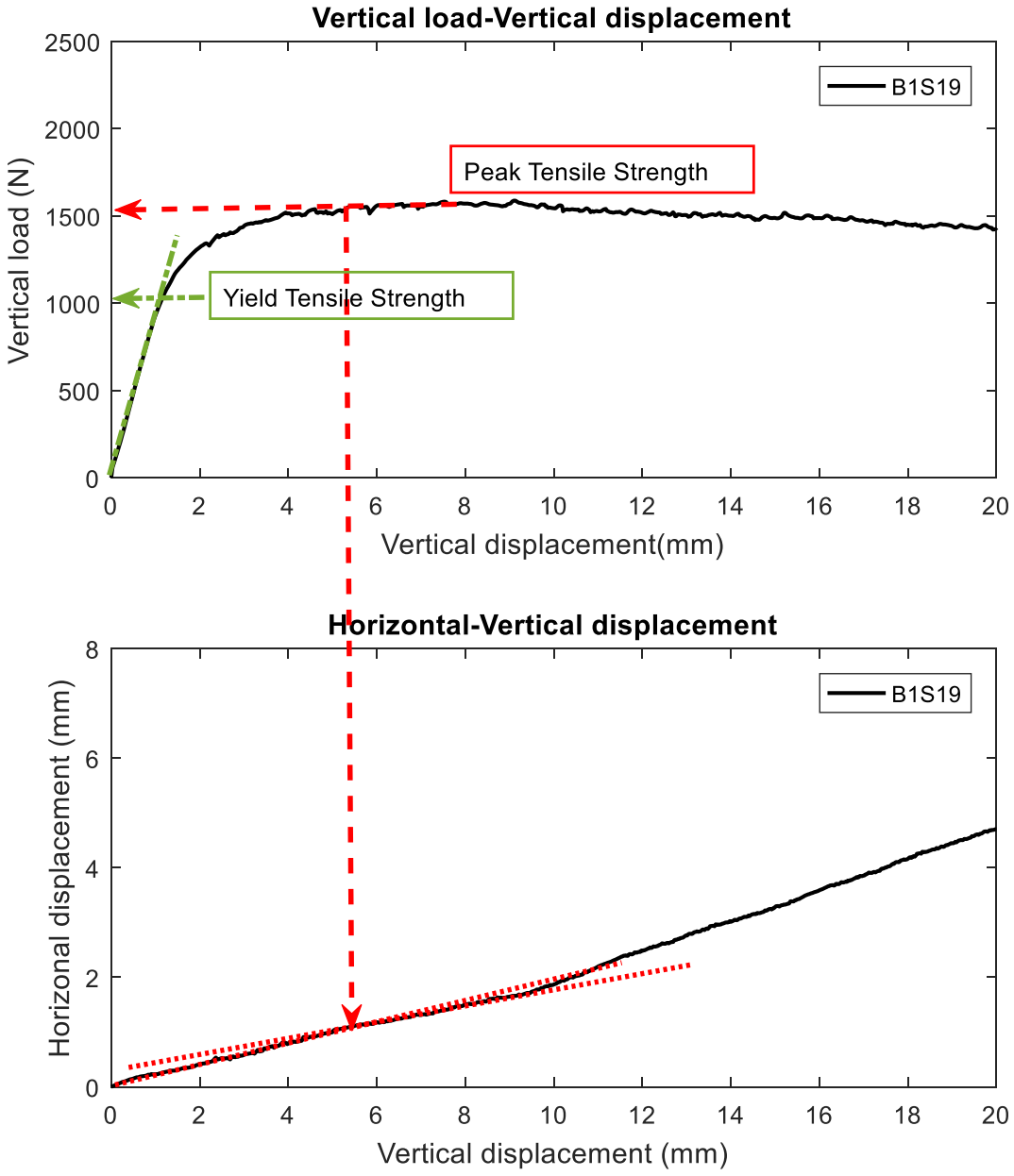

Figure 4. 22 Graph showing the yield and peak tensile strengths calculation for bentonite-sand samples (Loading approach= DPT, T= - 15 °C, Loading rate= 9 mm/min, Salinity= 1 g/L).

`

Table 4. 3 Tensile strength values for all tested samples.

Group	Sample	Temperature (˚C)	Salinity (g/L)	Test	Loading rate (mm/min)	Maximum applied load (N)		Tensile strength (kpa)	
						Yield	Peak	Yield	Peak
K-01	K1S01	- 15	1	RST	1	1933	3738	477	922
	K1S02				3	2135	4349	526	1072
	K1S03				9	2324	4572	573	1127
K-02	K1S04			FST	1	1839	4016	453	990
	K1S05				3	2178	4645	537	1145
	K1S06				9	2411	5270	595	1300
K-03	K1S07			DPT	1	1153	1743	293	444
	K1S08				3	1435	1959	365	499
	K1S09				9	1634	2181	416	555
K-04	K1S10	- 10	1	RST	1	1557	2839	384	700
	K1S11				3	1765	3497	435	862
	K1S12				9	1918	3701	473	913
K-05	K1S13			FST	1	1570	3341	387	824
	K1S14				3	1899	3577	468	882
	K1S15				9	2196	4007	542	988
K-06	K1S16			DPT	1	900	1359	229	346
	K1S17				3	1106	1578	282	402
	K1S18				9	1317	1734	335	441
K-07	K1S19	- 5	1	RST	1	1186	1865	292	460
	K1S20				3	1383	2400	341	592
	K1S21				9	1500	2510	370	619
K-08	K1S22			FST	1	1204	2309	297	569
	K1S23				3	1444	2399	356	592
	K1S24				9	1599	2624	394	647
K-09	K1S25			DPT	1	580	925	148	235
	K1S26				3	717	1050	183	267
	K1S27				9	892	1179	227	300
K-10	K0S01	- 5	0	RST	1	1090	2283	269	563
	K0S02				3	1246	2555	307	630
	K0S03				9	1342	2749	331	678
K-11	K0S04			FST	1	1195	2558	295	631
	K0S05				3	1304	2778	322	685
	K0S06				9	1398	2930	345	723
K-12	K0S07			DPT	1	607	949	155	242
	K0S08				3	812	1095	207	279
	K0S09				9	1197	1400	305	356
K-13	K3S01	- 5	3	RST	1	740	1552	182	383
	K3S02				3	1034	1997	255	492
	K3S03				9	1044	2307	257	569

`

Group	Sample	Temperature (°C)	Salinity (g/L)	Test	Loading rate (mm/min)	Maximum applied load (N)		Tensile strength (kpa)	
						Yield	Peak	Yield	Peak
K-14	K3S04	- 5	3	FST	1	709	1899	175	468
	K3S05				3	1046	2044	258	504
	K3S06				9	1164	2359	287	582
K-15	K3S07			DPT	1	345	841	88	214
	K3S08				3	395	945	101	241
	K3S09				9	520	1046	132	266
K-16	K1S28	- 2	1	RST	1	552	1073	136	265
	K1S29				3	716	1255	177	309
	K1S30				9	803	1380	198	340
K-17	K1S31			FST	1	418	1306	103	322
	K1S32				3	498	1348	123	332
	K1S33				9	749	1582	185	390
K-18	K1S34			DPT	1	279	530	71	135
	K1S35				3	384	648	98	165
	K1S36				9	508	727	129	185
K-19	K1S37	- 1	1	RST	1	330	636	81	157
	K1S38				3	446	850	110	210
	K1S39				9	541	998	133	246
K-20	K1S40			FST	1	242	869	60	214
	K1S41				3	261	923	64	228
	K1S42				9	422	1105	104	272
K-21	K1S43			DPT	1	165	355	42	90
	K1S44				3	238	445	61	113
	K1S45				9	329	515	84	131
K-22	K1S46	- 0.5	1	RST	1	125	428	31	106
	K1S47				3	251	565	62	139
	K1S48				9	342	686	84	169
K-23	K1S49			FST	1	181	546	45	135
	K1S50				3	189	585	47	144
	K1S51				9	284	782	70	193
K-24	K1S52			DPT	1	82	237	21	60
	K1S53				3	146	308	37	78
	K1S54				9	202	366	51	93
K-25	K1S55	0	1	RST	1	81	279	20	69
	K1S56				3	107	357	26	88
	K1S57				9	150	421	37	104
K-26	K1S58			FST	1	99	349	24	86
	K1S59				3	114	421	28	104
	K1S60				9	171	499	42	123
K-27	K1S61			DPT	1	21	70	5	17
	K1S62				3	44	120	11	30

`

Group	Sample	Temperature (°C)	Salinity (g/L)	Test	Loading rate (mm/min)	Maximum applied load (N)		Tensile strength (kpa)	
						Yield	Peak	Yield	Peak
K-27	K1S63	0	1	DPT	9	83	201	20	50
B-01	B1S01	- 15	1	RST	1	1499	3666	382	933
	B1S02				3	2203	4514	561	1149
	B1S03				9	2796	5365	712	1366
B-02	B1S04			FST	1	1830	4503	451	1110
	B1S05				3	2726	5101	672	1258
	B1S06				9	3478	5845	858	1441
B-03	B1S07			DPT	1	1448	2003	357	494
	B1S08				3	2049	2396	505	591
	B1S09				9	2468	2643	609	652
B-04	B1S10	- 10	1	RST	1	1212	3002	309	764
	B1S11				3	1697	3631	432	924
	B1S12				9	2156	4299	549	1094
B-05	B1S13			FST	1	1139	3590	281	885
	B1S14				3	1807	4041	446	996
	B1S15				9	2650	4595	653	1133
B-06	B1S16			DPT	1	1059	1558	261	384
	B1S17				3	1705	1998	420	493
	B1S18				9	2012	2206	496	544
B-07	B1S19	- 5	1	RST	1	899	2157	229	549
	B1S20				3	1297	2736	330	696
	B1S21				9	1603	3109	408	791
B-08	B1S22			FST	1	660	2632	163	649
	B1S23				3	1128	2781	282	686
	B1S24				9	1502	3198	370	789
B-09	B1S25			DPT	1	600	1020	148	252
	B1S26				3	1078	1376	266	339
	B1S27				9	1461	1603	360	395
B-10	B0S01	- 5	0	RST	1	954	2394	243	609
	B0S02				3	1419	3000	361	764
	B0S03				9	2000	3809	509	970
B-11	B0S04			FST	1	874	2599	216	641
	B0S05				3	1073	3032	265	748
	B0S06				9	2022	3564	499	879
B-12	B0S07			DPT	1	815	1238	201	305
	B0S08				3	1294	1551	319	382
	B0S09				9	1586	1842	391	454
B-13	B3S01	- 5	3	RST	1	594	1568	146	387
	B3S02				3	716	2306	177	569
	B3S03				9	1566	3002	386	740
B-14	B3S04			FST	1	466	2376	119	605

`

Group	Sample	Temperature (°C)	Salinity (g/L)	Test	Loading rate (mm/min)	Maximum applied load (N)		Tensile strength (kpa)	
						Yield	Peak	Yield	Peak
B-14	B3S05	- 5	3	FST	3	641	2504	163	637
	B3S06				9	1080	3148	275	801
B-15	B3S07			DPT	1	548	955	135	235
	B3S08				3	962	1205	237	297
	B3S09				9	1200	1556	296	384
B-16	B1S28	- 2	1	RST	1	671	1320	165	326
	B1S29				3	1007	1800	248	444
	B1S30				9	1232	2202	304	543
B-17	B1S31			FST	1	400	1663	102	423
	B1S32				3	602	1689	150	430
	B1S33				9	981	2226	250	567
B-18	B1S34			DPT	1	333	610	82	150
	B1S35				3	568	822	142	203
	B1S36				9	834	1008	206	249
B-19	B1S37	- 1	1	RST	1	427	754	105	186
	B1S38				3	597	1201	147	296
	B1S39				9	772	1494	190	368
B-20	B1S40			FST	1	301	1019	77	259
	B1S41				3	473	1088	120	277
	B1S42				9	744	1590	189	405
B-21	B1S43			DPT	1	210	402	52	99
	B1S44				3	420	576	104	142
	B1S45				9	590	751	145	185
B-22	B1S46	- 0.5	1	RST	1	275	499	68	123
	B1S47				3	351	807	87	199
	B1S48				9	455	1050	112	259
B-23	B1S49			FST	1	221	729	56	186
	B1S50				3	303	750	77	191
	B1S51				9	456	1152	116	293
B-24	B1S52			DPT	1	129	257	32	63
	B1S53				3	301	399	74	98
	B1S54				9	402	548	99	135
B-25	B1S55	0	1	RST	1	148	302	36	74
	B1S56				3	222	499	55	123
	B1S57				9	253	614	62	151
B-26	B1S58			FST	1	99	345	24	85
	B1S59				3	146	361	36	89
	B1S60				9	157	619	39	153
B-27	B1S61			DPT	1	56	141	14	36
	B1S62				3	149	209	38	53
	B1S63				9	201	291	51	74

`

4.5 A comparison among different measuring approaches

The results show very significant differences among different approaches The peak tensile strength values measured by RST and FST are almost twice the values obtained by DPT under the same temperature and loading condition due to the increase in the contact area between loading strips and samples in RST and FST, while the DPT keeps the same loading area and provides more reliable results. The yield tensile strengths measured by RST and FST are comparable, as shown in Figures 4.24 and 4.25. For example, the tensile strength values of the bentonite-sand samples of a salinity 1 g/L at – 15 °C and loading rate of 9 mm/min are 1366 kPa, 1441 kPa, and 652 kPa when they tested by RST, FST, and DPT, respectively. Different behaviors may be observed for samples at the same conditions when they tested using the three loading approaches even if they have the same testing conditions and stress history. For example, the kaolinite-sand samples with a salinity of 1 g/L at temperature -0.5 °C and loading rate of 1 mm/min show a ductile, brittle, and brittle-ductile behaviors when RST, FST, and DPT tests are performed, respectively as shown in Figure 4.23.

The yield tensile strengths measured by RST and FST are comparable to the peak tensile strength obtained by DPT. At temperature -15 °C and loading rate 9 mm/min, the yield tensile strengths of kaolinite-sand samples measured by RST and FST were 573 and 595 kPa, respectively. The peak tensile strength obtained by DPT was 555 kPa. At temperature -1 °C and loading rate 1 mm/min, the yield tensile strengths of bentonite-sand samples determined by RST and FST were 105 and 77 kPa, respectively. The peak tensile strength obtained by DPT was 99 kPa.

In this research, the loading strips of RST and FST tests are designed to have a contact width less than one-sixth the diameter of the sample according to ASTM D3967 – 16 for splitting tensile strength of rocks. In addition to a well-controlled procedure for sample preparation is followed to produce homogeneous samples, as mentioned in Chapter 3 to minimize the impact of the predetermined plan of failure.

All tested samples except a few tests at - 10 °C and - 15 °C are failed at axial displacement from 10 mm to 20 mm, this means that the contact area is continuously increased with time during RST and FST tests, while Equation 2.3 of the splitting test is derived based on the assumption that

the applied load is a line load. The previous observation may reveal the main source for overestimating the true strength by splitting tests.

The yield tensile strength is calculated using the same equations at the end of the elastic region to reduce the effect of plastic deformation resulting from the penetration of loading strips into the frozen samples. From Figure 4.24, the peak tensile strength values of kaolinite-sand samples with salinity of 1 g/L at – 15 °C and loading rate of 9 mm/min are 1127 kPa, 1300 kPa, and 555 kPa, respectively when FST, RST, and DPT tests are performed, while the elastic tensile strength values of the same samples are 573 kPa, 595 kPa, and 416 kPa corresponding to RST, FST, and DPT, respectively. In other words, the peak tensile strength obtained by FST for this sample is 2.3 times the peak tensile strength determined by DPT, whereas the elastic tensile strength calculated from RST for this sample is less than 1.4 times that is computed from DPT.

From Figure 4.25, the peak tensile strength values obtained by RST and FST tests for bentonite-sand samples with a salinity of 1 g/L at - 15 °C and a loading rate of 9 mm/min are 210 %, 221 % of the tensile strength obtained by DPT, respectively. On the other hand, the yield tensile strength values according to RST and FST tests are 117 % and 141 % of the tensile strength computed by DPT, respectively. The peak tensile strength values of bentonite-sand samples with a salinity of 1 g/L at - 1 °C and a loading rate of 3 mm/min are 208 % and 195 % of that obtained by DPT, while the elastic tensile strength values are 141 % and 115 %, respectively.

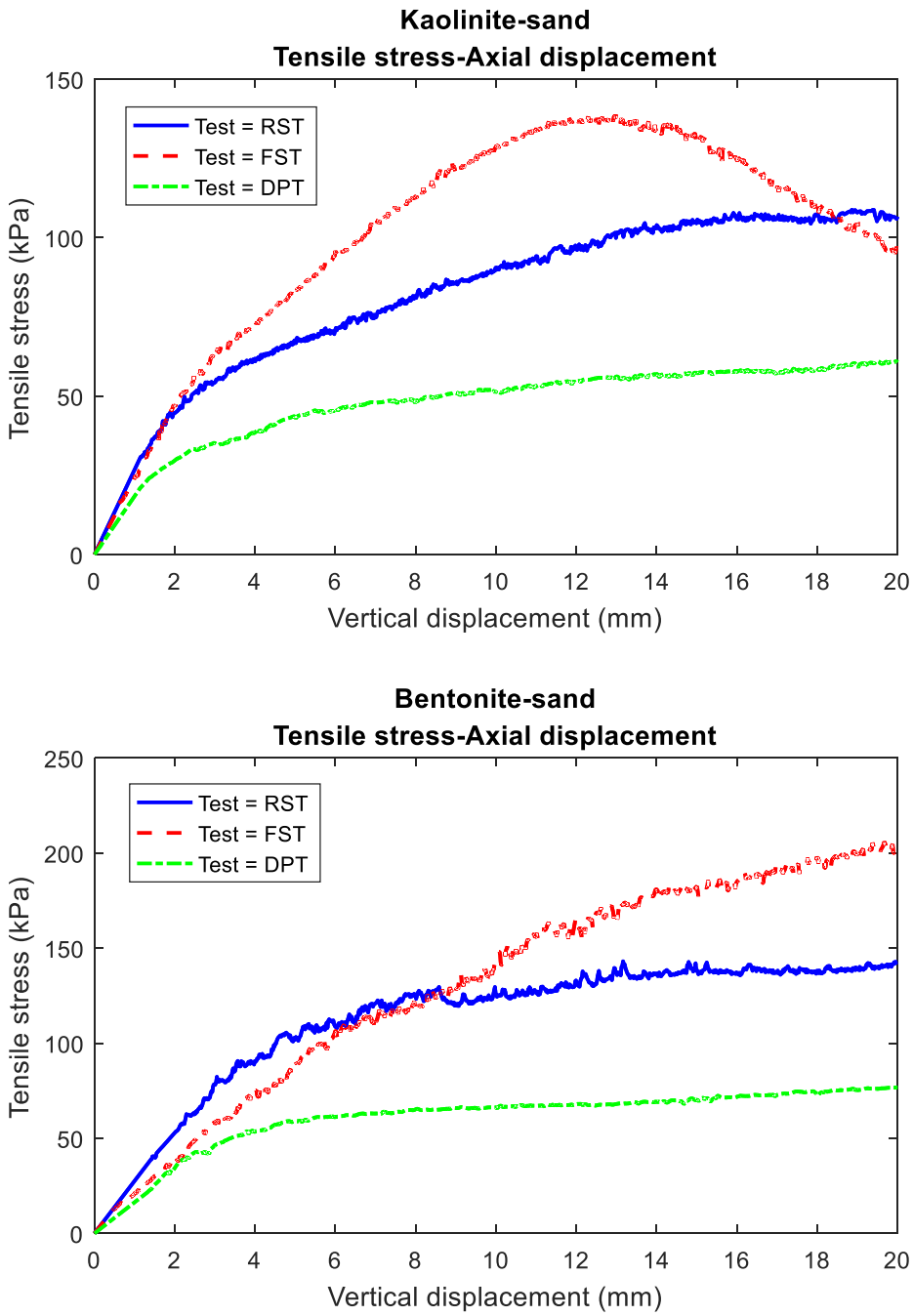

Figure 4. 23 Tensile strength-vertical displacement curves obtained from RST, FST, and DPT tests (T= - 0.5 °C, Loading rate= 1 mm/min, Salinity= 1 g/L).

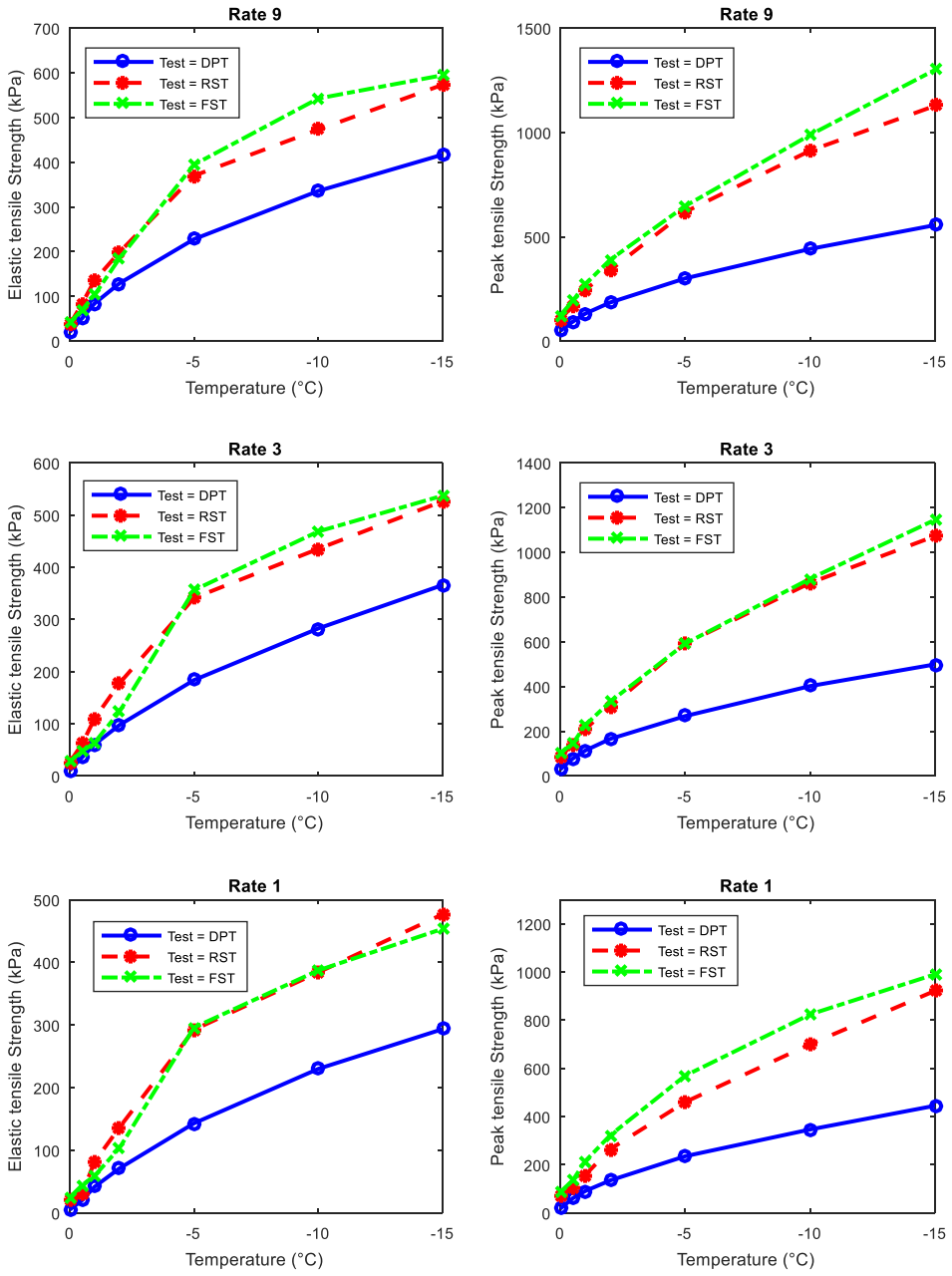

Figure 4. 24 Yield and peak tensile strength-temperature curves of kaolinite-sand samples (Salinity= 1 g/L).

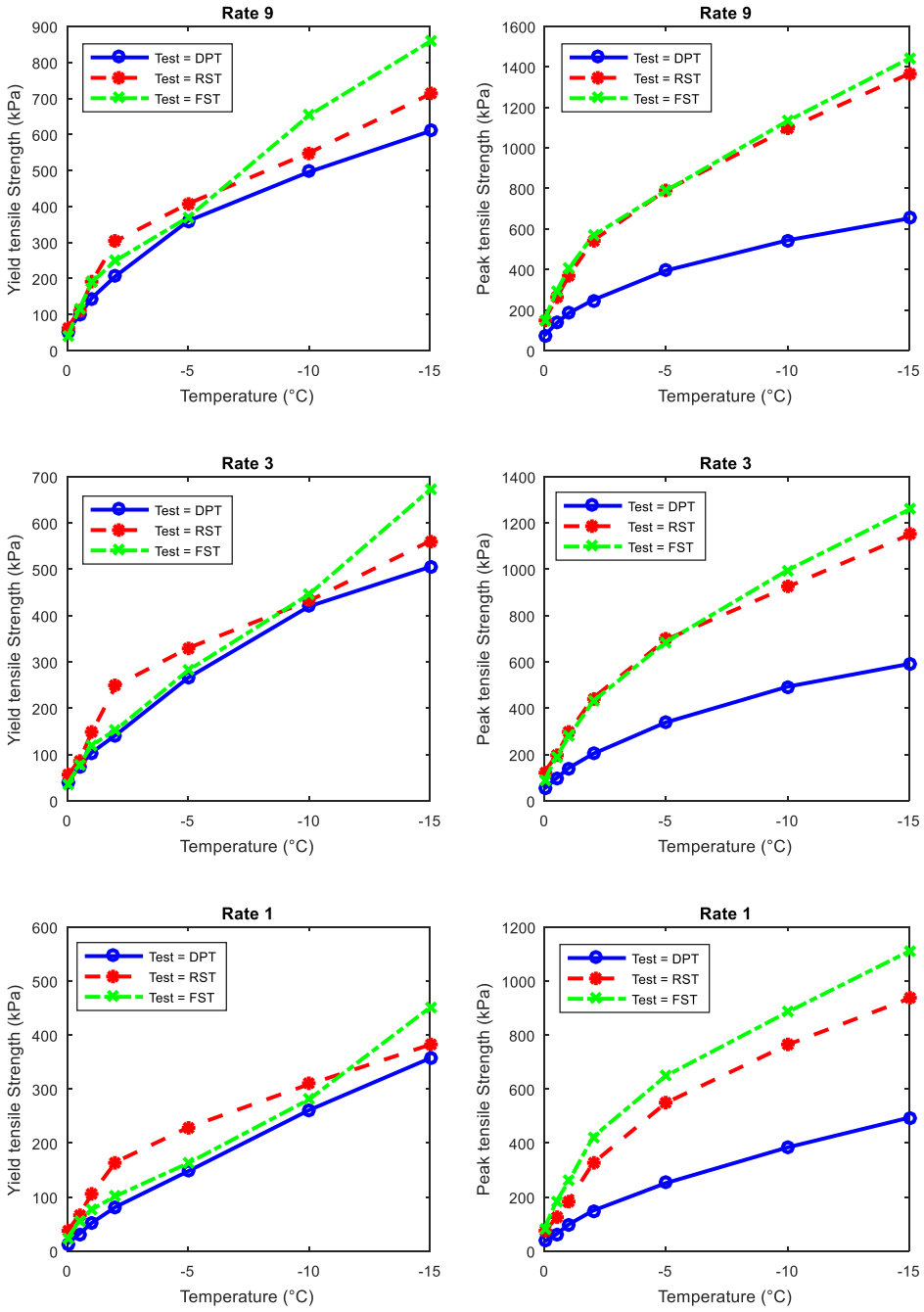

Figure 4. 25 Yield and peak tensile strength-temperature curves of bentonite-sand samples (Salinity= 1 g/L).

`

4.6 Factors affecting the tensile strength of frozen samples

4.6.1 Temperature

For the temperature range from -15 to 0 °C, remarkable differences in vertical load-vertical displacement relations for kaolinite-sand and bentonite-sand samples at different temperatures are observed. At temperatures below -5°C, there is a hardening behavior, softening behavior, and peak strength were noticed, and the post-peak softening behavior is accompanied by a change in the slope of horizontal displacement-vertical displacement curve. At frozen fringe temperatures, all the load-displacement curves show a linear elastic trend followed by a strain-hardening behavior without a post-peak softening behavior as shown in Figures 4.28 to 4.33. For kaolinite-sand samples with a salinity of 1 g/L that are tested by DPT test under a loading rate of 9 mm/min, the peak tensile strength increases more than 11 times from 50 kPa (axial load = 201 N) to 555 kPa (axial load = 2181 N) when the temperature drops from 0 °C to - 15 °C, respectively.

Moreover, the decrease in temperature is usually accompanied by an increase in the brittleness of samples which is appeared in a decrease in plastic deformation, strain hardening, and a quick drop of tensile strength after failure. The lateral deformation also decreases with the drop in temperature, as shown in Figures from 4.28 to 4.33. The failure of bentonite-sand samples tested by DPT at a strain rate of 3 mm/min is converted from brittle failure, through brittle-plastic failure, to ductile failure when temperature increases from - 15 to 0 °C.

From the post-failure pictures, samples display very similar failure modes at - 10 °C under different loading rates, and a typical vertical splitting fracture passing through the center of the sample was observed for the samples tested by the splitting tests, while side fractures were noticed in DPT samples (see Figure 10). kaolinite-sand and bentonite-sand samples at - 1 °C showed a strong viscoplastic behavior which is reflected by the deep penetration of the loading strip into the frozen samples, while the same fracture was observed in DPT samples (see Figure 4.19).

A good correlation is observed between the temperature and the tensile strength, and the correlation equation for both kaolinite-sand and bentonite-sand samples in a temperature range from 0°C to -15°C and loading rates of 1,3, and 9 mm/min are found to be a power-law type. Also, the tensile strength-temperature curve shows a non-linear behavior for the three indirect tensile strength tests and under different loading rates. Initially, the tensile strength is found to be

increased rapidly at temperatures ranging from 0 to - 2 °C as a result of quick growth in ice matrix, then a transition region is observed at temperatures ranging from - 2 °C to - 5 °C. Eventually, the degree of the non-linearity of the tensile strength-temperature relationship reduced with the drop in temperature below -5°C due to the reduction in free water and the growth in the ice strength as shown in Figures 4.34 and 4.35.

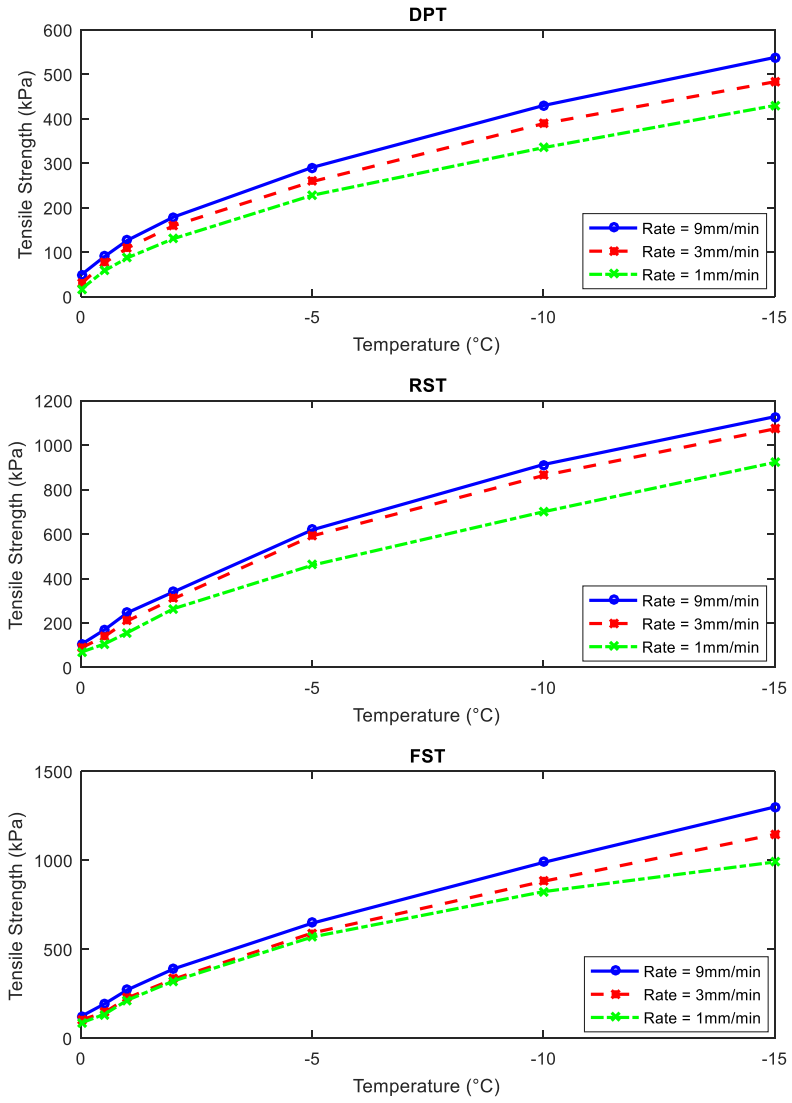

Figure 4. 26 Peak tensile strength-temperature curve of kaolinite-sand samples (Loading approach= RST, FST, and DPT, Salinity= 1 g/L).

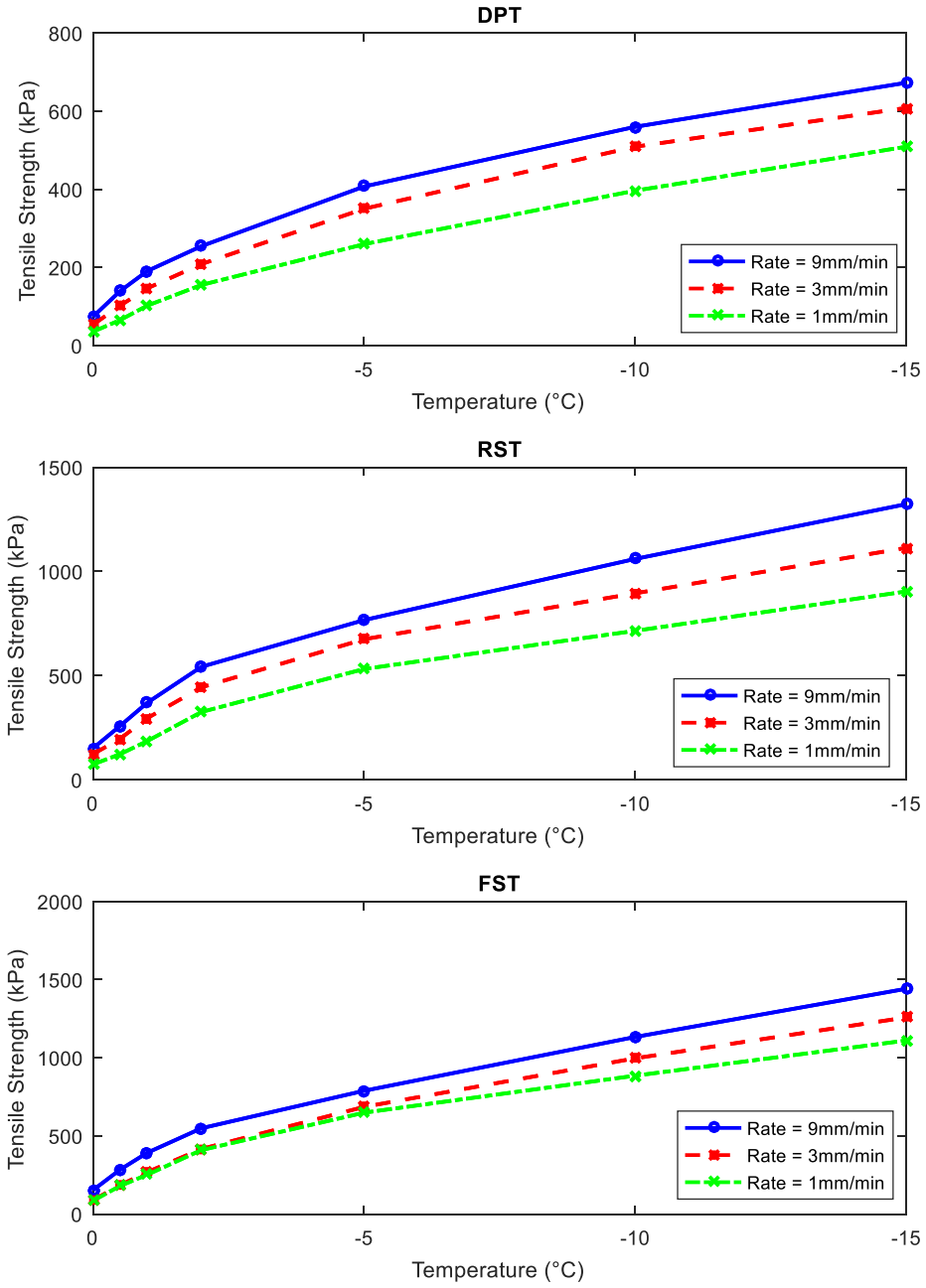

Figure 4. 27 Peak tensile strength-temperature curve of bentonite-sand samples (Loading approach= RST, FST, and DPT, Salinity= 1 g/L).

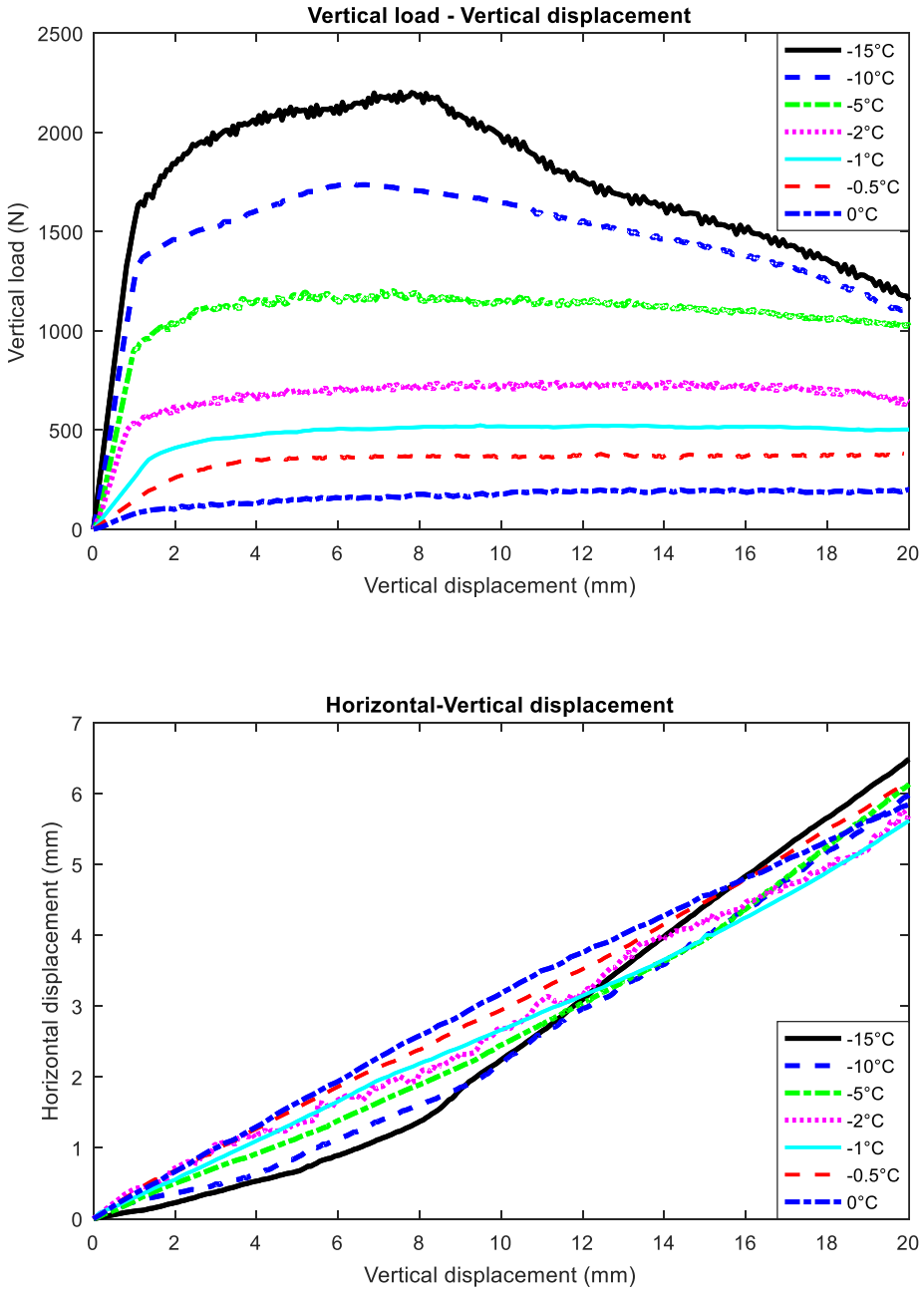

Figure 4.28 Vertical load-vertical displacement curves of tensile strength tests performed on kaolinite-sand samples (Loading approach= DPT, Loading rate= 9 mm/min, Salinity= 1 g/L,).

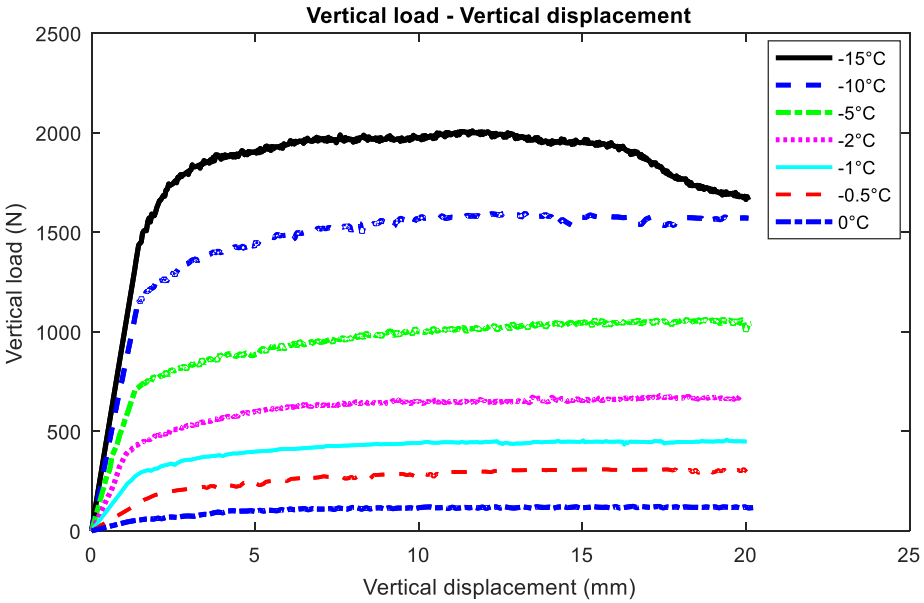

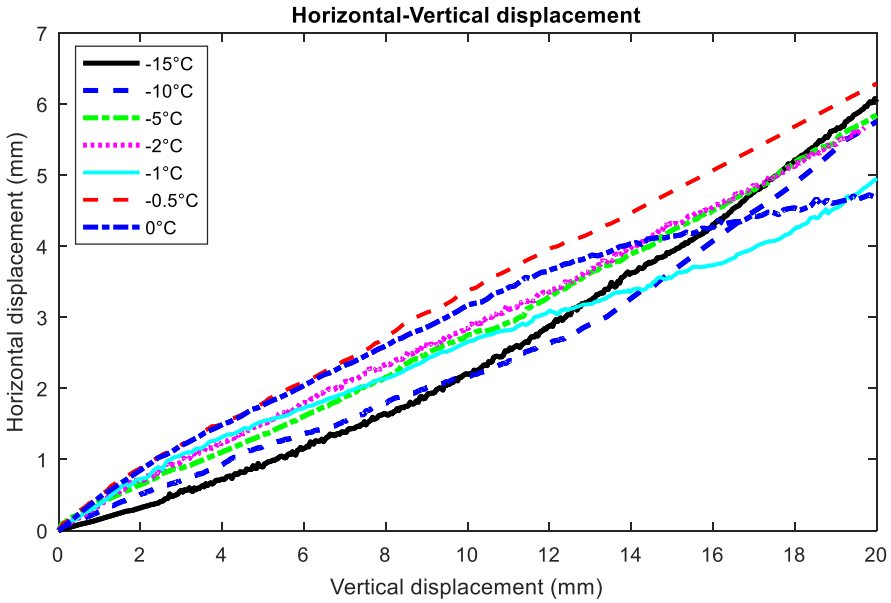

Figure 4. 29 Vertical load-vertical displacement curves of tensile strength tests performed on kaolinite-sand samples (Loading approach= DPT, Loading rate= 3 mm/min, Salinity= 1 g/L).

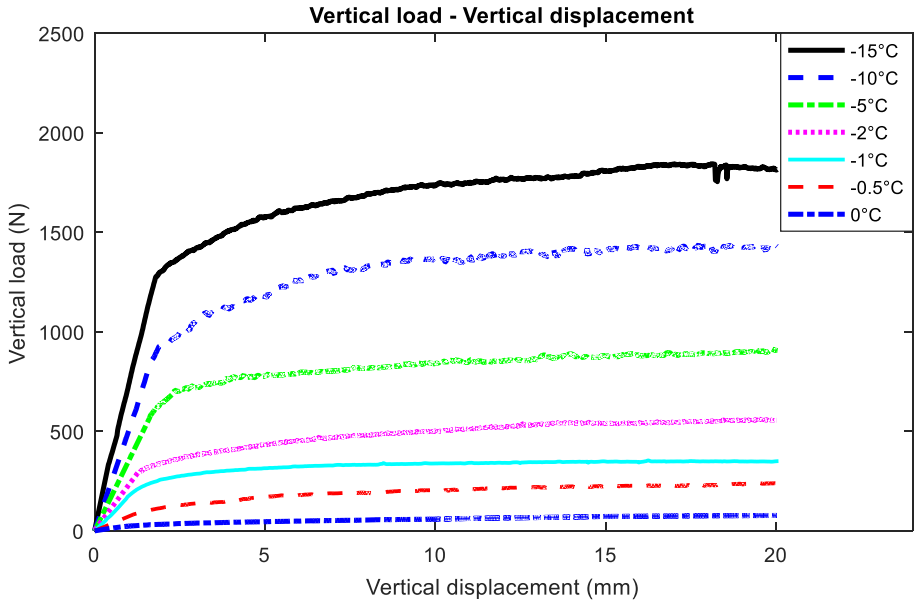

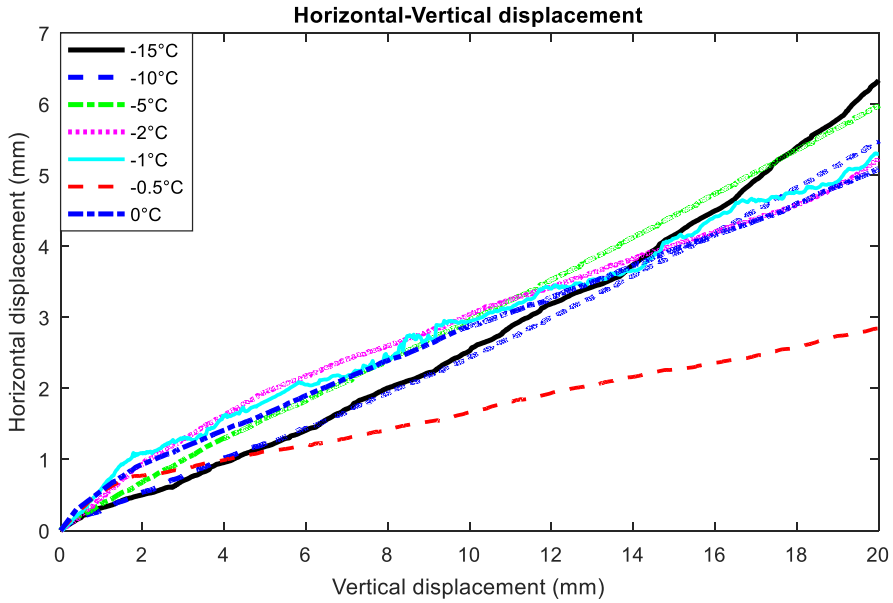

Figure 4. 30 Vertical load-vertical displacement curves of tensile strength tests performed on kaolinite-sand samples (Loading approach= DPT, Loading rate= 1 mm/min, Salinity= 1 g/L).

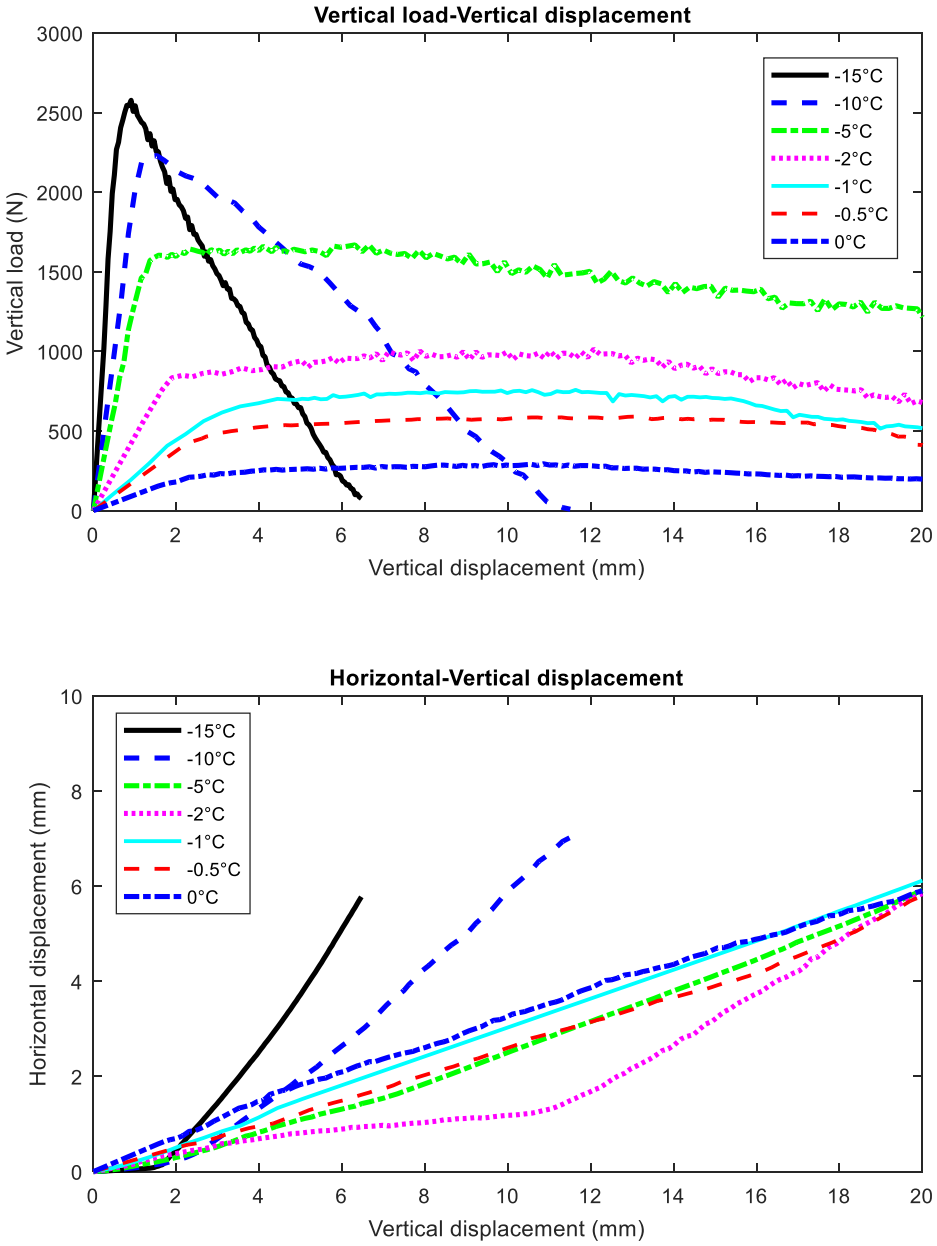

Figure 4. 31 Vertical load-vertical displacement curves of tensile strength tests performed on bentonite -sand samples (Loading approach= DPT, Loading rate= 9 mm/min, Salinity= 1 g/L).

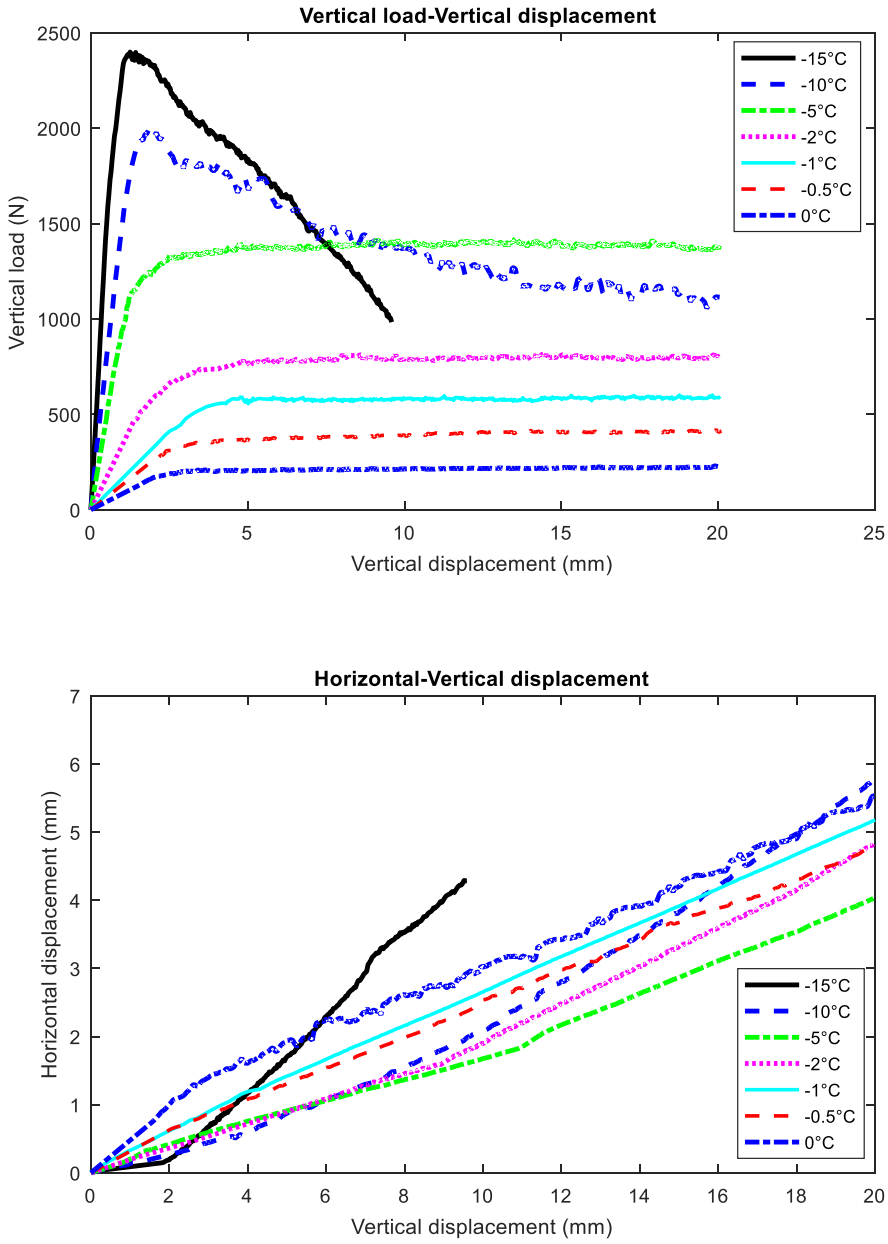

Figure 4.32 Vertical load-vertical displacement curves of tensile strength tests performed on bentonite -sand samples (Loading approach= DPT, Loading rate= 3 mm/min, Salinity= 1 g/L).

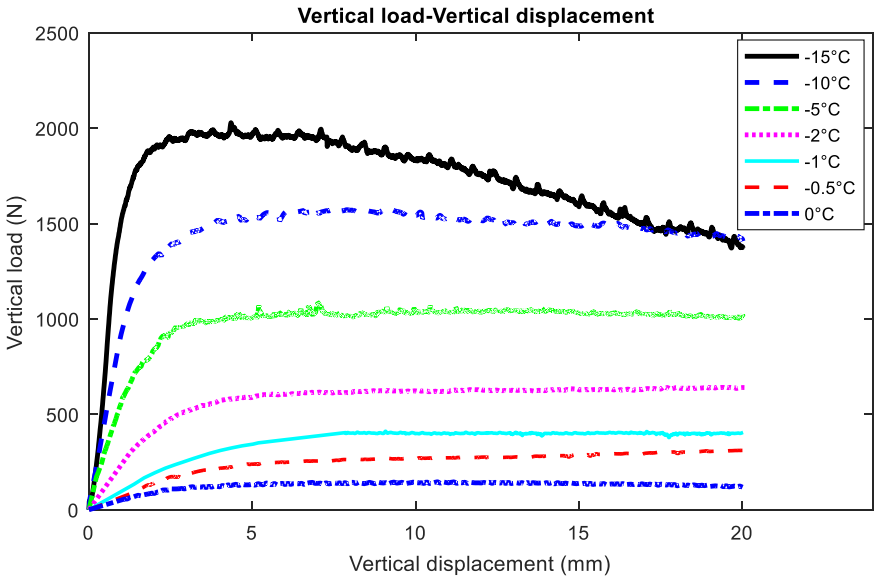

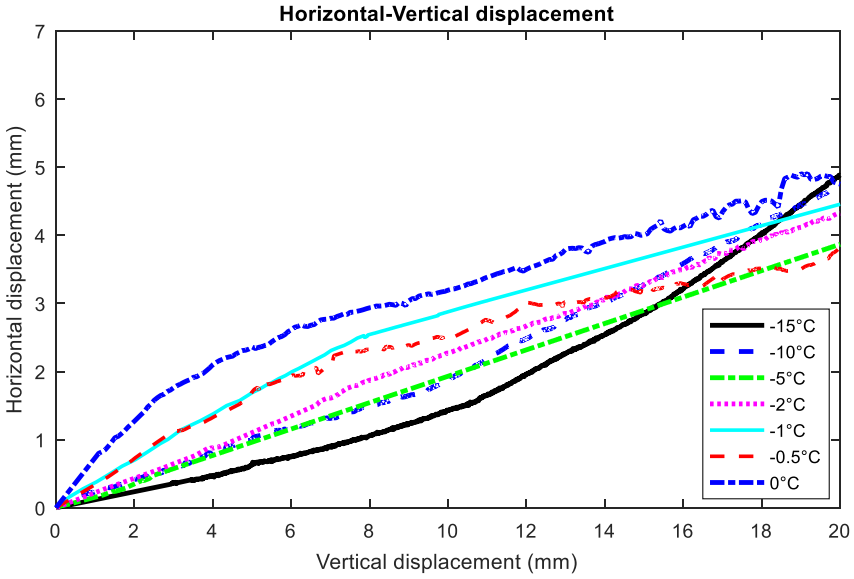

Figure 4.33 Vertical load-vertical displacement curves of tensile strength tests performed on bentonite -sand samples (Loading approach= DPT, Loading rate= 1 mm/min, Salinity= 1 g/L).

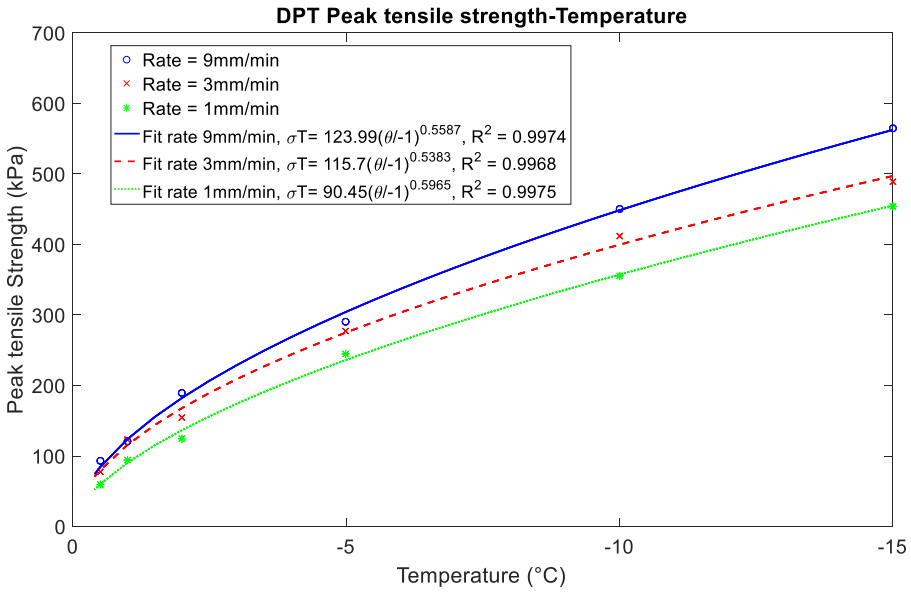

Figure 4. 34 Curves showing the correlation between peak tensile strength and temperature for kaolinite-sand samples (Loading approach= DPT, Salinity= 1 g/L).

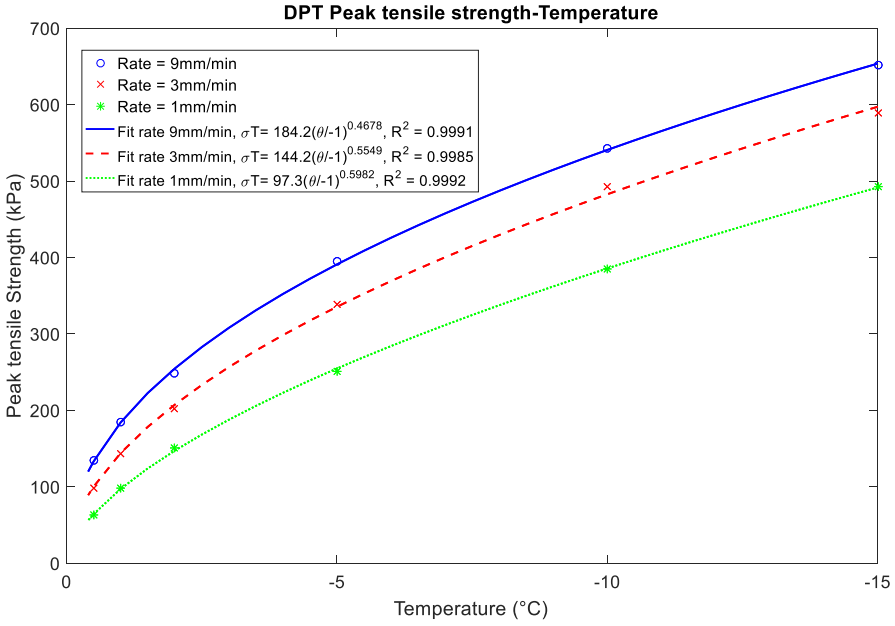

Figure 4. 35 Curves showing the correlation between peak tensile strength and temperature for bentonite-sand samples (Loading approach= DPT, Salinity= 1 g/L).

`

4.6.2 Loading rate

The loading rate influences both the tensile strength value and deformation behavior of the tested samples. The increase in loading rate usually leads to increasing the tensile strength (see Figure 4.36) and brittleness of samples, but its impact depending on varies parameters such as the testing method, temperature, salinity, and composition of the soil sample. Figure 4.17 shows the remarkable effect of strain rate on group B-03 samples. The tensile strength values corresponding to loading rates of 1 mm/min, 3 mm/min, and 9 mm/min are 494 kPa, 591 kPa, and 652 kPa, respectively. The failure mode changed from brittle failure at loading rates of 9 and 3 mm/min to ductile failure at a loading rate of 1 mm/min, and the failure mode changed from brittle at 9 and 3 mm/min to ductile at 1 mm/min (see Figure 4.9). The stain rate also influences the axial deformations and strain failure, particularly at low temperatures. From Figure 4.4, the samples of group K-01 failed at strains of 7.5 and 12.5 mm at loading rates of 9 mm/min and 3 mm/min, respectively compared to 16mm at 1 mm/min.

To simplify the effect of strain rate on the peak tensile strength, the power-law relationship between strain rates and the peak tensile is linearized by plotting in a log-log graph. From Figure 4.36, the effect of strain rate on the tensile strength of frozen soil is largely influenced by the temperature. At temperatures above - 5 °C, the relation is a broken-line graph with a slope break at a strain rate of 0.0295 S^{-1}, and the first part of the line of lower strain rates has a slope greater than the slope of the second part, while the relation becomes almost a straight line at temperatures below -5°C. Also, the tensile strength of the samples with a salinity of 3 g/L is affected by the strain rate more than the samples of 0 g/L at the same temperature of -5 °C. The results show that the sensitivity of the tensile strength of frozen soil to the strain rate depends on the temperature and the salinity of the sample as well for the same testing method.

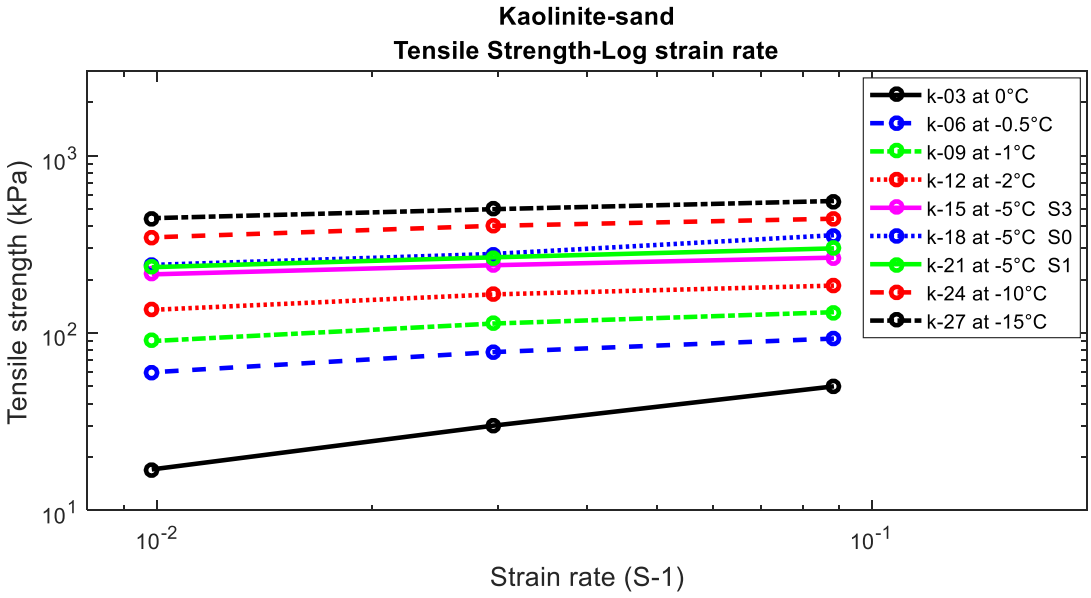

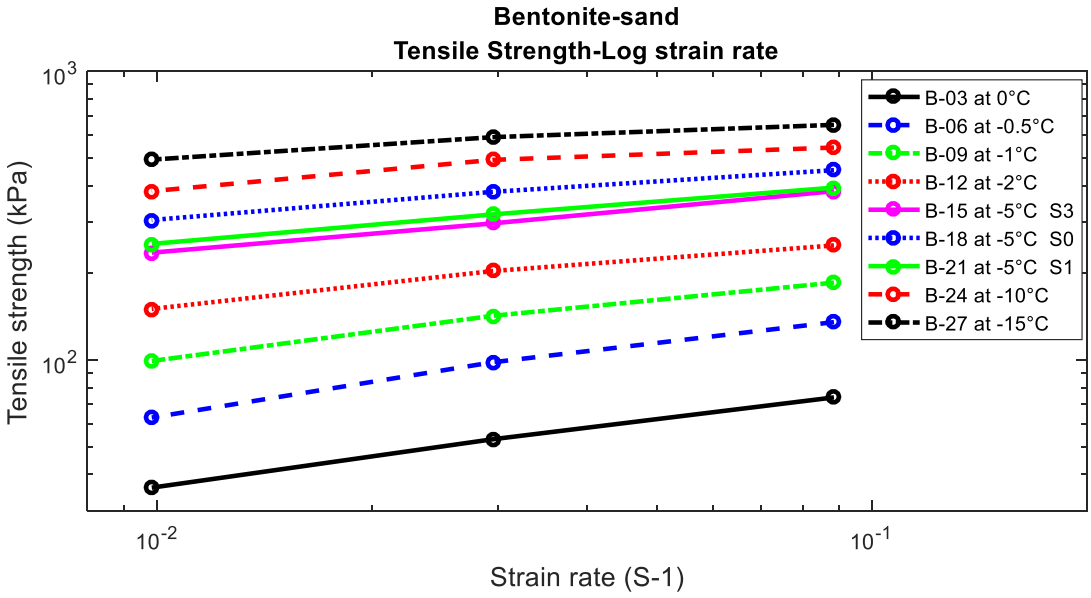

Figure 4. 36 Log-log plot of tensile strength-strain rate curves for sandy clay samples at a temperature range from - 15 to 0 °C (Loading approach= DPT, Salinity= 1 g/L).

`

4.6.3 Salinity

The salinity of the tested samples has a strong effect on the tensile strength and behavior of the frozen sandy clay soil. The non-saline soil samples fail at higher tensile stresses and behave more brittle compared to the samples of salinity of 1 g/L and 3 g/L. On the contrary, the samples of salinity of 3 g/L have the lowest tensile strength values with more ductile behavior due to the increase in the unfrozen water content.

The values of the peak tensile strength for bentonite-sand samples with a salinity of 0 g/L measured by DPT at a temperature - 5 °C and loading rates of 1, 3, and 9 mm/min changed by 11 %, 3 %, and 12 %, respectively. On the other hand, the peak tensile strength of samples with salinity of 3 g/L varied by -10 %, - 15 %, and - 6 % at a temperature - 5 °C and loading rates of 1, 3, and 9 mm/min, respectively compared to the samples with a salinity of 1 g/L. Also, the failure of non-saline soil samples becomes more brittle, whereas the behavior of the samples with a salinity of 3 g/L is more ductile due to the reduction in ice content as shown in Figures 4.37 and 4.38.

Finally, the salinity affects the sensitivity of the tensile strength of frozen soil to the strain rate, as mentioned in the previous section 4.6.2 (see Figure 4.36).

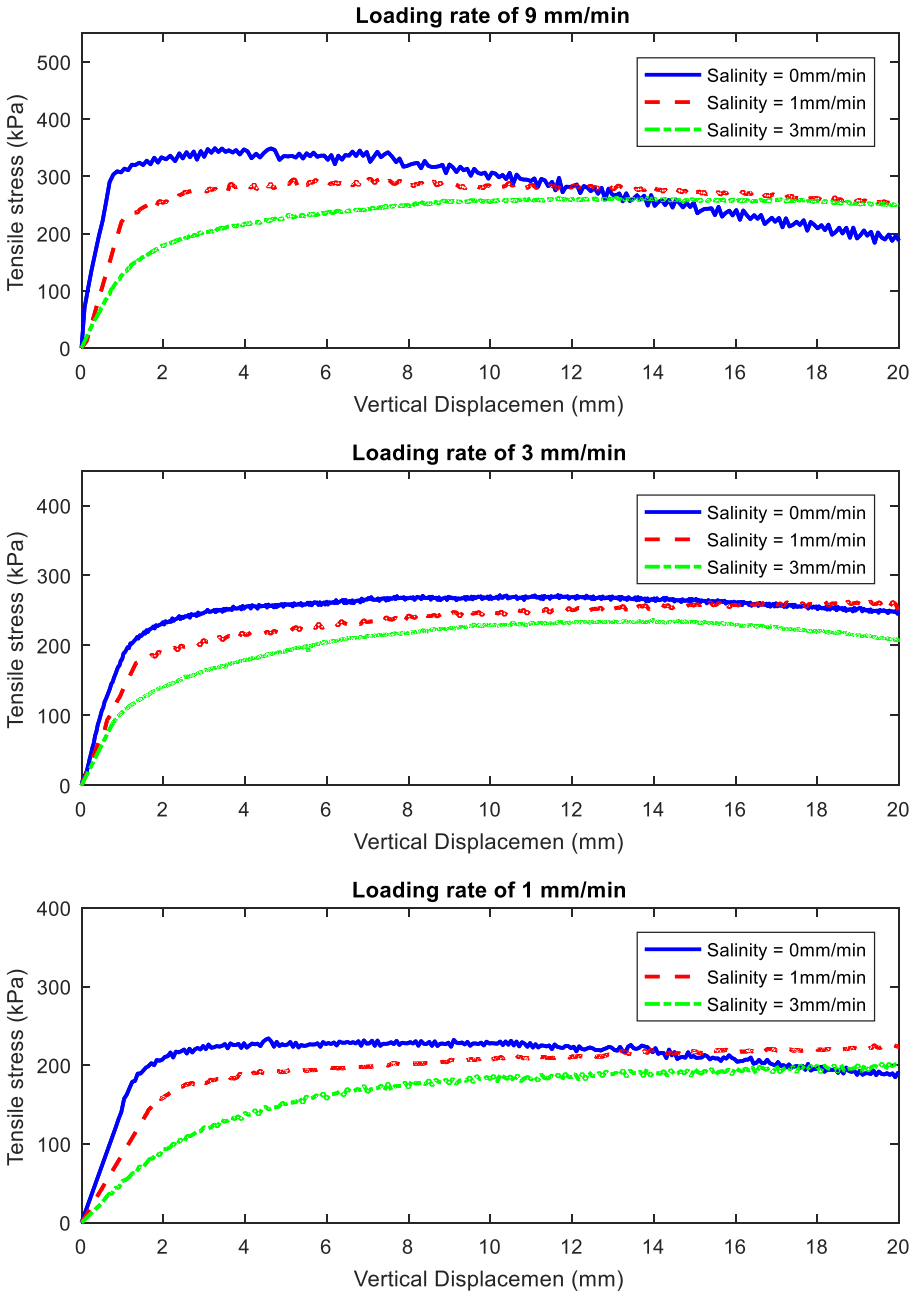

Figure 4. 37 Tensile strength-vertical displacement curves of kaolinite-sand samples with various salinities of 0, 1, 3 g/L (Loading approach= DPT, T= -5 °C).

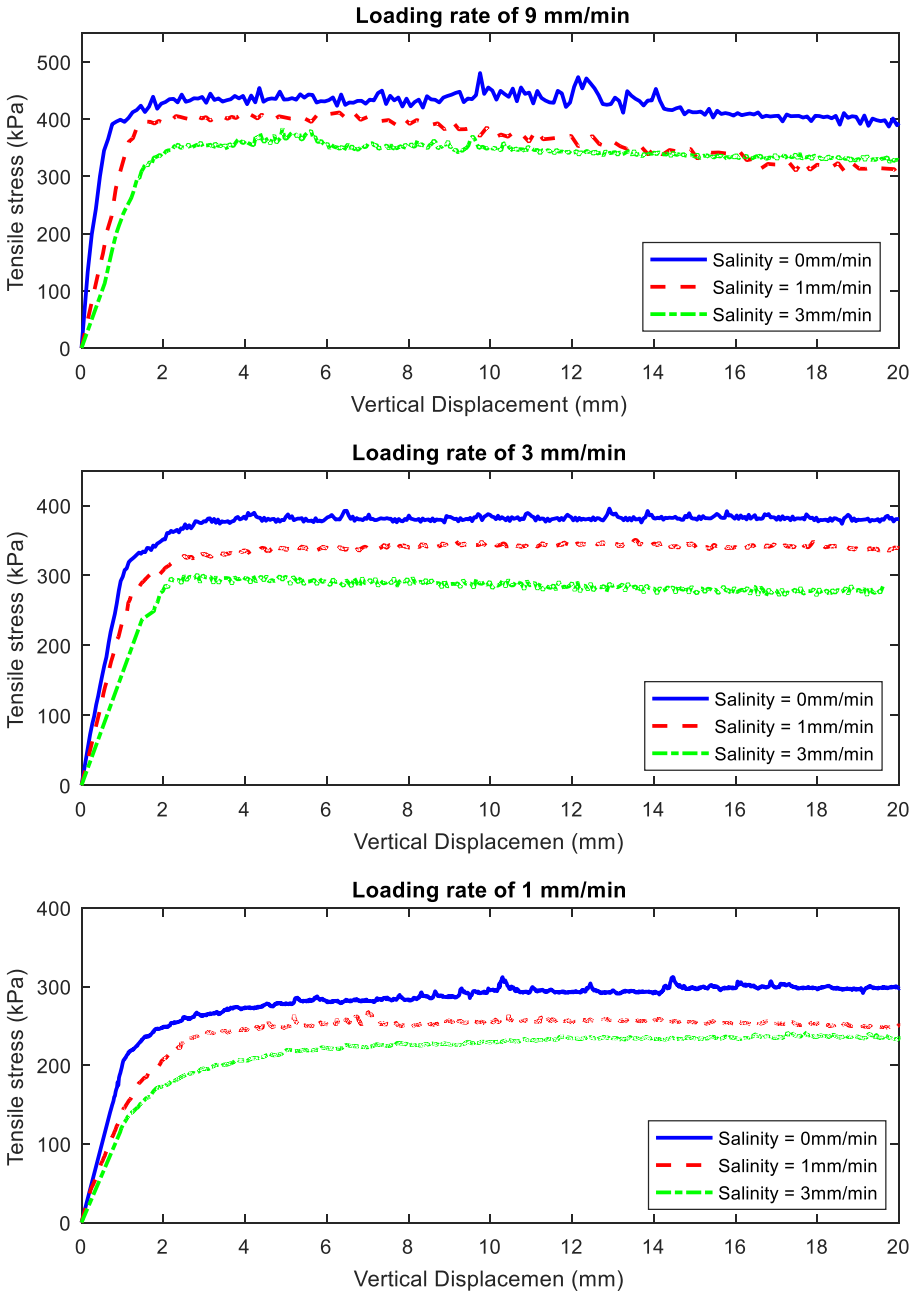

Figure 4. 38 Tensile strength-vertical displacement curves of bentonite-sand samples with various salinities of 0, 1, 3 g/L (Loading approach= DPT, T= -5 °C).

`

4.6.4 Clay mineralogy

The freezing temperature of soil depends on several parameters such as the surface area of the soil particles, the soil grains size distribution, the density, the mineralogical composition, and the chemical composition of the soil. To study the effect of clay mineralogy in this research, two types of sandy clay samples are prepared using the same procedure, composition proportions, and materials except for the clay mineral.

From the results of hydrometer tests, the grain size of the bentonite particles is finer than the kaolinite particles, which results in increasing the amount of mixing water for bentonite-sand samples by more than 300 % of that for kaolinite-sand samples to reach the same percentage of saturation (120 % liquid limit).

The results of the three tensile strength testing methods reveal that the tensile strength values of bentonite-sand samples are higher than that for kaolinite-sand samples in the temperature range from - 15 °C to 0 °C and at loading rates of 1, 3, and 9 mm/min. The difference between the tensile strength values of bentonite-sand and kaolinite-sand increases with the decrease in temperature and the increase in a loading rate. For example, the peak tensile strength obtained by DPT for the bentonite-sand sample at temperature - 10 °C and loading rate of 9 mm/min is 123 % the peak tensile strength of the kaolinite-sand sample at the same testing conditions, and the behaviour of the bentonite-sand sample is more brittle than kaolinite- sand sample. The peak tensile strength obtained by DPT for the kaolinite-sand sample at temperature - 10 °C and loading rate of 1 mm/min is equal to the peak tensile strength of the bentonite-sand sample at the same testing conditions, but the behavior of the bentonite-sand sample is more ductile than kaolinite-sand sample as shown in Figures 4.39 and 4.40.

The bentonite-sand samples generally behave more brittle than kaolinite-sand samples. At temperatures below – 5 °C and at high loading rates, while a ductile behavior was observed for both sandy clay soils at temperatures above - 5 °C due to the high unfrozen water content of bentonite-sand samples at temperatures above - 5 °C.

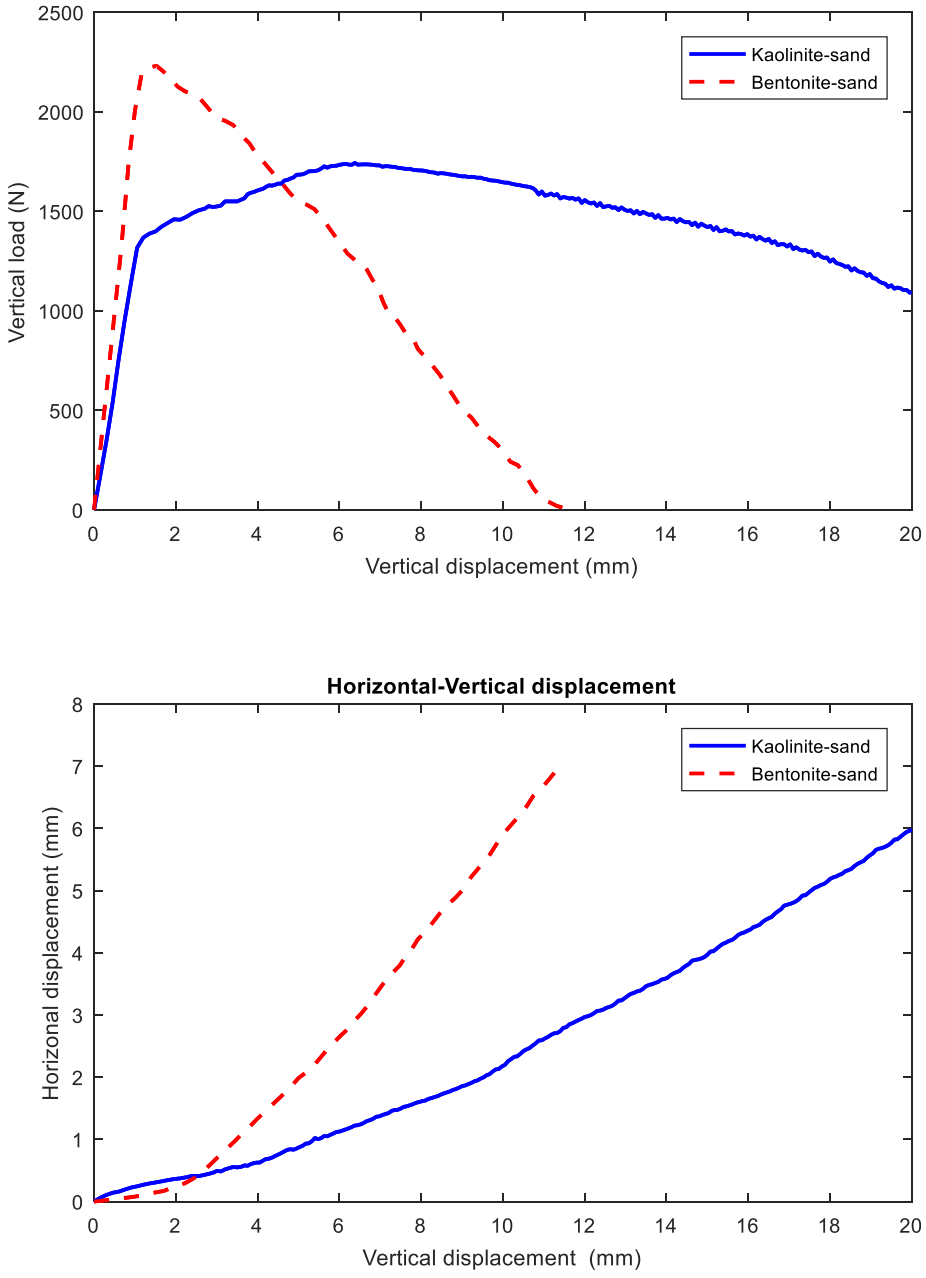

Figure 4. 39 Vertical load-vertical displacement curves of tensile strength tests performed on samples with different clay mineralogy (Loading approach= DPT, T= - 10 °C, Loading rate= 9 mm/min, Salinity= 1 g/L).

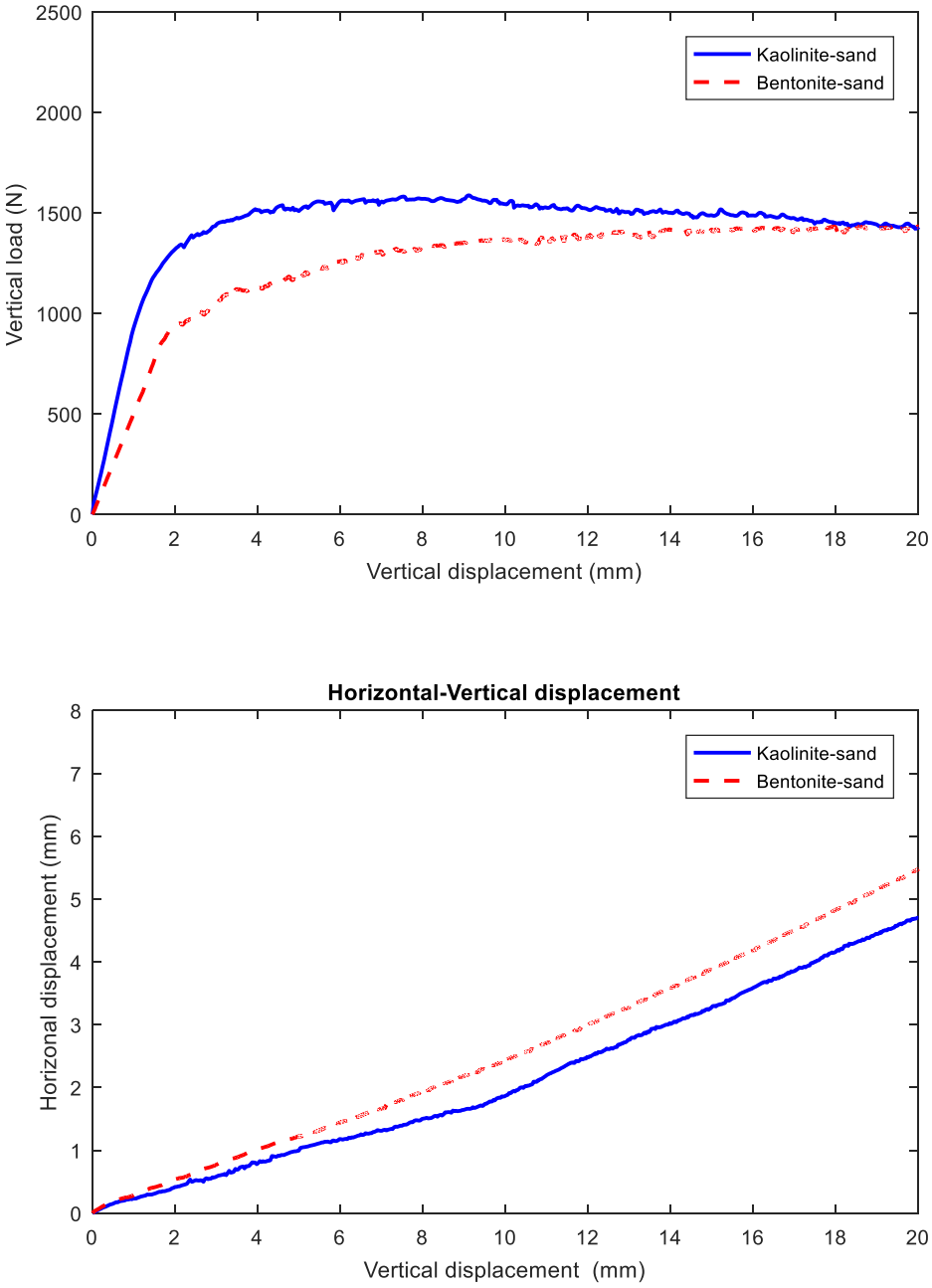

Figure 4. 40 Vertical load-vertical displacement curves of tensile strength tests performed on samples with different clay mineralogy (Loading approach= DPT, T= - 10 °C, Loading rate= 1 mm/min, Salinity= 1 g/L).

`

4.7 Summary

One hundred sixty-two indirect tension tests are carried out to investigate the parameters affecting the tensile strength and deformation behavior of frozen sandy clay samples. These parameters are the temperature, loading rate, salinity, testing method, and the clay mineralogy. The temperature is found to significantly affect the tensile strength of the tested sandy clay frozen soils, and their behavior becomes similar to a weak rock at low temperatures (the tensile strength of frozen sand-clay soil at -15°C increased by about 1000% its strength at 0°C). The strain rate also has a strong influence on the tensile strength, the deformation behavior, and the failure of frozen soil and the sensitivity of the tensile strength to the strain rate depends on the magnitude of the strain rate and the temperature of the frozen soil. Both the tensile strength and the deformation behavior of saline samples are greatly affected by the salinity of frozen samples (the tensile strength of saline samples of 3 g/L is decreased by more than 20% compared to the non-saline samples). The impact of indirect tensile strength testing method is easily observed in the significant difference between the results of the three indirect tests (the values of the tensile strength calculated by RST and FST are almost twice that determined by DPT). Eventually, the tensile strength values of the bentonite-sand samples are found to be greater than these for kaolinite-sand samples due to the higher content of ice and cohesion. Also, the behavior of bentonite-sand samples to temperature is observed to be more complex due to the very large surface area of the bentonite particles that results in large changes in the unfrozen water content at different temperatures.

`

Chapter 5

LABORATORY TESTS ON TEMPERATURE-DEPENDENT UNIAXIAL COMPRESSIVE STRENGTH AND STRESS RELAXATION

This chapter is mainly composed of two parts; the first part focuses on the uniaxial compressive strength (UCS) of frozen sandy clay soils, including the test setup used, procedure followed, and the various parameter affecting the UCS of the frozen soil such as a temperature, loading rate, clay mineral, and test setup. Furthermore, Young's modulus and Poisson's ratio are calculated for all tested samples to study the different factors that can affect their values. To achieve the objective of this part, a series of fifty-four UCS tests carried out in both the Building Envelope Performance Laboratory (BEPL) of Concordia University and the Geotechnical Laboratory (GL) of Polytechnique Montréal using two different setups.

The second part of this chapter studies the stress relaxation test, which is a substantial alternative for the conventional creep test that focuses on creep parameters independent of material flow law. This part involves sixteen stress relaxation tests performed on sandy clay frozen soils at different temperatures, loading rates, and stress levels to investigate the effect of the different parameters on the test results.

5.1 UCS test set-up

The uniaxial compressive strength (UCS) tests are performed in both the BEPL and GL. The UCS tests are carried out in the BEPL laboratory using the same setup of the indirect tensile strength tests (Chapter 4) after replacing the loading strips as shown in Figure 5.1, while the following setup (see Figure 5.2) is used for testing the frozen sandy clay samples at GL laboratory:

1. Environmental chamber manufactured by CSZ: a dual-purpose environmental chamber with a temperature range from - 45 to 170 °C is designed to either operate independently or to deliver the temperature-conditioned air to remote cells.
2. Freezing cell: a mini freezer with an upright clear door provided by a well-insulated extension, and the necessary openings are drilled to pass the loading frame through its walls. The freezing cell is connected to the cold air unit by two insulated flexible ducts.

`

3. Instron 1350 loading system: a 100 kN computer-controlled servo-hydraulic loading system with a high precision strain control is used.
4. Sub-frame: the same sub-frame is transferred to GL laboratory, but the PVC fittings are replaced by two stainless steel holders for mounting the non-insulated LVDTs. The sub-frame provided with a pair of loading plates made of stainless steel of grade 420 for UCS test with a diameter of 63.5 mm (2.5 inches).
5. Data acquisition and PC: MTS Flex Test SE controller designed to work with MTS series 793 software and Windows operating system.
6. Removable special holders: A two-part holders of inner diameters 50.8 mm (2 inches) and 63.5 (2.5 inches) are used to adjust the frozen soil sample at the center of the platens, as shown in Figure 5.3.

Figure 5. 1 Set-up of UCS test used at BEPL Laboratory.

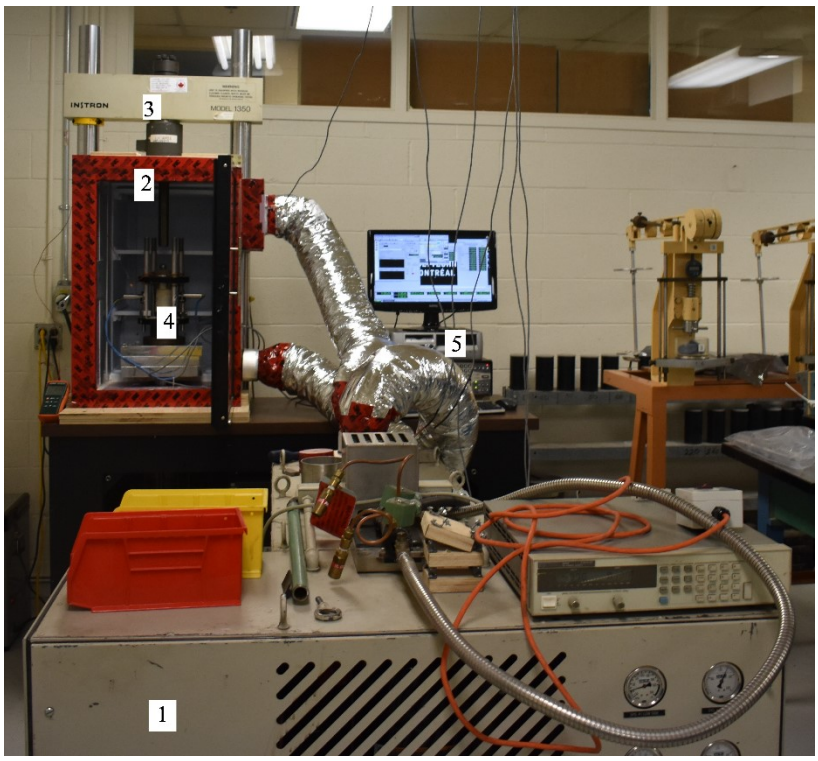

Figure 5. 2 Set-up of UCS test used at the GL Laboratory.

Figure 5. 3 Holders used for positioning frozen samples before the UCS test.

`

5.1.1 Measuring devices

The axial and horizontal displacements were measured via a high accuracy linear variable displacement transducers (LVDTs) of range 50 mm produced by HP series 24DCDT, in addition to the bottom platen readings that are taken continuously by Instron 1350 software. For the temperature measurements, Easy View RTD type K with a temperature range from - 20 to 250 °C and 0.1 °C /1 °C resolution is used inside the freezing cell during the test, and the maximum, minimum, and average readings can be recalled after testing (see Figure 5.1).

5.1.2 UCS test procedure

The UCS test is performed at BEPL laboratory using the same procedure of the indirect tension tests (Chapter 4), whereas the procedure of testing at GL of Polytechnique Montréal can be described as the following:

1. The temperature of the portable freezer is adjusted to be lower than the test temperature by 5°C using the digital control button according to the calibration chart,
2. After reaching the required temperature, the samples are placed in the portable freezer and transferred to GL laboratory.
3. The samples are stored for a minimum of 24 hours before testing at the test temperature,
4. The faces of the loading tools are cleaned properly before placing the sample.
5. The temperature of the environmental chamber is adjusted to the temperature of testing as per the calibration chart,
6. the packing of the sample is removed before testing, and then the sample is placed in the environmental chamber when the temperature drops and remains constant at the test temperature,
7. The holders are installed on loading tools for positioning of the sample between loading plates of the sub-frame to ensure proper loading, then LVDTs are conducted to the sample, and finally bearing plates are seated, and the holders are removed before loading.
8. The sample is kept for at least 1 hour before starting the UCS test.
9. Test logging file is initiated containing all information (i.e., Name of the sample, the date, the test performed, the temperature, and the loading rate), then the loading rate is entered, and the test is started.

`

10. After failure, the test is stopped, and the logging file is saved.

5.2 General results of UCS tests

The fifty-four UCS tests are divided into eighteen groups according to the test temperature and the test location. The samples are tested at a temperature range from 0 to the – 15 °C in BEPL laboratory, while four groups are tested in GL at temperatures of – 10 °C and - 15 °C. Table 5.1 shows the details of the tested groups at GL and BEPL laboratories. The name of each group composed of two letters, the first is the clay mineral and the second letter is the university where the test is done (i.e., KP means UCS for Kaolinite-sand samples at Polytechnique Montréal)

At each temperature, two groups of frozen sandy clay soils, kaolinite-sand and bentonite-sand, are tested to investigate the behavior of different clay minerals. Each group composed of three samples are tested at different loading rates of 1 mm/min, 3 mm/min, and 9 mm/min to study its influence on the UCS of the frozen soil. The results of the fourteen groups tested in BEPL laboratory and the photos taken for the samples after failure tested at temperatures -15 and -1°C are shown in Figures from 5.4 to 5.9, while the results of the other groups are shown in Figures form B 57 and B 71. The results of the groups tested in GL and the photos taken after failure are shown in Figures from 5.10 to 5.15. Finally, Table 5.2 records the uniaxial compressive strength values for all tested groups at GL and BEPL laboratories.

`

Table 5. 1 Details of UCS tested groups at GL and BEPL laboratories.

Laboratory	Group	Sample	Temperature	Loading rate
BEPL Concordia University	KC-01	CK1 - CK3	- 15	1, 3, and 9 mm/min
	BC-01	CB1 - CB3	- 15	1, 3, and 9 mm/min
	KC-02	CK4 – CK6	- 10	1, 3, and 9 mm/min
	BC-02	CB4 – CB6	-10	1, 3, and 9 mm/min
	KC-03	CK7 – CK9	- 5	1, 3, and 9 mm/min
	BC-03	CB7 – CB9	- 5	1, 3, and 9 mm/min
	KC-04	CK10 – CK12	- 2	1, 3, and 9 mm/min
	BC-04	CB10 – CB12	- 2	1, 3, and 9 mm/min
	KC-05	CK13 – CK15	- 1	1, 3, and 9 mm/min
	BC-05	CB13 – CB15	- 1	1, 3, and 9 mm/min
	KC-06	CK16 – CK18	- 0.5	1, 3, and 9 mm/min
	BC-06	CB16 – CB18	- 0.5	1, 3, and 9 mm/min
	KC-07	CK19 – CK21	0	1, 3, and 9 mm/min
	BC-07	CB19 – CB21	0	1, 3, and 9 mm/min
GL Polytechnique Montréal	KP-01	CK22 – CK24	- 15	1, 3, and 9 mm/min
	BP-01	CB22 – CB24	- 15	1, 3, and 9 mm/min
	KP-02	CK25 – CK27	- 10	1, 3, and 9 mm/min
	BP-02	CB25 – CB27	- 10	1, 3, and 9 mm/min

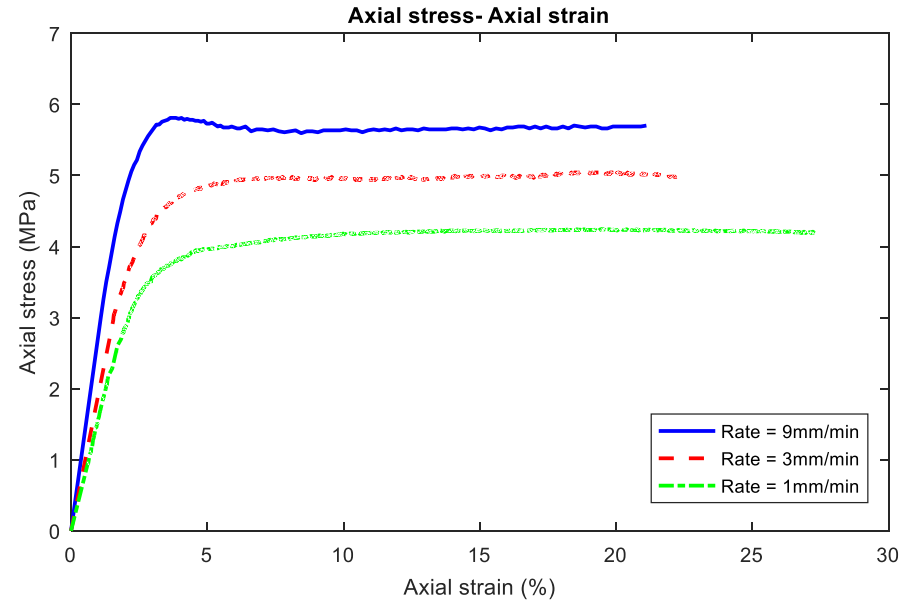

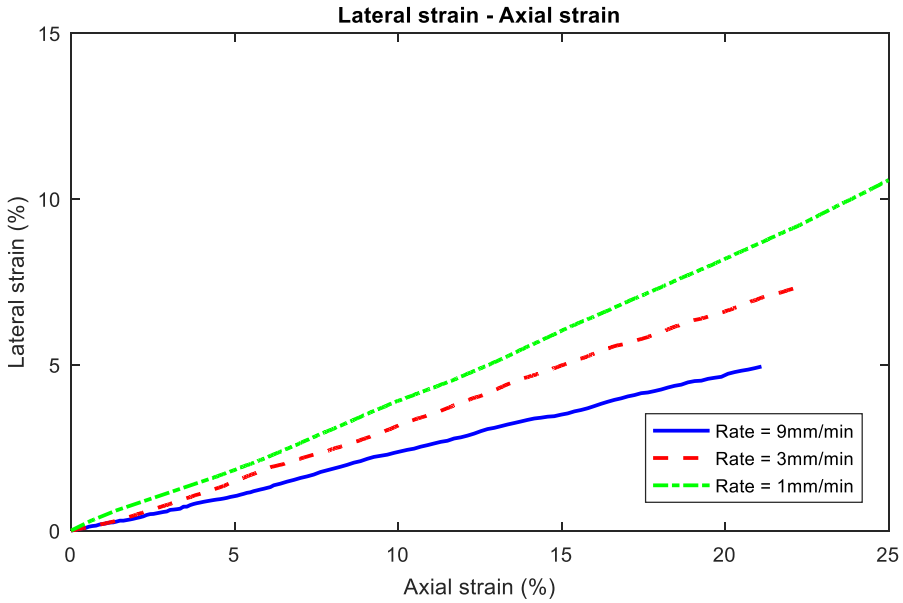

Figure 5. 4 Results of UCS tests performed on group KC-01 (T= - 15 °C, Laboratory= BEPL).

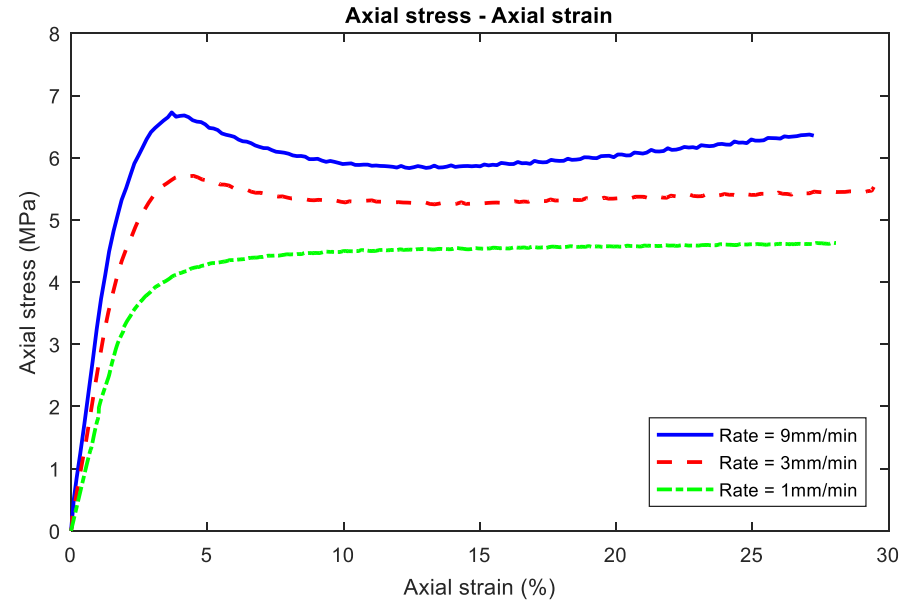

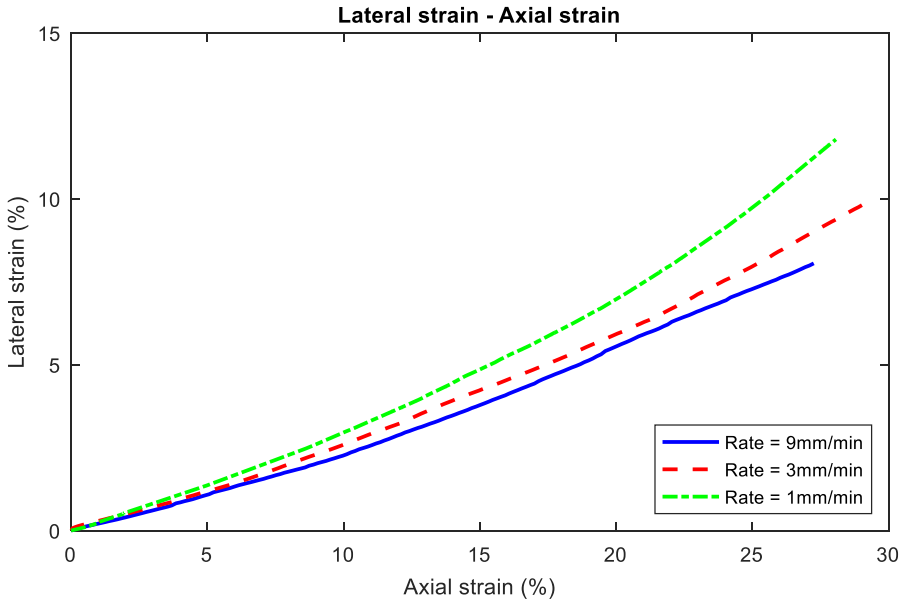

Figure 5. 5 Results of UCS tests performed on group BC-01 (T= - 15 °C, Laboratory= BEPL).

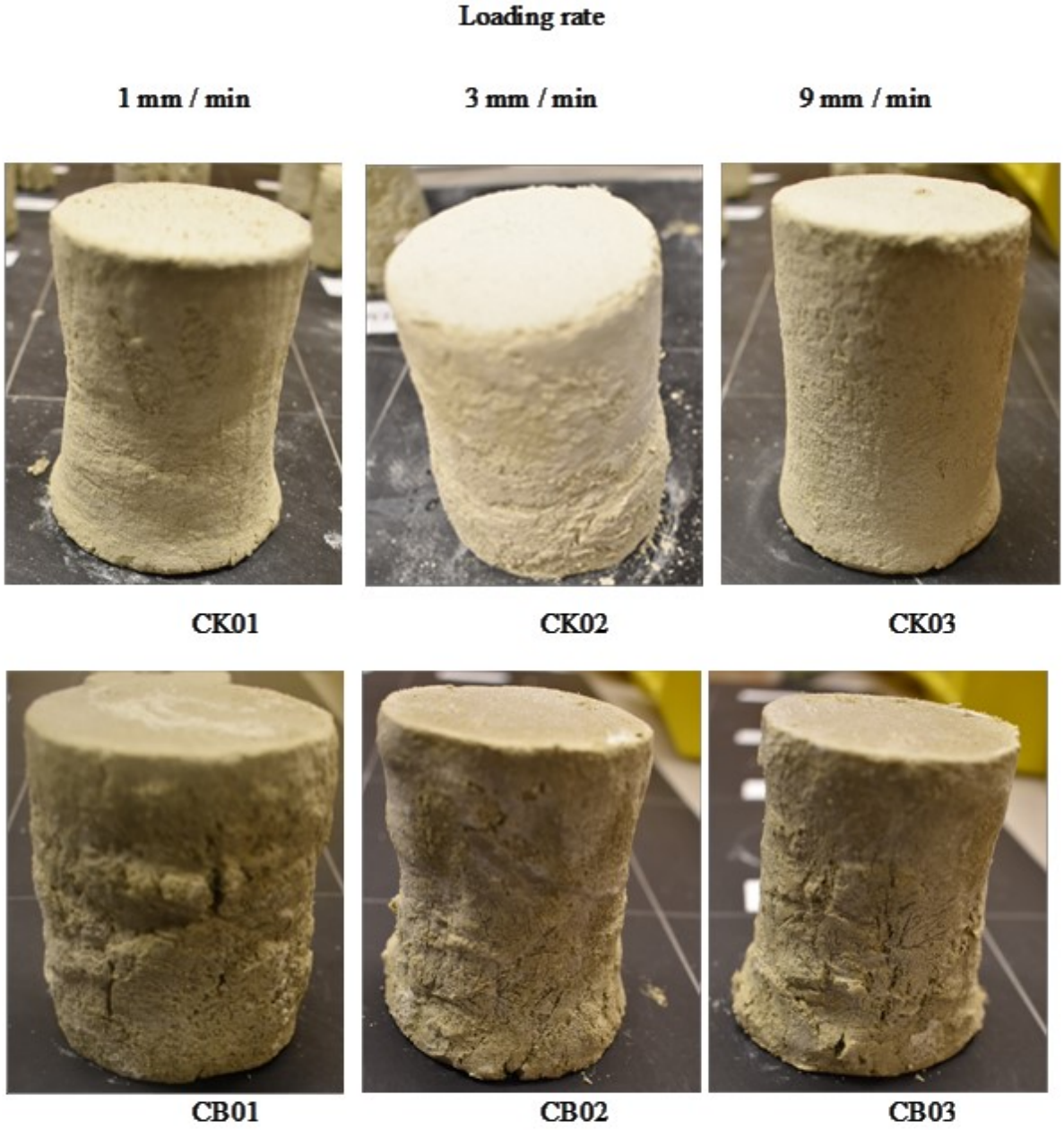

Figure 5. 6 Post-failure pictures of UCS tested samples (T= - 15 °C, Laboratory= BEPL).

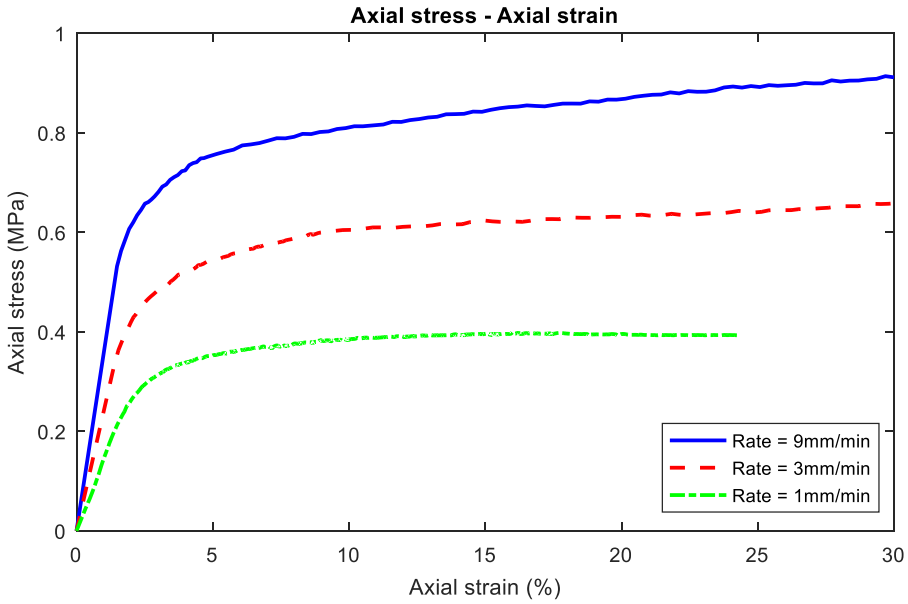

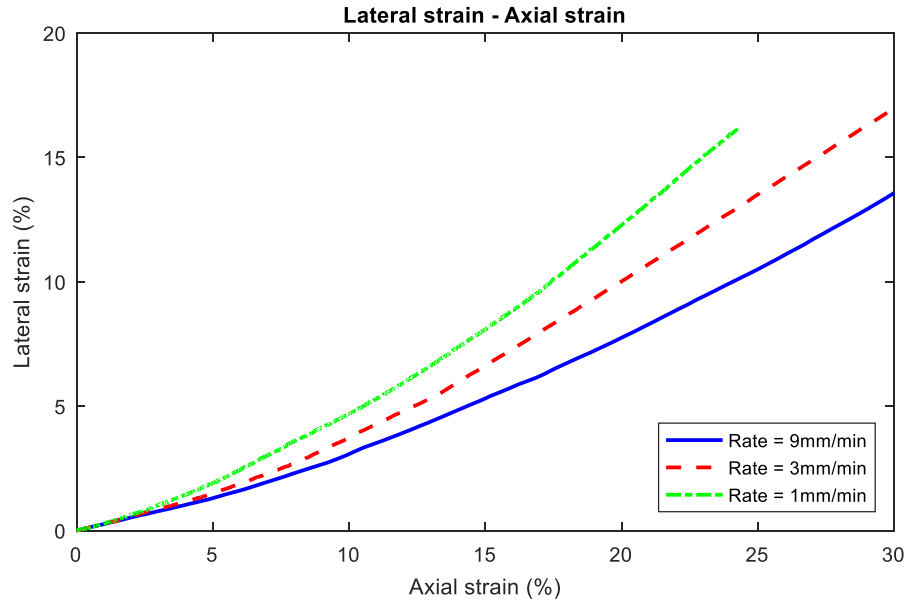

Figure 5.7 Results of UCS tests performed on group KC-05 (T= - 1 °C, Laboratory= BEPL).

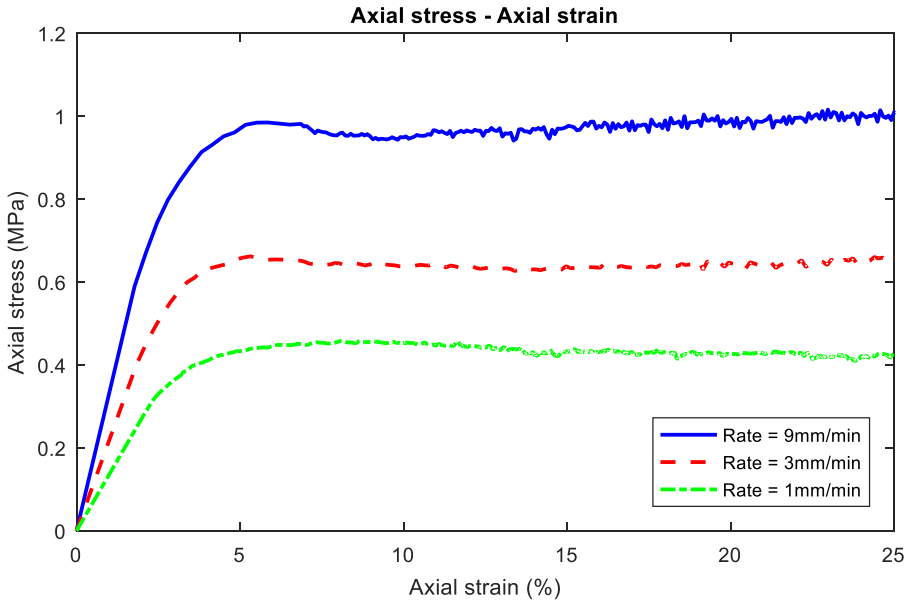

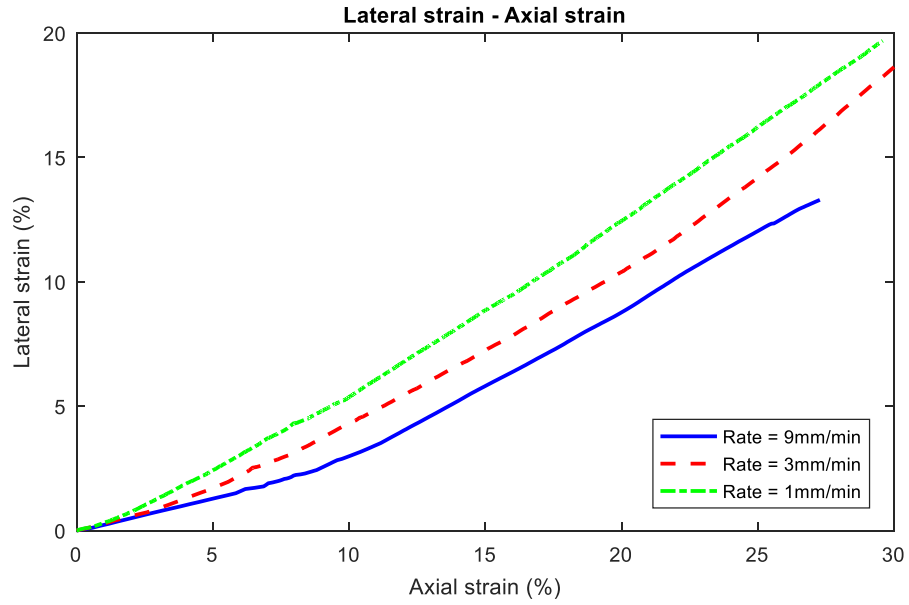

Figure 5. 8 Results of UCS tests performed on group BC-05 (T= - 1 °C, Laboratory= BEPL).

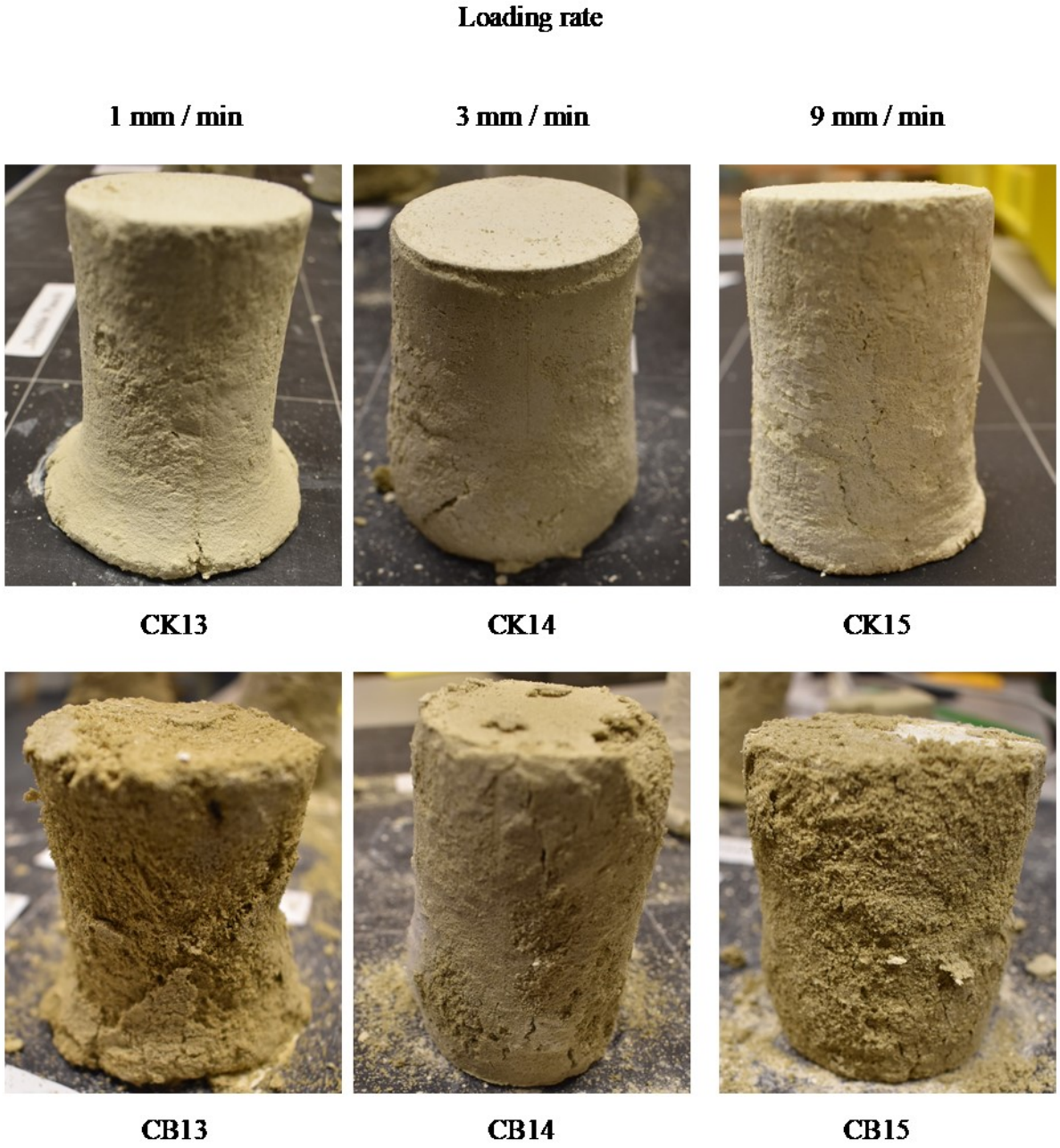

Figure 5.9 Post-failure pictures of UCS tested samples (T= - 1 °C, Laboratory = BEPL).

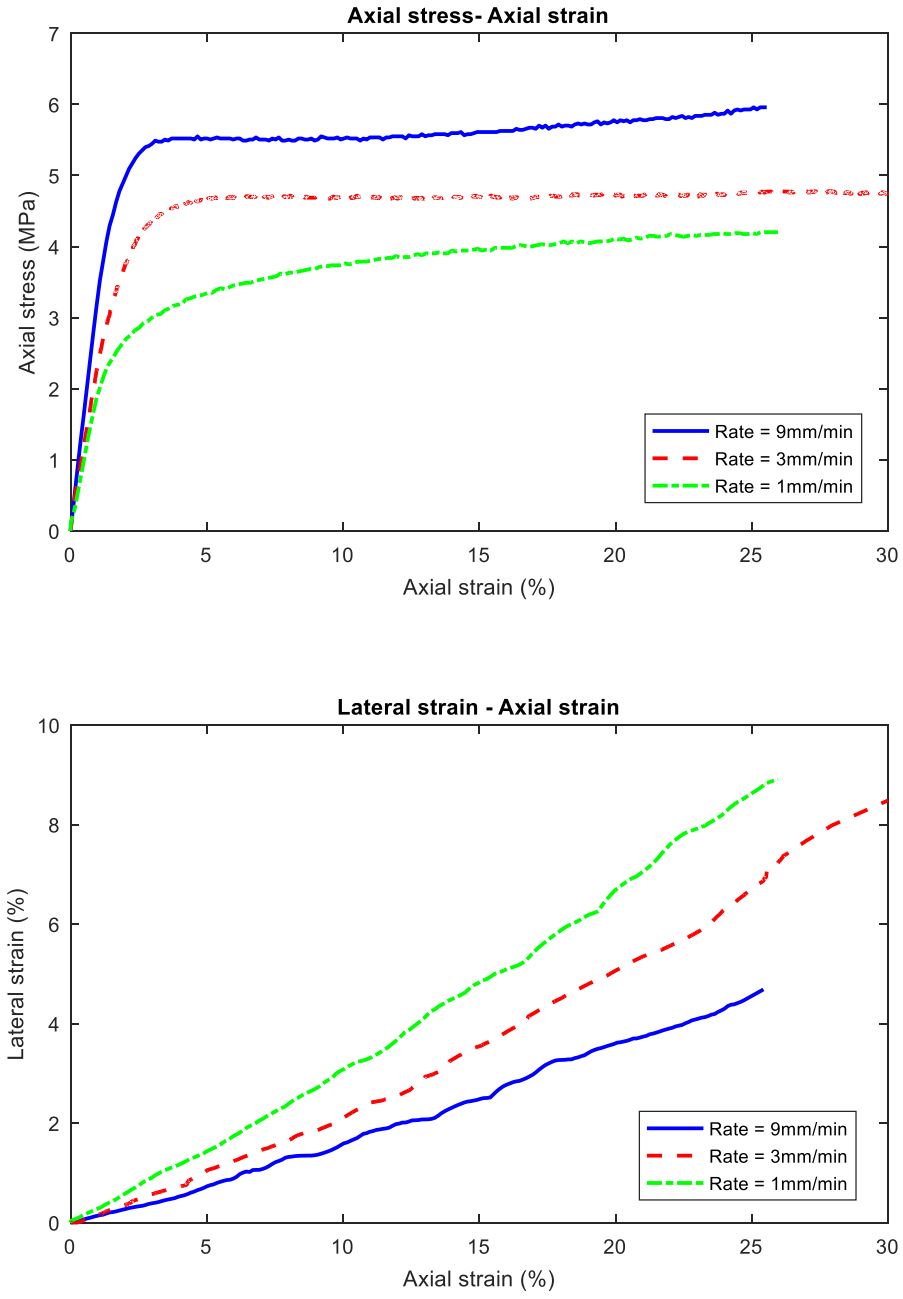

Figure 5. 10 Results of UCS tests performed on group KP-01 (T= - 15 °C, Laboratory= GL).

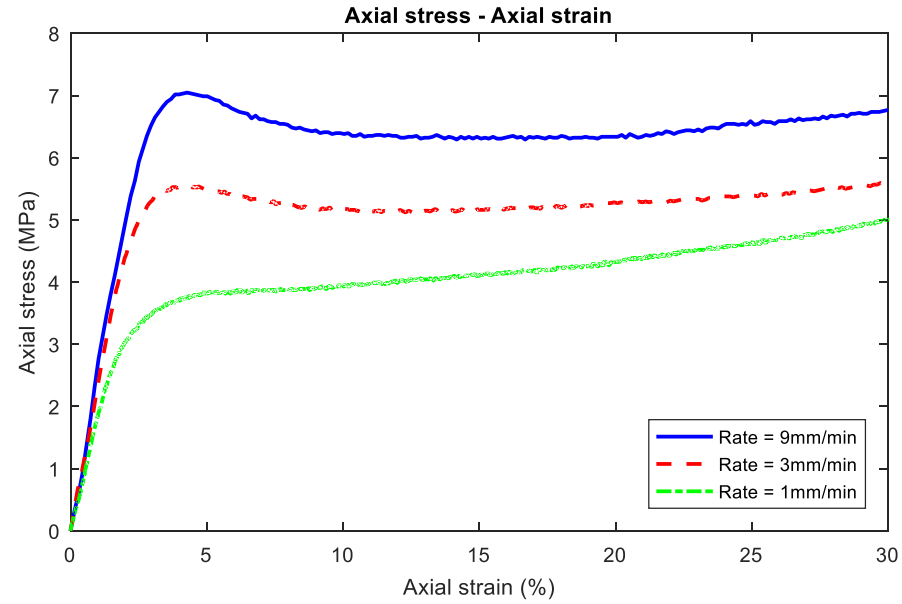

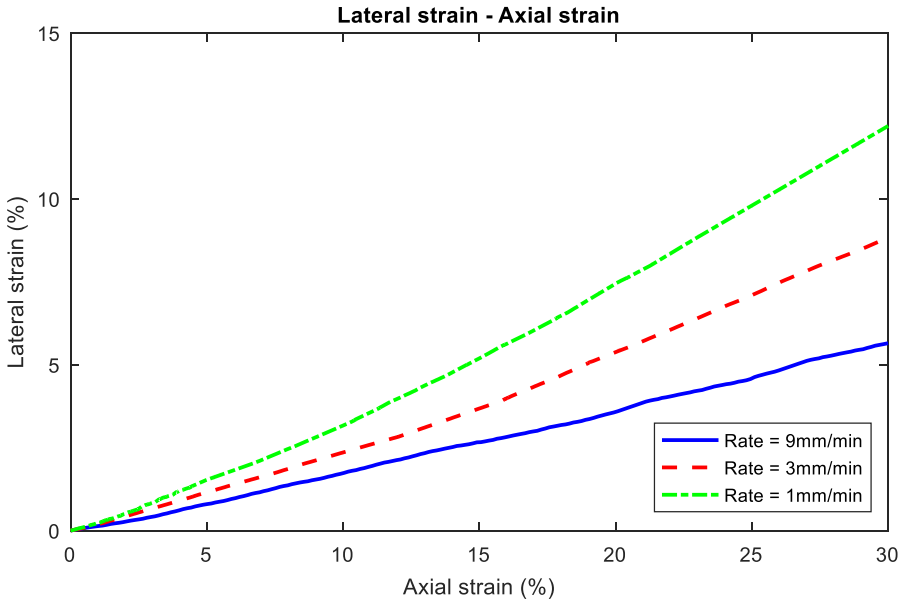

Figure 5. 11 Results of UCS tests performed on group BP-01 (T= - 15 °C, Laboratory= GL).

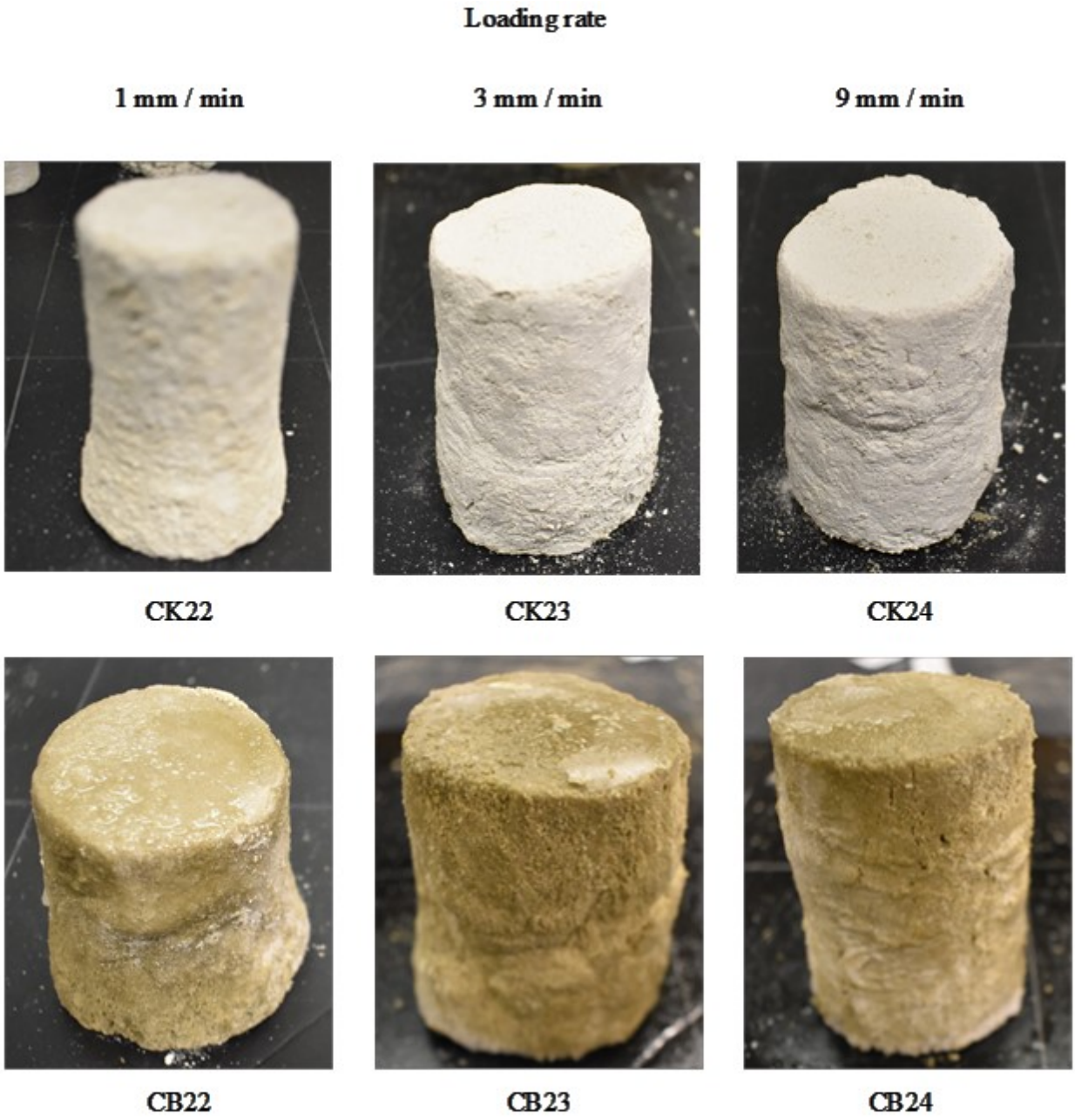

Figure 5. 12 Post-failure pictures of UCS tested samples (T= - 15 °C, Laboratory= GL).

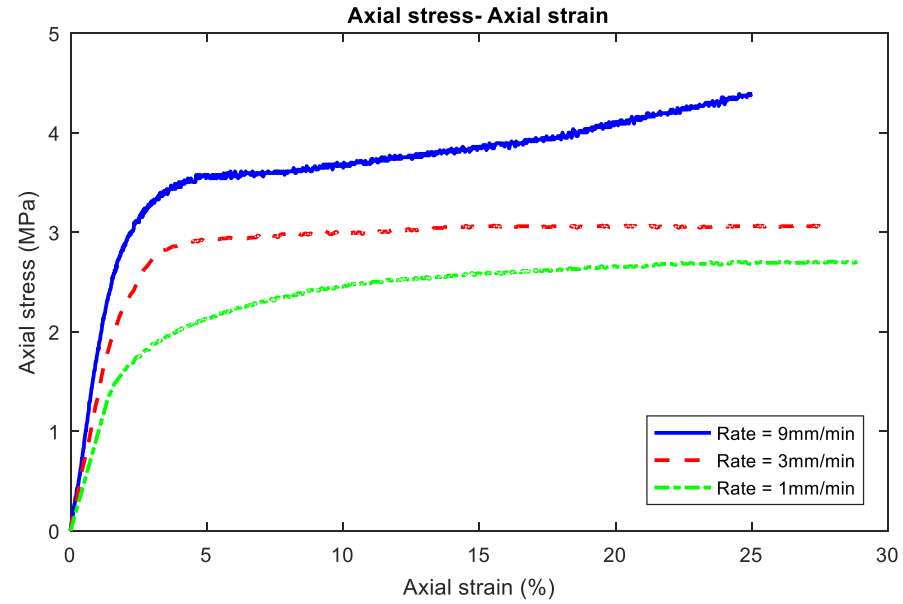

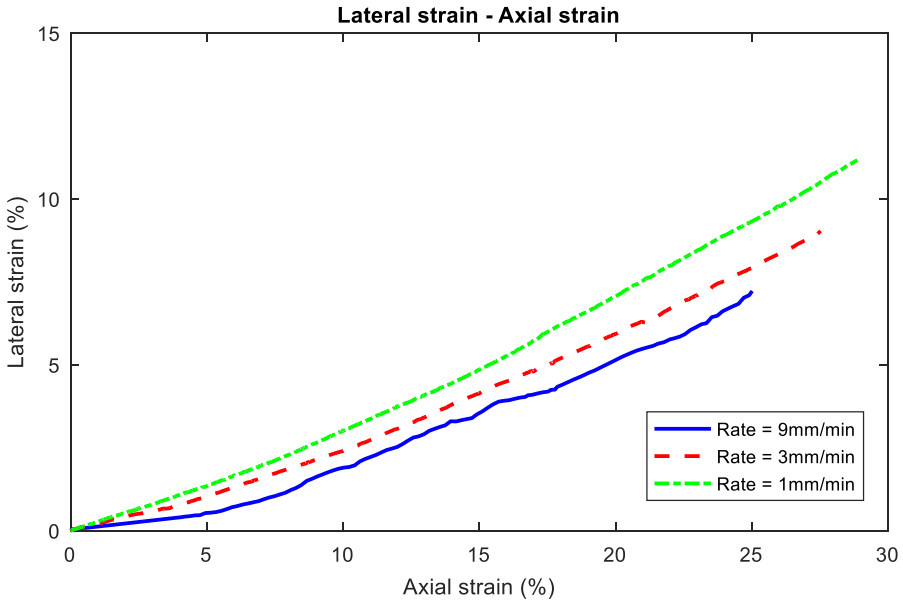

Figure 5. 13 Results of UCS tests performed on group KP-02 (T= - 10 °C, Laboratory= GL).

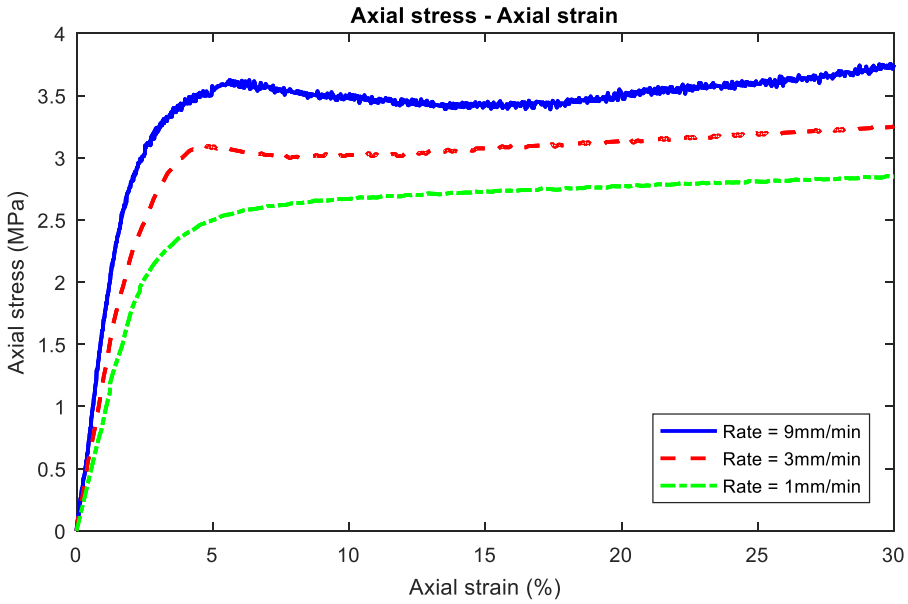

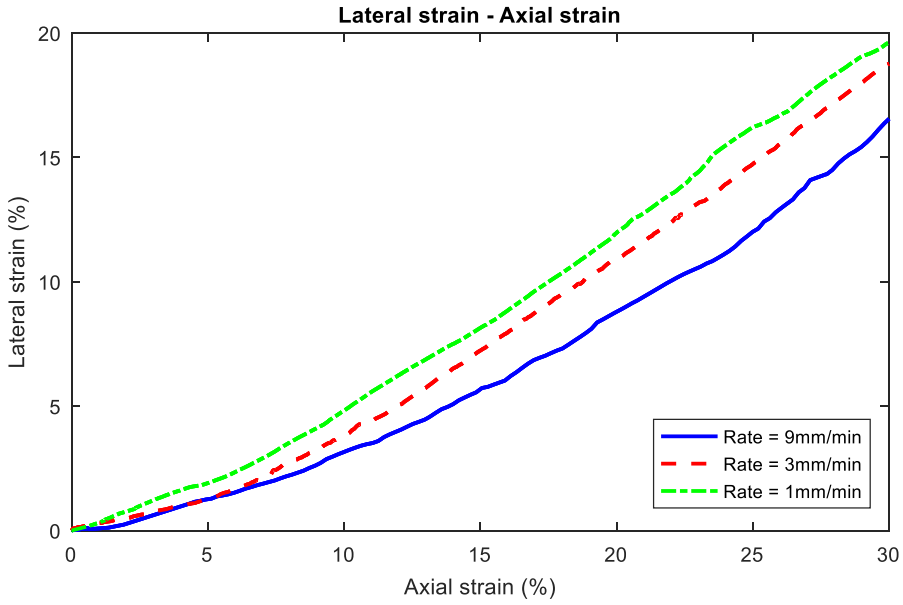

Figure 5. 14 Results of UCS tests performed on group BP-02 (T= - 10 °C, Laboratory= GL).

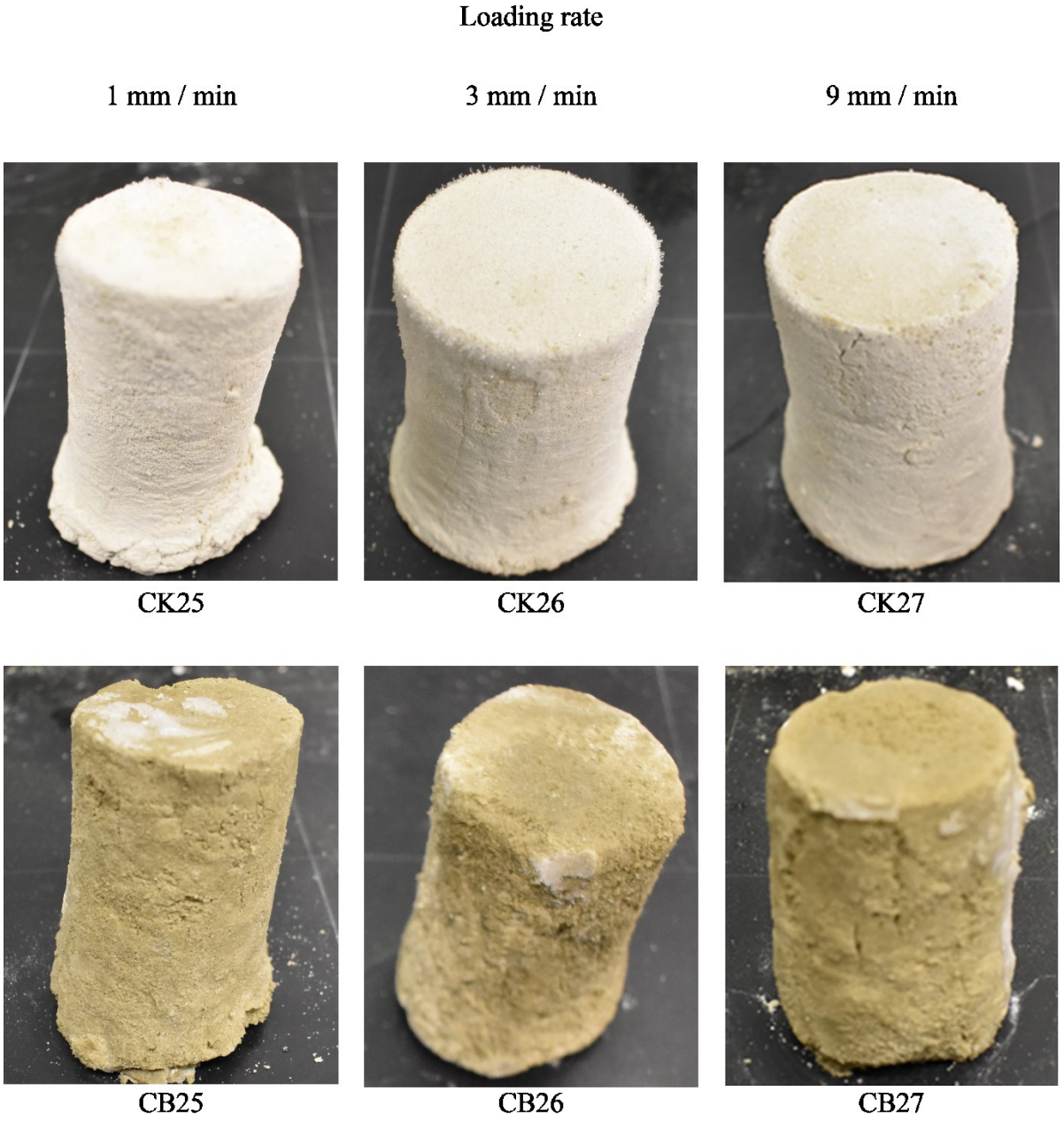

Figure 5. 15 Post-failure pictures of UCS tested samples (T= - 10 °C, Laboratory= GL).

`

The uniaxial compressive stress (σc) is calculated using Equation 5.1 by dividing the applied compressive load by the initial cross-sectional area of the frozen sample, and the uniaxial compressive strength (UCS) is picked from axial stress-axial strain curve at failure as shown in Figure 5.16, and the

$$\sigma c = \frac{P}{\pi b^2} \tag{5.1}$$

where σc is the uniaxial compressive stress of the frozen sample in MPa, P is the applied load at failure in N, and b is the sample radius in mm.

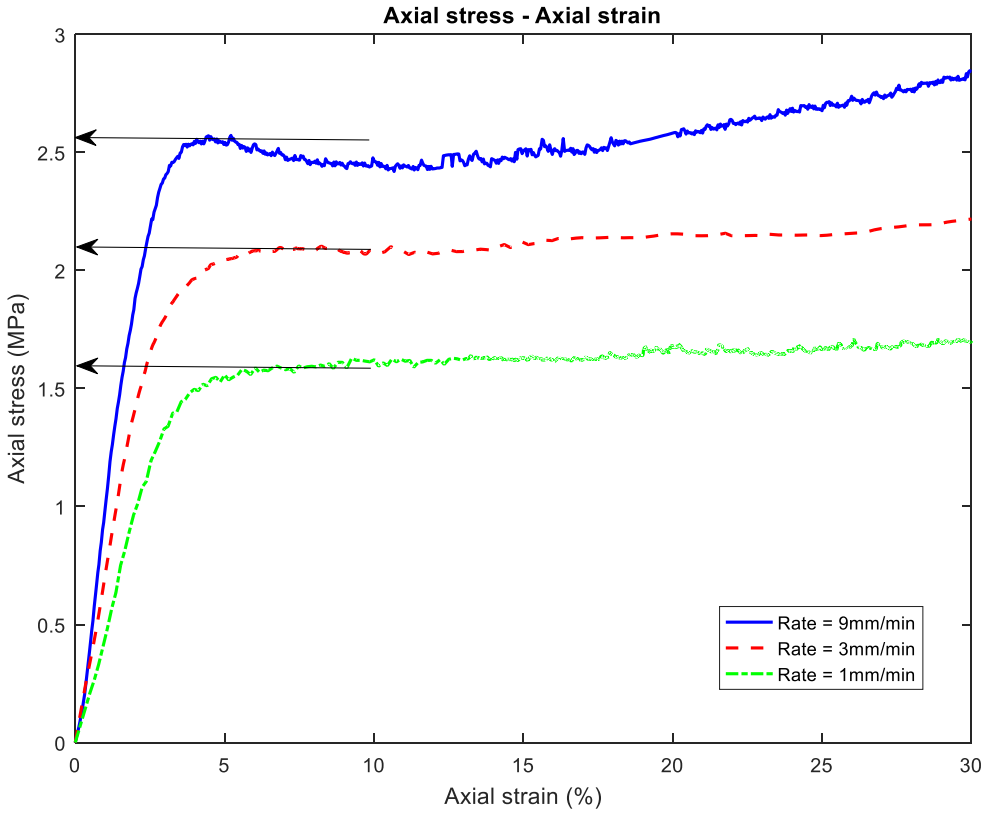

Figure 5. 16 Graph showing the UCS calculation for group BC-03.

Young's modulus, E, can be determined by several methods. In this research, Young's modulus is calculated by the tangent method at fixed stress levels of 50 % of the UCS. The tangent Young's modulus, Et is calculated using Equation 5.2, by dividing the change in stress by the

change in the axial strain at fixed stress levels of 25 % and 75 % to avoid the effect of the nonlinearities at low, high-stress levels. In some cases, at temperatures close to the melting point and low loading rates, the stress level 75 % is replaced by the end of the linear portion such as the samples at – 1 °C as shown in Figure 5.17.

$$Et = \frac{\Delta\sigma c}{\Delta\varepsilon \mathrm{v}} \tag{5.2}$$

where Et is the tangent Young's modulus of the frozen sample in MPa; $\Delta\sigma c$ is the change in applied stress in MPa; $\Delta\varepsilon \mathrm{v}$ is the change in the axial strain.

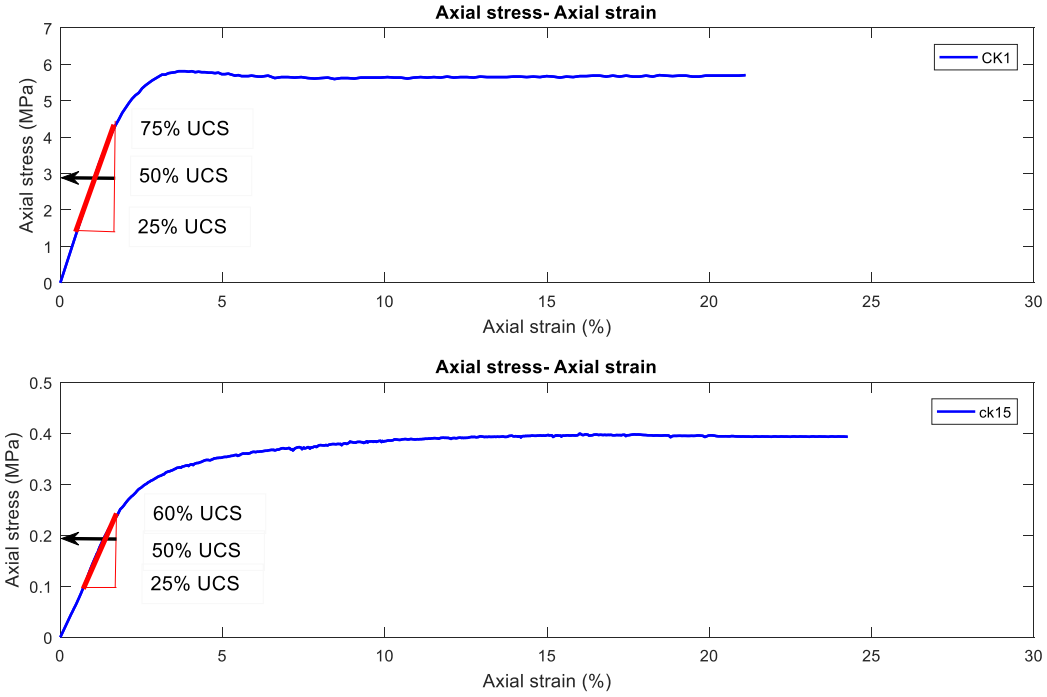

Figure 5. 17 Graph showing tangent Young's modulus calculation.

The value of Poisson's ratio, υ, is calculated by dividing the change in lateral strain by the change in the axial strain as given in Equation 5.3, and the change in the lateral and vertical strain is determined in the same manner as the Young's modulus, Et to obtain more reliable and accurate results.

`

$$\nu = \frac{\Delta\varepsilon l}{\Delta\varepsilon \mathrm{v}} \tag{5.3}$$

where υ is Poisson's ratio; $\Delta\varepsilon l$ is the change in the lateral strain; $\Delta\varepsilon$v is the change in the axial strain.

Table 5. 2 UCS and deformation parameters values for the UCS tested samples

Group	Sample	Temperature (°C)	Lab	Loading rate (mm/min)	UCS (MPa)	E (MPa)	υ
KC-01	CK1	- 15	BEPL	9	5.81	241	0.19
	CK2			3	4.95	192	0.22
	CK3			1	4.09	157	0.25
KC-02	CK4	- 10	BEPL	9	3.94	159	0.20
	CK5			3	3.29	118	0.23
	CK6			1	2.65	92	0.26
KC-03	CK7	- 5	BEPL	9	2.29	81	0.22
	CK8			3	1.81	56	0.25
	CK9			1	1.29	40	0.28
KC-04	CK10	- 2	BEPL	9	1.20	39	0.25
	CK11			3	0.87	26	0.27
	CK12			1	0.59	17	0.31
KC-05	CK13	- 1	BEPL	9	0.83	26	0.27
	CK14			3	0.61	18	0.30
	CK15			1	0.39	12	0.33
KC-06	CK16	- 0.5	BEPL	9	0.63	20	0.29
	CK17			3	0.49	14	0.32
	CK18			1	0.29	10	0.35
KC-07	CK19	0	BEPL	9	0.47	15	0.32
	CK20			3	0.33	12	0.34
	CK21			1	0.20	9	037

`

Group	Sample	Temperature (°C)	Lab	Loading rate (mm/min)	UCS (MPa)	E (MPa)	υ
KP-01	CK22	- 15	GL	9	5.51	247	0.18
	CK23			3	4.68	178	0.23
	CK24			1	4.16	116	0.27
KP-02	CK25	- 10	GL	9	3.54	152	0.19
	CK26			3	2.99	134	0.22
	CK27			1	2.56	77	0.28
BC-01	CB1	- 15	BEPL	9	6.71	258	0.17
	CB2			3	5.38	233	0.21
	CB3			1	4.47	165	0.24
BC-02	CB4	- 10	BEPL	9	4.42	170	0.18
	CB5			3	3.71	145	0.23
	CB6			1	2.98	100	0.25
BC-03	CB7	- 5	BEPL	9	2.57	92	0.20
	CB8			3	2.09	67	0.25
	CB9			1	1.59	47	0.27
BC-04	CB10	- 2	BEPL	9	1.43	43	0.23
	CB11			3	0.95	31	0.26
	CB12			1	0.71	21	0.29
BC-05	CB13	- 1	BEPL	9	0.98	29	0.25
	CB14			3	0.65	20	0.28
	CB15			1	0.45	14	0.30
BC-06	CB16	- 0.5	BEPL	9	0.75	23	0.26
	CB17			3	0.50	15	0.30
	CB18			1	0.39	11	0.32
BC-07	CB19	0	BEPL	9	0.48	17	0.29
	CB20			3	0.42	12	0.33
	CB21			1	0.38	9	0.35

`

Group	Sample	Temperature (°C)	Lab	Loading rate (mm/min)	UCS (MPa)	E (MPa)	υ
BP-01	CB22	- 15	GL	9	7.03	263	0.17
	CB23			3	5.51	227	0.22
	CB24			1	3.81	154	0.25
BP-02	CB25	- 10	GL	9	3.59	148	0.20
	CB26			3	3.09	130	0.24
	CB27			1	2.72	88	0.27

5.3 Factors affecting the UCS

5.3.1 Temperature

It is found that the temperature has a remarkable effect on compressive strength of sandy clay frozen samples, and the UCS of all tested samples increases at the temperature range from - 15 to 0 °C with the decrease in temperature due to the increase in the ice content and strength. For example, kaolinite-sand samples at a loading rate of 9 mm/min, the UCS value increases more than 12 times from 470 kPa at 0 °C to 5810 kPa at - 15 °C, while the UCS of bentonite-sand samples increases by 14 times at a loading rate of 9 mm/min when a temperature drops from - 15 to 0 °C. The failure strain also decreases for the tested sandy clay soils with a decrease in temperature. For kaolinite-sand samples at a loading rate of 9 mm/min, the failure strain values at temperatures of -15 °C and 0 °C are 3.69 % and 6.67 %, respectively; and failure strain decreased by 220 % when the temperature drops from 0 °C to - 15 °C for the bentonite-sand samples at a loading rate of 9 mm/min .

At temperatures above - 15 °C, the unfrozen water content is enough to maintain the plastic behavior of both frozen sandy clay soils. For the bentonite-sand samples at temperatures below - 5 °C and loading rates of 3 and 5 mm/min, an apparent peak compressive strength can be observed with small strain-softening followed by strain hardening, while the behavior of kaolinite-sand samples is close to the ideal plastic behavior as shown in Figure 5.18. The post-peak softening behavior is accompanied by a change in horizontal strain-vertical strain cure due to dilation. At warm temperatures and low loading rates, the vertical stress-vertical strain becomes linear elastic trend followed by a strain-hardening behavior without a post-peak softening behavior.

`

From Figure 5.6, kaolinite-sand and bentonite-sand samples display similar failure modes under different loading rates at a temperature of - 15 °C, while the samples display a viscoplastic behavior at - 1 °C which is reflected by the large lateral deformation near to the bottom platen as shown Figure 5.9.

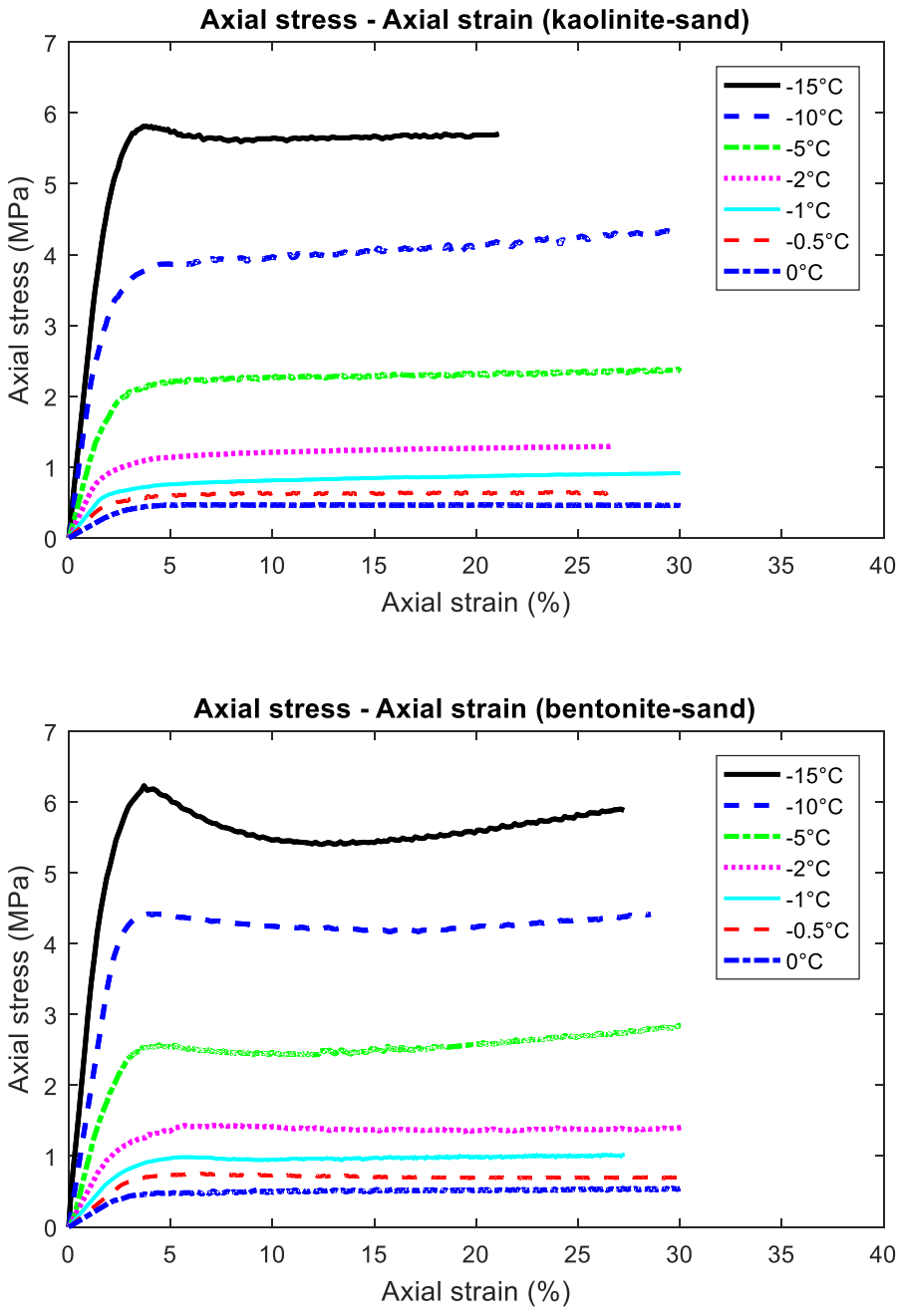

Figure 5. 18 The axial stress-axial strain curves of the tested samples at a loading rate of 9 mm/min.

`

Figures 5.19 and 5.20 show a good correlation between the temperature and UCS for both kaolinite-sand and bentonite-sand samples in a temperature range from - 15 to 0 °C and loading rates of 1, 3, and 9 mm/min, and power-law equations are effective for all correlations. The UCS-temperature curve shows a non-linear behavior due to the quick growth in the ice matrix followed by a transition region, then the relationship between the UCS and temperatures becomes almost a straight line. The limits of each stage depend on several parameters such as soil type, unfrozen water content, and loading rate. For kaolinite-sand, the UCS-temperature curve becomes a straight line at temperatures between - 2 and - 5 °C, while UCS-temperature relationship for bentonite-sand samples is almost a straight line at temperatures below - 5 °C. Also, the effect of loading rate can be reflected by the increase in values of the coefficient A of the power-law equation.

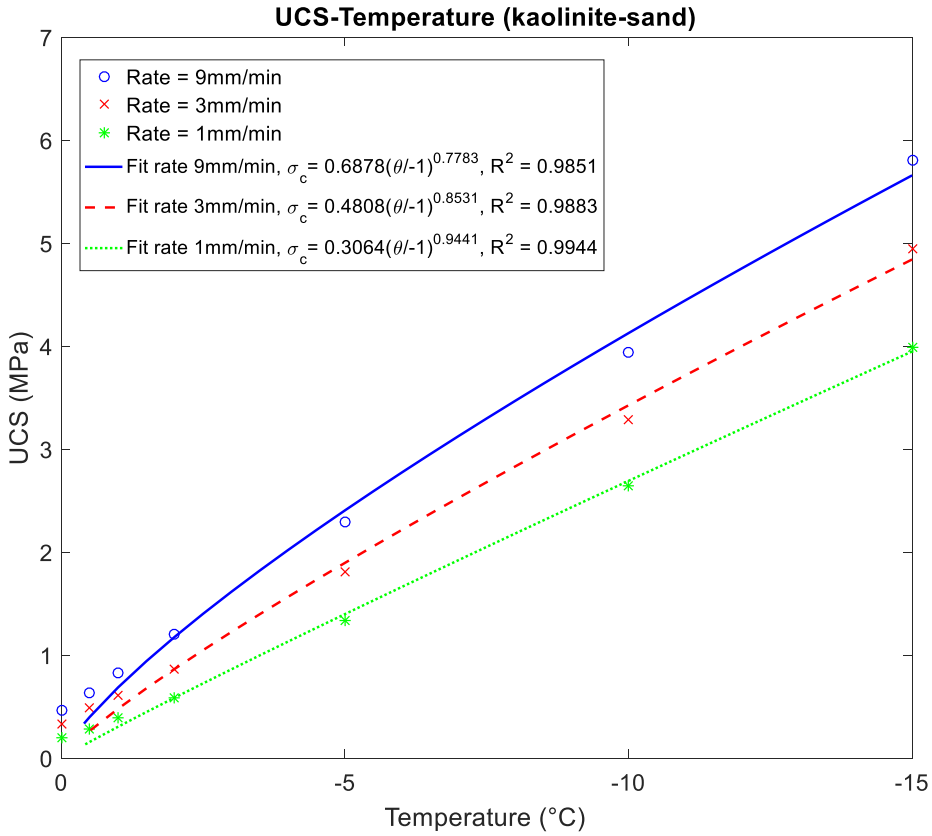

Figure 5.19 Curves showing the correlation between UCS and temperature for kaolinite - sand samples (Laboratory= BEPL).

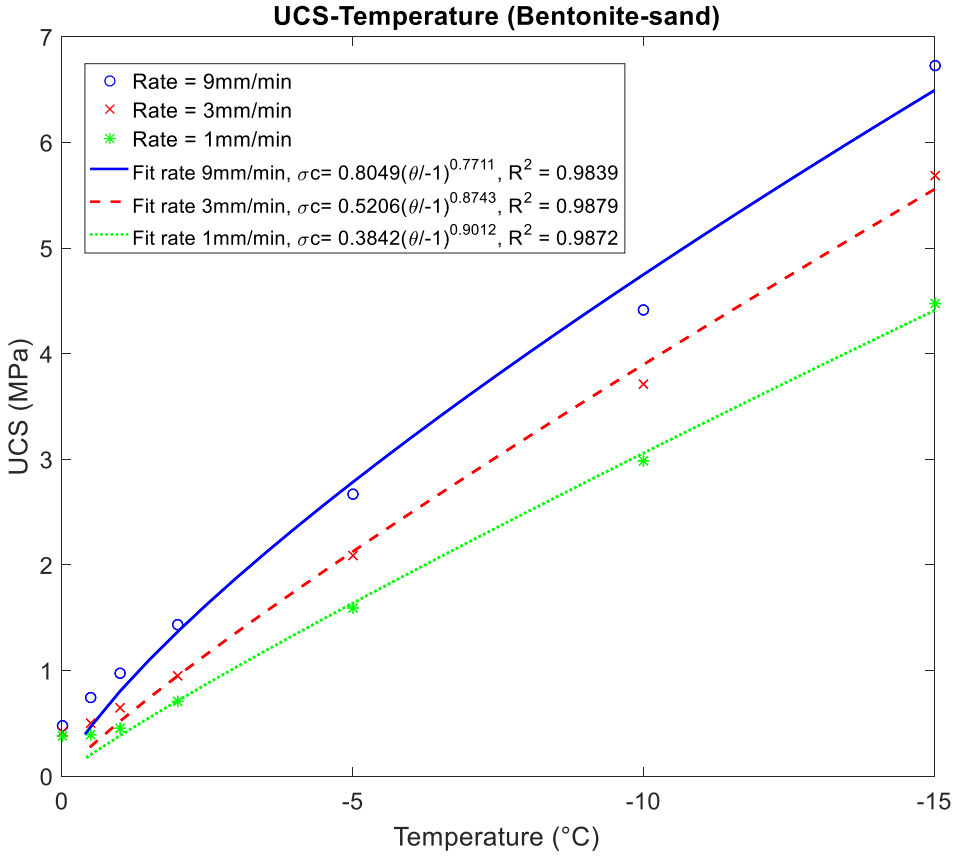

Figure 5.20 Curves showing the correlation between UCS and temperature for bentonite-sand samples (Laboratory= BEPL).

5.3.2 Loading rate

The loading rate affects the UCS of the tested frozen sandy clay soils at a temperature range of - 15 to 0 °C due to the presence of unfrozen water. For the kaolinite-sand samples at a temperature of -1 °C, the UCS values increase by 213 % and 136 % at loading rates of 9 and 3, respectively compared to the UCS at 1mm/min (see Figure 5.7). The UCS values of bentonite-sand samples at - 15 °C are 6.71, 5.38, and 4.47 MPa corresponding to loading rates of 9, 3, and 1 mm/min, respectively as shown in Figure 5.5.

The loading rate also influences both the deformation and failure behavior of frozen sandy clay soils. No brittle failure is observed during the UCS tests in a temperature range from - 15 to 0 °C and loading rates of 1, 3, 9 mm/min. Only a stress-strain curve with a peak and small strain-

softening are observed only at a loading rate of 9 mm/min and a temperature of - 15 °C for the kaolinite-sand samples, and at loading rates of 3 and 9 mm/min and temperatures below - 5 °C for the bentonite-sand samples. The increase in loading rate improves the stiffness of the tested samples, which is manifested in the increase of the axial stress-axial strain curve slope, as shown in Figures from 5.4 to 5.9.

The power-law relationship between strain rates and the UCS is linearized on the log-log plot to investigate the impact of strain rate on the UCS at different temperatures, as shown in Figure 5.21. The strain rates influence the UCS of frozen kaolinite-sand, but this effect is temperature-dependent. Generally, the relation between UCS and the strain rate is a broken-line graph with a slope break at a strain rate of 0.0295 S^{-1}, and the part of lower strain rates has a slope steeper than that of higher strain rate, but the relation becomes almost a straight line at temperatures below –10 °C as shown in Figure 5.21.

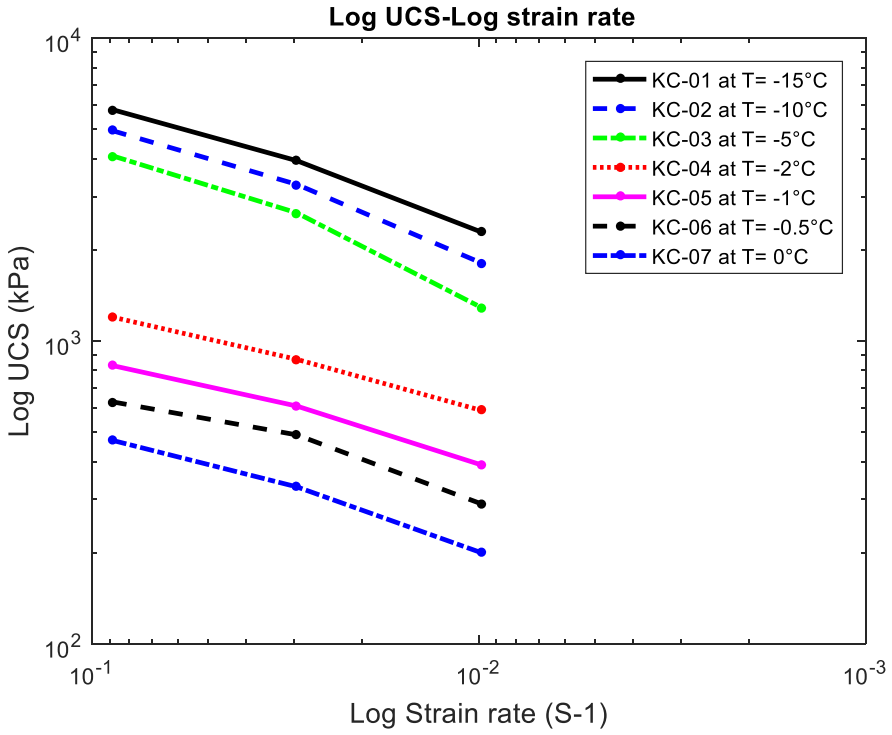

Figure 5. 21 Log-log plot of UCS- strain rate curves of kaolinite-sand samples at a temperature range from - 15 to 0 °C (Laboratory= BEPL).

`

5.3.3 Clay mineralogy

The UCS of frozen soil depends on various parameters such as the grains surface area and size distribution, the density, the mineralogical composition, and the chemical composition of the soil. In this research, the UCS tests are performed on both kaolinite-sand and bentonite-sand frozen soil to investigate the influence of clay mineralogy on UCS.

The results of the UCS tests show that the UCS values of bentonite-sand samples are higher than that for kaolinite-sand samples in the temperature range from - 15 °C to 0 °C and loading rates of 1, 3, and 9 mm/min due to the higher cohesion and the ice content. The bentonite-sand samples display more brittle behavior with a peak and strain-softening below - 5 °C, while the brittle behavior is observed at temperature - 15 °C for kaolinite-sand samples. From Figure 5.22, the ratio of the UCS of bentonite-sand samples to kaolinite-sand samples is 15 % at temperatures of - 15 °C and loading rate of 9 mm/min, while it is 27 % at temperatures of 0 °C and loading rate of 3 mm/min.

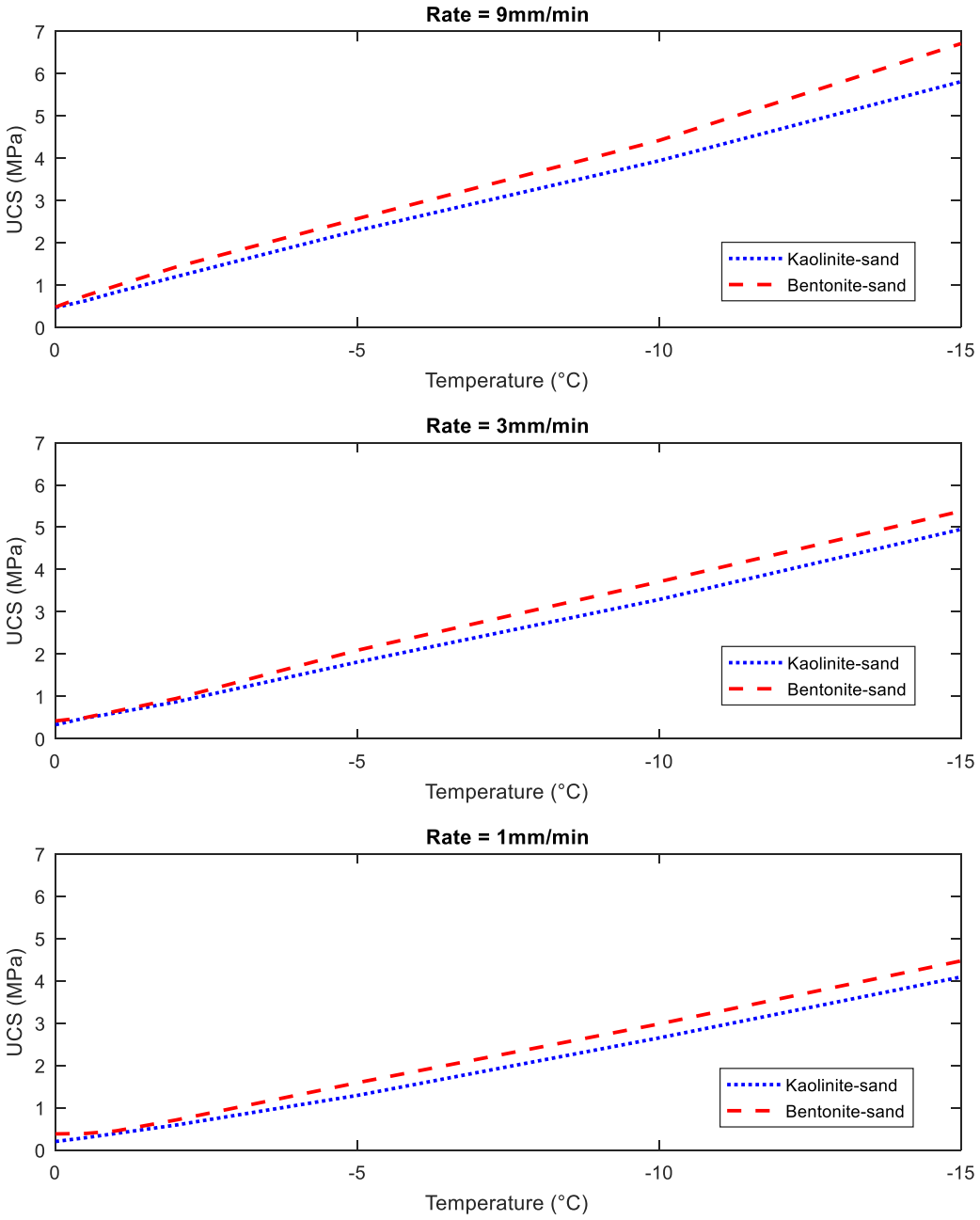

Figure 5. 22 The UCS-temperature curves at a temperature range from - 15 to 0 °C (Laboratory= BEPL).

`

5.3.4 Setup used

The UCS tests are performed in two laboratories using two different setups. The UCS tests take place in BEPL at Concordia University laboratory inside a large environmental chamber provided with a small accurate loading device with a maximum capacity of 15 kN and PC monitor to control the test from the environmental chamber. On the other hand, while the setup used in GL at Polytechnique Montréal composed of a freezing unit connected to cooling system via a flexible duct, and the cell is placed through a loading device of 100 kN capacity.

For the former setup, all samples are placed inside the chamber at the test temperature, and the surface preparation is done in the chamber before testing if needed, so there is no additional time for the adaptation nor thermal disturbance. For the latter setup, the samples need enough time not less than one hour after putting in the freezing cell to avoid any effect of the thermal disturbance during transferring and positioning into the freezing cell.

The results of both laboratories show that there is no significant difference in the UCS values obtained from both laboratories, and the difference between UCS values decreases by the decrease in temperature and the increase in loading rate. The kaolinite-sand samples show more sensitive to thermal disturbance than bentonite-sand samples. Figure 5.23 shows the results of UCS tests performed in both laboratories for kaolinite-sand samples, and the ratio between the UCS obtained from BEPL to GL is 103 % at - 15 °C and a loading rate of 1 mm/min, while it increased 109 % at - 10 °C and a loading rate of 9 mm/min. For bentonite-sand samples tested in BEPL and GL, the UCS values at - 15 °C and a loading rate of 9 mm/min are 6.71 and 7.04 MPa, respectively; while UCS values at a temperature of - 10 °C and a loading rate of 3 mm/min are 3.71 and 3.17 MPa, respectively (see Figure 5.24).

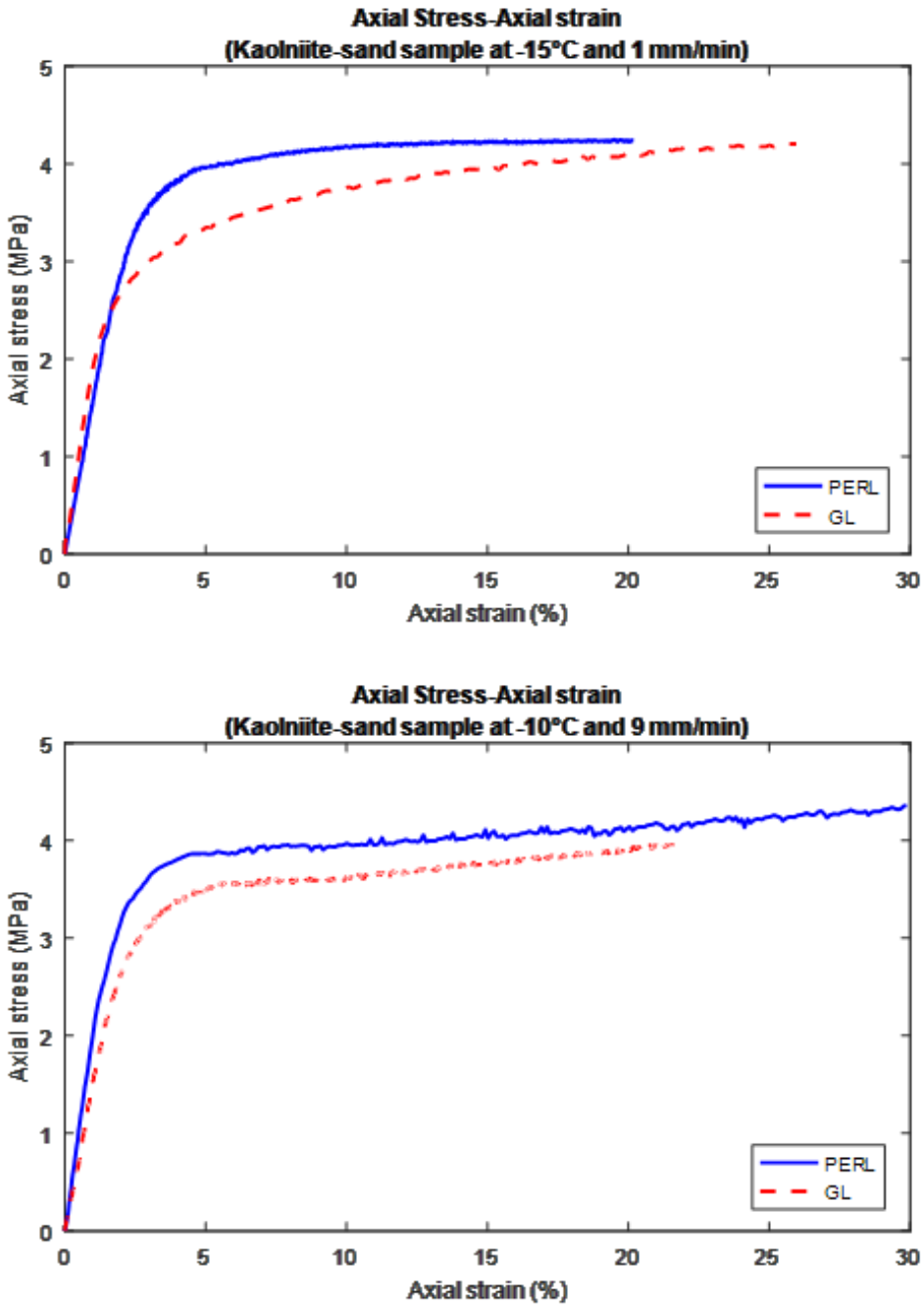

Figure 5. 23 Axial stress-axial strain curve of kaolinite-sand samples at BEPL and GL laboratories.

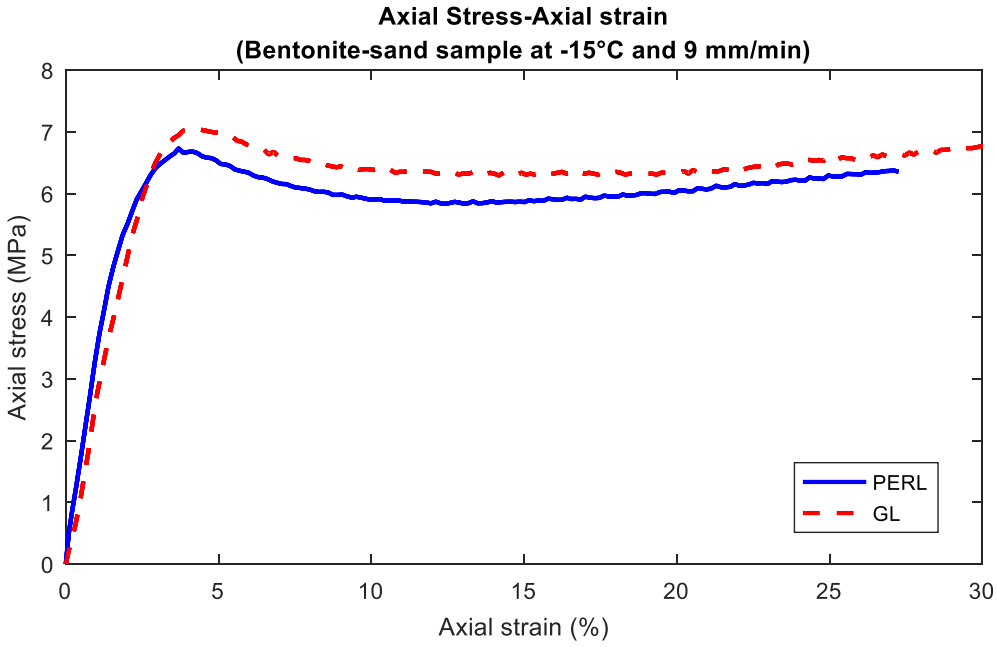

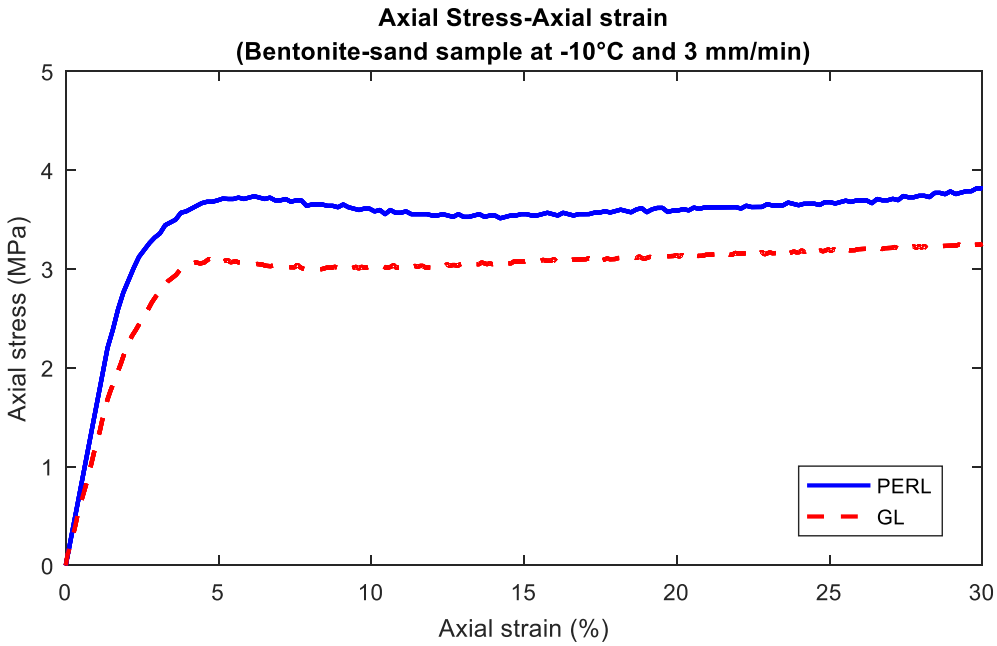

Figure 5.24 Axial stress-axial strain curve of bentonite-sand samples at BEPL and GL laboratories.

`

5.4 Temperature-dependent elastic deformation parameters

Young's modulus, E and Poisson's ratio, υ are important stiffness parameters that are used in settlement calculation and the elastic deformation analysis. The tangent method is used to calculate Young's modulus, E, and Poisson's ratio at 50 % of the UCS, as mentioned in section 5.3. Their values are found to be sensitive to the temperature of the soil, loading rate, and the soil type.

The values of Young's modulus, E, and Poisson's ratio, υ are found to be strongly dependent on temperature. The value of Young's modulus for the kaolinite-sand sample at - 15 °C increased by 1200 % compared to its value at - 0.5 °C and a loading rate of 9 mm/min as shown in Figure 5.25, while the value of Young's modulus for bentonite-sand sample at - 15 and - 0.5 °C are 258 MPa and 23 MPa, respectively at a loading rate of 9 mm/min (see Figure 5.26). Poisson's ratio value decreased from 0.29 at - 0.5 °C to 0.19 at - 15 °C at a loading rate of 9 mm/min for kaolinite-sand samples, whereas the value of Poisson's ratio for bentonite-sand samples decreased by 35 % when the temperature decreased from - 0.5 °C to - 15 °C at same loading rate of 9 mm/min as shown in figures 5.25 and 5.26.

Also, the loading rate has a strong effect on Young's modulus and Poisson's ratio at a certain temperature. For the kaolinite-sand sample at - 15 °C, the value of Young's modulus is 241 MPa at a loading rate of 9 mm/min compared to 157 MPa at a loading rate of 1 mm/min (see Figure 5.25). Poisson's ratio value for bentonite-sand samples at - 10 °C and loading rates of 9 and 1 mm/min are 0.18 and 0.25, respectively, as shown in Figure 5.26.

From Figures 5.25 and 5.26, the bentonite-sand samples have higher values of Young's modulus, E compared to kaolinite-sand samples, whereas the values of Poisson's ratio values for bentonite-sand samples are lower than kaolinite-sand samples.

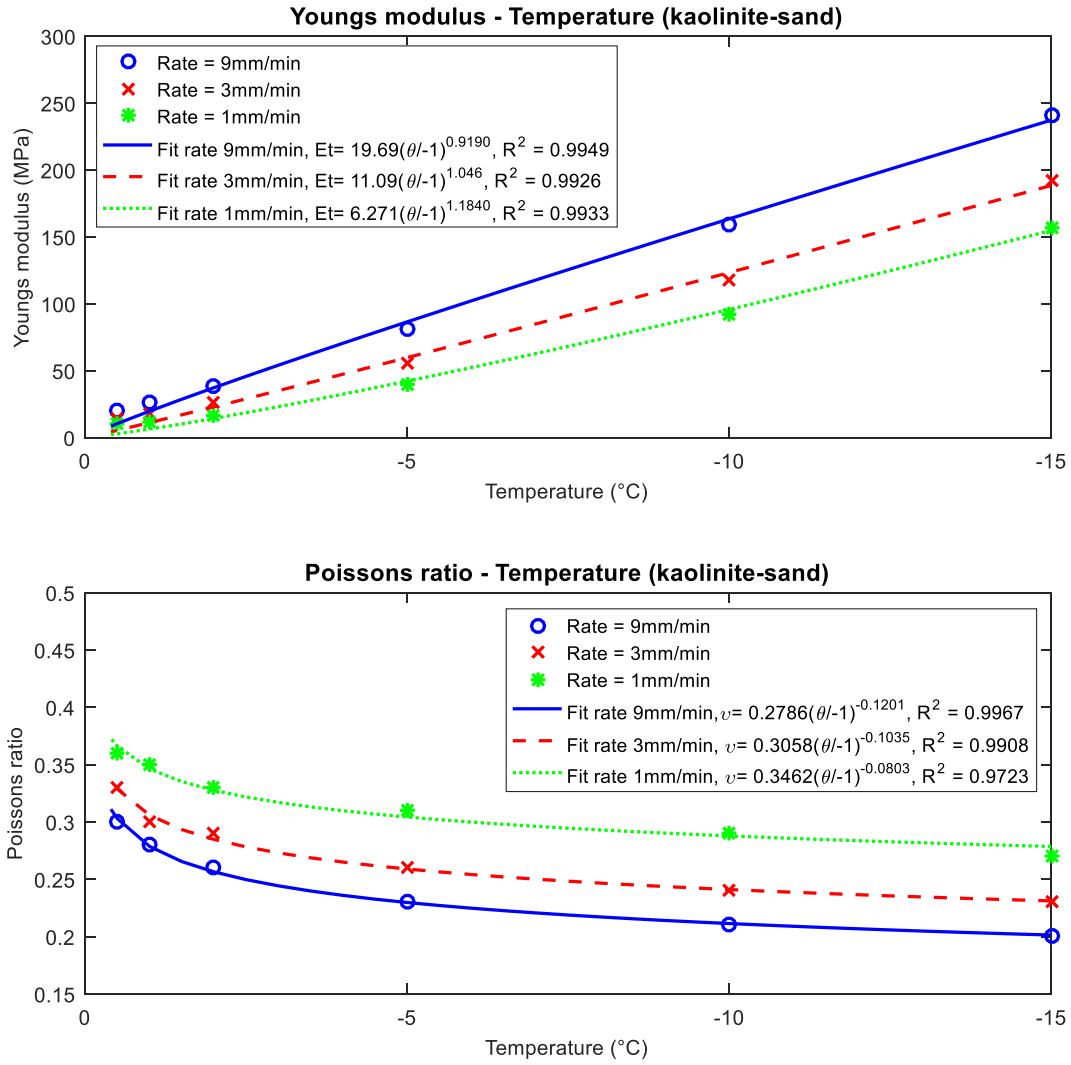

Figure 5. 25 Curves showing the correlation between elastic deformation parameters and temperature of kaolinite-sand samples.

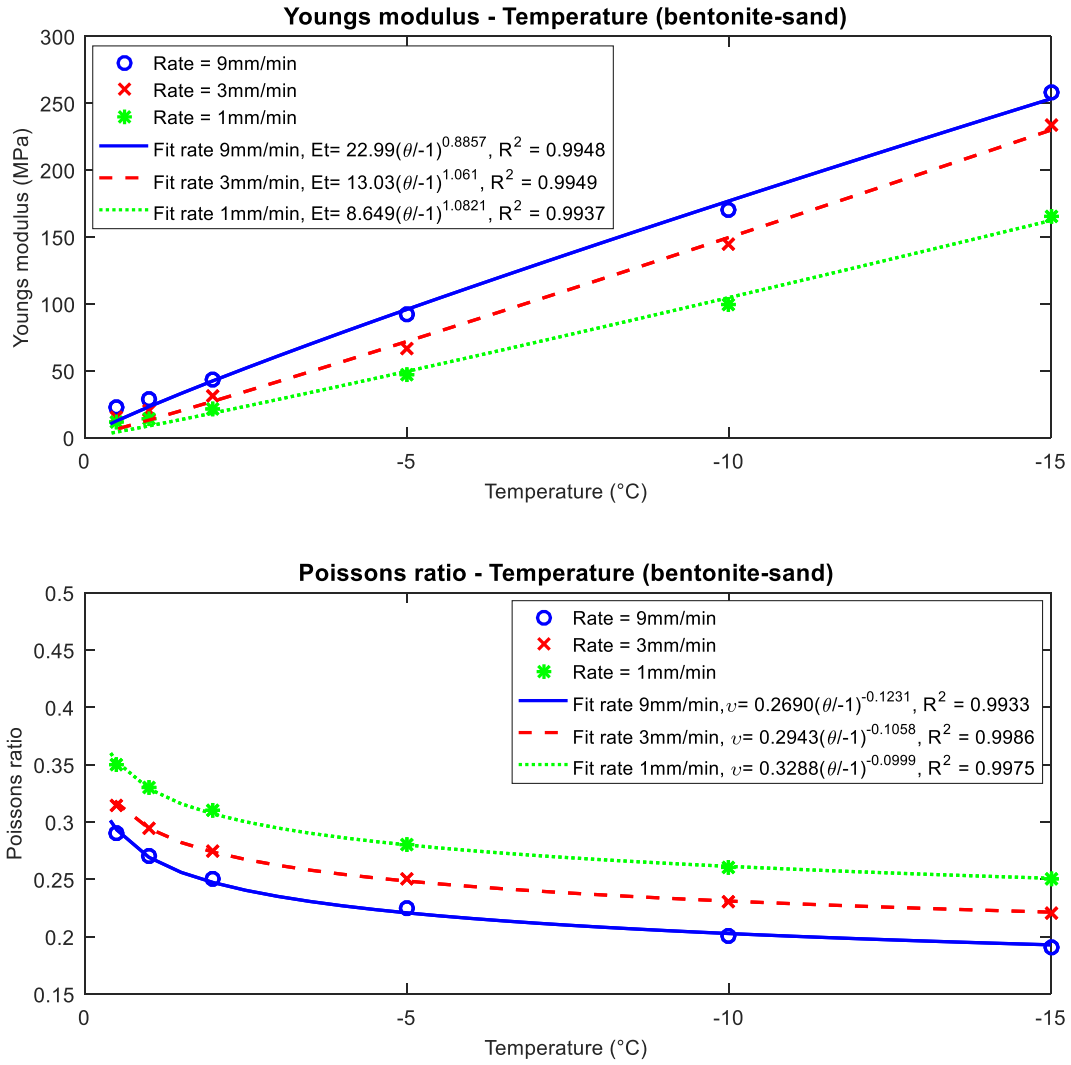

Figure 5. 26 Curves showing the correlation between elastic deformation parameters and temperature of bentonite-sand samples.

`

5.5 Stress relaxation test

The stress relaxation is a time-dependent reduction in stress under a constant strain due to soil creep. From the previous definition, the stress relaxation test is the opposite of the creep test in which the strain is constant, while the stress is recorded against time. Therefore, the stress relaxation test is a good alternative to the conventional creep test, because there is no flow due to the controlled strain and the stress redistribution associated with the previous loading steps are considered as well.

A series of sixteen uniaxial compression stress relaxation (UCSR) tests are performed on both kaolinite-sand and bentonite-sand samples in BEPL of Concordia University using the same setup and procedure of the UCS test. The UCSR tests are performed at three different stress levels of 25, 50, and 75 % of its UCS, at four temperatures of - 1, - 5, - 10, and – 15 °C, and under loading rates of 1 and 9 mm/min to investigate the various parameters affecting the relaxation test.

The results of UCSR tests are divided into two groups according to the soil type, and the details of the kaolinite-sand group are recorded in Tables 5.3, while Table 5.4 shows the details of the kaolinite-sand group. The stress-strain curve and axial stress-time curves for all tested samples at temperatures -15 and -1°C are shown in Figures from 5.27 to 5.34, while the results of the other groups are shown in Figures form B 72 and B 79.

Table 5.3 Details of the stress relaxation test for kaolinite-sand samples

Group	Temperature	Test	Loading rate
CK28	-15	UCSR	1 mm/min
CK29	-15	UCSR	9 mm/min
CK30	-10	UCSR	1 mm/min
CK31	-10	UCSR	9 mm/min
CK32	-5	UCSR	1 mm/min
CK33	-5	UCSR	9 mm/min
CK34	-1	UCSR	1 mm/min
CK35	-1	UCSR	9 mm/min

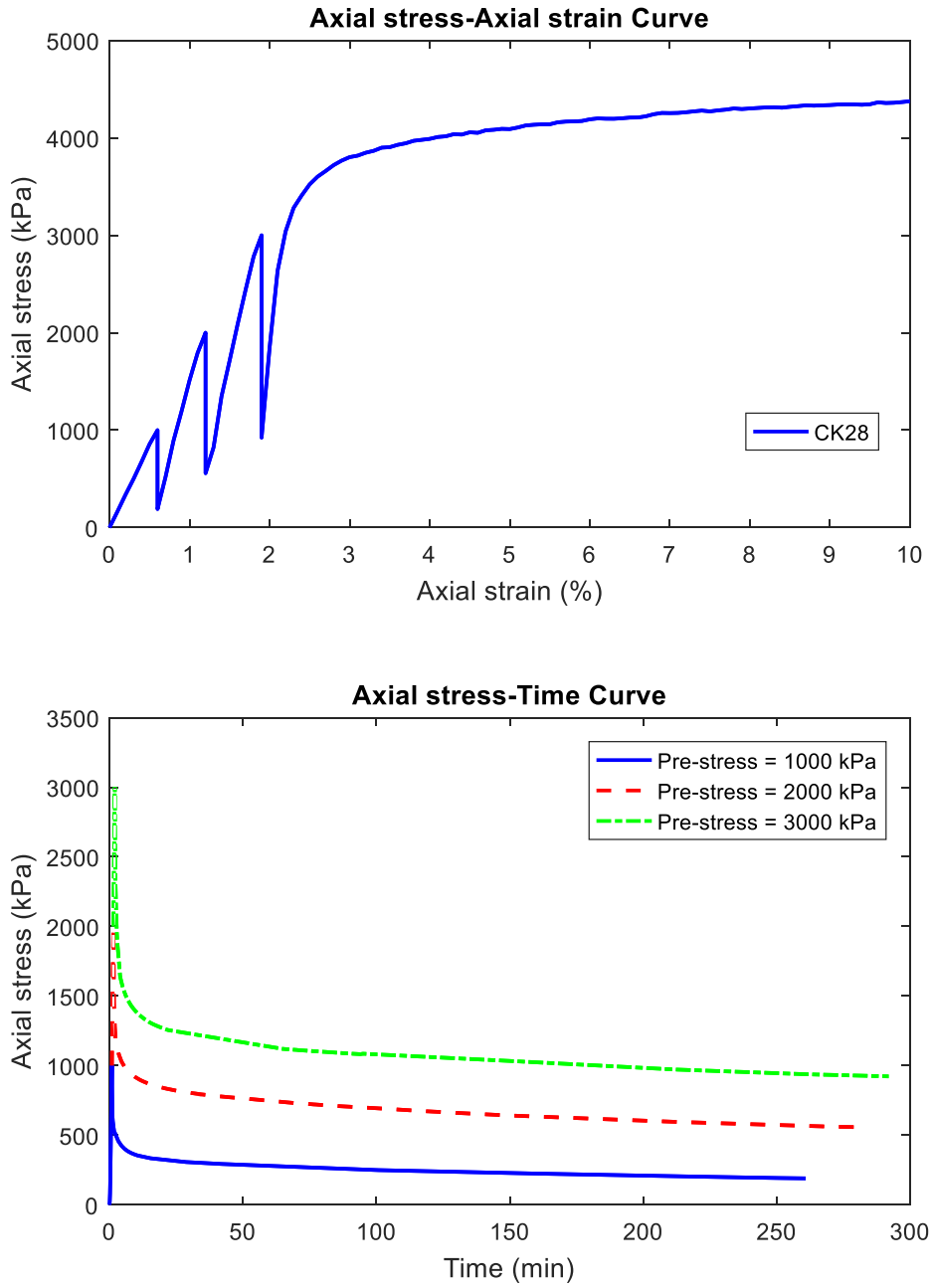

Figure 5. 27 Results of the stress relaxation test performed on sample CK28 (T= - 15 °C and Loading rate= 1 mm/min).

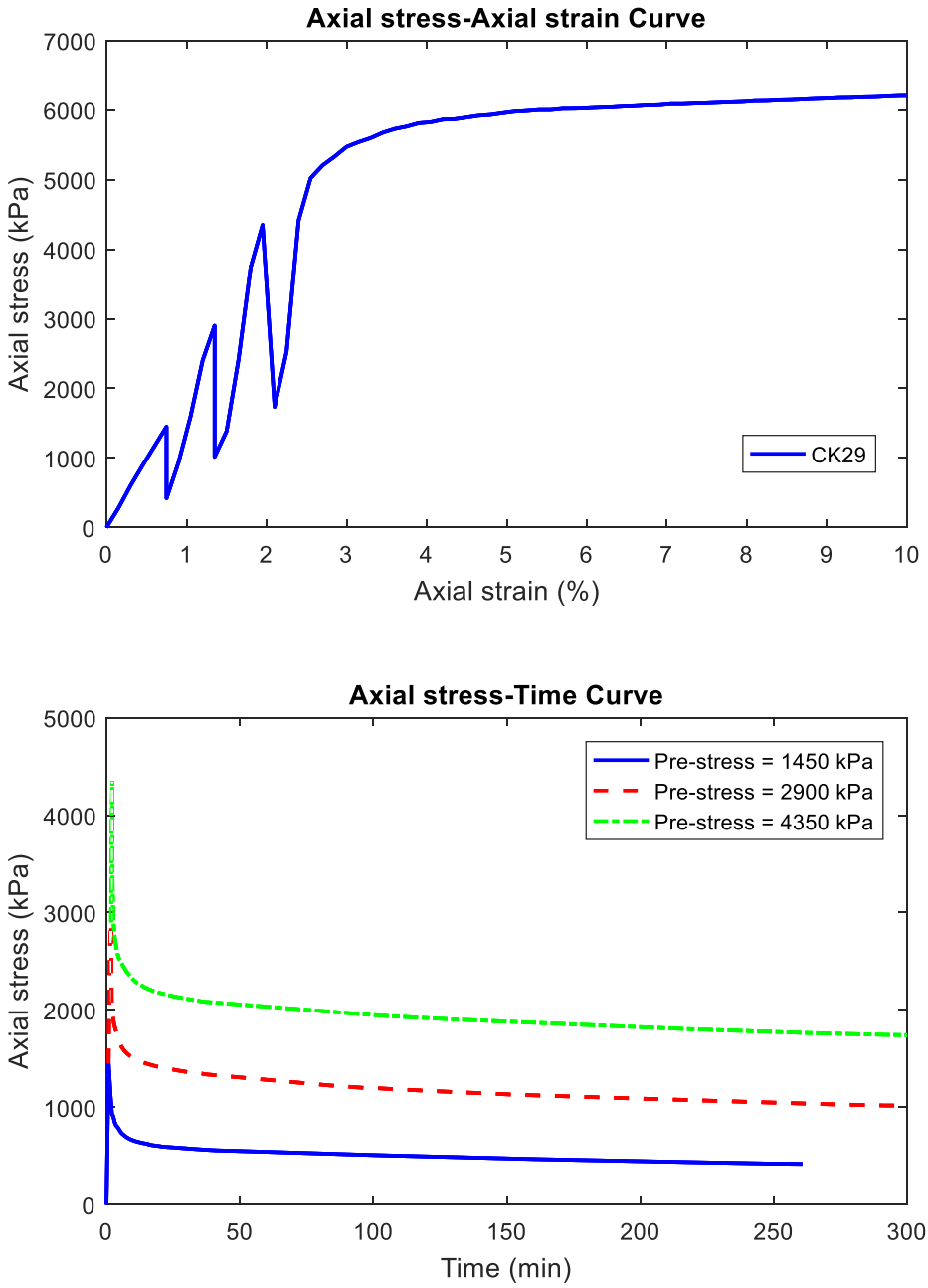

Figure 5. 28 Results of the stress relaxation test performed on sample CK29 (T= - 15 °C and Loading rate= 9 mm/min).

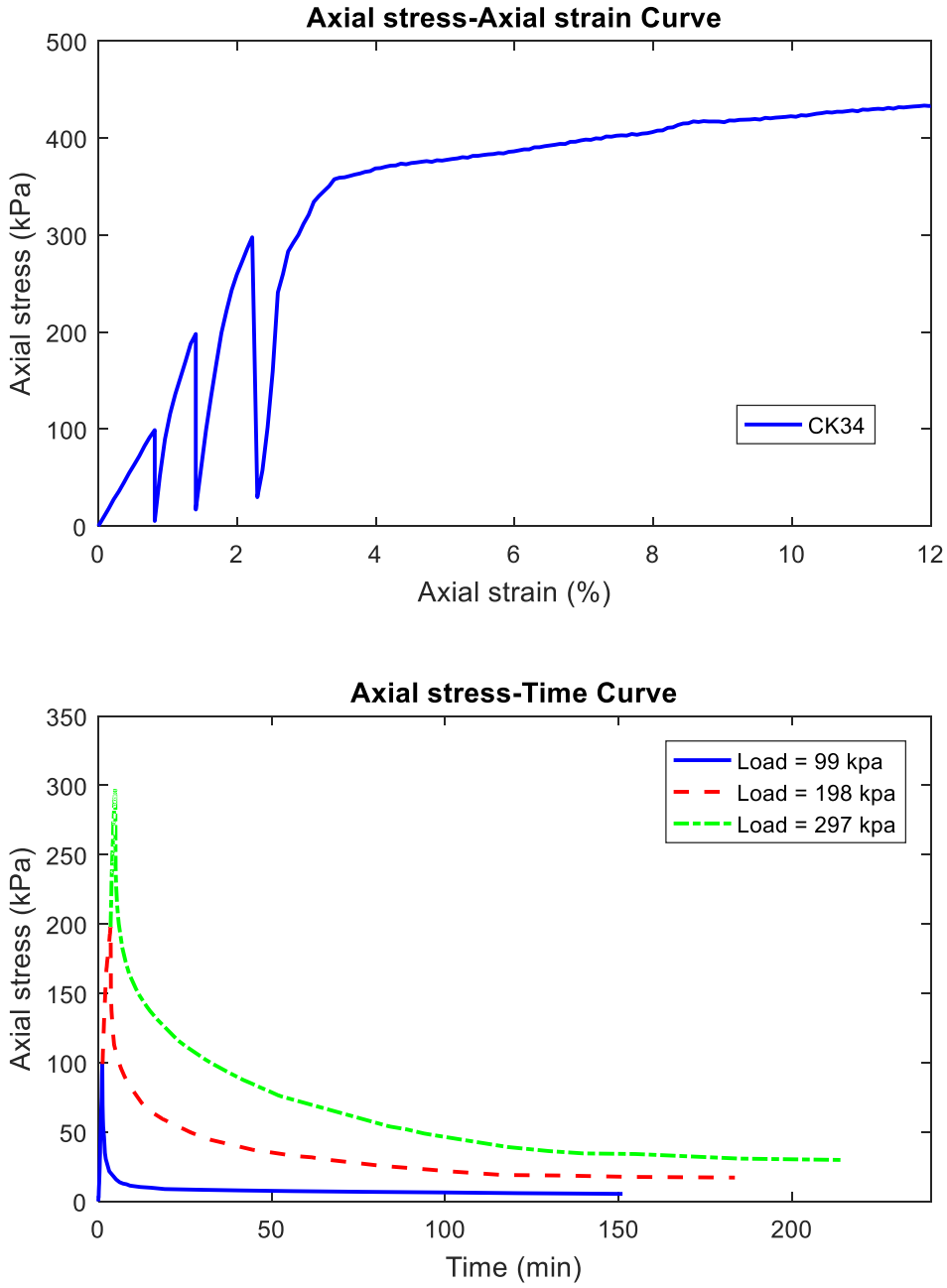

Figure 5. 29 Results of the stress relaxation test performed on sample CK34 (T= - 1 °C and Loading rate= 1 mm/min).

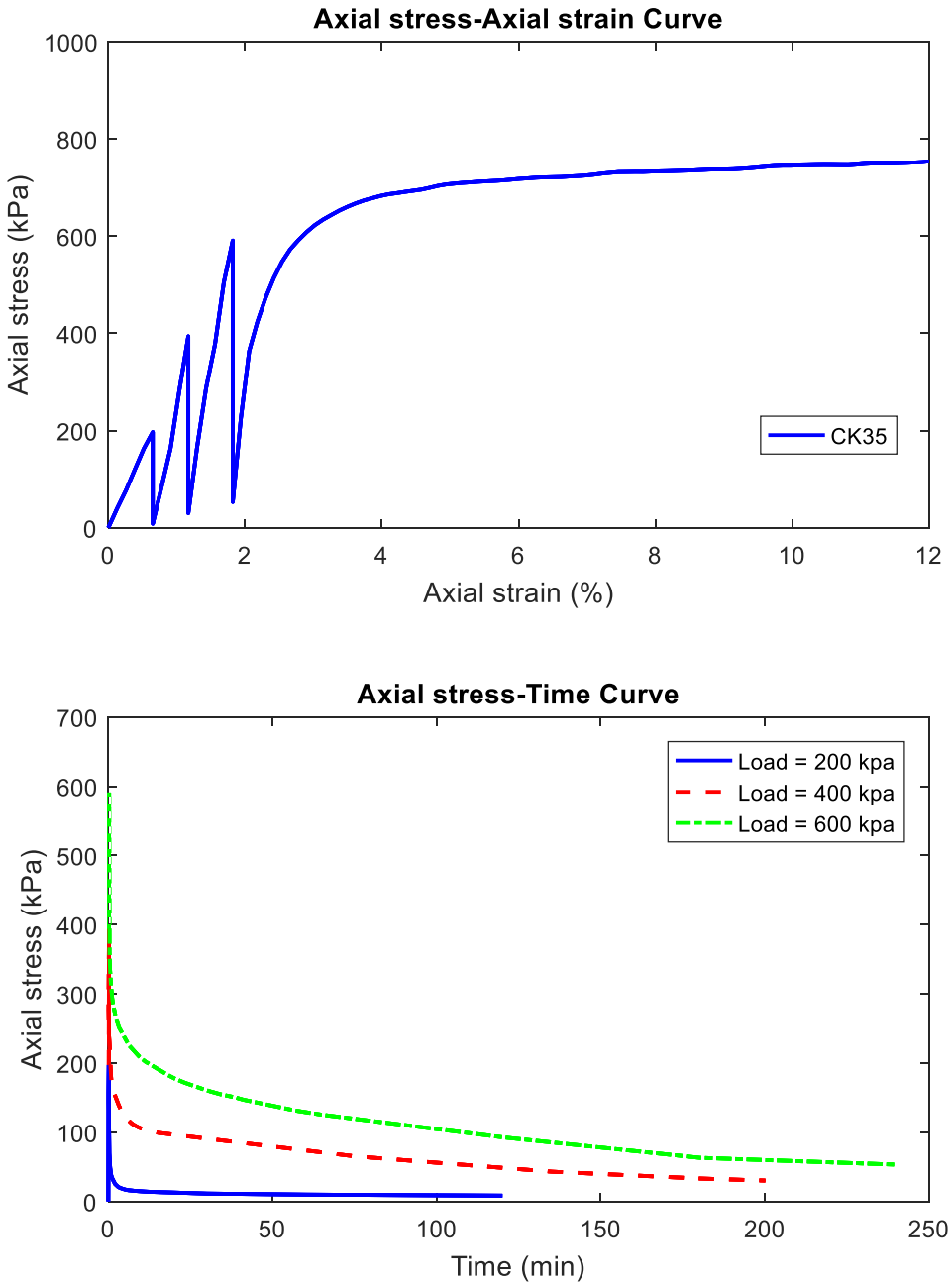

Figure 5. 30 Results of the stress relaxation test performed on sample CK35 (T= - 1 °C and Loading rate= 9 mm/min).

`

Table 5. 4 Details of the stress relaxation test for bentonite-sand samples.

Sample	Temperature	Test	Loading rate
CB28	- 15	UCSR	1 mm/min
CB29	- 15	UCSR	9 mm/min
CB30	- 10	UCSR	1 mm/min
CB31	- 10	UCSR	9 mm/min
CB32	- 5	UCSR	1 mm/min
CB33	- 5	UCSR	9 mm/min
CB34	- 1	UCSR	1 mm/min
CB35	- 1	UCSR	9 mm/min

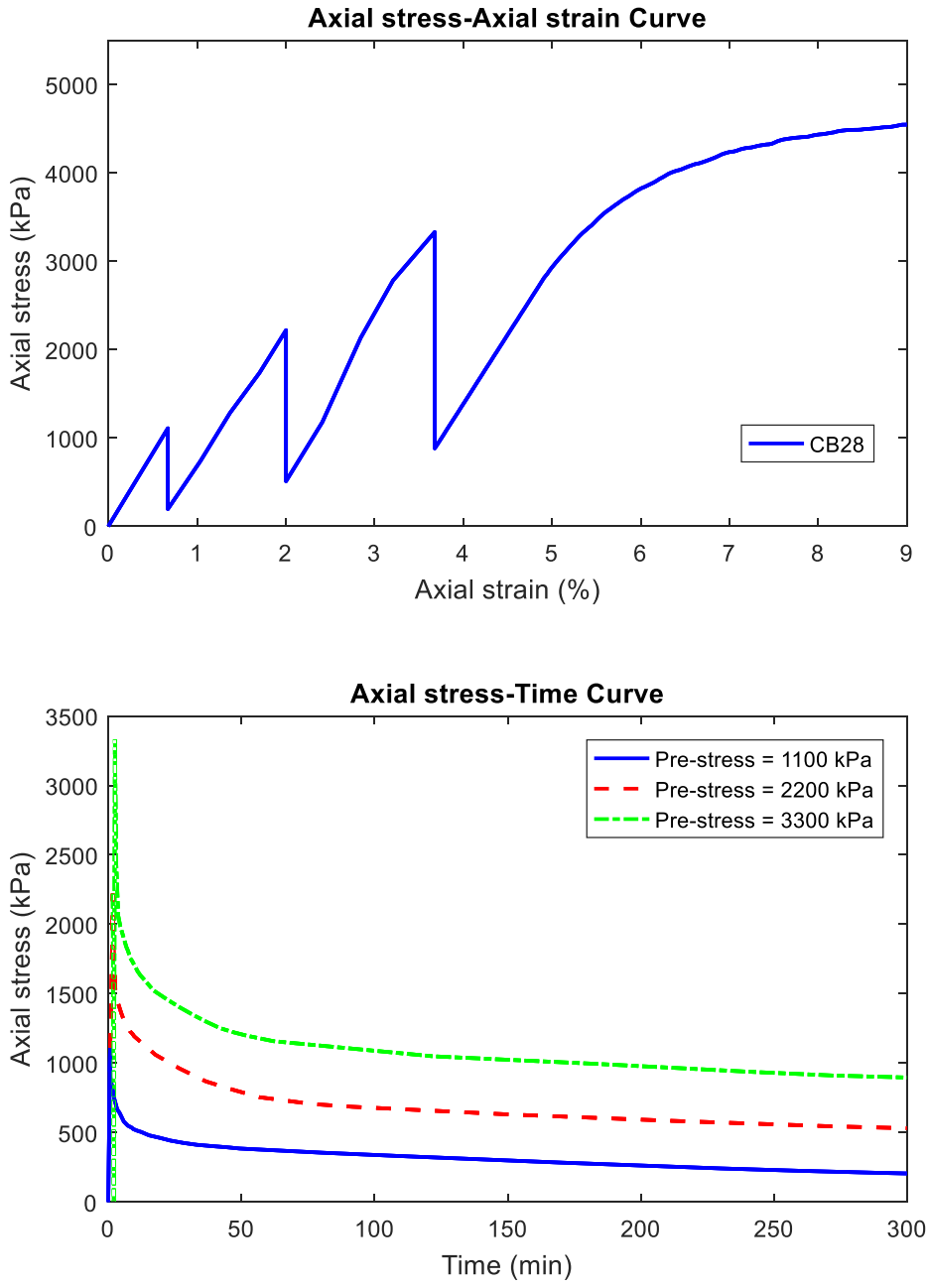

Figure 5. 31 Results of the stress relaxation test performed on sample CB28 (T= - 15 °C and Loading rate= 1 mm/min).

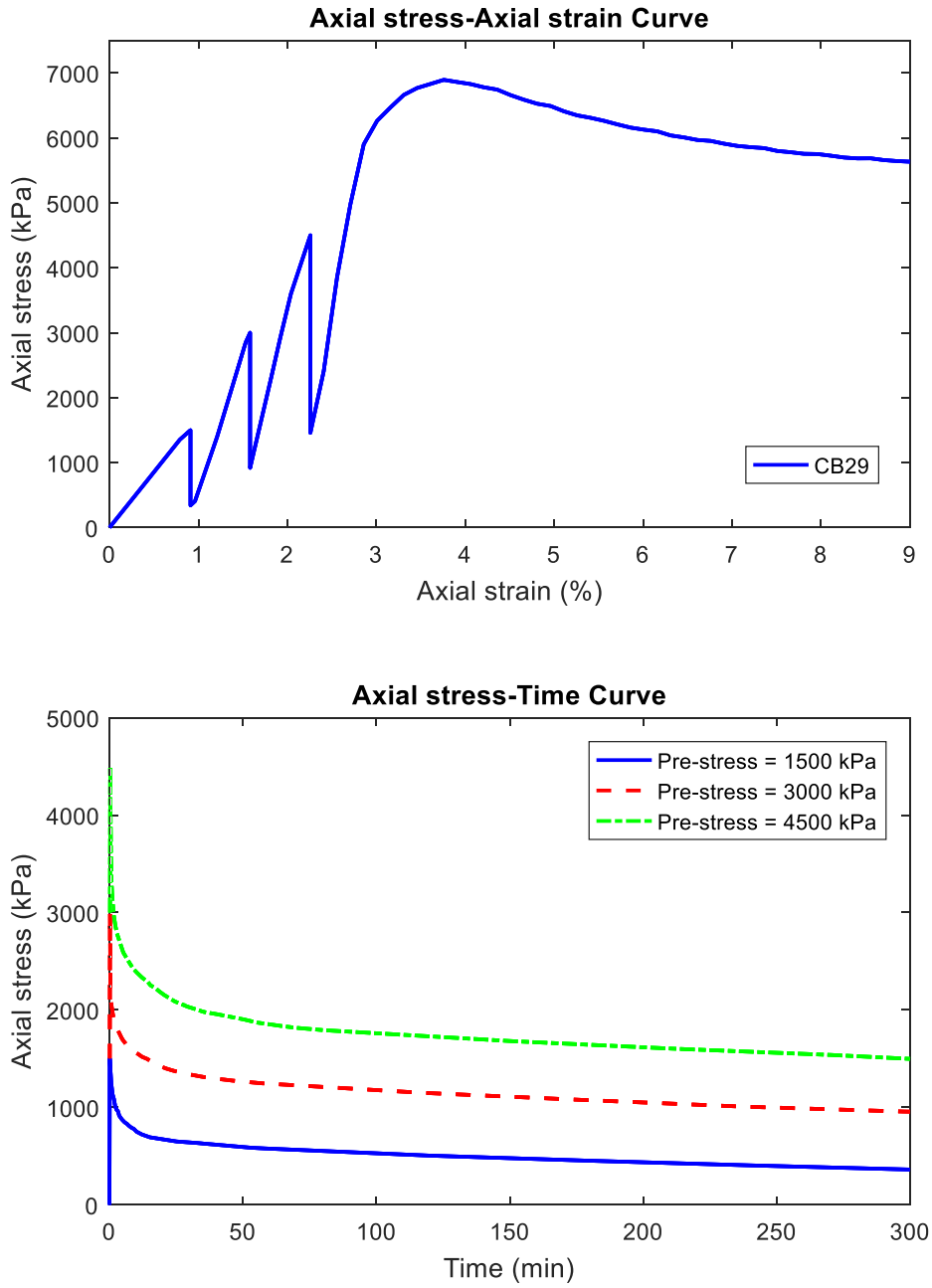

Figure 5. 32 Results of the stress relaxation test performed on sample CB29 (T= - 15 °C and Loading rate= 9 mm/min).

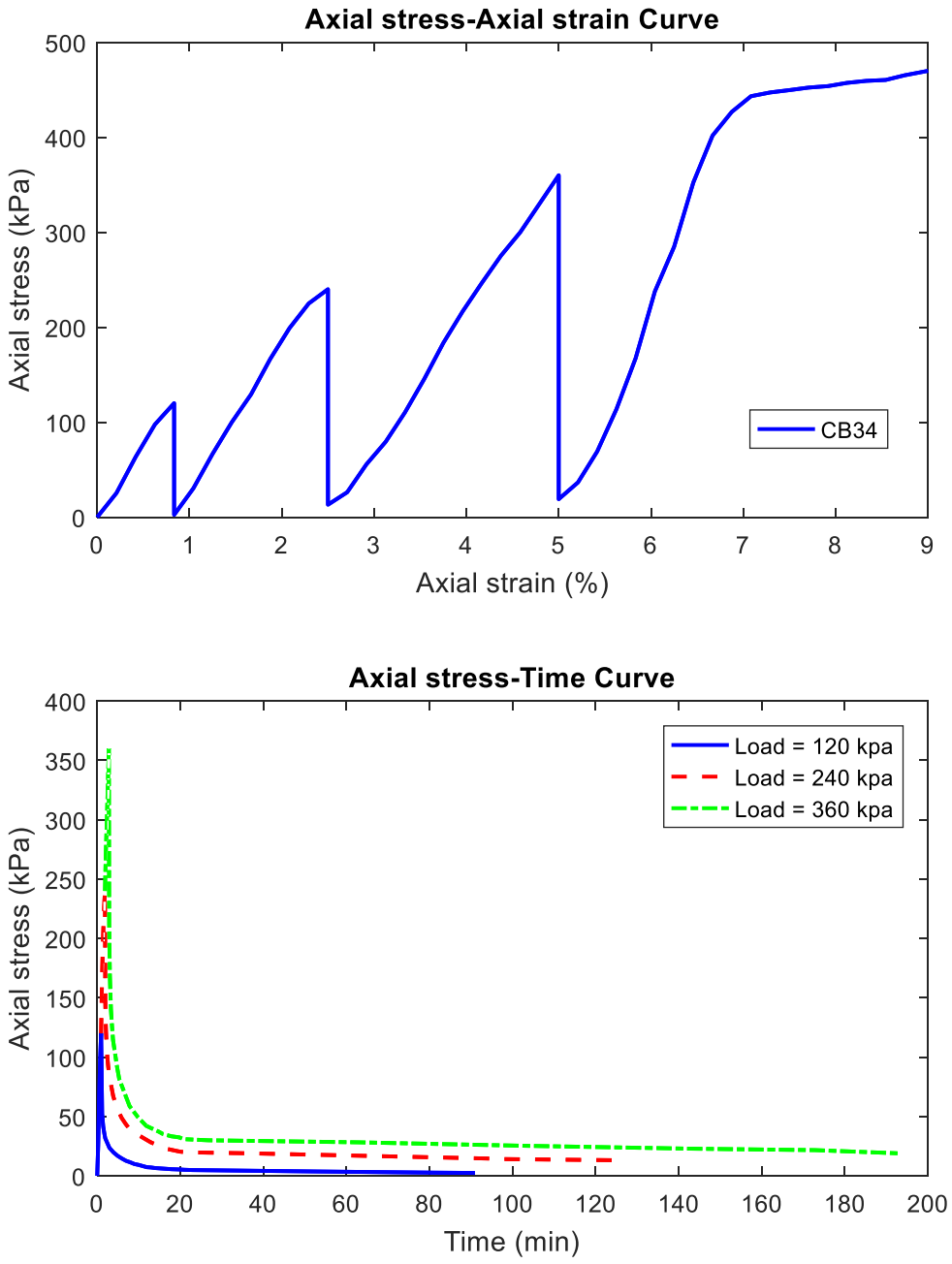

Figure 5. 33 Results of the stress relaxation test performed on sample CB34 (T= - 1 °C and Loading rate= 1 mm/min).

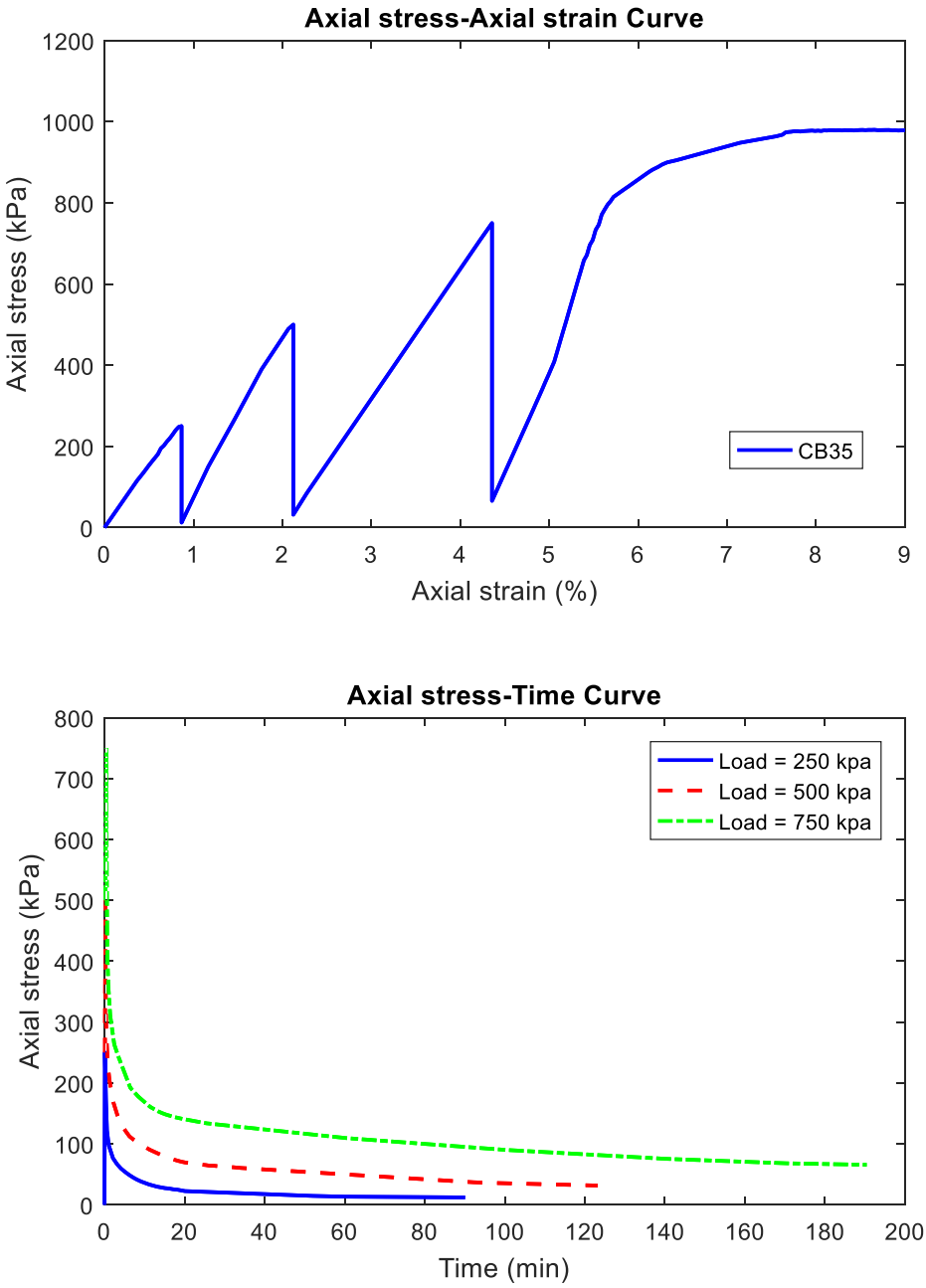

Figure 5.34 Results of the stress relaxation test performed on sample CB35 (T= - 1 °C and Loading rate= 9 mm/min).

`

5.6 Factors affecting the relaxation test results

5.6.1 Temperature

The results of UCSR tests show that the stress relaxation of sandy clay frozen soils is greatly affected by the temperature. Both the immediate stress relaxation and the rate of the stress relaxation are deceased with the decrease in the temperature. Figure 5.35 shows that the stress of kaolinite-sand samples at a loading rate of 9 mm/min, the stress level of 75 % of the UCS value, and temperatures – 1 °C and – 15 °C is finally relaxed by 91 % and 60 %, respectively of its initial value.

The stress-time curve can be divided into three parts are an immediate or primary, transition, and secondary stress relaxation. The primary stress relaxation varies linearly with time, then a nonlinear transition stress relaxation, and finally, a linear secondary relaxation occurs until attaining the final relaxation. For bentonite-sand samples at a loading rate of 1 mm/min, the stress level of 25 % of its UCS, and at temperatures of - 1 °C and - 15 °C. The stress is immediately relaxed by 74 % and 28 %, respectively after 1 minute, while the stress relaxed during the transition stage by 19 % and 38 % in 10 and 50 minutes, respectively. Laterally, a secondary relaxation occurs, and the stress is reduced by 5 % and 15 % at 90 and 360 minutes, respectively.

At temperature -1°C and loading rate 1 mm/min, kaolinite-sand and bentonite-sand samples display a strong viscoplastic behavior which is reflected by the significant primary stress relaxation, as shown in Figure 5.36.

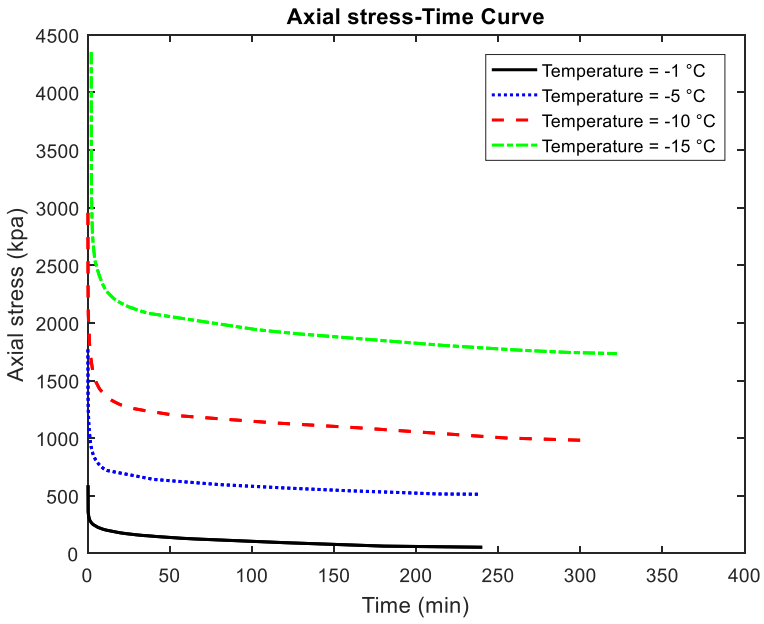

Figure 5.35 Axial stress-time curve of kaolinite-sand samples (Loading rate= 9 mm/min, Stress level= 75% of its UCS).

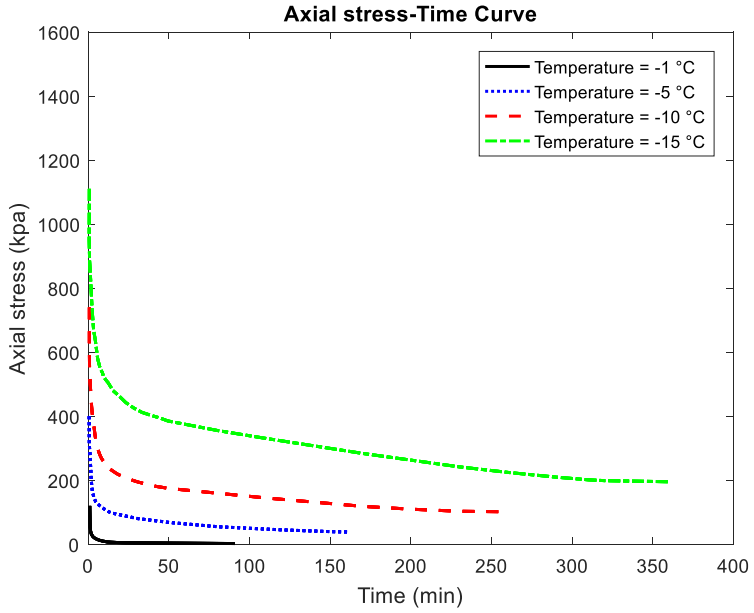

Figure 5. 36 Axial stress-time curve of bentonite-sand samples (loading rate= 1 mm/min, Stress level= 25 % of its UCS).

`

5.6.2 Loading rate

The loading rate is an important external factor that influences the stress relaxation test results, and the increase in the loading rate decreases the primary relaxation, the rate of stress relaxation, and the final relaxation stress. The kaolinite-sand samples at - 10 °C, a stress level of 75 % of its UCS value, and loading rates of 1 and 9 mm/min are immediately relaxed by 43 % and 39 %, respectively after 1 minute; while the final stress relaxation values are 78 % and 69 %, respectively (see Figure 5.35 and 5.37).

The frozen sandy clay soils seem to be sensitive to the loading rate at all temperatures due to the presence of unfrozen water. Figures 5.36 and 5.38 show that the bentonite-sand sample at a temperature of- 1 °C, a stress level of 25 % of its UCS, and loading rate of 9 mm/min is relaxed by 94 % compared to 98 % at a loading rate of 1mm/min.

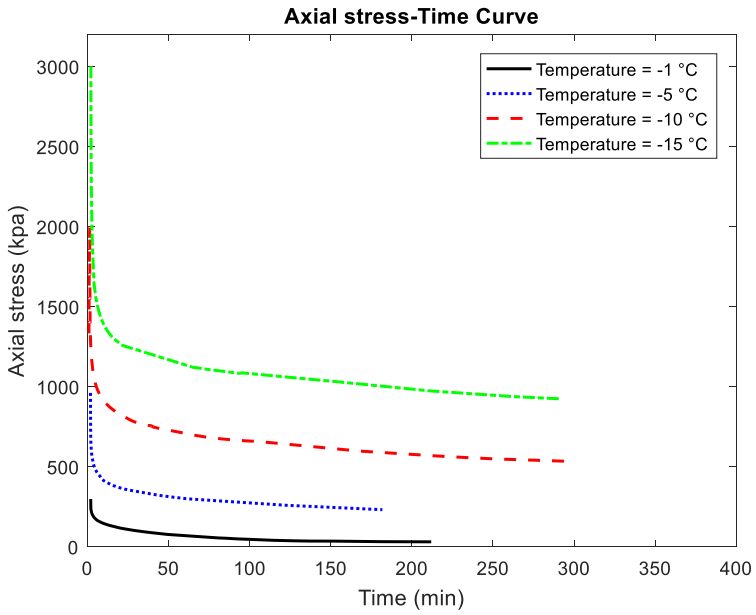

Figure 5. 37 Axial stress-time curve of kaolinite-sand samples (loading rate= 1 mm/min, Stress level= 75 % of its UCS)

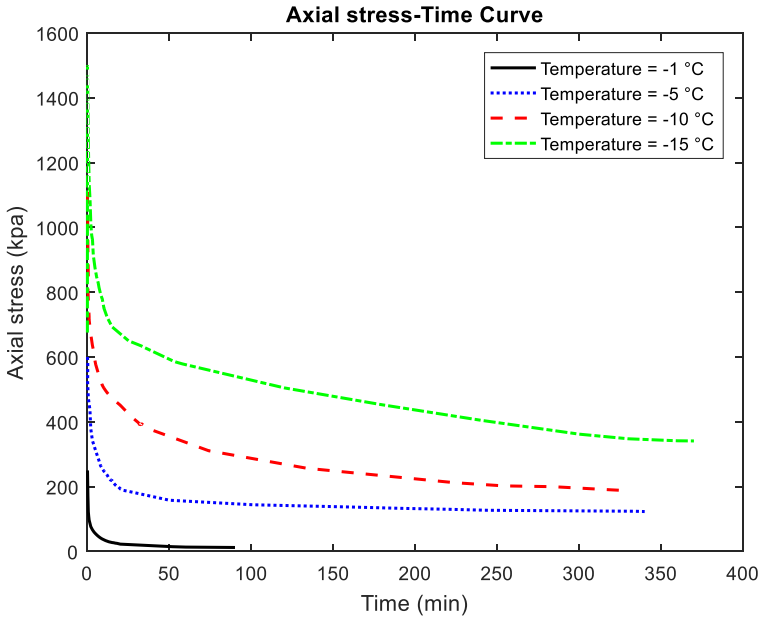

Figure 5.38 Axial stress-time curve of bentonite-sand samples (loading rate= 9 mm/min, Stress level= 25% of its UCS)

`

5.6.3 Stress level

The relaxation test accounts for the stress redistribution that occurred during the previous steps. The results of stress relaxation tests show that the primary relaxation, stress relaxation rate, and the final relaxation are reduced by the increase in the stress level. From the results of UCSR tests for bentonite-sand at - 15 °C, a loading rate of 9 mm/min, and stress levels of 25 %, 50 %, and 75 % of its UCS, the observed primary relaxations are 36 %, 33 %, and 31 % , respectively after 1 minute , while the final stress relaxation values are 74 %, 70 %, and 64 %, respectively (see Figure 5.32).

The results of UCSR tests reveal that the stress level influences the stress relaxation for all samples. Figure 5.33 shows that the final stress relaxations of bentonite-sand samples at - 1°C and loading rate of 1mm/min are 98 %, 95 %, and 94 % at stress levels of 25 %, 50 %, and 75 % of the UCS, respectively, whereas the final stress relaxation of kaolinite-sand samples at – 15 °C and loading rate of 9 mm/min are 71 %, 65 %, and 60% at stress levels of 25 %, 50 %, and 75 % of the UCS, respectively (see Figure 5.28).

5.6.4 Clay mineral

The results of UCSR tests show that the finer grains, the higher primary and final relaxations at the temperature range from - 1 °C to -15 °C. Figures 5.39 shows that at - 1 °C and loading rate of 1 mm/min, both the primary and the final relaxation of bentonite-sand samples, of finer grains, is larger that of kaolinite-sand samples at all stress levels. For example, the primary relaxation at a stress level of 75 % of its UCS is 72 % for bentonite-sand sample compared to 43% for kaolinite-sand sample. Bentonite-sand samples at - 15 °C and loading rate of 9 mm/min have higher primary and final relaxation of all stress levels compared to the bentonite-sand samples, while the transition relaxation is smaller than that for kaolinite-sand sample (see Figure 5.40).

At low temperatures, the behavior of bentonite-sand is similar to kaolinite-sand samples as shown in Figure 5.40, while bentonite-sand samples display more viscoplastic behavior than kaolinite-sand samples which reflected by the significant primary stress relaxation (see Figure 5.39).

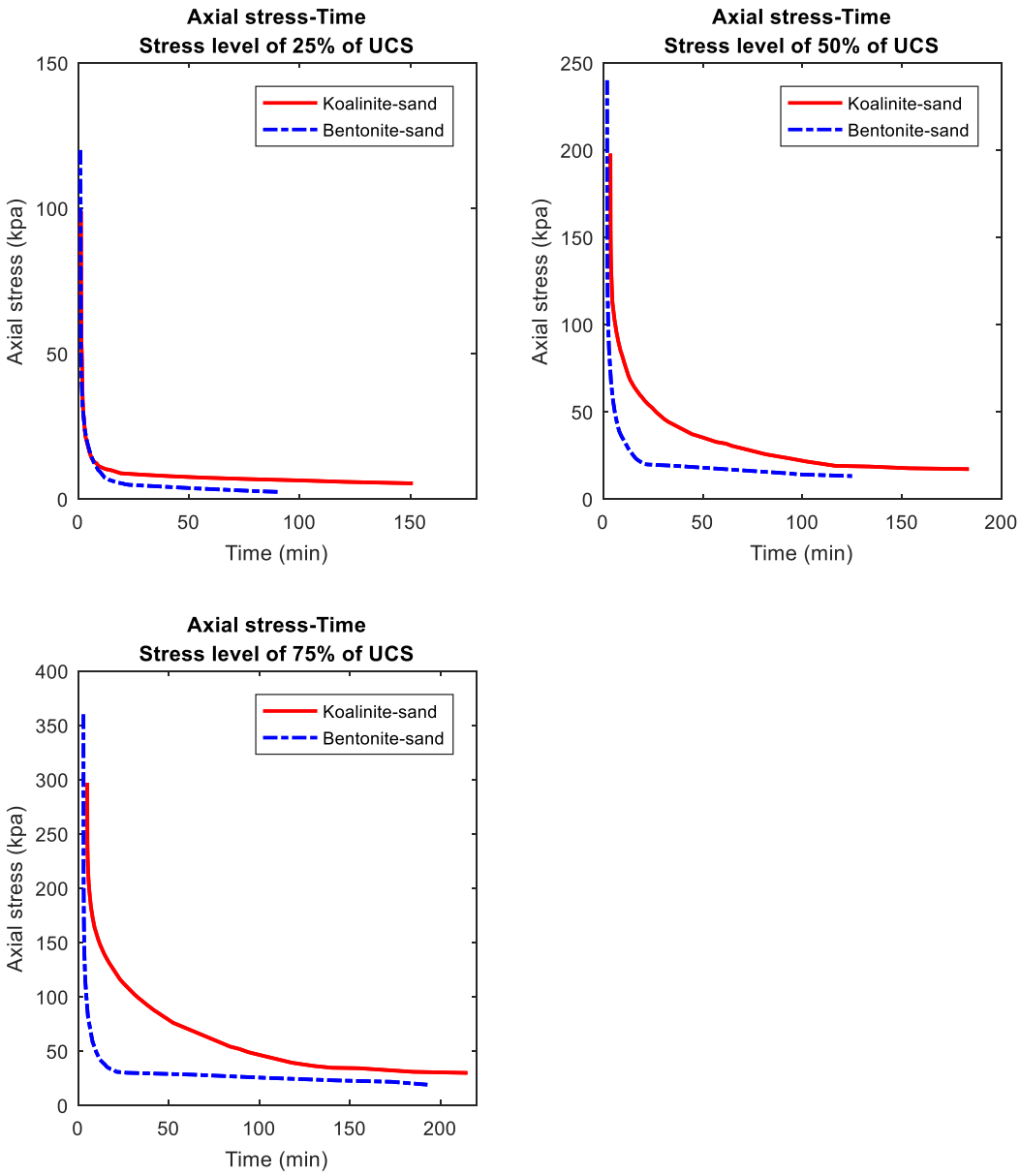

Figure 5. 39 Axial stress-time curve of sandy clay samples (T= - 1 °C, Loading rate= 1 mm/min).

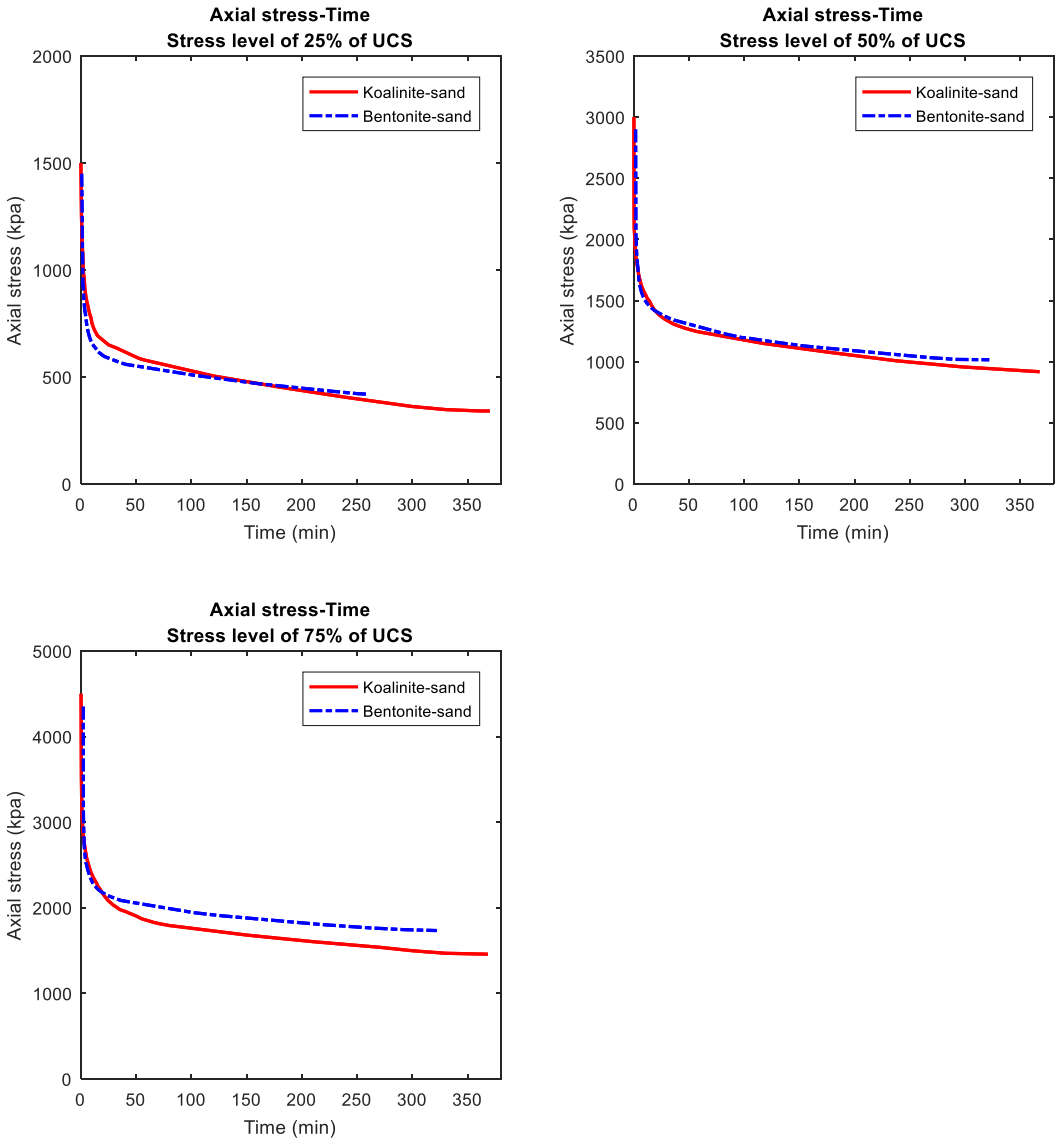

Figure 5. 40 Axial stress-time curve of sandy clay samples (T= - 15 °C, Loading rate= 9 mm/min).

`

5.7 Summary

Fifty-four UCS tests carried out at a temperature range from – 15 to 0 °C in BEPL and GL laboratories to study the various parameters affecting the UCS of frozen sandy clay soils, deformation, and failure behaviors. These parameters are temperature, loading rate, clay mineral, and test setup used. The drop in temperature greatly increases UCS, stiffness, and brittleness of the samples due to the increase in ice content and strength. The loading rate is investigated at different rates of 1, 3, and 9 mm/min, and the results show that the loading rate affects the UCS in the temperature range from – 15 to 0 °C due to the presence of the unfrozen water, and its effect increases at temperatures close to the melting point.

Two clay minerals used in this research are bentonite and kaolinite. The very small particle size of clay minerals increases the surface area that results in the presence of a large amount of unfrozen bound water, so no brittle failure is observed at the temperatures range from -15 to - 1 °C and loading rates of 1 and 9 mm/min for both kaolinite and bentonite samples. At temperatures below - 10 °C, the samples display a plastic behavior with a small peak and strain- softening.

The UCS tests carried out in a cold room or large environmental chamber and a small freezing cell connected with a source of cold air. The results obtained from both setups show a small variation in UCS due to the precautions taken before testing. The Bentonite-sand samples are more sensitive to the thermal disturbances.

Sixteen uniaxial compression stress relaxation (UCSR) tests are performed at BEPL laboratory to investigate the factors affecting stress relaxation such as temperature, loading rate, stress level, and clay mineral. The results show that the primary relaxation, relaxation rate, and final relaxation decreases with the decrease in temperature and the increase in both the loading rate and the stress level.

`

Chapter 6

CONCLUSION AND RECOMMENDATION FOR FUTURE WORK

6.1 Summary of thesis contributions and conclusions

This research proposes a practical approach for preparing saturated frozen clay soil samples with specific unit weight. Also, it presents various approaches for measuring tensile and compressive mechanical properties and the factors affecting their values. Finally, the stress relaxation test was studied as an alternative to the Findings related to the conventional creep test.

6.1.1 A Practical approach for preparing artificially frozen sandy clay samples

- From the sandy clay trial mixes, the water content of 110 % the liquid limit or more is high enough to produce homogenous and saturated samples. On condition of providing proper mixing for adequate time using a suitable mixer.
- The consolidation is an important process during samples preparation because it determines the density and porosity of soil to obtain samples of relatively high tensile strength free of ice lenses and to simulate the effect of the overburden pressure on-site.
- The evaporation and sublimation of moisture during freezing lead to a reduction in the water content, which results in a reduction in both ice content and the cohesion between the particles, so the surface of the samples should be protected inside the freezing mold, and then the mold was preserved in a multi-ply bag after air removal.
- Ice lenses formation can be limited or prevented by quick cooling under very low temperatures. In this research, the samples were frozen at - 40 °C.

6.1.2 Temperature-dependent tensile strength of frozen sandy clay soils

- The loading approach has a drastic effect on the tensile strength of frozen clay soil. The values of the tensile strength obtained from the splitting tests are almost double that of the double punch tests due to the increase in the contact area between loading strips and samples in RST and FST, while the DPT keeps the same loading area. Also, The deformation behavior also may vary according to the loading approach, even if they have the same testing conditions and stress history. The kaolinite-sand samples at -

`

0.5 °C and a loading rate of 1 mm/min showed a ductile, brittle, and brittle-ductile behavior when they were tested using RST, FST, and DPT methods, respectively.

- DPT is an effective and conservative approach.
- The splitting test is an inappropriate test for clay soils at warm temperature and low loading rate, but if the splitting tensile test is the only available test, the yield tensile strength shall be used instead of the peak tensile strength based on the comparable results of the peak tensile strength of DPT and the yield strength of RST and FST. At temperatures below at - 5 °C, the yield strength of RST and FST can be used after multiplying by a factor of safety (e.g., 75%.).
- The tensile strength of frozen sandy clay soil is temperature-dependent, and it mainly depends on the ice content and ice strength. At temperatures below -5°C, there is a hardening behavior, softening behavior, and peak tensile strength, while at warm temperatures the behavior becomes linear elastic followed by a strain-hardening.
- The tensile strength and deformation behavior of frozen sandy clay soil also depends on the loading rate. At a certain temperature, the tensile strength increases with the increase in loading rate, and this growth in tensile strength depending on temperature, soil type, and testing method. The increase in the loading rate due to the presence of the unfrozen water, but beyond a particular loading rate, the increase in strength became very minimal.
- The mode of failure and the failure strain were found to be temperature and loading rate-dependent. The mode of failure of RST and FST was a typical vertical splitting fracture passing through the center of the sample at low temperatures, while the behavior becomes viscoplastic which is reflected by the strong penetration of the loading strip into the sample at high temperatures and low loading rates. The mode of failure for DPT was a side fracture in the temperature range from – 15 to 0 °C.
- The salinity of the pore fluid affects both the tensile strength and the deformation behavior of the frozen sandy clay soils. The tensile strength decreases with an increase in salinity due to unfrozen water content. Also, the salinity increases the sensitivity of the tensile strength to the temperature and strain rate.

`

- The results of the tensile strength obtained from the three testing methods showed that the values of the tensile strength of bentonite-sand samples were higher than those of kaolinite-sand samples in the temperature range from -15 to 0 °C and at loading rates of 1, 3, and 9 mm/min due to the higher cohesion of bentonite-sand samples.

6.1.3 Temperature-dependent compressive strength of a frozen sandy clay soil

- The uniaxial compressive strength of the sandy clay frozen soil is strongly improved by decreasing the temperature. The uniaxial compressive strength of frozen sandy clay soils at - 15 °C was 14 times greater than the same samples at 0 °C. The uniaxial compressive strength increased exponentially with decreases in temperature up to a certain temperature, and then the relation became linear at temperatures around - 5 °C depending on clay mineral, loading rate, and salinity.
- The loading rate has a remarkable effect on the uniaxial compressive strength of frozen sandy clay soil, and the influence of the loading rate increases at with the increase in temperature due to the presence of unfrozen water. Brittle failure was observed only at – 15 °C and loading rate of 9 mm/min for the kaolinite-sand samples, and at loading rates of 3 and 9 mm/min below -5°C for the bentonite-sand samples.
- The strength of the bentonite-sand samples was higher than those of the kaolinite-sand samples in the temperature range from 0 °C to -15 °C, and loading rates of 1, 3, and 9 mm/min as a result of the higher cohesion and the ice content.
- The uniaxial compressive strength tests at - 10 and - 15 °C were performed using two different setups to study the effect of the setup on the uniaxial compressive strength. One setup was in the large environmental chamber, and the other was with the freezing unit. The results of both setups showed that there was no significant difference in the uniaxial compressive values, but kaolinite-sand samples were more sensitive to thermal disturbances due to the sample transferring and poisoning before testing.
- The ratio of the uniaxial compressive strength to tensile strength increases with the decrease in temperature and the increase in loading rate.
- The temperature has a significant effect on both Young's modulus, E, and Poisson's ratio, υ. The value of Young's modulus for the bentonite- sand sample at - 15 °C is

`

fifteen times greater than that at 0 °C. The loading rate also affects Young's modulus and Poisson's ratio. The values of Young's modulus for the bentonite-sand sample at -15 °C are 241 MPa and 157 MPa at rates of 9 mm/min and 1 mm/min, respectively. Poisson's ratio increases with the increase in the temperature and the decrease in loading rate.

6.1.4 Temperature-dependent stress relaxation of a frozen sandy clay soil

- The stress-time curve of the uniaxial compression stress relaxation test can be divided into three parts: an immediate or primary stress relaxation, a transition, and a secondary stress relaxation. Both the primary and secondary portions were linearly varied with time, while the transition relaxation is nonlinear with time.
- During the primary stress relaxation, the rate of stress relaxation decrease with the drop in temperature and the increase in loading rate. The kaolinite-sand samples at a loading rate of 9 mm/min relaxed by 91 % and 60 % at temperatures of - 1°C and – 15 °C, respectively. The bentonite-sand samples relaxed by 98% and 94% at a temperature of - 1 °C, a stress level of 25 % of its UCS, and loading rate of 1 and 9 mm/min, respectively.
- During the transition and secondary relaxation, the relaxation times increase with the decrease in temperature and the increase in loading rate. For the bentonite-sand samples at a loading rate of 1 mm/min, a stress level of 25 % of its UCS, and at temperatures of - 1 °C and - 15 °C, the stress relaxed during the transition stage by 19 % and 38 % after 10 and 50 minutes, respectively, while the stress reduced by 5 % and 15 % at 90 and 360 minutes, respectively during the secondary relaxation.
- The stress level affects the stress relaxation test results. The primary relaxation and final stress relaxation decreased with the increase in stress level, while in the transition relaxation and the secondary relaxation, the relaxation time increased with the increase in the stress level.
- The results of the stress relaxation tests show that bentonite-sand samples have more stress relaxation than kaolinite-sand samples. The primary and final relaxation rates of bentonite-sand samples are greater than those of kaolinite-sand samples at all temperatures, loading rates, and stress levels. In contrast, the transition and secondary

`

relaxation time of bentonite-sand samples were lower than that of kaolinite-sand samples.

6.2 Recommendation for future work

The findings of this research highlighted several areas that need further investigation, and the following are the recommendations for future work:

- The satisfactory results obtained from the double punch tests encourage further investigation to ensure its convenience for different types of frozen soil at various temperatures.
- Artificially frozen artificial clay soils seemed very beneficial to study the mechanical properties of frozen clay soils due to their homogeneity, constant composition, and well-bonded ice. Therefore, the need arises to investigate real in-situ clay soils to check the effectiveness of using artificially frozen clay soils.
- Although the study of the most influential parameters on strength and deformation behavior of frozen sandy clay soil, there are other factors such as water content, density, etc. need to be investigated.
- The lateral deformation is measured in this research at the middle of samples; however, the lateral deformation is not uniform particularly at temperatures above -5 and low loading rates; therefore different radial gauges are recommended to study the deformation behavior at higher temperatures and lower loading rates.
- Constitutive modeling on the strain hardening, plastic behavior of samples during a failure is recommended.
- A study of the microstructure of frozen samples during the stress relaxation test for a better understanding of the redistribution of the stresses, particularly at frozen fringe temperatures is also recommended.
- It would be useful to study the behavior of the frozen soil during the stress relaxation tests with stress levels above the elastic limit.

`

REFERENCES

Akagawa, S., & Nishisato, K. (2009). Tensile strength of frozen soil in the temperature range of the frozen fringe. *Cold Regions Science and Technology*, 57(1), 13-22.

Akazawa, T. (1943). New test method for evaluating internal stress due to compression of concrete (the splitting tension test)(part 1). *J Jpn Soc Civ Eng*, 29, 777-787.

Andersland, O. B., & Ladanyi, B. (2013). An introduction to frozen ground engineering. Springer Science & Business Media.

Anderson, D. M., & Morgenstern, N. R. (1973). Physics, chemistry and mechanics of frozen ground: A review. *In North American Contribution to the Proceedings of the Second International Conference on Permafrost Yakutsk, USSR*, (pp. 257-288).

ASTM, C128. (2015). Standard test method for relative density (specific gravity) and absorption of coarse aggregate. *West Conshohocken, PA: ASTM*.

ASTM, C136. (2014). Standard test method for sieve analysis of fine and coarse aggregates.

ASTM, C78. (2016). Standard test method for flexural strength of concrete (using simple beam with third-point loading). In American society for testing and materials.

ASTM, D 3967. (2016). Standard Test Method for Splitting Tensile Strength of Intact Rock Core Specimens. *ASTM International, West Conshohocken, PA*.

ASTM, D 4318. (n.d.). Standard test methods for liquid limit, plastic limit, and plasticity index of soils.

ASTM, D2216. (2010). Standard Test Methods for Laboratory Determination of Water (Moisture) Content of Soil and Rock by Mass. *West Conshohocken, PA: ASTM International*.

ASTM, D4083. (2016). Suggested practice for description of frozen soils (visual-manual procedure. *ASTM Geotechnical Testing Journal*, 1(4).

ASTM, D442. (2007). Standard test method for particle-size analysis of soils.

`

ASTM, D790. (2017). Standard test methods for flexural properties of unreinforced and reinforced plastics and electrical insulating materials.

ASTM, D854. (2014). Standard test methods for specific gravity of soil solids by water pycnometer. *ASTM International, West Conshohocken.*

Azmatch, T. F., Sego, D. C., Arenson, L. U., & Kevin, W. B. (2010). Tensile Strength of Frozen Soils Using Four-Point Bending Test. *63rd Canadian Geotechnical Conference & 6th Canadian Permafrost Conference*, 436–42.

Azmatch, T. F., Sego, D. C., Arenson, L. U., & Kevin, W. B. (2011). Tensile Strength and Stress-Strain Behaviour of Devon Silt under Frozen Fringe Conditions. *Cold Regions Science and Technology*, 68(1–2):85–90.

Baker, T. H. W. (1976). Transportation, preparation, and storage of frozen soil samples for laboratory testing. In Soil specimen preparation for laboratory testing *ASTM International.*

Bing, H., & Ma, W. (2011). Laboratory investigation of the freezing point of saline soil. *Cold Regions Science and Technology*, 67(1-2), 79-88.

Bortolotti, L. (1988). Double-punch test for tensile and compressive strengths in concrete. *Materials Journal*, 85(1), 26-32.

Bragg, R. A., & Andersland, O. B. (1981). Strain rate, temperature, and sample size effects on compression and tensile properties of frozen sand. *Engineering Geology*, 18(1-4), 35-46.

C109, A. (2008). Standard Test Method for Compressive Strength of Hydraulic Cement Mortars (Using 2-in. or 50-mm Cube Specimens. West Conshohocken PA.: ASTM International.

Carneiro, F. L. (1943). Um novo método para determinacão da resistência à tração dos concretos. *Anais 5a reunião da Associação Brasileira de Normas Técnicas (ABNT) em São Paulo*, 127-129.

Chen, W. F. (1969). Double punch test for tensile strength of concrete. 70-18.

Chen, W. F., & Drucker, D. C. (1969). Bearing capacity of concrete blocks or rock. *Journal of Engineering Mechanics*.

`

Chen, W. F., & Yuan, R. L. (1980). Tensile strength of concrete: double-punch test. *Journal of the Structural Division*, 106(8), 1673-1693.

Christ, M., & Kim, Y. C. (2009). Experimental study on the physical-mechanical properties of frozen silt. *KSCE Journal of Civil Engineering*, 13(5), 317-324.

Colback, P. S. B. (1966). An analysis of brittle fracture initiation and propagation in the Brazilian test. *In 1st ISRM Congress. International Society for Rock Mechanics and Rock Engineering*.

Coviello, A., Lagioia, R., & Nova, R. (2005). On the measurement of the tensile strength of soft rocks. *Rock Mechanics and Rock Engineering*, 38(4), 251-273.

Dillon, H. B., & Andersland, O. B. (1966). Predicting unfrozen water contents in frozen soils. . *Canadian geotechnical journal*, 3(2), 53-60.

Dismuke, T. D., Chen, W. F., & Fang, H. Y. (1972). Tensile strength of rock by the double-punch method. *Rock mechanics*, 4(2), 79-87.

Fang, H. Y., & Chen, W. F. (1971). New method for determination of tensile strength of soils. *Highway Research Board.*

Haynes, F. D. (1978). Strength and deformation of frozen silt. *In Proceedings of the Third International Conference on Permafrost Edmonton, Alberta, Canada*, (pp. 655-661).

Haynes, F. D., & Karalius, J. A. (1977). Effect of temperature on the strength of frozen silt (No. CRREL-77-3). *Cold Regions Research and Engineering Lab Hanover NH.*

Haynes, F. D., Karalius, J. A., & Kalafut, J. (1975). Strain Rate Effect on the Strength of Frozen Silt (No. CRREL-RR-350). *COLD REGIONS RESEARCH AND ENGINEERING LAB HANOVER NH.*

Hivon, E. G., & Sego, D. C. (1995). Strength of frozen saline soils. *Canadian Geotechnical Journal*, 32(2), 336-354.

`

Hivon, E., & Sego, D. C. (1990). Determination of the unfrozen water content of saline permafrost using time-domain reflectometry (TDR). *In Proceeding of the 5th Canadian Permafrost Conference*, (pp. 257-262). Quebec City, Quebec, Canada.

Hu, X. D., Wang, J. T., & Yu, R. Z. (2013). Uniaxial compressive and splitting tensile tests of artificially frozen soils in tunnel construction of Hong Kong. *Journal of Shanghai Jiaotong University (Science)*, 18(6), 688-692.

Iravanian, A., & Bilsel, H. (2016). Strength Characterization of Sand-Bentonite Mixtures and the Effect of Cement Additives. *Marine Georesources & Geotechnology*, 34(3), 210-218.

Jessberger, H. L. (1981). A state-of-the-art report. Ground freezing: mechanical properties, processes and design. *Engng Geol.*, 18, 5–30.

Johnston, G. H. (1963). Soil sampling in permafrost areas.

Konrad, J. M., & Morgenstern, N. R. (1981). The segregation potential of a freezing soil. *Canadian Geotechnical Journal*, 18(4), 482-491.

Kozlowski, T. (2009). Some factors affecting supercooling and the equilibrium freezing point in soil–water systems. *Cold Regions Science and Technology*, 59(1), 25-33.

Lade, P. V. (2009). Creep, stress relaxation, and rate effects in sand. *In Proceedings of the 17th International Conference on Soil. Alexandria, Egypt*, (pp. 5-9).

LeBlanc, A. M., Allard, M., Carbonneau, A. S., Oldenborger, G. A., L'Hérault, E., Sladen, W. E., ... & Mate, D. (2011). Assessing permafrost conditions and landscape hazards in support of climate change adaptation in Pangnirtung, Nunavut. *Geological Survey of Canada*, 59.

Lee, M. Y., Fossum, A., Costin, L. S., & Bronowski, D. (2002). Frozen soil material testing and constitutive modeling.

Leroueil, S., Tardif, J., Roy, M., Rochelle, P.L., and Konrad, J.M. (1991). Effects of frost on the mechanical behaviour of Champlain Sea clays. *Canadian Geotechnical Journal*, 28(5): 690-697.

`

Li, H., Yang, H., Chang, C., & Sun, X. (2001). Experimental investigation on compressive strength of frozen soil versus strain rate. *Journal of cold regions engineering*, 15(2), 125-133.

Li, X., Zhang, J., Liu, K., & Zhang, X. N. (2006). Finite element modeling of geomaterial using digital image processing and computerized tomography identification. *Yantu Lixue(Rock and Soil Mechanics)*, 27(8), 1331-1334.

Michalowski, R. L., & Zhu, M. (2006). Frost heave modelling using porosity rate function. *International journal for numerical and analytical methods in geomechanics*, 30(8), 703-722.

Ming, F., Li, D., Zhang, M., & Zhang, Y. (2017). A novel method for estimating the elastic modulus of frozen soil. *Cold Regions Science and Technology*, 141, 1-7.

Molins i Borrell, C. A. (2008). Double Punch Test to control the energy dissipation in tension of FRC (Barcelona test).

Mujika, F. (2006). On the difference between flexural moduli obtained by three-point and four-point bending tests. *Polymer Testing*, 25(2), 214-220.

Nixon, J. F., & Morgenstern, N. R. (1974). Thaw–consolidation tests on undisturbed fine-grained permafrost. *Canadian Geotechnical Journal*, 11(1), 202-214.

Patterson, D. E., & Smith, M. W. (1985). Unfrozen water content in saline soils: results using time-domain reflectometry. ". *Canadian Geotechnical Journal*, 22(1), 95-101.

Sarfarazi, V., & Schubert, W. (2017). Numerical simulation of tensile failure of concrete in direct, flexural, double punch tensile and ring tests. *Periodica Polytechnica Civil Engineering*, 61(2), 176-183.

Savigny, K. W., & Morgenstern, N. R. (1986). In situ creep properties in ice-rich permafrost soil. *Canadian Geotechnical Journal*, 23(4), 504-514.

Shloido, G. A. (1968). Determining the tensile strength of frozen ground. *Power Technology and Engineering (formerly Hydrotechnical Construction)*, 2(3), 238-240.

Sladen, W. E. (2011). Permafrost. Geological Survey of Canada.

`

Thusyanthan, N. I., Take, W. A., Madabhushi, S. P. G., & Bolton, M. D. (2007). Crack initiation in clay observed in beam bending. *Geotechnique*, 57(7), 581-594.

Wang, B., Paudel, B., and Li, H. (2016). Behaviour of retrogressive thaw slumps in northern Canada—three-year monitoring results from 18 sites. *Landslides*, 13(1): 1-8.

Xu, X., Wang, Y., Yin, Z., & Zhang, H. (2017). Effect of temperature and strain rate on mechanical characteristics and constitutive model of frozen Helin loess. *Cold Regions Science and Technology*, 136, 44-51.

Yamamoto, Y., & Springman, S. M. (2017). Three-and four-point bending tests on artificial frozen soil samples at temperatures close to 0 C. *Cold Regions Science and Technology*, 134, 20-32.

Yu, Y., Zhang, J., & Zhang, J. (2009). A modified Brazilian disk tension test. *International Journal of Rock Mechanics and Mining Sciences*, 2(46), 421-425.

Yuanlin, Z., & Carbee, D. L. (1987). Creep and strength behavior of frozen silt in uniaxial compression (No. CRREL-87-10). COLD REGIONS RESEARCH AND ENGINEERING LAB HANOVER NH.

Yue, Z. Q., Chen, S., & Tham, L. G. (2003). Finite element modeling of geomaterials using digital image processing. *Computers and Geotechnics*, 30(5), 375-397.

Zhongyan, S., Wanwei, P., & Yongzhi, L. (1995). Tensile Strength of Frozen Saturated Loess [J]. *Journal of Glaciolgy and Geocryology*, 4.

Zhou, G., Hu, K., Zhao, X., Wang, J., Liang, H., & Lu, G. (2015). Laboratory investigation on tensile strength characteristics of warm frozen soils. *Cold Regions Science and Technology*, 113, 81-90.

`

APPENDIX A

MATERIALS TESTS RESULTS

A 1 Particle size analysis test

A 1.1 Sand

The sand sample used for sieve analysis

Mass of sand before washing = 139.00 g

Mass of sand after washing = 136.80 g

Mass of sand after sieving = 136.80 g

Table A1 Data of particle size distribution test for sand.

Sieve No.	Opening (mm)	Mass retained on sieve (g)	Mass Cumulative retained (g)	% Cumulative retained	Total percent passed (%)
40	0.425	0.0	0.0	0.0	100.0
50	0.300	8.1	8.1	5.9	94.1
70	0.212	55.0	63.1	46.1	53.9
80	0.180	24.9	88.0	64.3	35.7
100	0.150	19.5	107.5	78.6	21.4
140	0.106	15.9	123.4	90.2	9.8
200	0.075	10.1	133.5	97.6	2.4
Pan		3.3	136.8	100.0	0.0

`

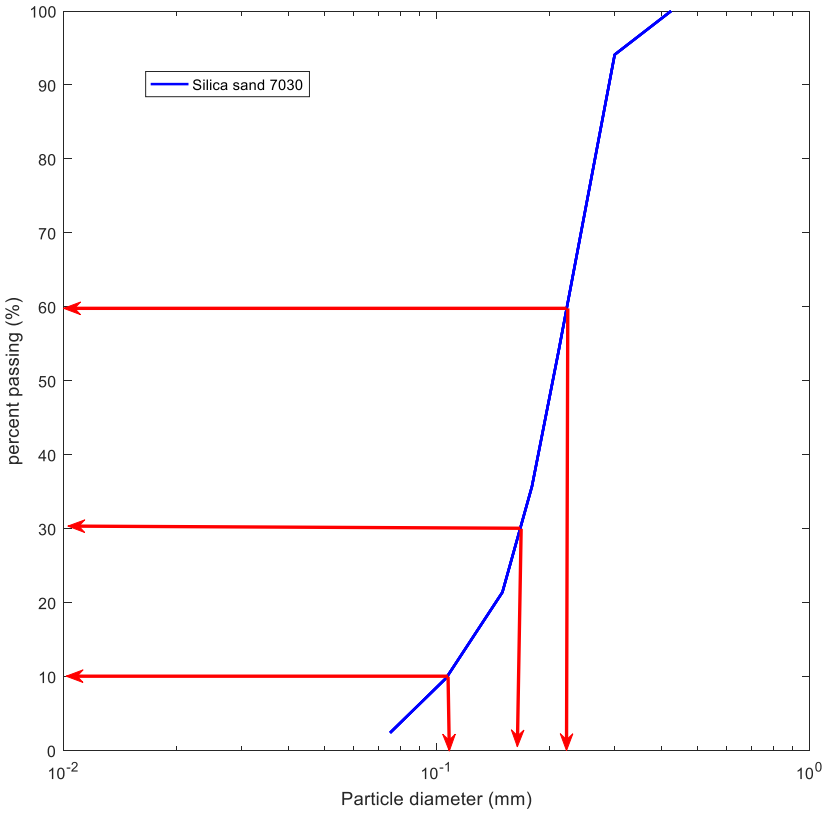

Figure A 1 Particle size distribution of silica sand 7030

$Cu = D_{60} / D_{10} = 0.23/0.11 = 2.1$

$Cc = (D_{30})^2/D_{10}*D_{60} = (0.175)^2 / (0.11 * 0.23) = 0.0529/0.054 = 1.21$

`

A 1.2 kaolinite

Table A2 Data of hydrometer test for kaolinite.

Time (min)	Temperature (°C)	Corrected reading (meniscus)	Effective depth	Fully Corrected reading	Particle diameter	Percentage finer than D (%)
0.25	24.8	47.85	8.450514	49.09	0.075814	87.3
0.5	24.8	47.35	8.532494	48.59	0.053868	86.1
1	24.8	46.85	8.614474	48.09	0.038273	84
2	24.8	45.35	8.860414	46.59	0.027447	82
5	24.8	44.35	9.024374	45.59	0.017519	79
10	24.8	41.85	9.434274	43.09	0.012666	77
15	24.7	40.85	9.598234	42.06	0.010439	76
30	24.7	40.35	9.680214	41.56	0.007441	74
60	24.2	39.85	9.762194	40.91	0.005288	73
120	24.1	39.35	9.844174	40.41	0.003758	72
240	23.5	38.85	9.926154	39.70	0.002689	70.9
720	23.5	37.85	10.09011	39.70	0.001565	68.7
1440	23.5	36.85	10.25407	39.70	0.001116	67.2

`

A 1.3 Bentonite

TableA3 Data of hydrometer test for bentonite.

Time (min)	Temperature (°C)	Corrected reading (meniscus)	Effective depth	Fully Corrected reading	Particle diameter	Percentage finer than D (%)
0.25	24.8	48.85	8.286554	50.09	0.075305	97.7
0.5	24.8	48.85	8.286554	50.09	0.053249	97.7
1	24.8	48.85	8.286554	50.09	0.037653	97.7
2	24.8	48.85	8.532494	50.09	0.027017	96.7
5	24.8	47.35	8.696454	48.59	0.01725	94.7
10	24.8	46.35	8.778434	47.59	0.012255	92
15	24.7	45.85	9.270314	47.09	0.010291	90
30	24.7	42.85	9.762194	44.09	0.007467	84
60	24.2	39.85	10.25407	41.09	0.005432	77
120	24.1	36.85	10.99189	38.09	0.00398	71
240	23.5	32.35	11.89367	33.59	0.002952	63
720	23.5	26.85	13.86119	28.09	0.00184	44
1440	23.5	14.85	16.296	16.09	0.001411	29.7

`

A 2 Atterberg limits data test

A 2.1 kaolinite

Table A4 Data of liquid limit tests for kaolinite

Test number	1	2	3	4
Number of blows	30	26	15	7
Mass of wet soil + container (g)	51.10	53.67	60.04	49.26
Mass of dry soil + container (g)	37.26	38.61	41.52	34.54
Water loss (g)	13.84	15.06	18.52	14.72
Container (g)	13.77	13.77	13.77	13.77
Mass of dry soil (g)	23.49	24.84	27.75	20.77
Water content (%)	58.92	60.63	66.74	70.87

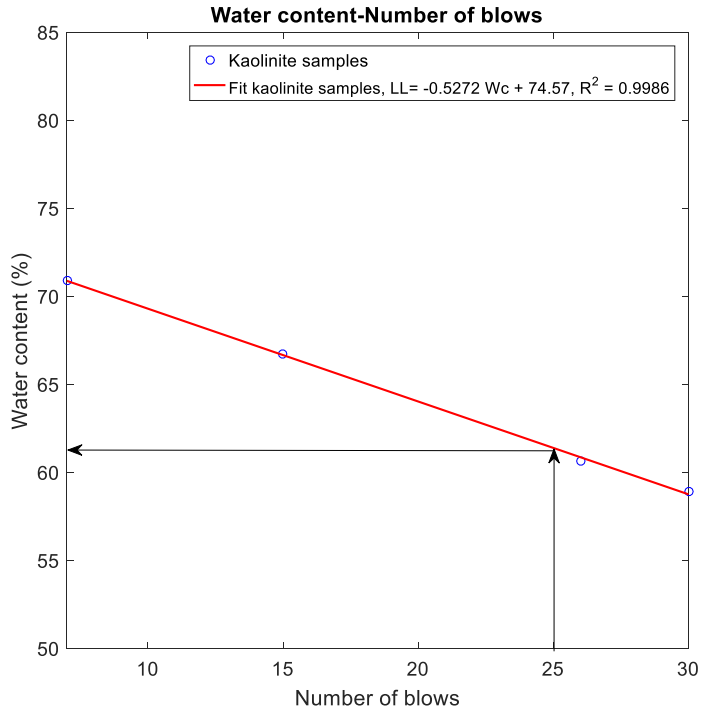

Figure A 2 Liquid limit of kaolinite

Liquid limit = **61** %

`

Table A5 Data of plastic limit tests for kaolinite

Test number	1	2	3
Mass of wet soil + container (g)	41.02	39.01	40.81
Mass of dry soil + container (g)	34.5	32.87	34.35
Water loss (g)	6.52	6.14	6.46
Container (g)	13.77	13.77	13.77
Mass of dry soil (g)	20.73	19.1	20.58
Water content (%)	31.45	32.15	31.39
Average plastic limit	31.66		

Plastic limit = 3**2** %

A 2.2 Bentonite

Table A6 Data of liquid limit tests for bentonite

Test number	1	2	3	4
Number of blows	40	32	23	17
Mass of wet soil + container (g)	45.59	49.64	52.12	47.72
Mass of dry soil + container (g)	23.88	24.61	24.59	22.95
Water loss (g)	21.71	25.03	27.53	24.77
Container (g)	13.77	13.77	13.77	13.77
Mass of dry soil (g)	10.11	10.84	10.82	9.18
Water content (%)	214.74	230.90	254.44	269.83

`

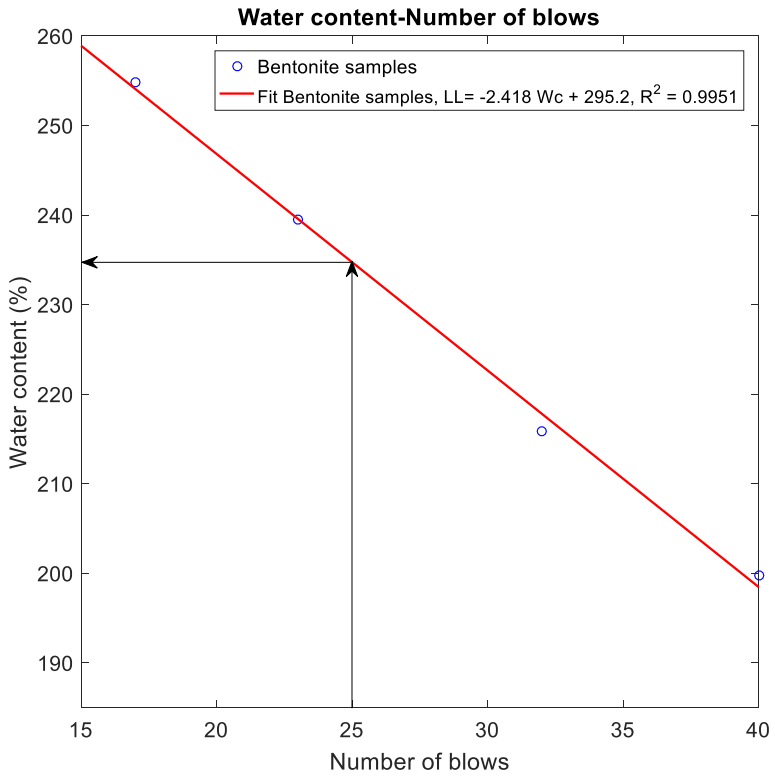

Figure A 3 Liquid limit of bentonite

Liquid limit = **235** %

Table A7 Data of plastic limit tests for bentonite

Test number	1	2	3
Mass of wet soil + container (g)	39.57	40.98	37.15
Mass of dry soil + container (g)	29.59	30.75	28.14
Water loss (g)	9.98	10.23	9.01
Container (g)	13.77	13.77	13.77
Mass of dry soil (g)	15.82	16.98	14.37
Water content (%)	63.08	60.25	62.70
Average plastic limit	62.01		

Plastic limit = **62** %

`

A 2.3 kaolinite-sand

Table A8 Data of liquid limit tests for kaolinite-sand

Test number	1	2	3	4
Number of blows	50	40	24	17
Mass of wet soil + container (g)	60.65	74.80	55.66	57.13
Mass of dry soil + container (g)	51.19	61.88	46.13	46.98
Water loss (g)	9.46	12.92	9.53	10.15
Container (g)	13.77	13.77	13.77	13.77
Mass of dry soil (g)	37.42	48.11	32.36	33.21
Water content (%)	25.28	26.86	29.45	30.56

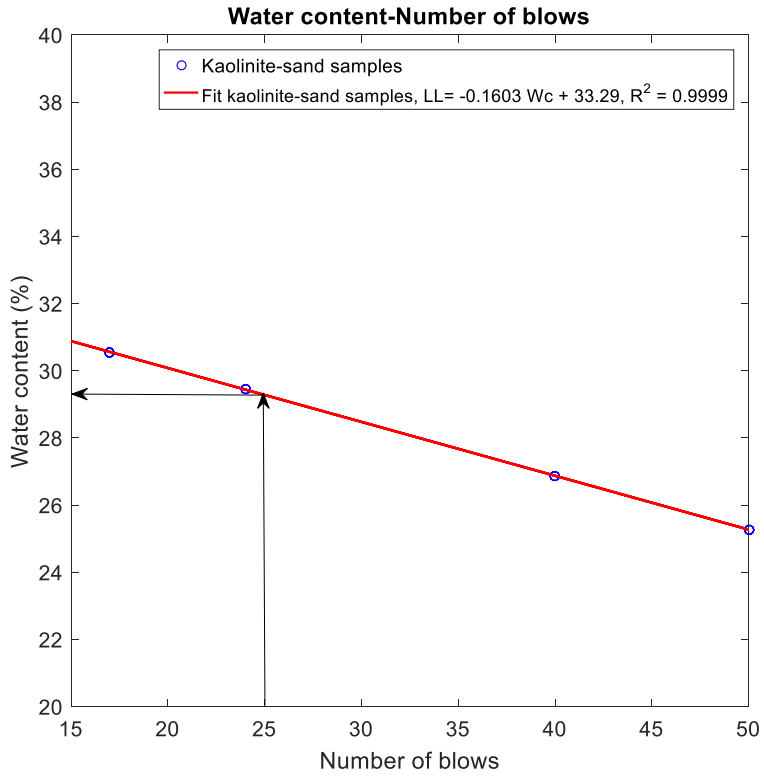

Figure A 4 Liquid limit of kaolinite-sand

Liquid limit = **30** %

`

Table A9 Data of plastic limit tests for kaolinite-sand

Test number	1	2	3
Mass of wet soil + container (g)	43.74	45.63	42.23
Mass of dry soil + container (g)	38.82	40.3	37.21
Water loss (g)	4.92	5.33	5.02
Container (g)	13.77	13.77	13.77
Mass of dry soil (g)	25.05	26.53	23.44
Water content (%)	19.64	20.09	21.42
Average plastic limit	20.38		

Plastic limit = **20** %

A 2.4 Bentonite-sand

Table A10 Data of liquid limit tests for bentonite-sand

Test number	1	2	3	4
Number of blows	35	23	19	15
Mass of wet soil + container (g)	49.23	55.16	57.78	65.30
Mass of dry soil + container (g)	31.11	33.07	33.99	37.12
Water loss (g)	18.12	22.09	23.79	28.18
Container (g)	13.77	13.77	13.77	13.77
Mass of dry soil (g)	17.34	19.30	20.22	23.35
Water content (%)	104.50	114.46	117.60	120.69

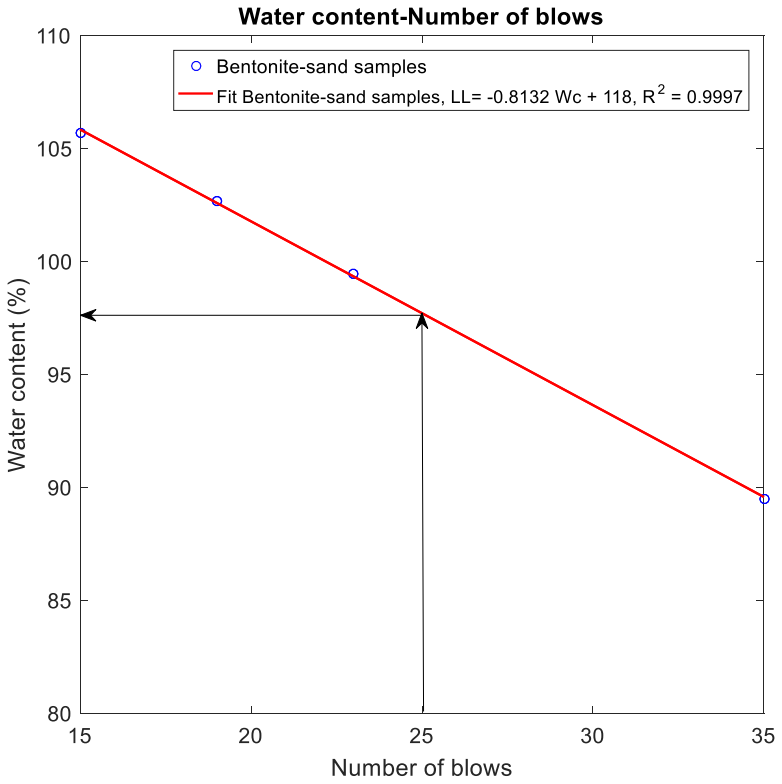

Figure A 5 Liquid limit of bentonite-sand

Liquid limit = **97** %

Table A11 Data of plastic limits test for bentonite-sand

Test number	1	2	3
Mass of wet soil + container (g)	44.21	43.73	40.04
Mass of dry soil + container (g)	36.39	36.29	33.22
Water loss (g)	7.82	7.44	6.82
Container (g)	13.77	13.77	13.97
Mass of dry soil (g)	22.62	22.52	19.25
Water content (%)	34.57	33.04	35.43
Average plastic limit	34.34		

Plastic limit = **34** %

`

A 3 Specific gravity

A 3.1 Sand

Table A12 Data of specific gravity of sand

Measurements	Unit	Test 1	Test 2
The mass of the oven dry soil solids finer than 4.75 mm	g	100.07	100.23
Mass of pycnometer (Mp)	g	185.13	185.13
The Volume of the pycnometer (Vp)	ml	494.86	494.86
Temperature of Test (Tt)	°C	18.5	18.50
The density of water at the test temperature (ρw,t)	g/cm3	0.998483	0.998502
The mass of the pycnometer and water (Mpw,t)	g	679.24	679.25
The mass of the pycnometer, water, and soil (Mpws,t)	g	741.54	741.66
Specific Gravity (Gt)		2.6488	2.6503
The temperature Coefficient (K)		1.00030	1.00030
Specific gravity at 20 °C (G 20°C) G 20°C = K* Gt		2.6496	2.6510
Specific gravity at 20 °C	**2.65**		

A 3.2 kaolinite

Table A13 Data of specific gravity of kaolinite

Measurements	Unit	Test 1	Test 2
The mass of the oven dry soil solids (Ms)	g	50.03	50.03
Mass of pycnometer (Mp)	g	185.13	185.13
The Volume of the pycnometer (Vp)	ml	494.86	494.86
Temperature of Test (Tt)	°C	18.60	18.60
The density of water at the test temperature (ρw,t)	g/cm3	0.998483	0.998483
The mass of the pycnometer and water (Mpw,t)	g	679.24	679.24
The mass of the pycnometer, water, and soil (Mpws,t)	g	710.21	710.15
Specific Gravity (Gt)		2.6249	2.6167
The temperature Coefficient (K)		1.00028	1.00028
Specific gravity at 20 °C (G 20°C) G 20°C = K* Gt		2.6257	2.6174
Specific gravity at 20 °C	**2.62**		

`

A 3.3 Bentonite

Table A14 Data of specific gravity of bentonite

Measurements	Unit	Test 1	Test 2
The mass of the oven dry soil solids (Ms)	g	50.01	50.00
Mass of pycnometer (Mp)	g	185.13	185.13
The Volume of the pycnometer (Vp)	ml	494.86	494.86
Temperature of Test (Tt)	°C	18.60	18.60
The density of water at the test temperature (ρw,t)	g/cm3	0.998483	0.998483
The mass of the pycnometer and water (Mpw,t)	g	679.24	679.24
The mass of the pycnometer, water, and soil (Mpws,t)	g	710.08	710.11
Specific Gravity (Gt)		2.6088	2.6138
The temperature Coefficient (K)		1.00028	1.00028
Specific gravity at 20 °C (G 20°C) G 20°C = K* Gt		2.6096	2.6145
Specific gravity at 20 °C	**2.61**		

`

APPENDIX B

EXPERIMENTAL PROGRAM RESULTS

B 1 Tensile strength tests results

Table B 1 Details of tensile strength tested groups at -10°C.

Group	Samples	Test	Salinity	Loading rate
K-04	K1S10-K1S12	RST	1 g/L	1, 3, and 9 mm/min
K-05	K1S13-K1S15	FST	1 g/L	1, 3, and 9 mm/min
K-06	K1S16-K1S18	DPT	1 g/L	1, 3, and 9 mm/min
B-04	B1S10-B1S12	RST	1 g/L	1, 3, and 9 mm/min
B-05	B1S13-B1S15	FST	1 g/L	1, 3, and 9 mm/min
B-06	B1S16-B1S18	DPT	1 g/L	1, 3, and 9 mm/min

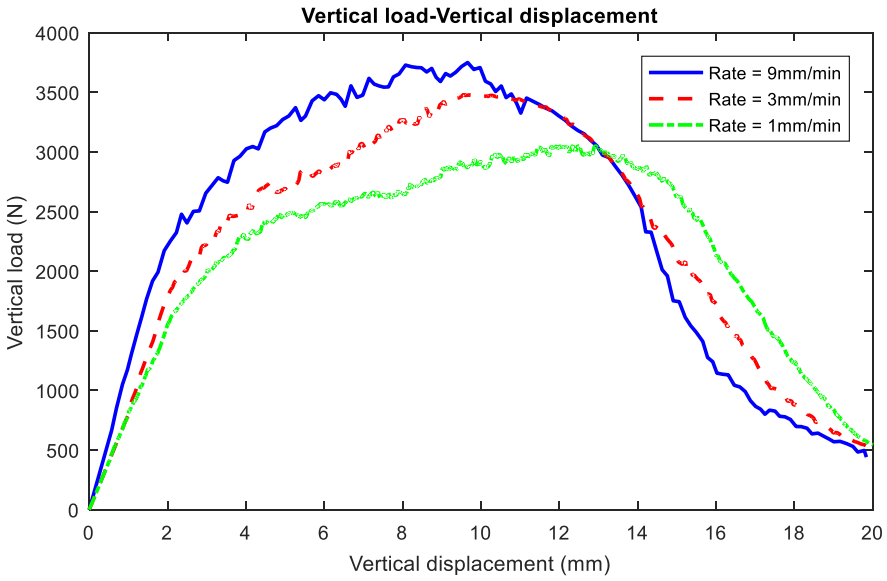

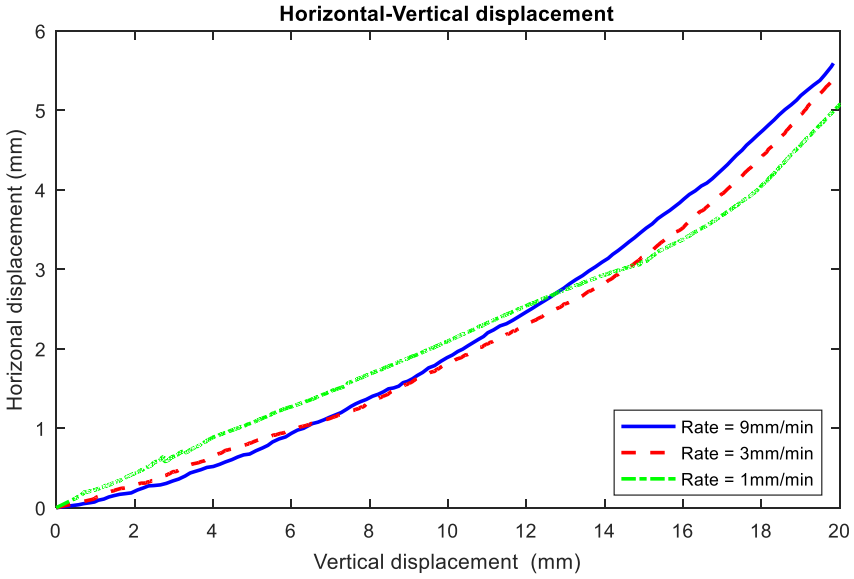

Figure B 1 Results of tensile strength tests performed on group K-04 (Loading approach= RST, T= - 10 °C, Salinity= 1 g/L).

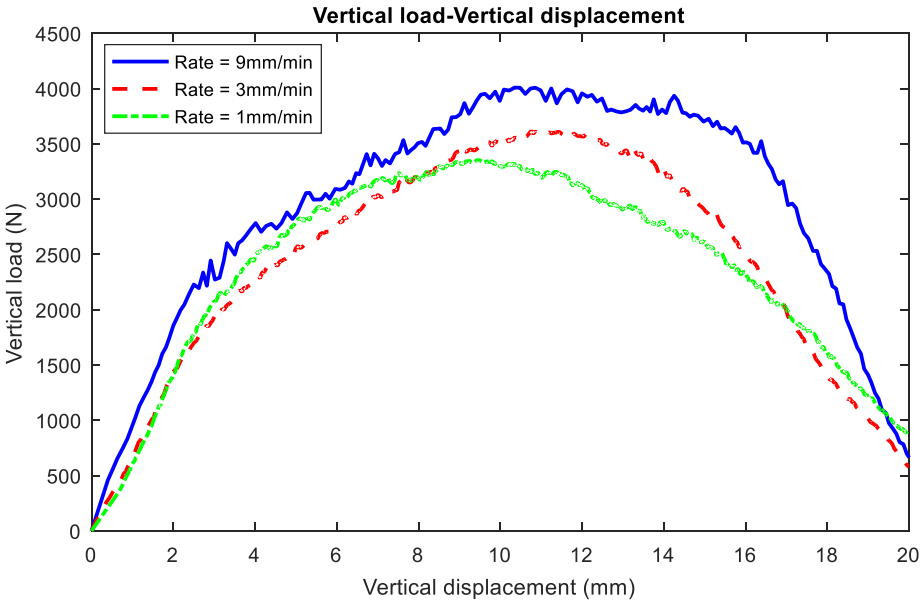

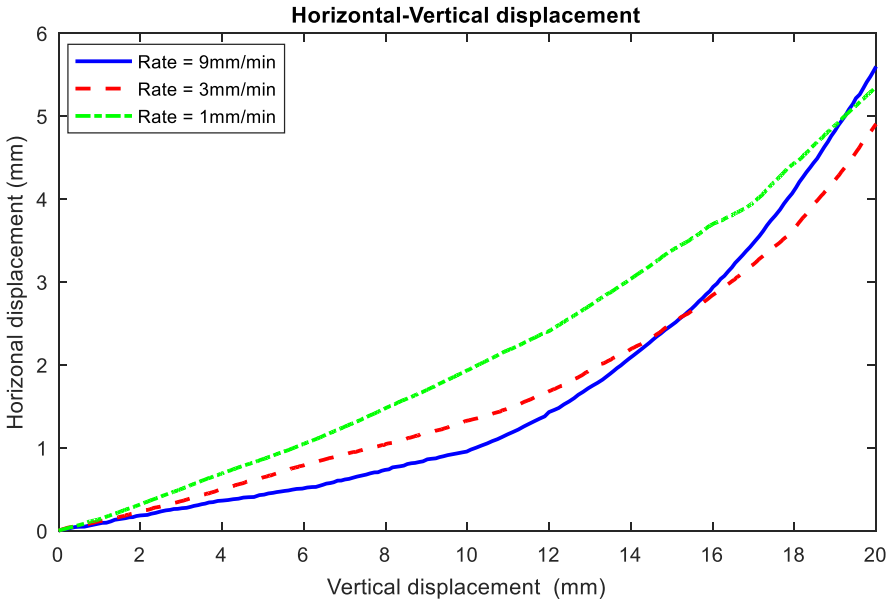

Figure B 2 Results of tensile strength tests performed on group K-05 (Loading approach= FST, T= - 10 °C, Salinity= 1 g/L).

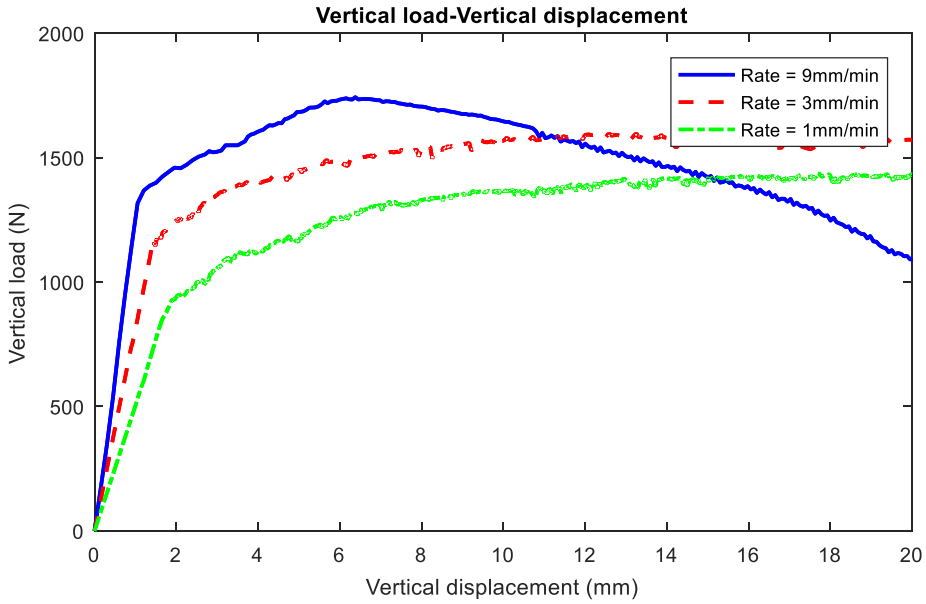

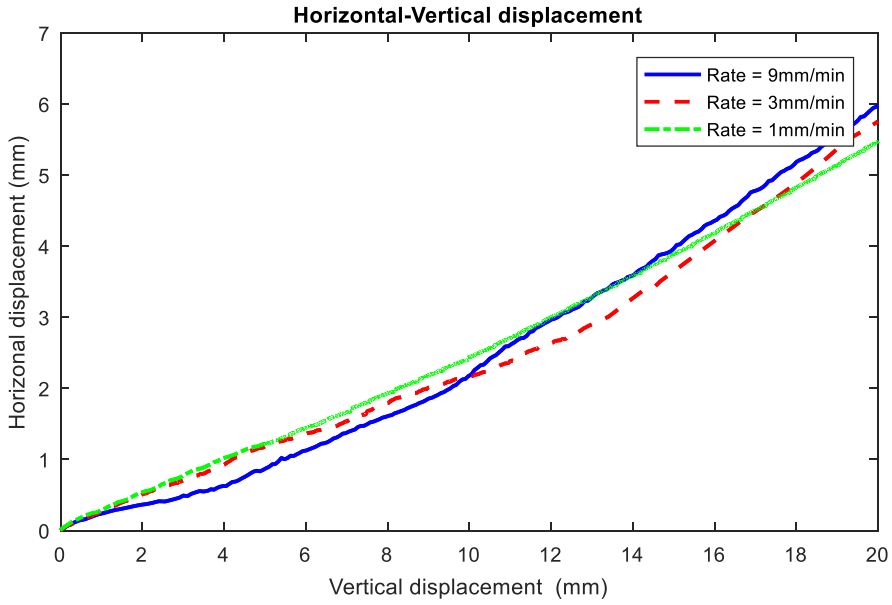

Figure B 3 Results of tensile strength tests performed on group K-06 (Loading approach= DPT, T= - 10 °C, Salinity= 1 g/L).

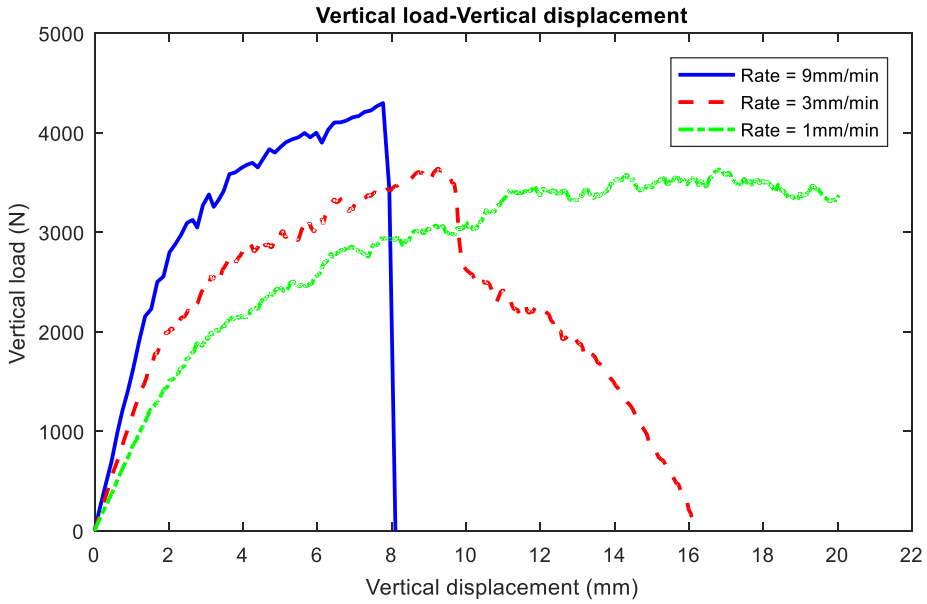

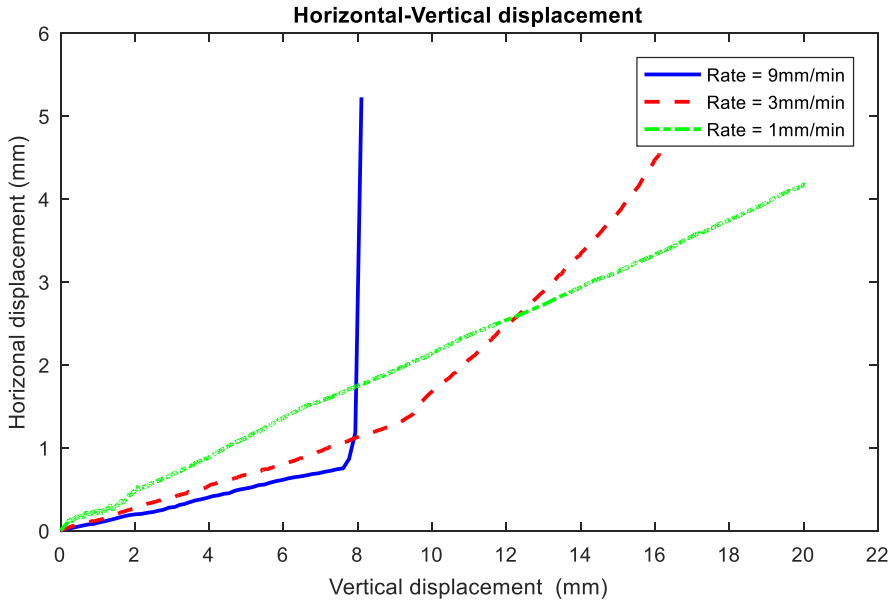

Figure B 4 Results of tensile strength tests performed on group B-04 (Loading approach= RST, T= - 10 °C, Salinity= 1 g/L).

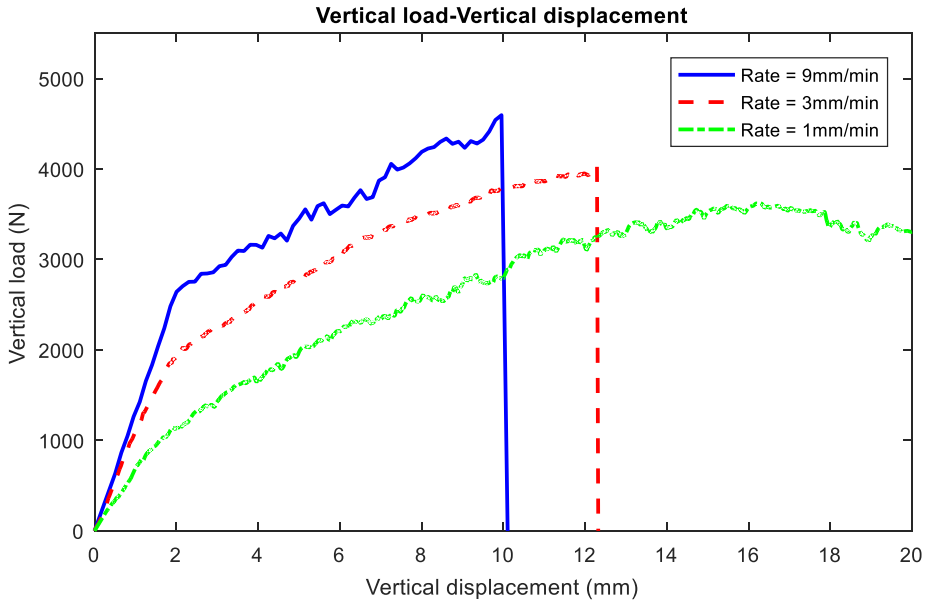

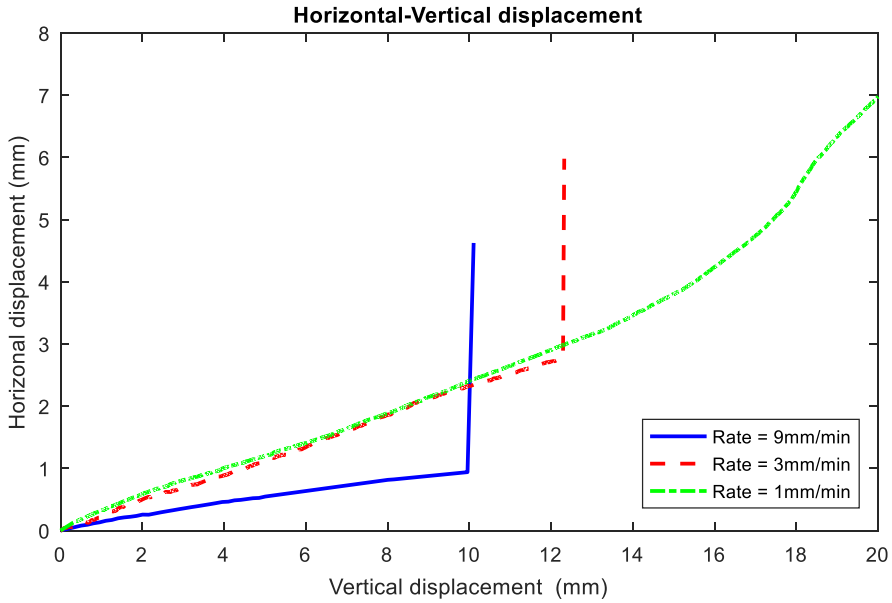

Figure B 5 Results of tensile strength tests performed on group B-05 (Loading approach= FST, T= - 10 °C, Salinity= 1 g/L).

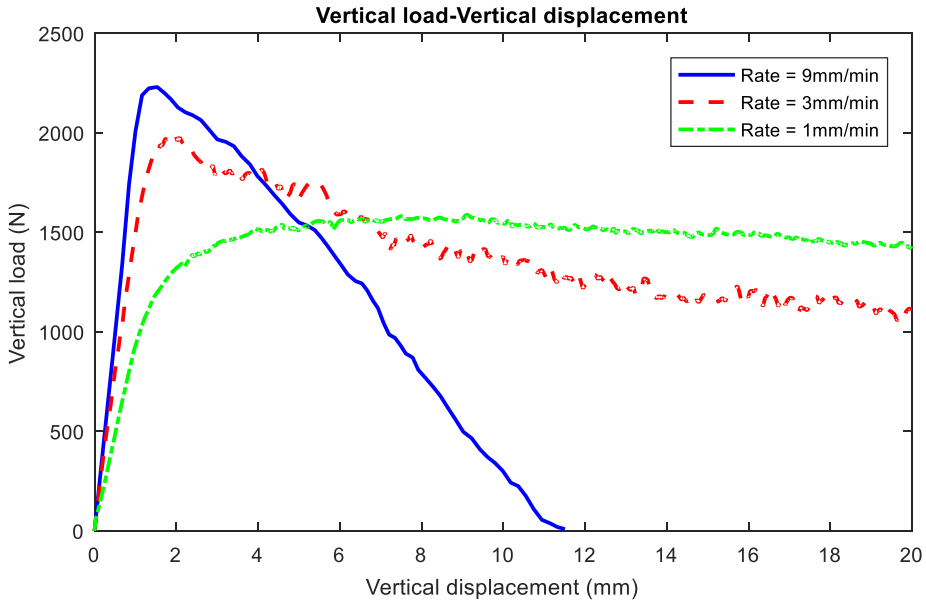

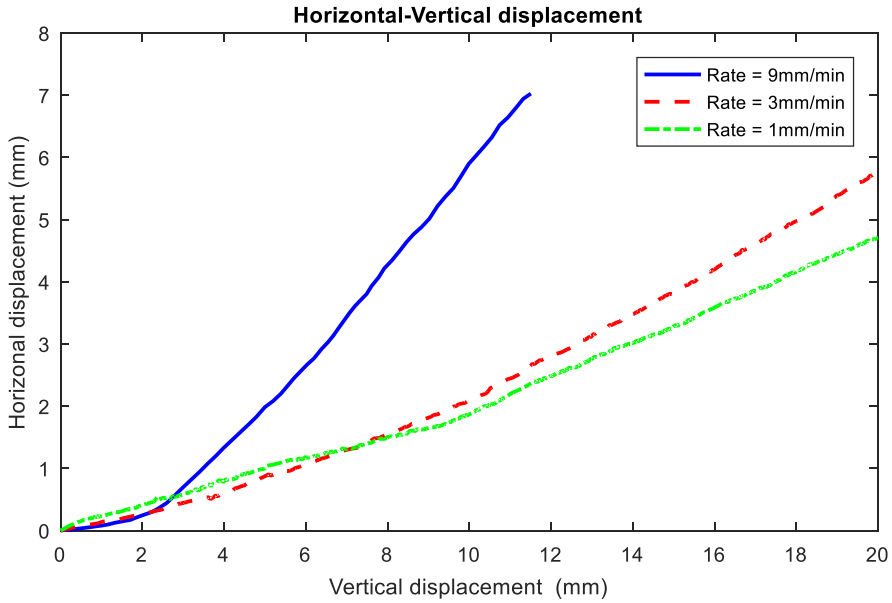

Figure B 6 Results of tensile strength tests performed on group B-06 (Loading approach= DPT, T= - 10 °C, Salinity= 1 g/L).

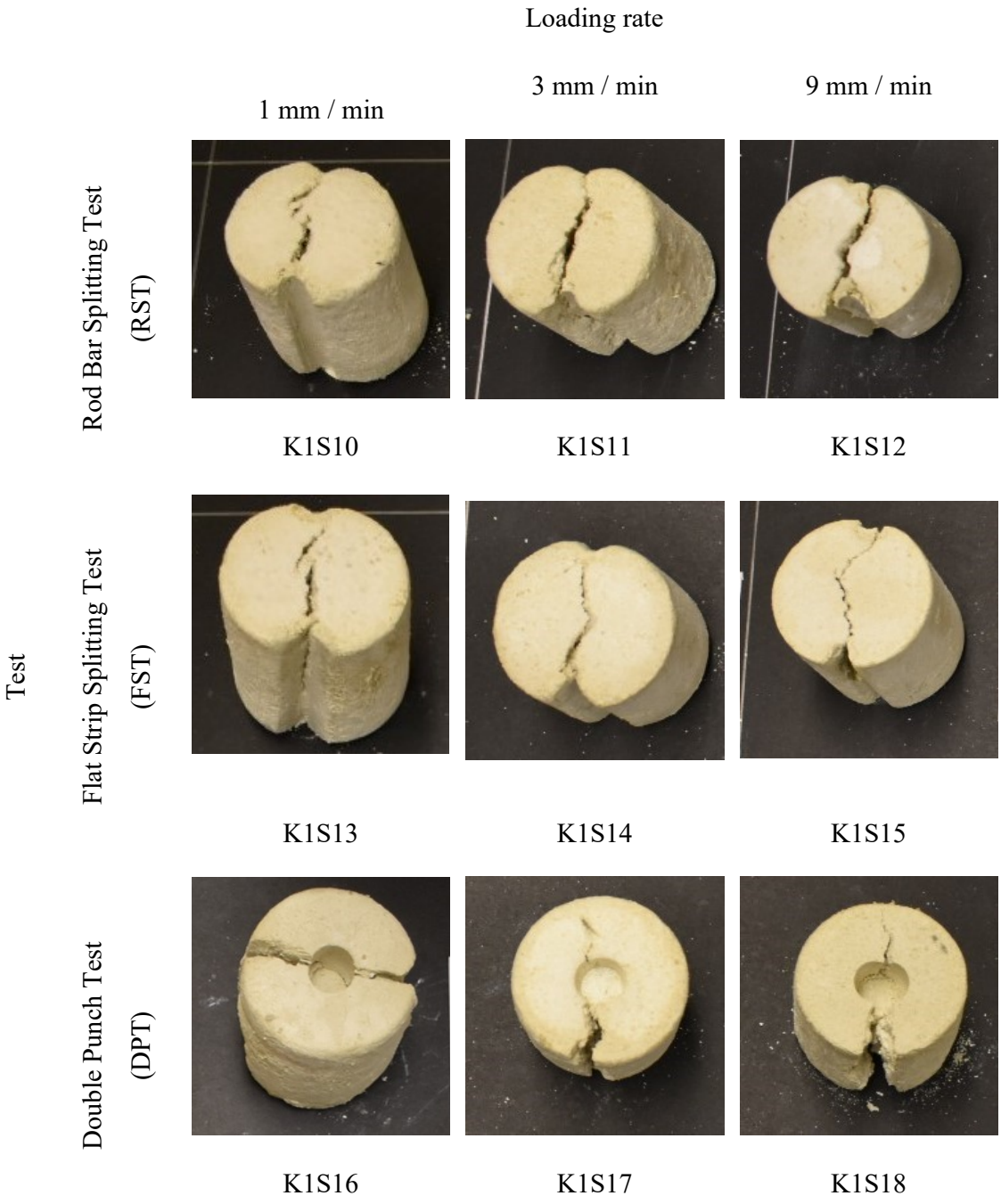

Figure B 7 Post-failure pictures of tested kaolinite-sand samples (T= - 10°C, Salinity = 1 g/L).

`

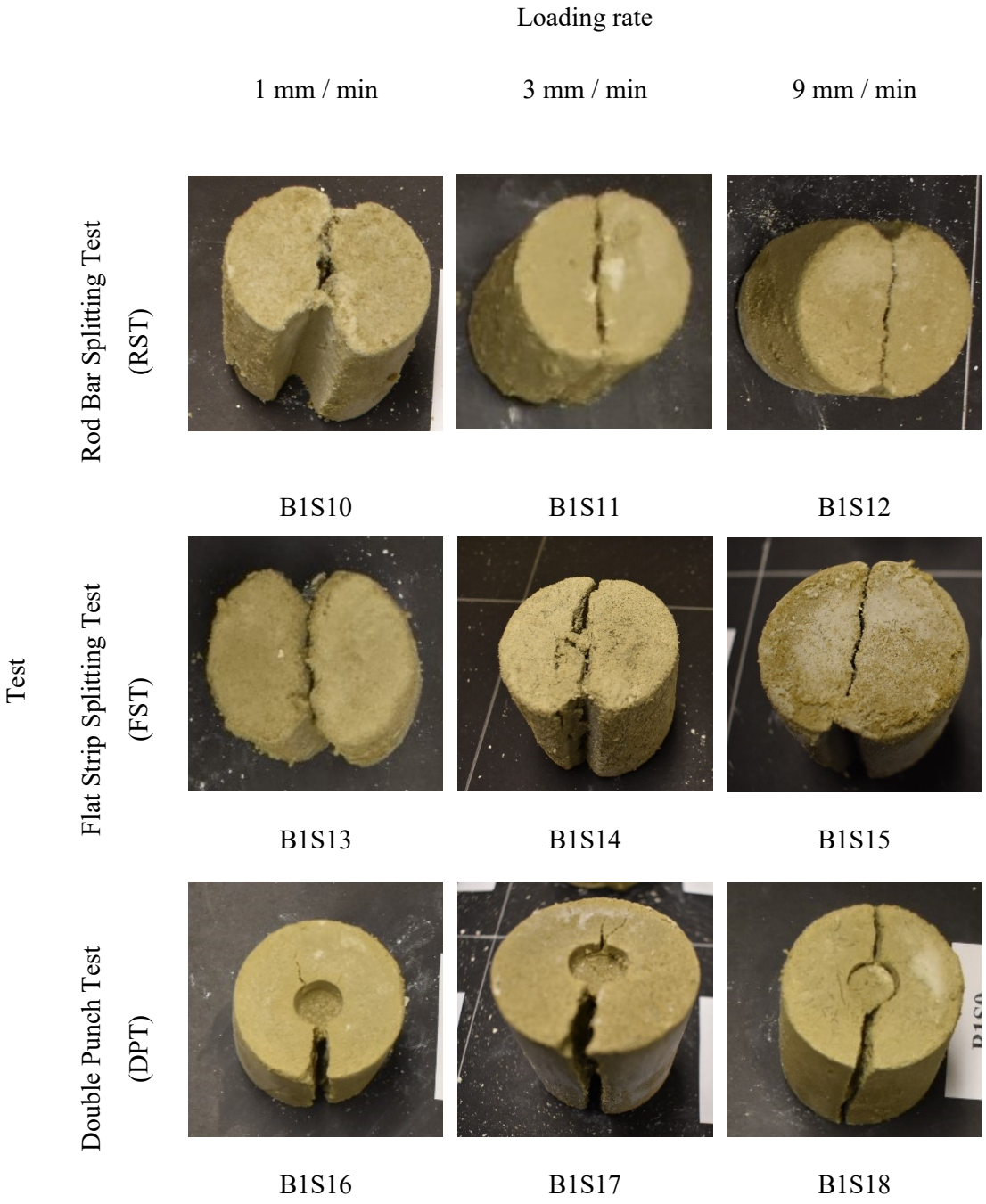

Figure B 8 Post-failure pictures of tested bentonite-sand samples (T= - 10 °C, Salinity= 1 g/L).

`

Table B 2 Details of tensile strength tested groups at -5°C.

Group	Samples	Test	Salinity	Loading rate
K-07	K1S19-K1S21	RST	1 g/L	1, 3, and 9 mm/min
K-08	K1S22-K1S24	FST	1 g/L	1, 3, and 9 mm/min
K-09	K1S25-K1S27	DPT	1 g/L	1, 3, and 9 mm/min
B-07	B1S19-B1S21	RST	1 g/L	1, 3, and 9 mm/min
B-08	B1S22-B1S24	FST	1 g/L	1, 3, and 9 mm/min
B-09	B1S25-B1S27	DPT	1 g/L	1, 3, and 9 mm/min
K-10	K0S01-K0S03	RST	0 g/L	1, 3, and 9 mm/min
K-11	K0S04-K0S06	FST	0 g/L	1, 3, and 9 mm/min
K-12	K0S07-K0S09	DPT	0 g/L	1, 3, and 9 mm/min
B-10	B0S01-B0S03	RST	0 g/L	1, 3, and 9 mm/min
B-11	B0S04-B0S06	FST	0 g/L	1, 3, and 9mm/min
B-12	B0S07-B0S09	DPT	0 g/L	1, 3, and 9 mm/min
K-13	K3S01-K3S03	RST	3 g/L	1, 3, and 9 mm/min
K-14	K3S04-K3S06	FST	3 g/L	1, 3, and 9 mm/min
K-15	K3S07-K3S09	DPT	3 g/L	1, 3, and 9 mm/min
B-13	B3S01-B3S03	RST	3 g/L	1, 3, and 9 mm/min
B-14	B3S04-B3S06	FST	3 g/L	1, 3, and 9 mm/min
B-15	B3S07-B3S09	DPT	3 g/L	1, 3, and 9 mm/min

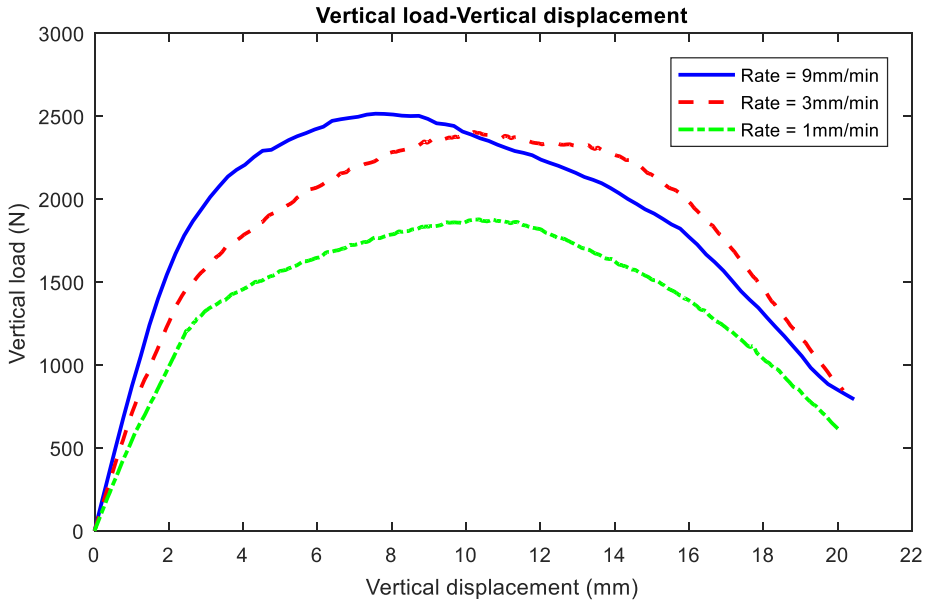

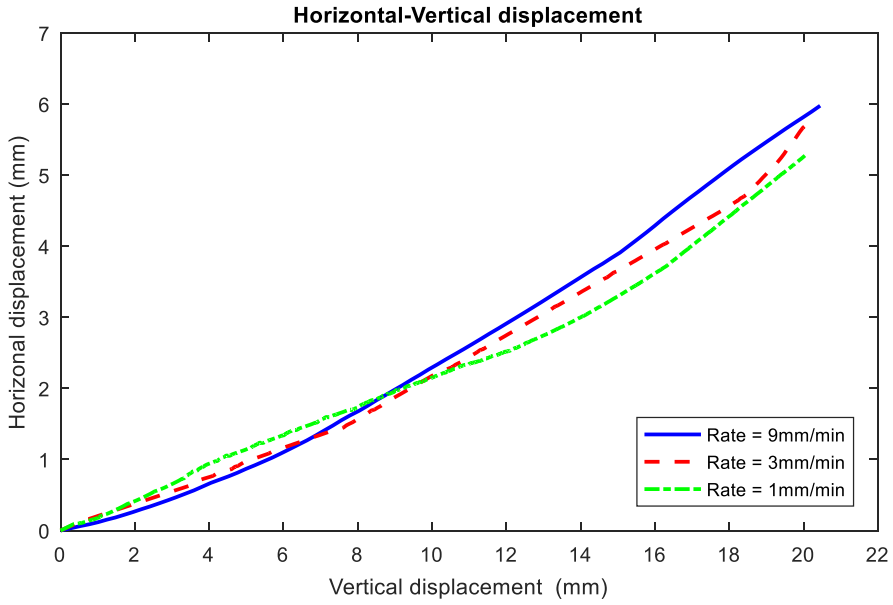

Figure B 9 Results of tensile strength tests performed on group K-07 (Loading approach= RST, T= - 5 °C, Salinity= 1 g/L).

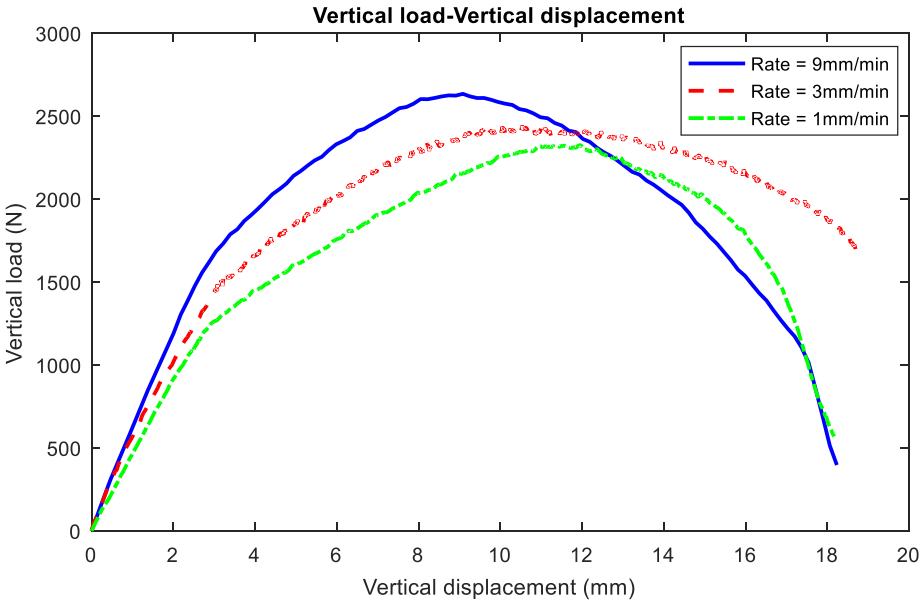

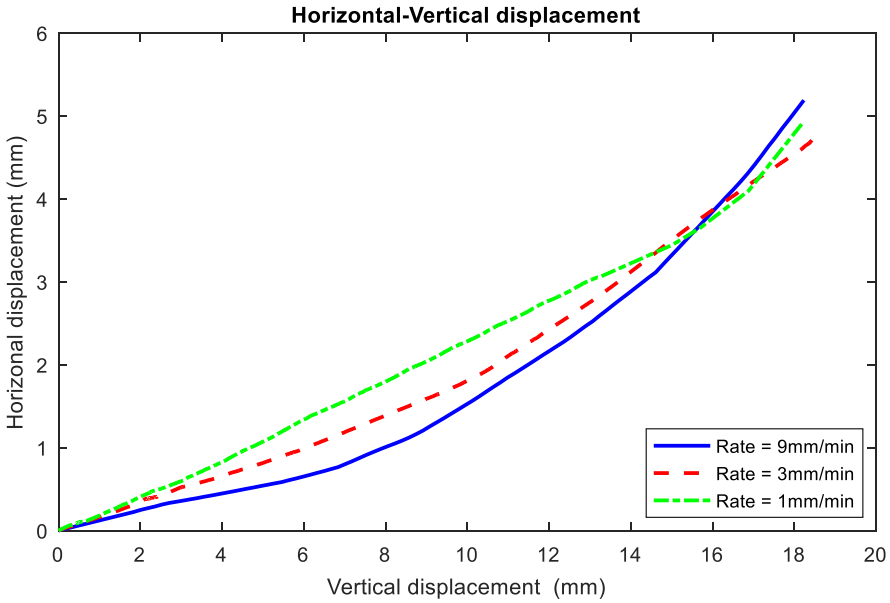

Figure B 10 Results of tensile strength tests performed on group K-08 (Loading approach= FST, T= - 5 °C, Salinity= 1 g/L).

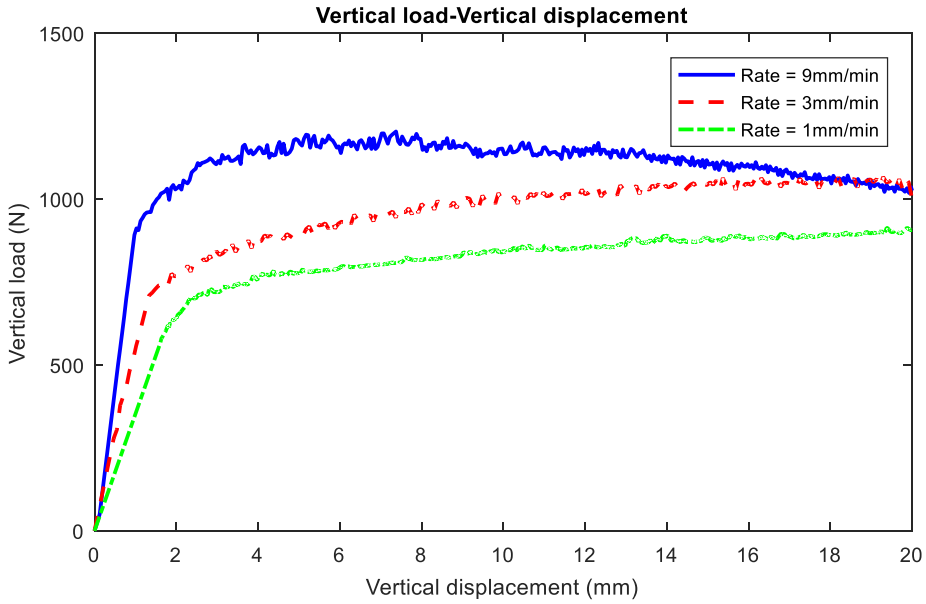

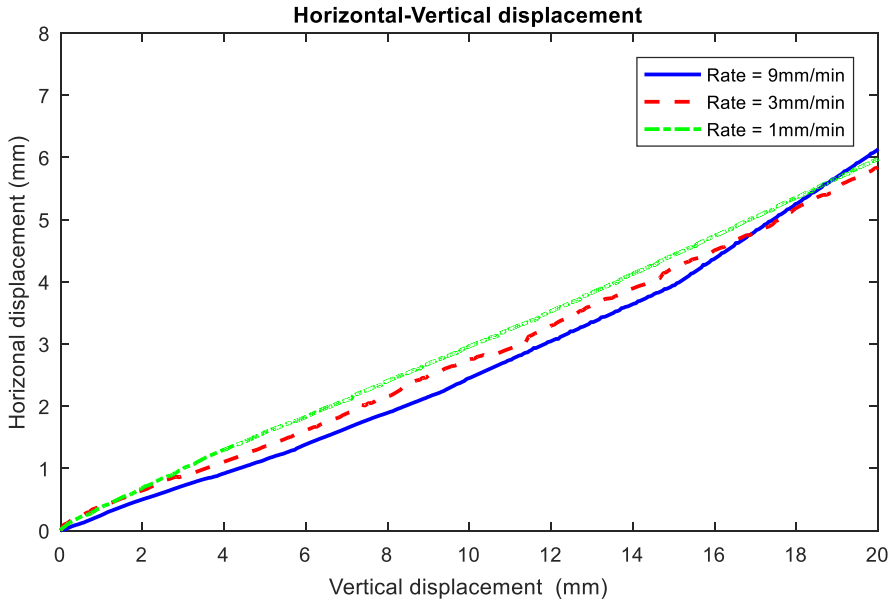

Figure B 11 Results of tensile strength tests performed on group K-09 (Loading approach= DPT, T= - 5 °C, Salinity= 1 g/L).

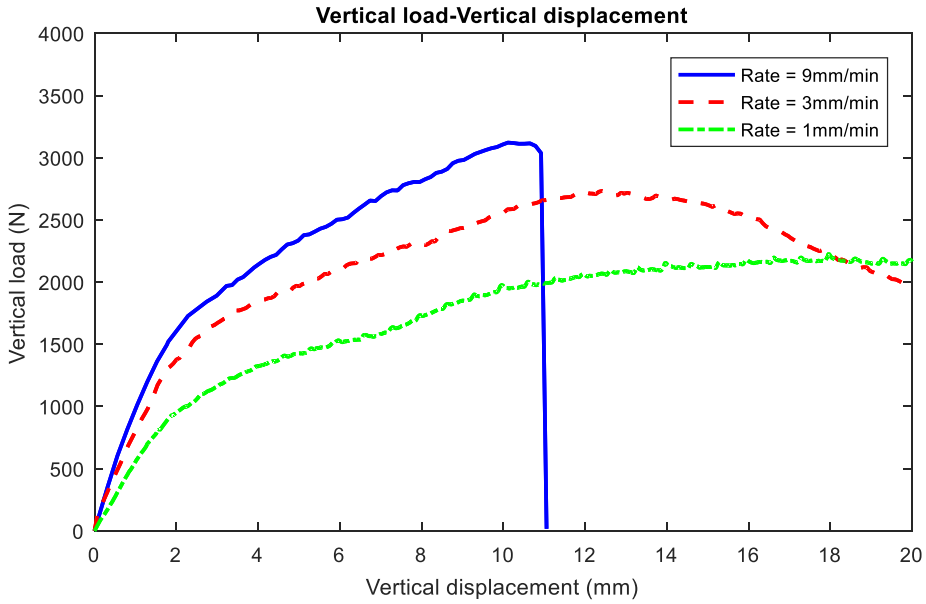

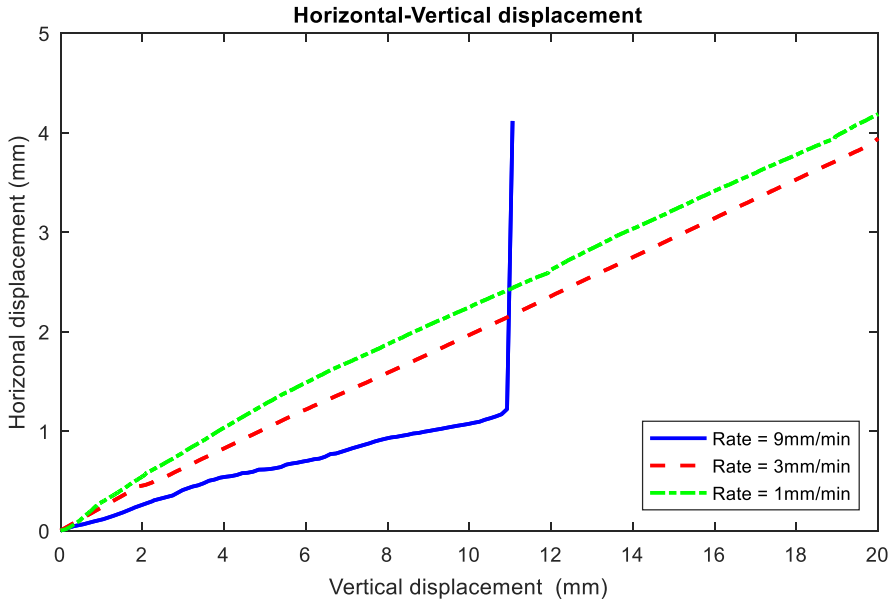

Figure B 12 Results of tensile strength tests performed on group B-07 (Loading approach= RST, T= - 5 °C, Salinity= 1 g/L).

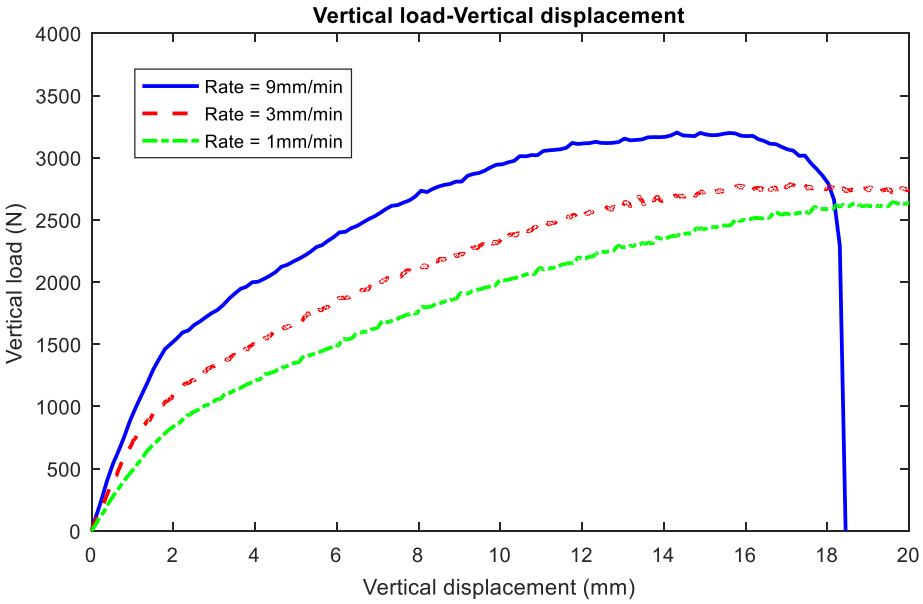

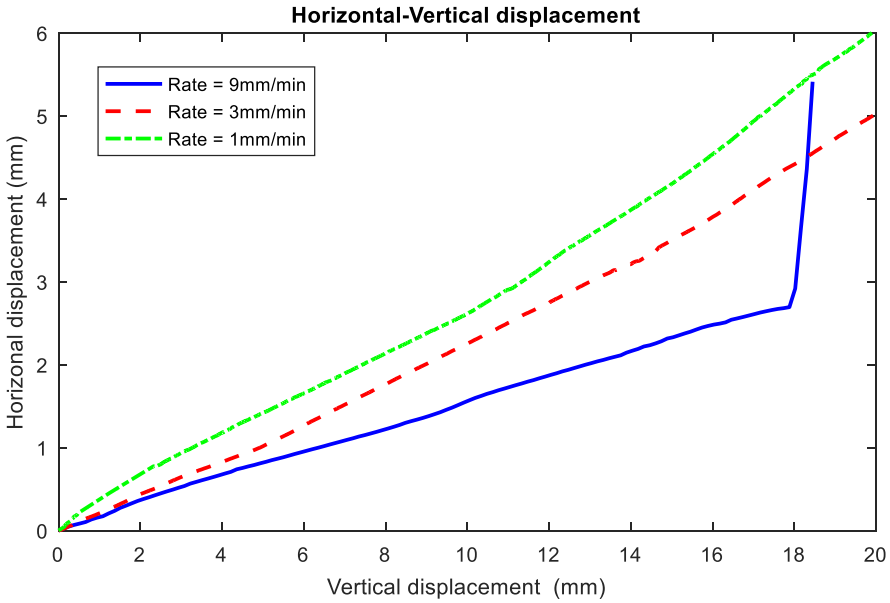

Figure B 13 Results of tensile strength tests performed on group B-08 (Loading approach= FST, T= - 5 °C, Salinity= 1 g/L).

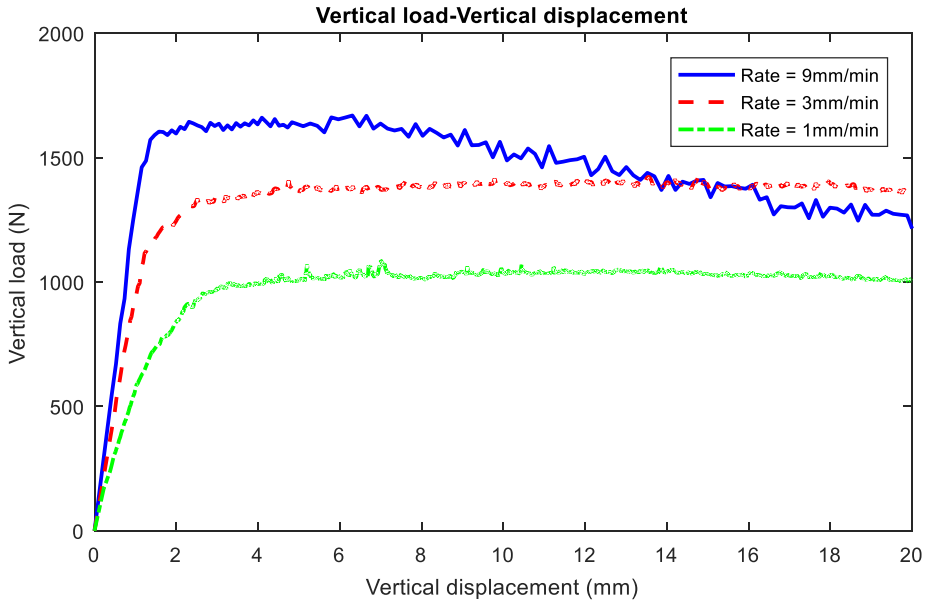

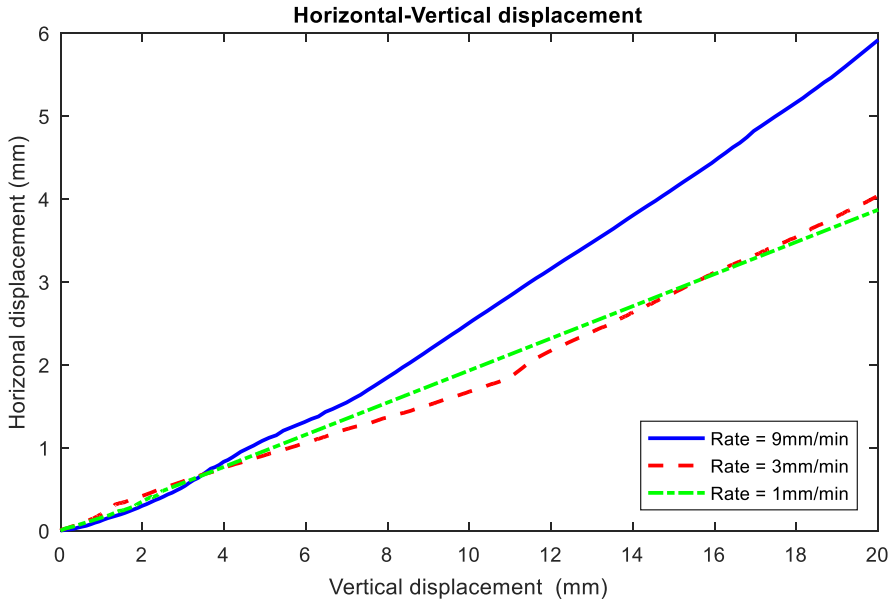

Figure B 14 Results of tensile strength tests performed on group B-09 (Loading approach= DPT, T= - 5 °C, Salinity= 1 g/L).

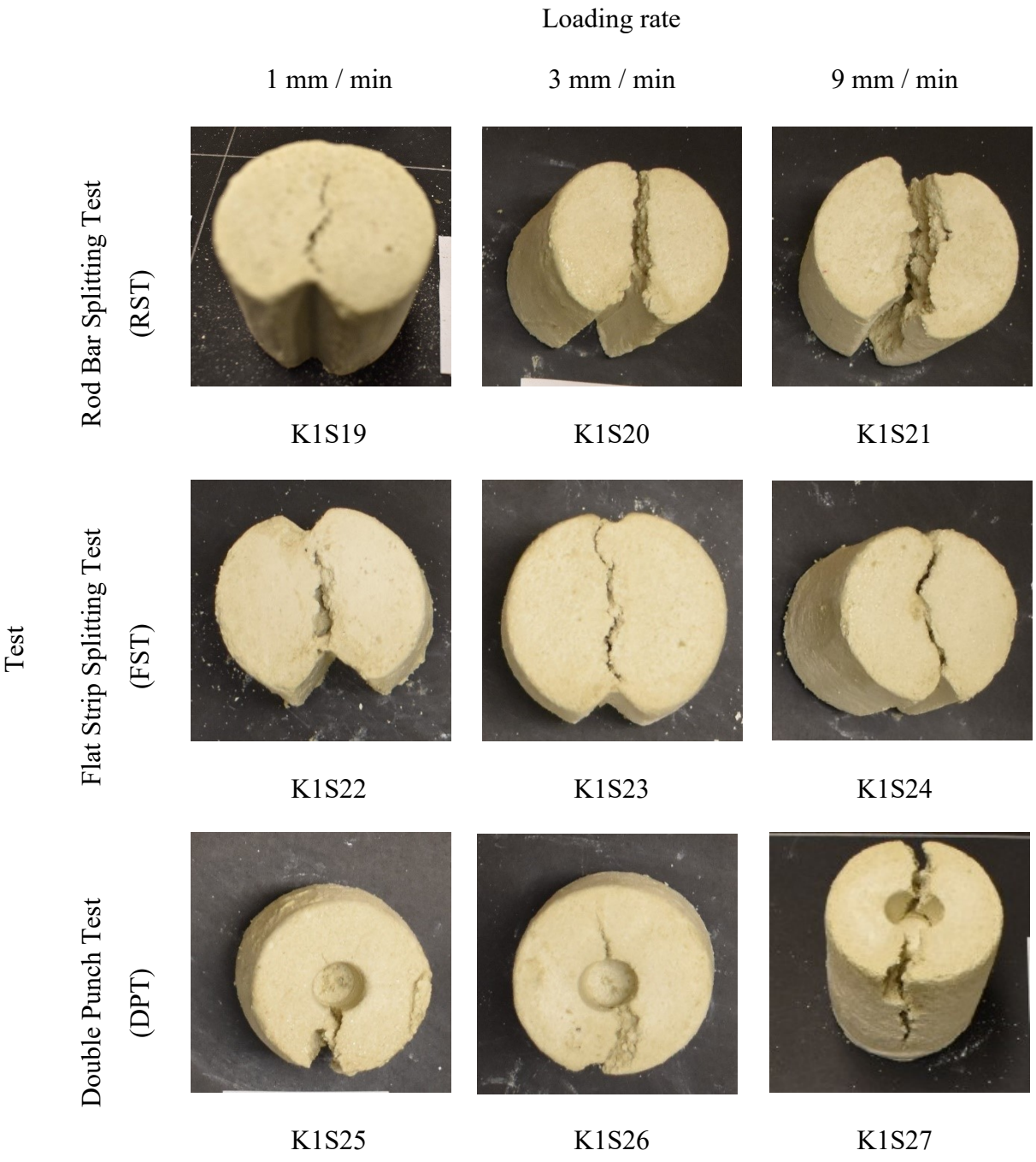

Figure B 15 Post-failure pictures of tested kaolinite-sand samples (T= - 5 °C, Salinity= 1 g/L).

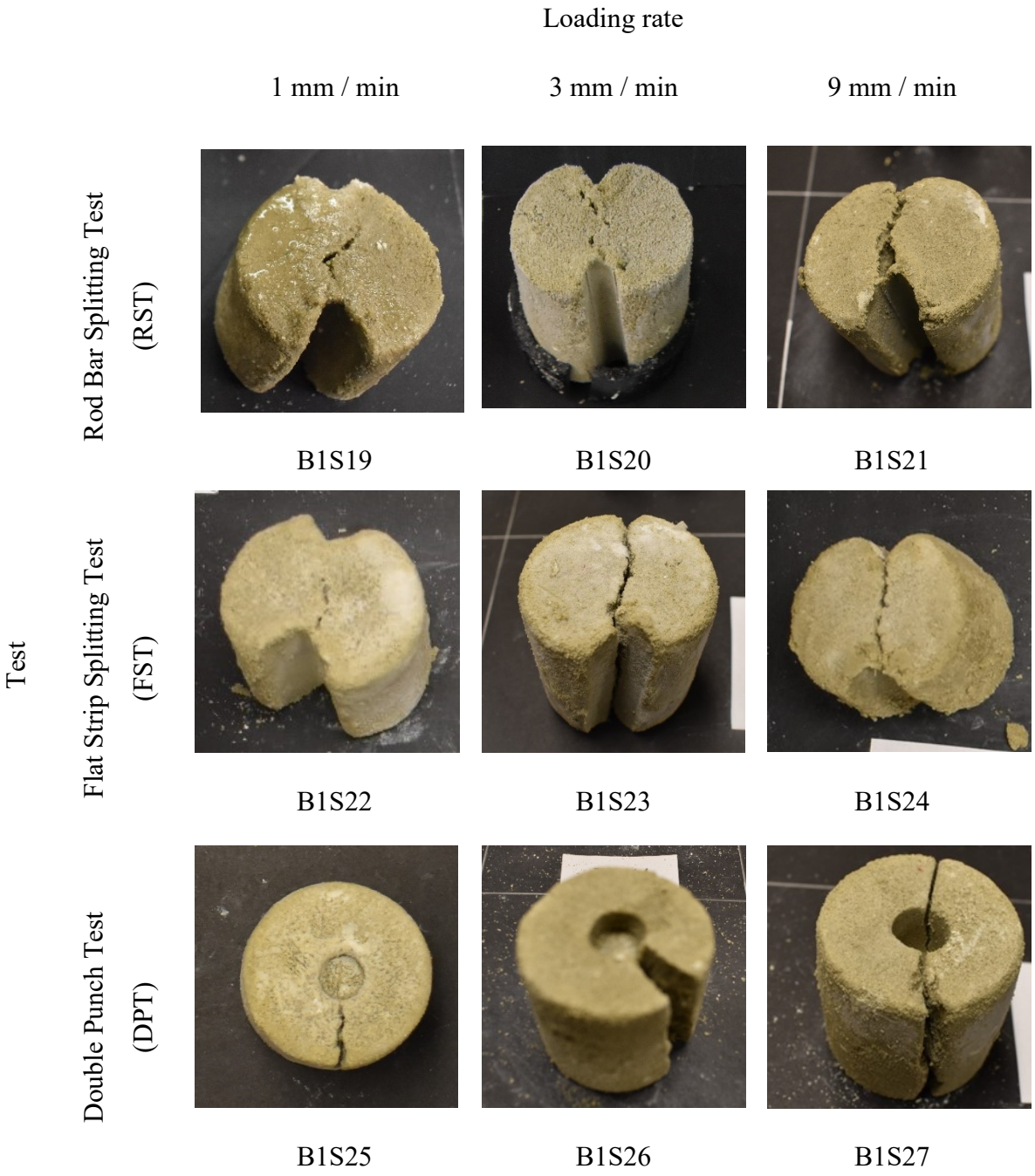

Figure B 16 Post-failure pictures of tested bentonite-sand samples (T= - 5 °C, Salinity= 1 g/L).

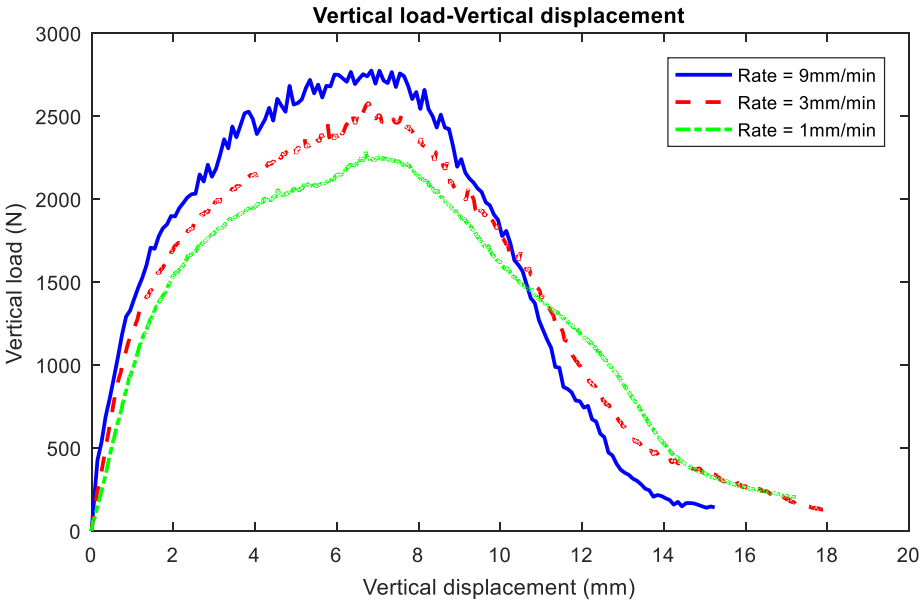

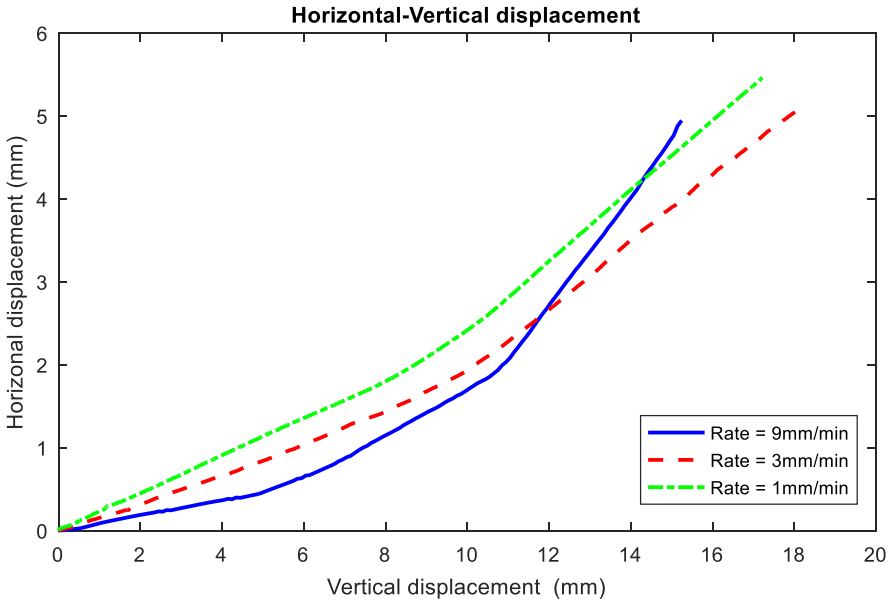

Figure B 17 Results of tensile strength tests performed on group k-10 (Loading approach= RST, T= - 5 °C, Salinity= 0 g/L).

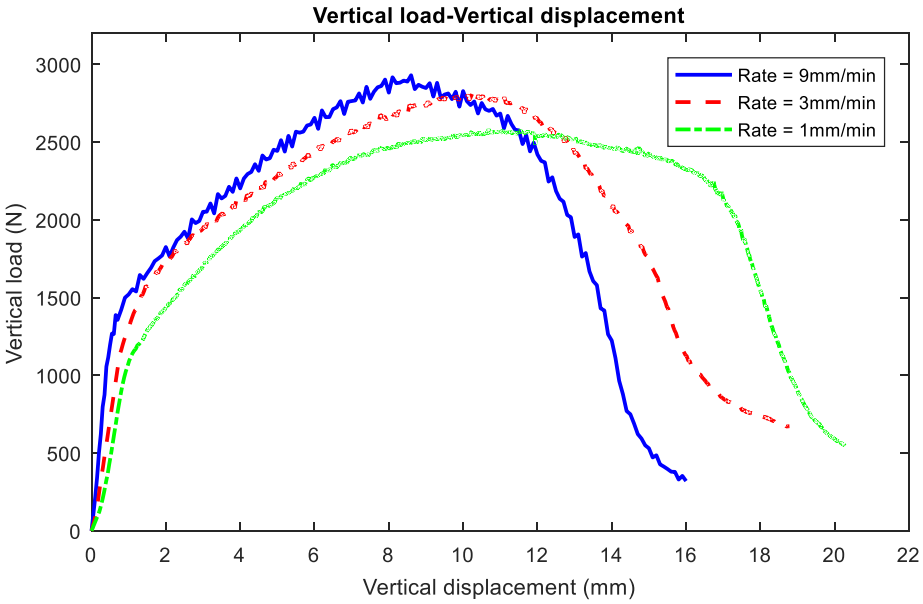

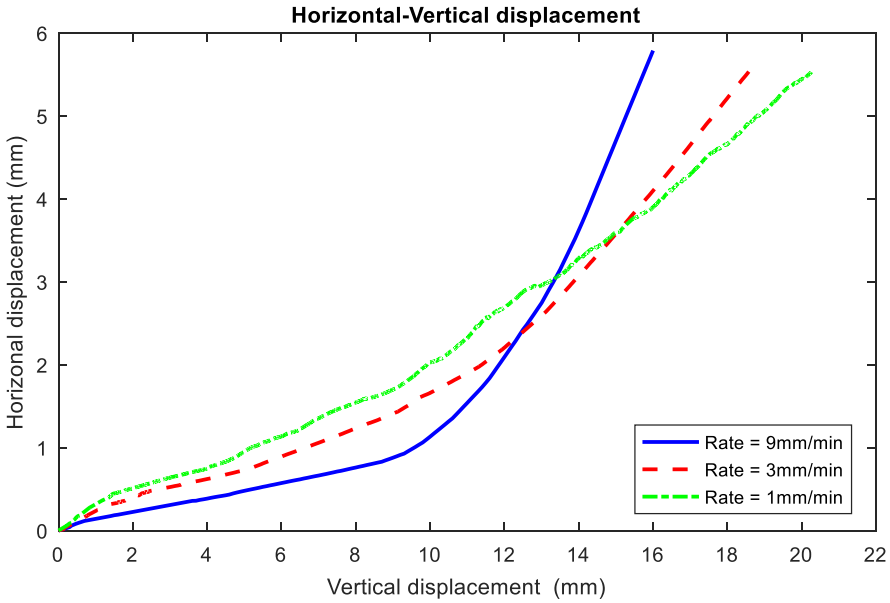

Figure B 18 Results of tensile strength tests performed on group k-11 (Loading approach= FST, T= - 5 °C, Salinity= 0 g/L).

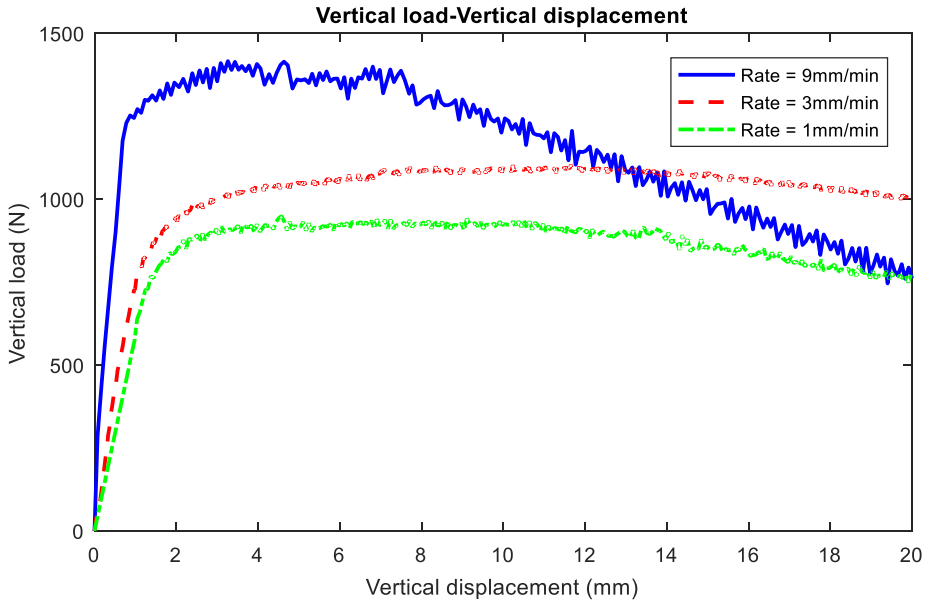

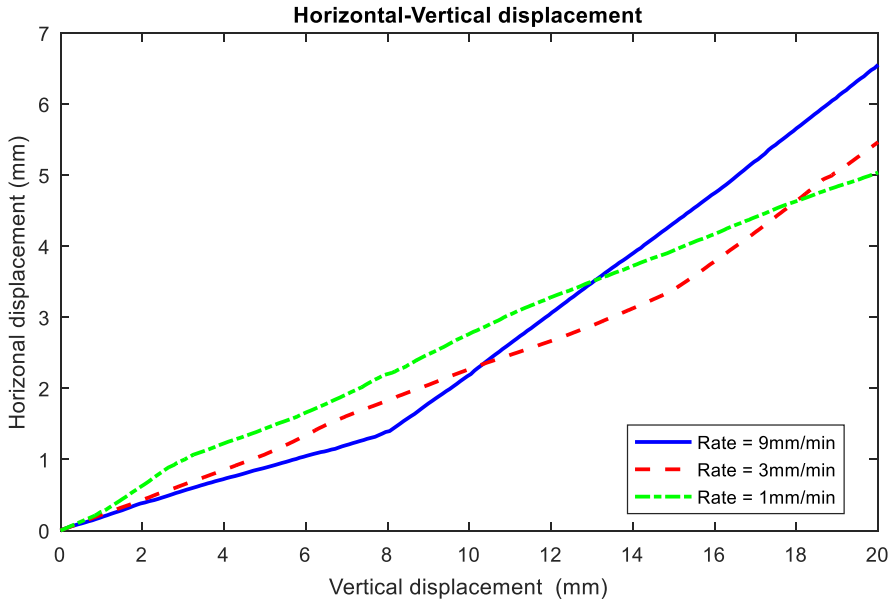

Figure B 19 Results of tensile strength tests performed on group k-12 (Loading approach= DPT, T= - 5 °C, Salinity= 0 g/L).

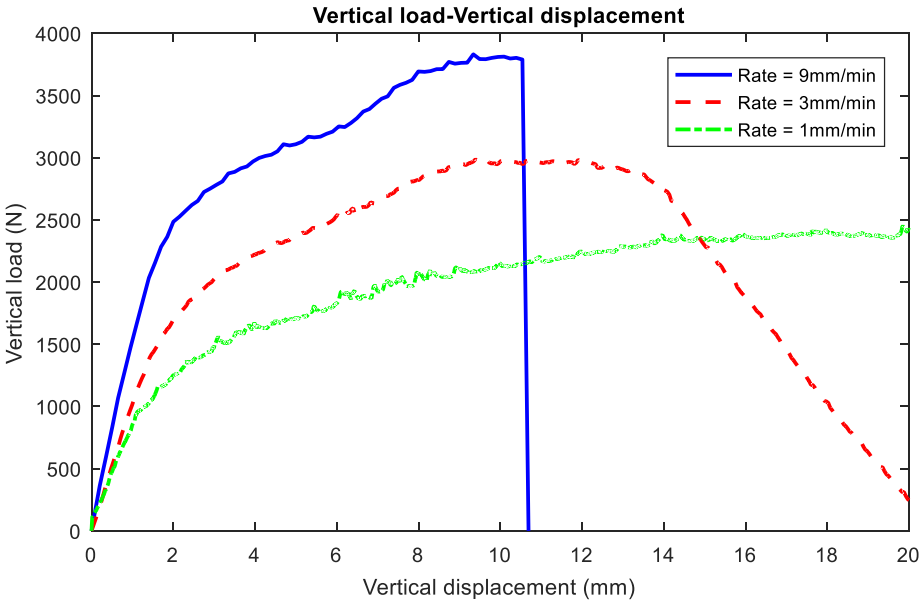

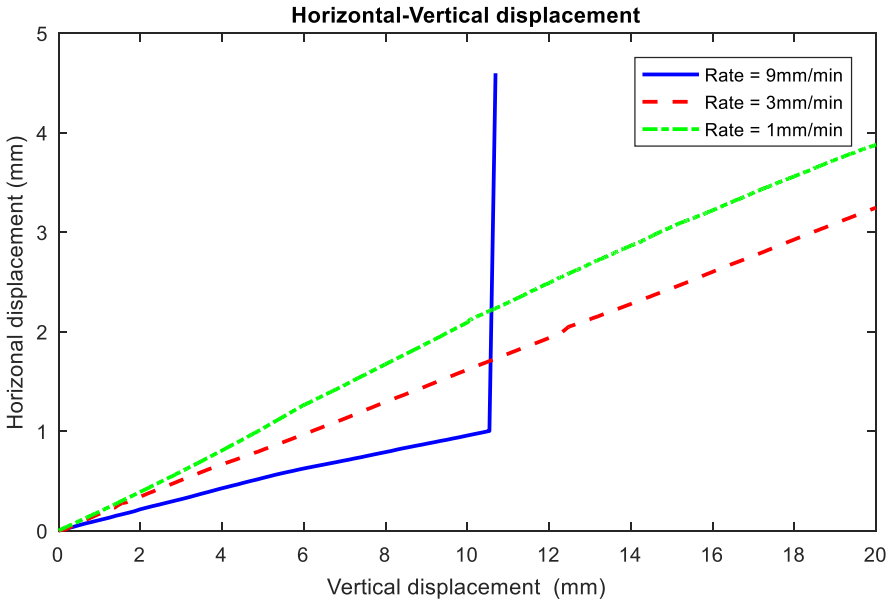

Figure B 20 Results of tensile strength tests performed on group B-10 (Loading approach= RST, T= - 5 °C, Salinity= 0 g/L).

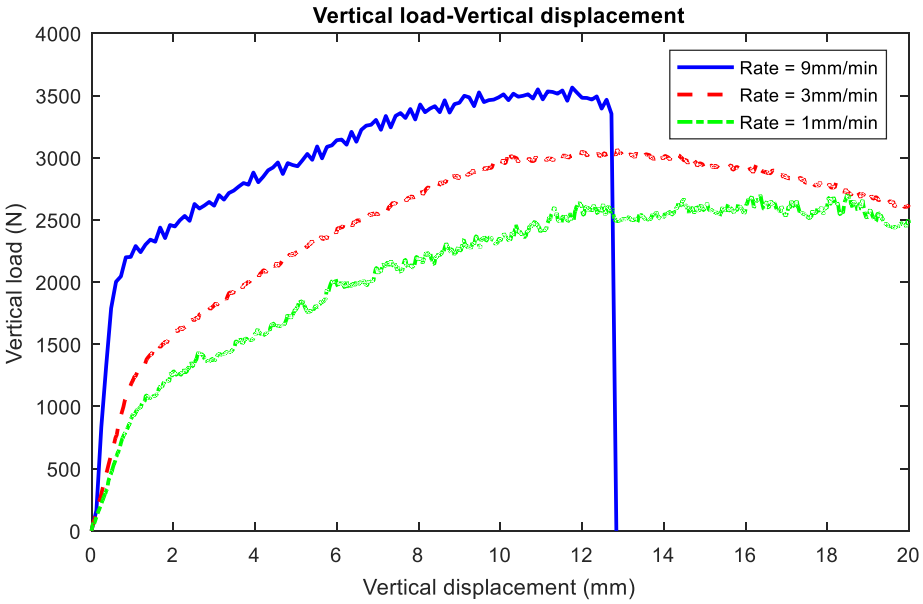

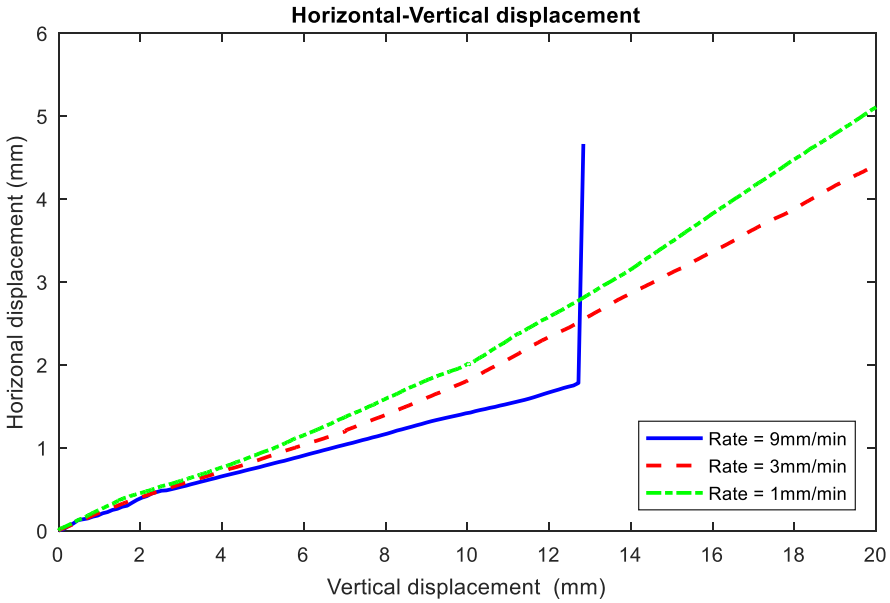

Figure B 21 Results of tensile strength tests performed on group B-11 (Loading approach= FST, T= - 5 °C, Salinity= 0 g/L).

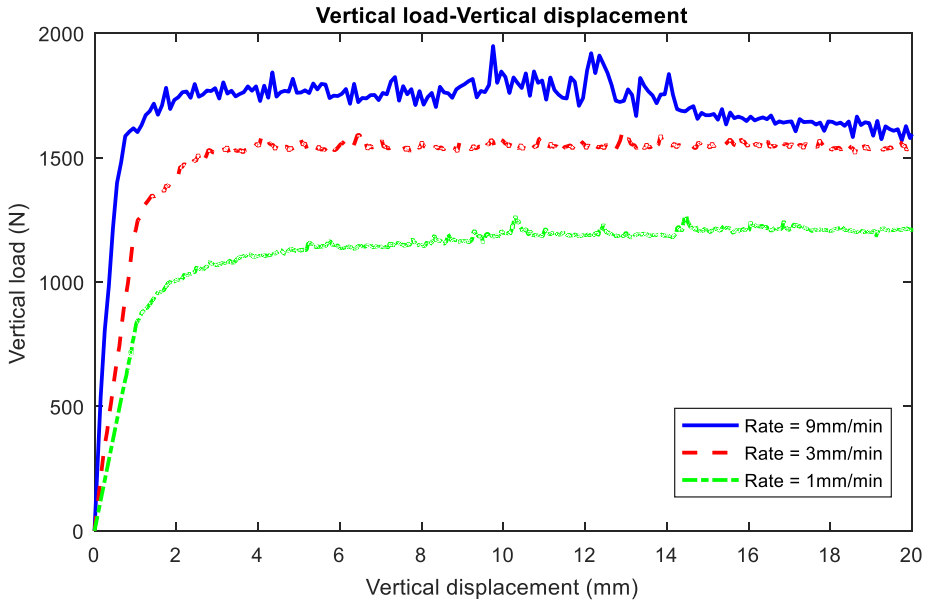

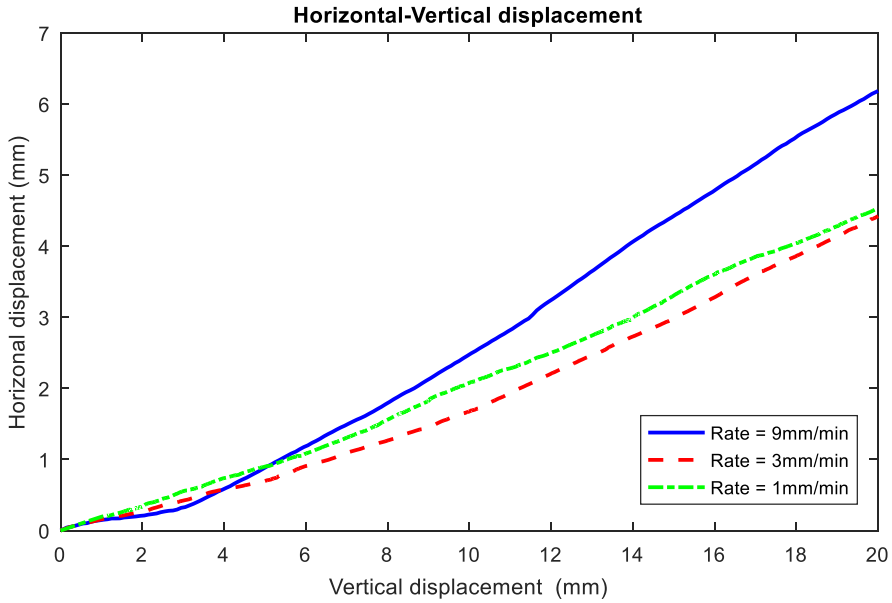

Figure B 22 Results of tensile strength tests performed on group B-12 (Loading approach= DPT, T= - 5 °C, Salinity= 0 g/L)

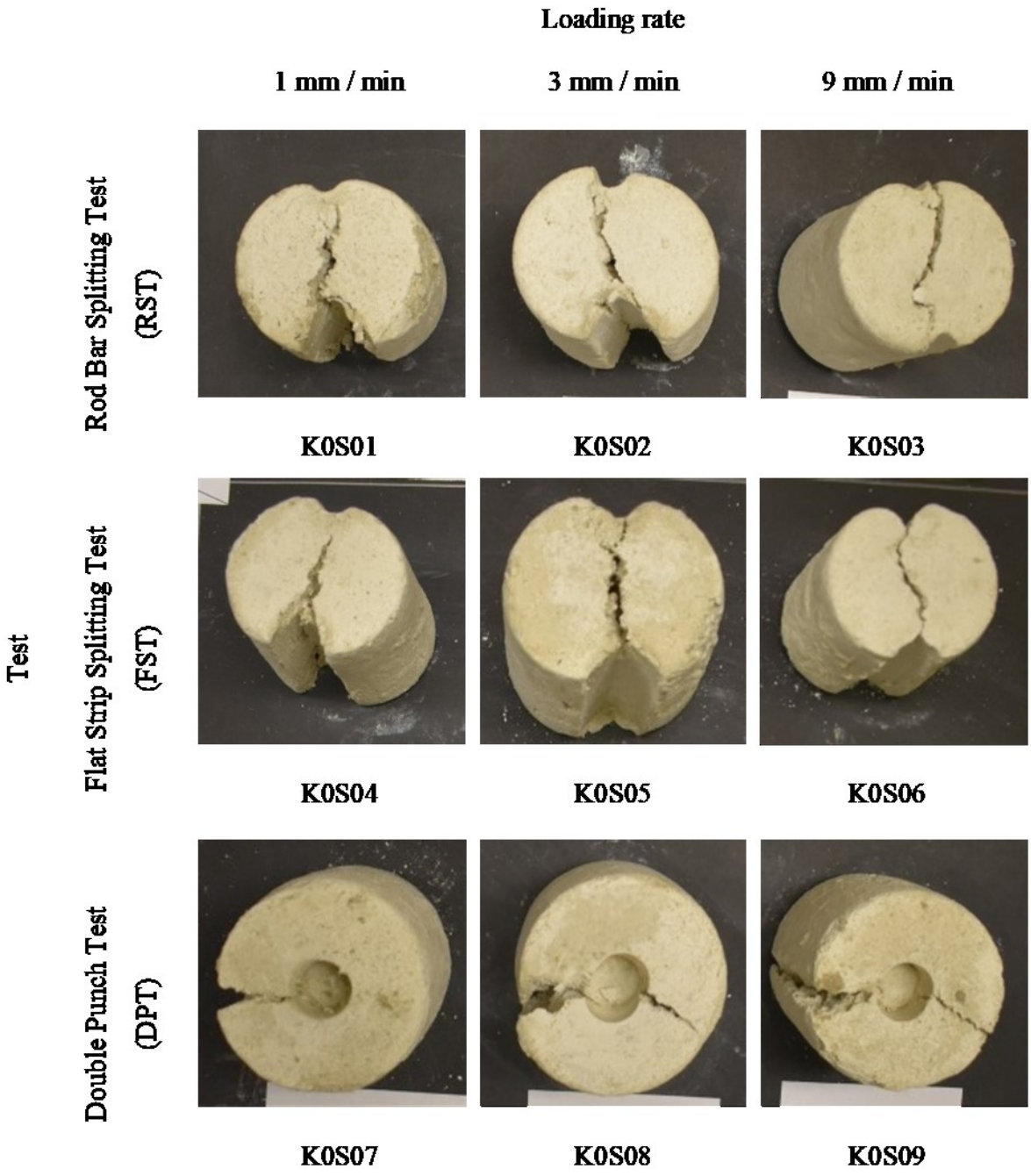

Figure B 23 Post-failure pictures of tested kaolinite-sand samples (T= - 5 °C, Salinity= 0 g/L).

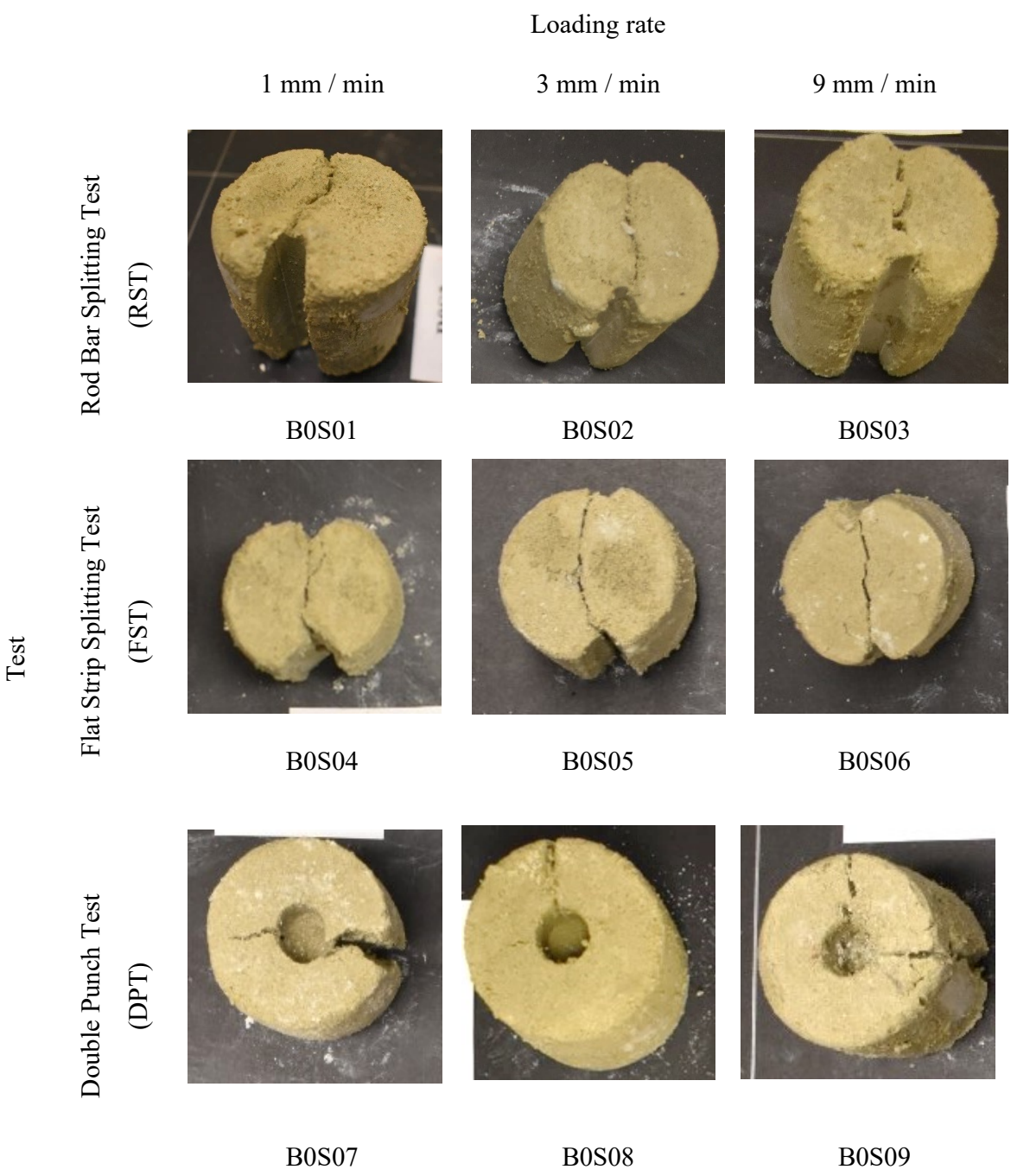

Figure B 24 Post-failure pictures of tested bentonite-sand samples (T= - 5 °C, Salinity= 0 g/L).

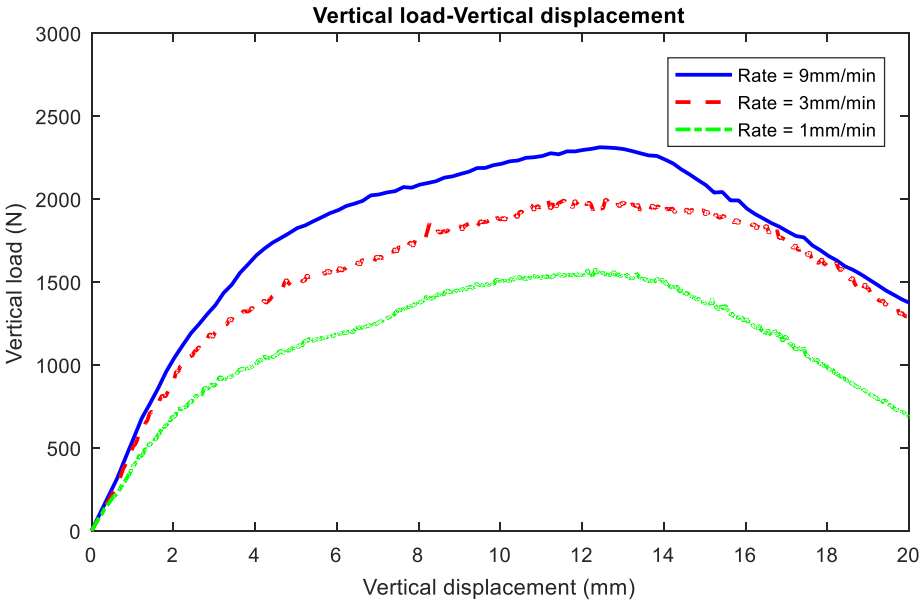

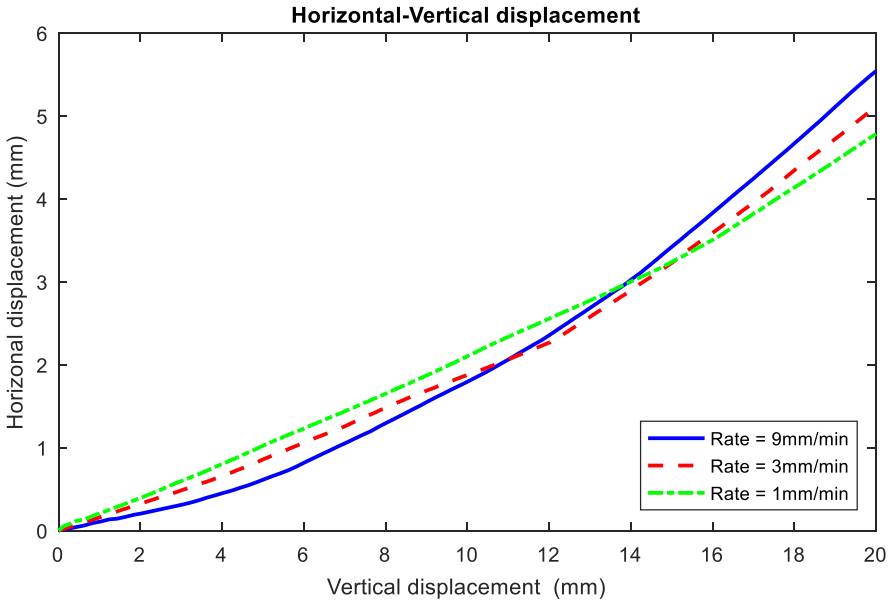

Figure B 25 Results of tensile strength tests performed on group K-13 (Loading approach= RST, T= - 5 °C, Salinity= 3 g/L).

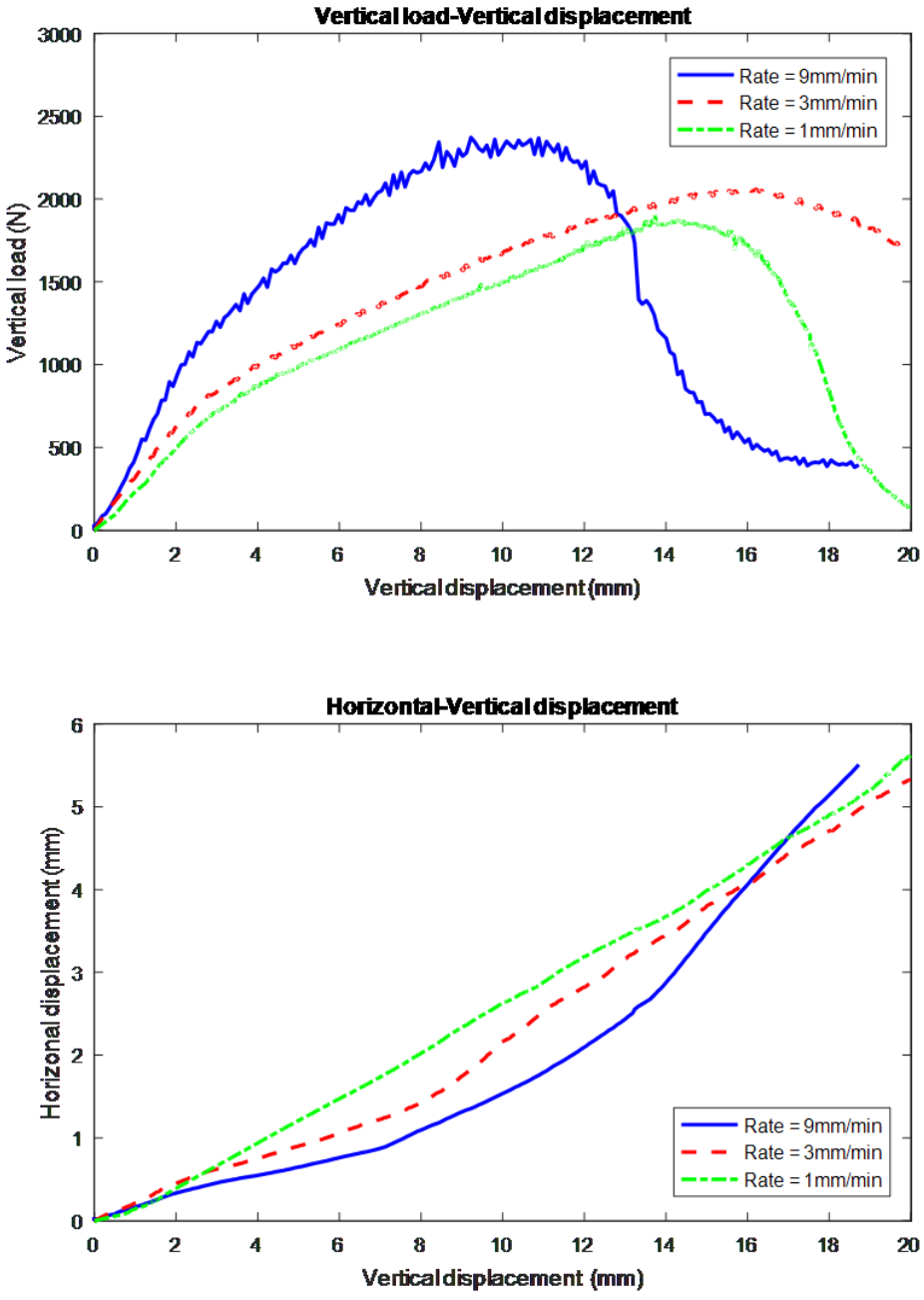

Figure B 26 Results of tensile strength tests performed on group K-14 (Loading approach= FST, T= - 5 °C, Salinity= 3 g/L).

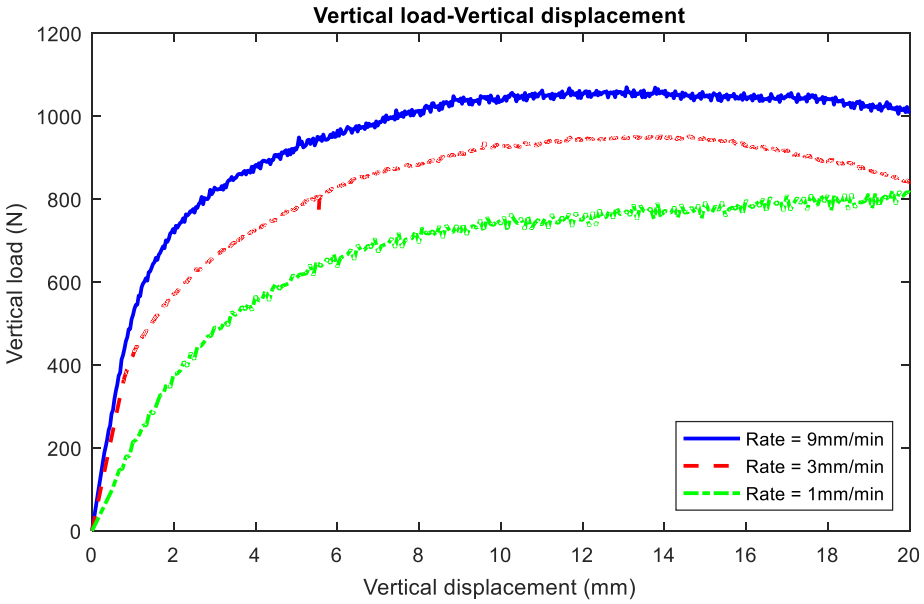

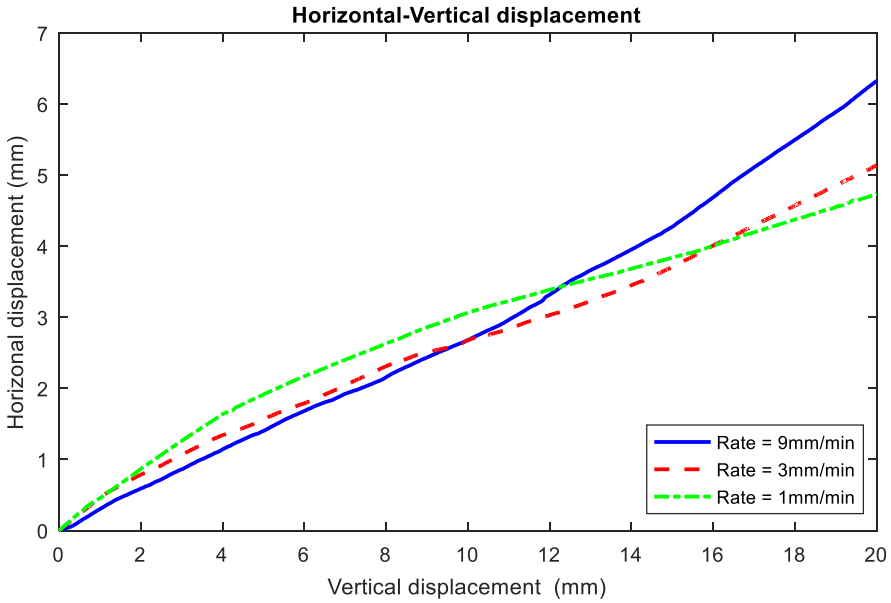

Figure B 27 Results of tensile strength tests performed on group K-15 (Loading approach= DPT, T= - 5 °C, Salinity= 3 g/L).

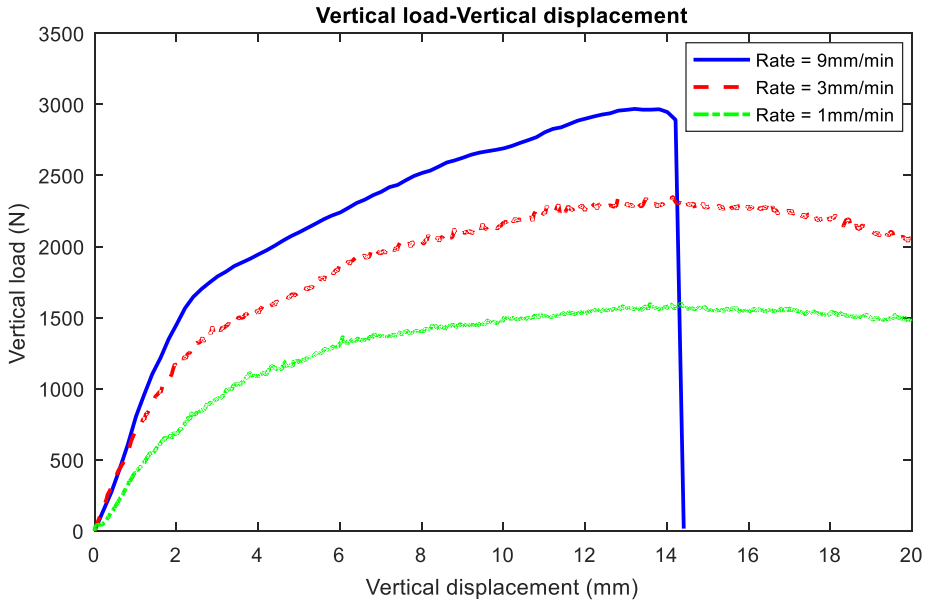

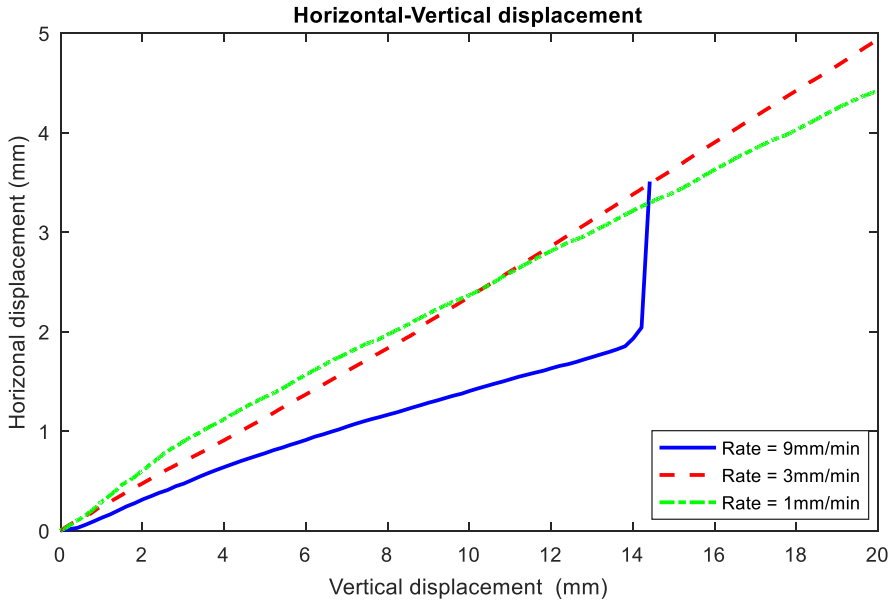

Figure B 28 Results of tensile strength tests performed on group B-13 (Loading approach= RST, T= - 5 °C, Salinity= 3 g/L).

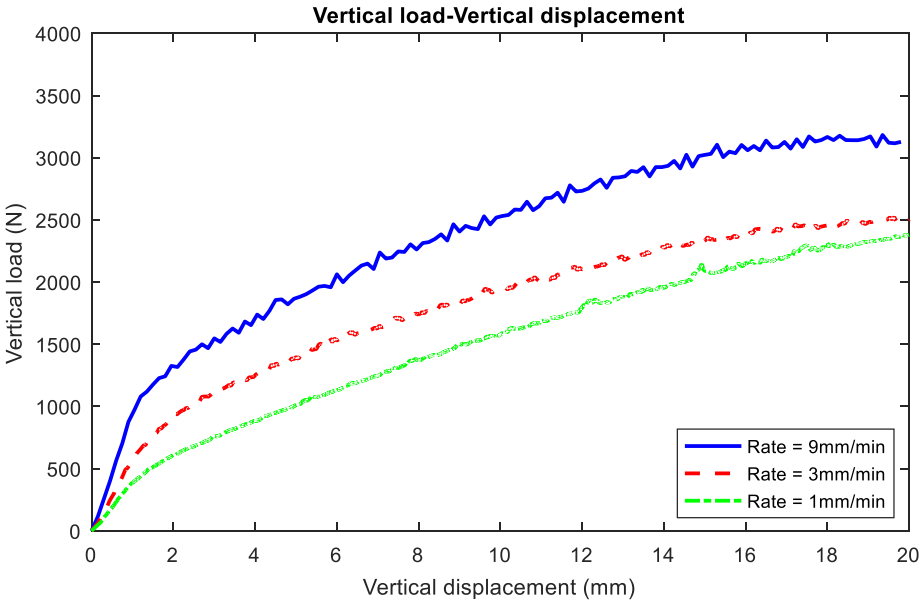

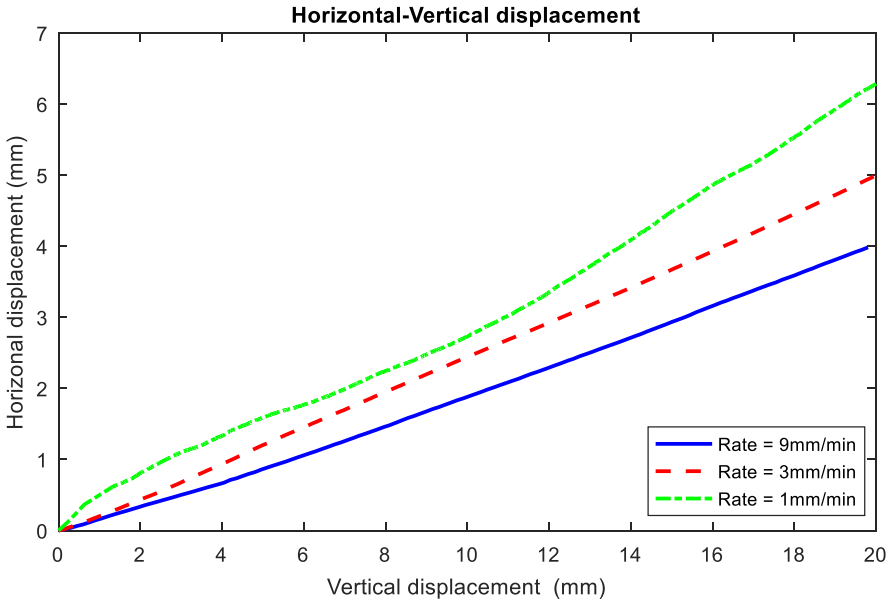

Figure B 29 Results of tensile strength tests performed on group B-14 (Loading approach= FST, T= - 5 °C, Salinity= 3 g/L).

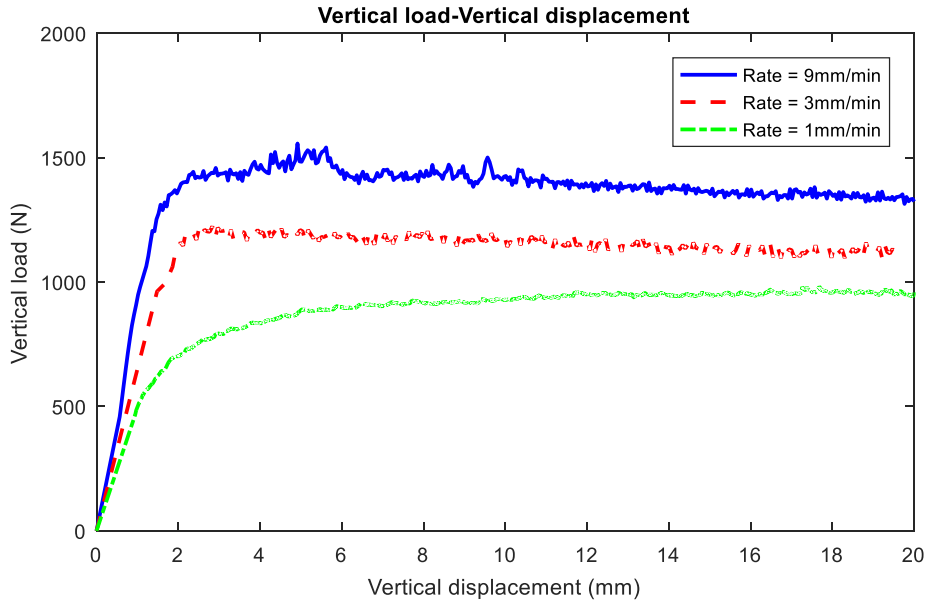

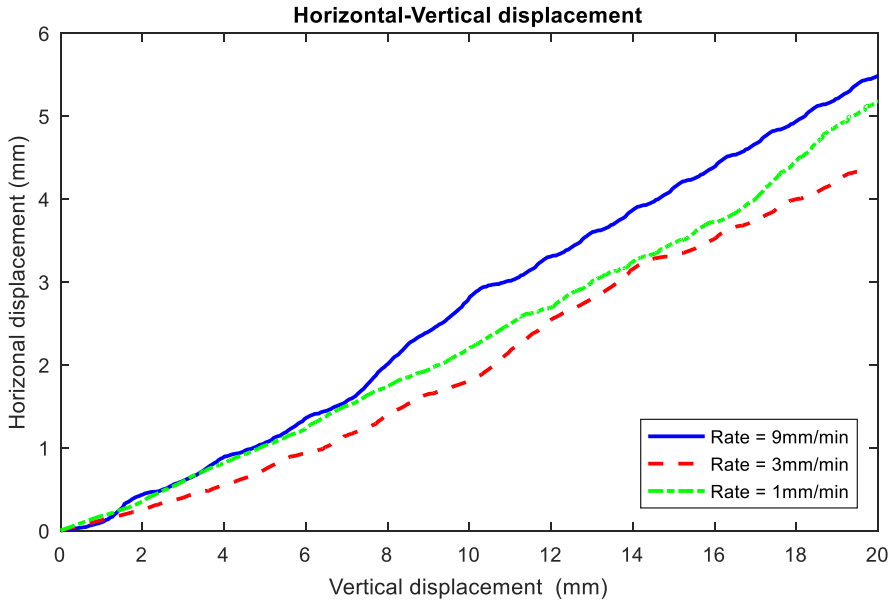

Figure B 30 Results of tensile strength tests performed on group B-15 (Loading approach= DPT, T= - 5 °C, Salinity= 3 g/L).

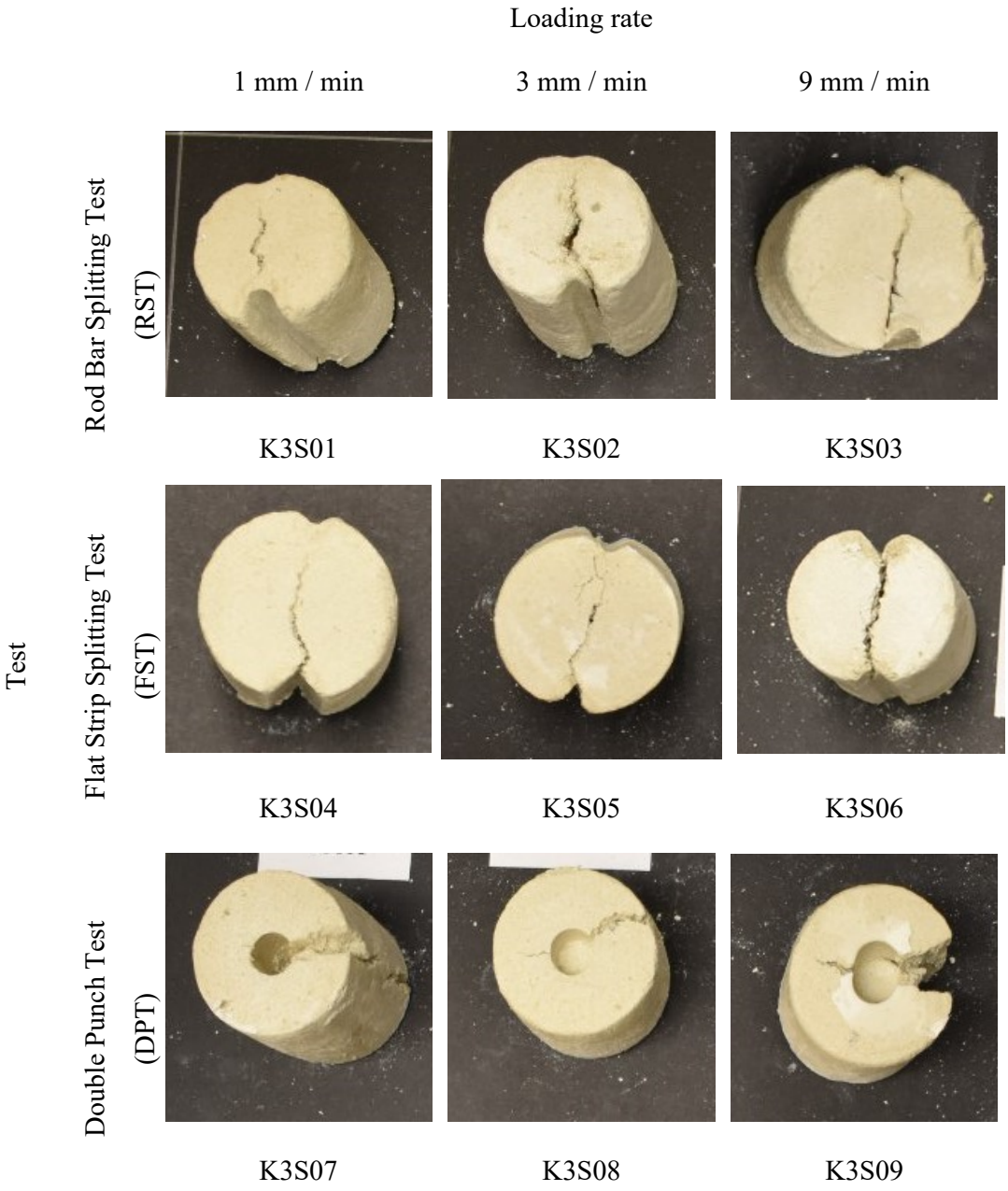

Figure B 31 Post-failure pictures of tested kaolinite-sand samples (T= - 5 °C, Salinity= 3 g/L).

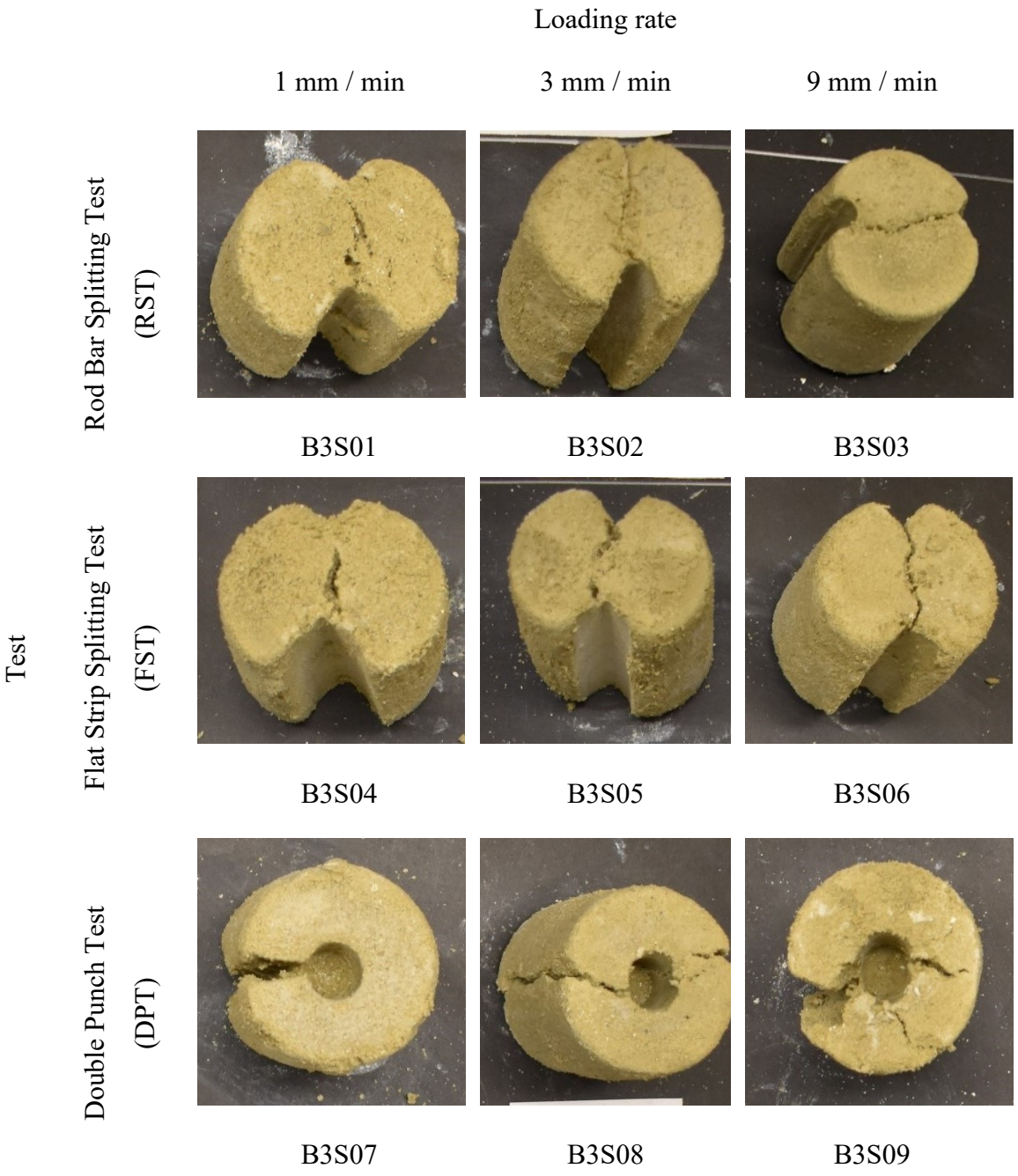

Figure B 32 Post-failure pictures of tested bentonite-sand samples (T= - 5 °C, Salinity= 3 g/L).

`

Table B 3 Details of tensile strength tested groups at -2°C.

Group	Samples	Test	Salinity	Loading rate
K-16	K1S28-K1S30	RST	1 g/L	1, 3, and 9 mm/min
K-17	K1S31-K1S33	FST	1 g/L	1, 3, and 9 mm/min
K-18	K1S34-K1S36	DPT	1 g/L	1, 3, and 9 mm/min
B-16	B1S28-B1S30	RST	1 g/L	1, 3, and 9 mm/min
B-17	B1S31-B1S33	FST	1 g/L	1, 3, and 9 mm/min
B-18	B1S34-B1S36	DPT	1 g/L	1, 3, and 9 mm/min

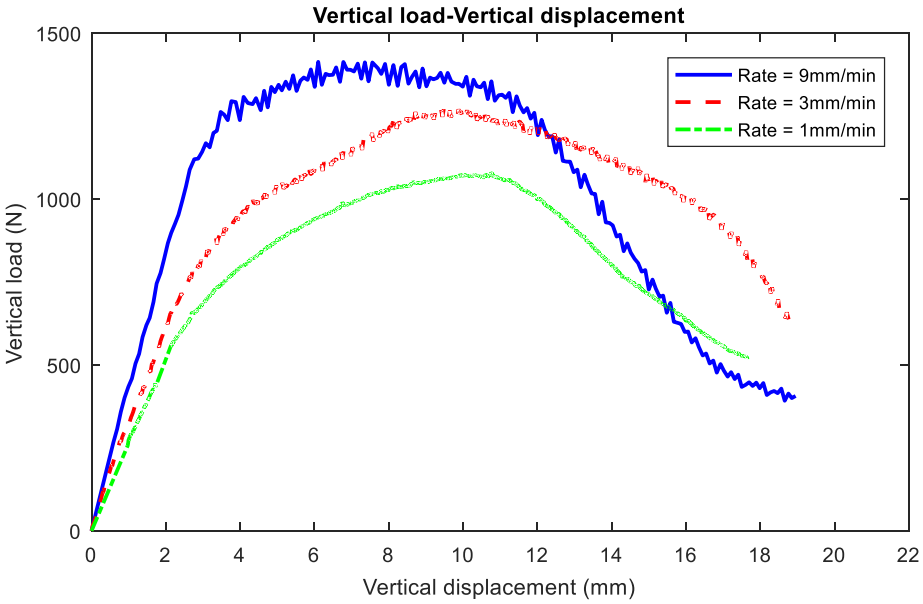

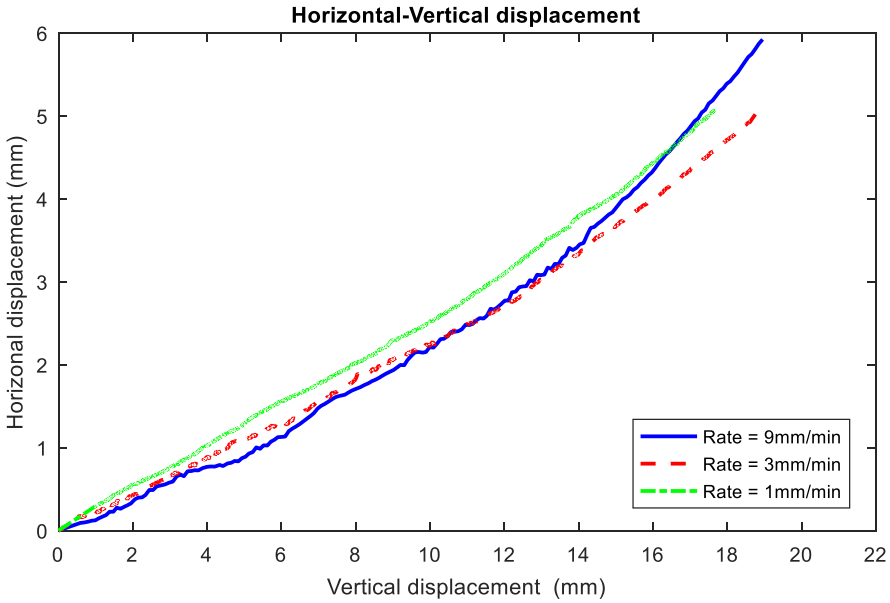

Figure B 33 Results of tensile strength tests performed on group K-16 (Loading approach= RST, T= - 2 °C, Salinity= 1 g/L).

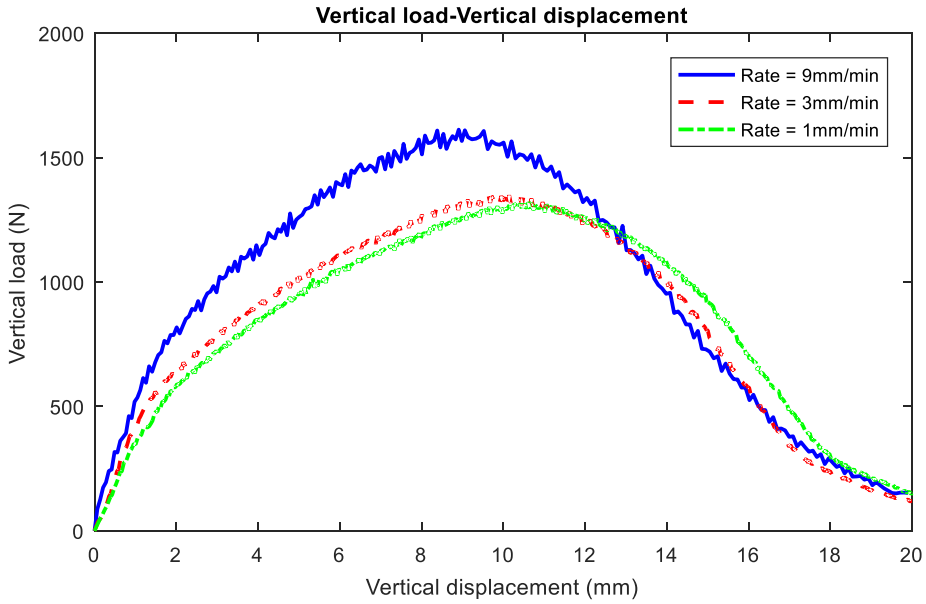

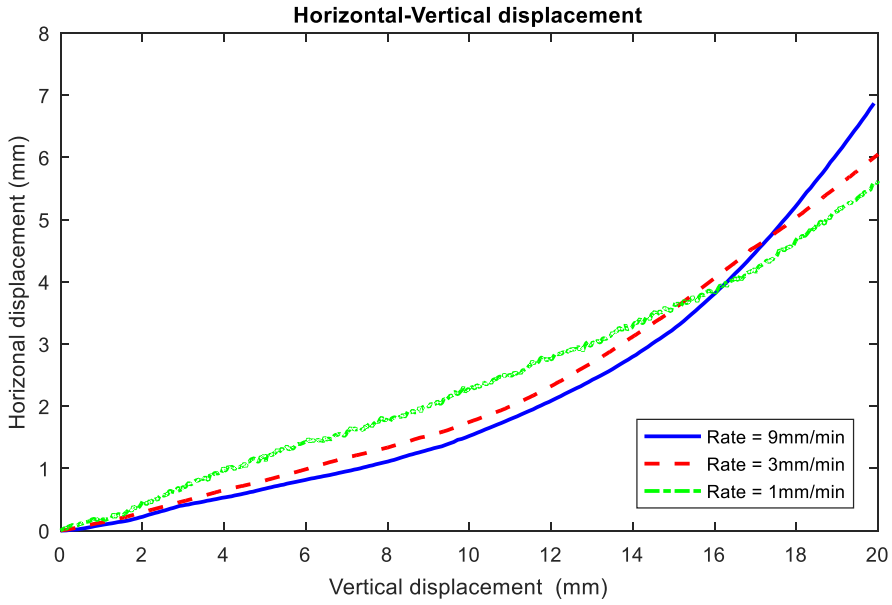

Figure B 34 Results of tensile strength tests performed on group K-17 (Loading approach= FST, T= - 2 °C, Salinity= 1 g/L).

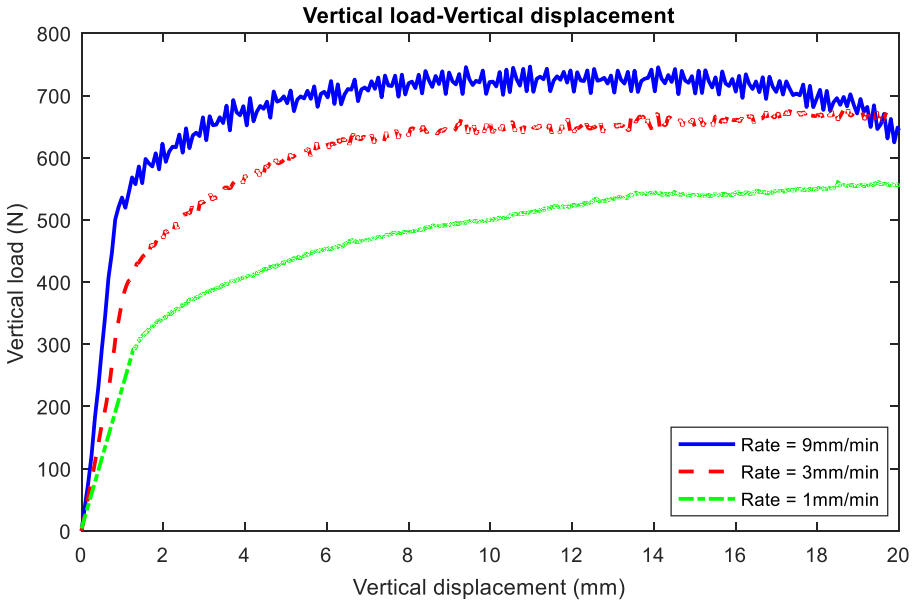

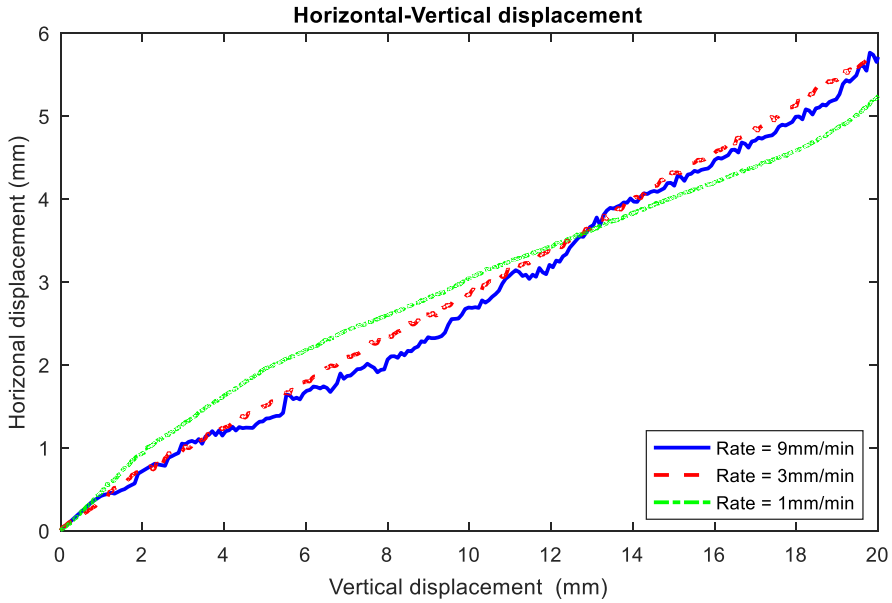

Figure B 35 Results of tensile strength tests performed on group K-18 (Loading approach= DPT, T= - 2 °C, Salinity= 1 g/L).

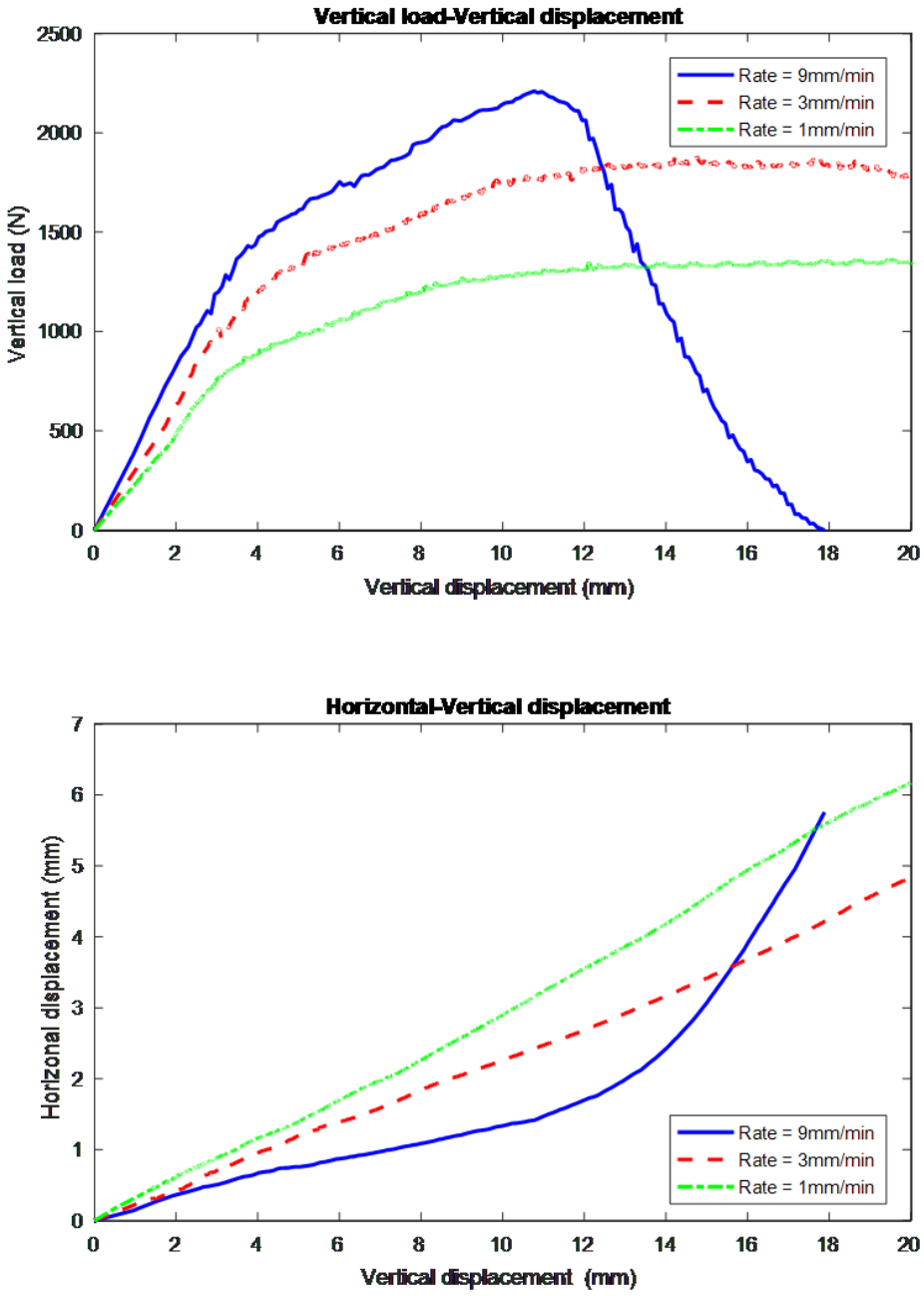

Figure B 36 Results of tensile strength tests performed on group B-16 (Loading approach= RST, T= - 2 °C, Salinity= 1 g/L).

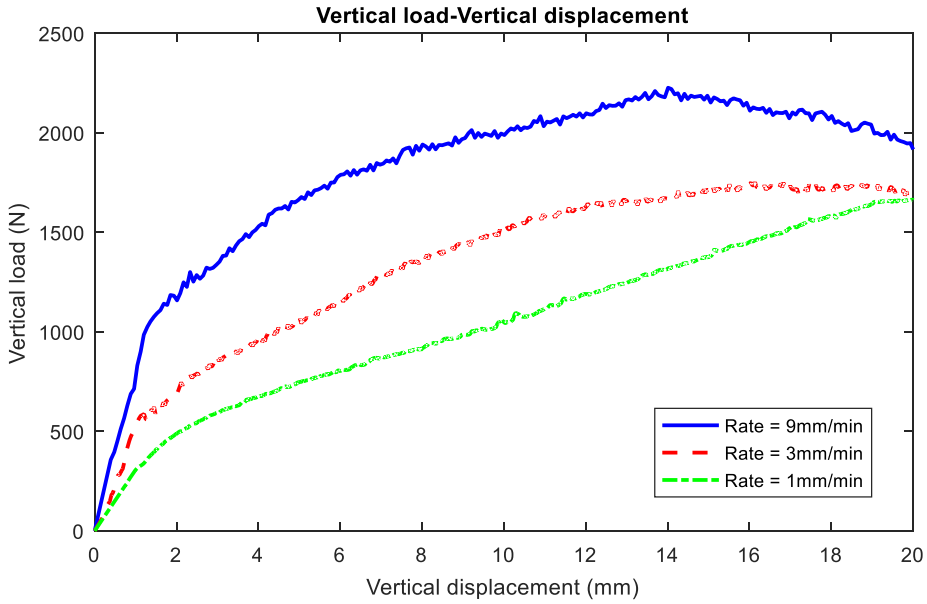

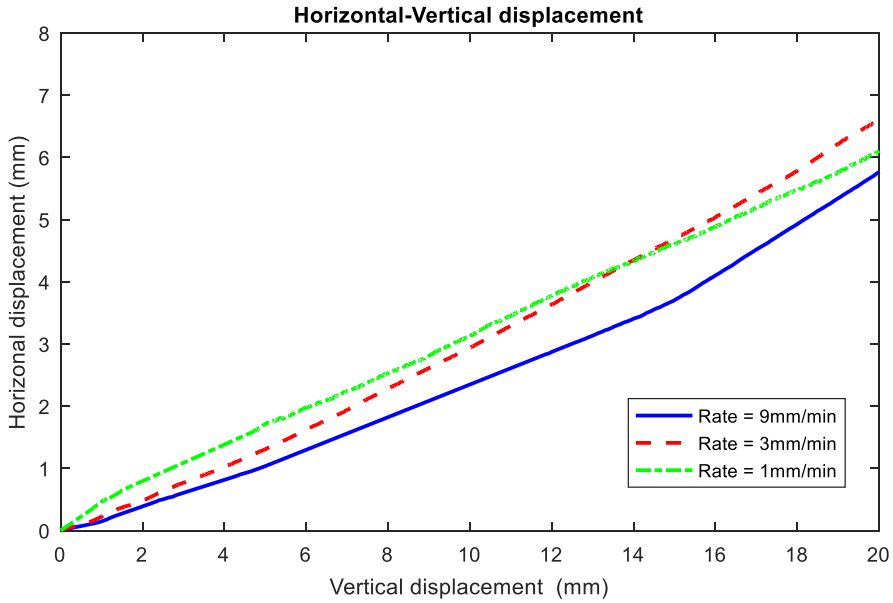

Figure B 37 Results of tensile strength tests performed on group B-17 (Loading approach= FST, T= - 2 °C, Salinity= 1 g/L).

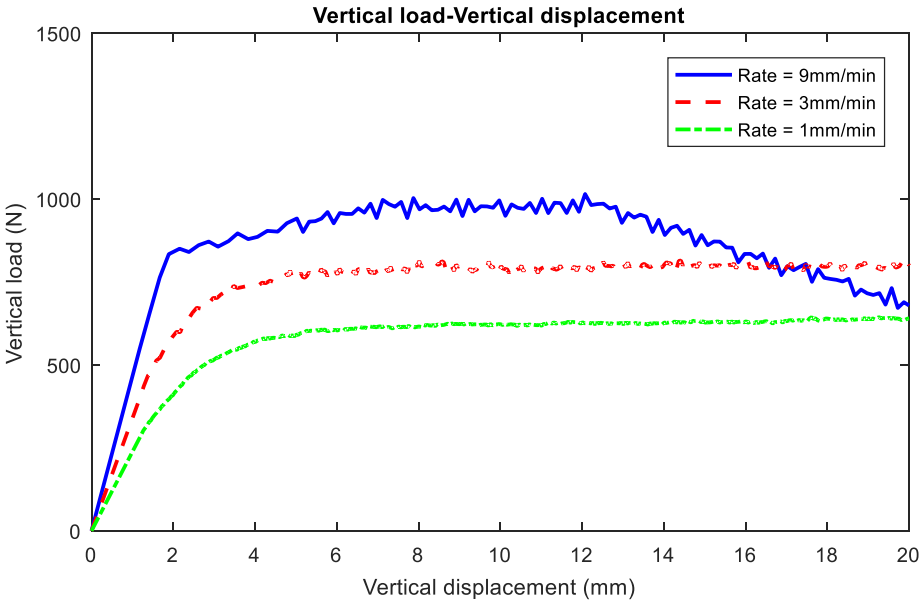

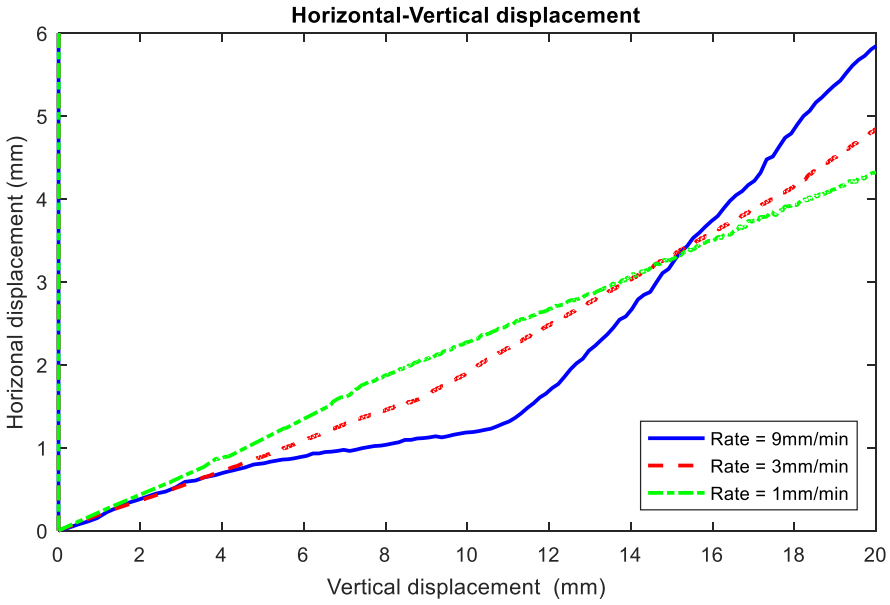

Figure B 38 Results of tensile strength tests performed on group B-18 (Loading approach= DPT, T= - 2 °C, Salinity=1 g/L).

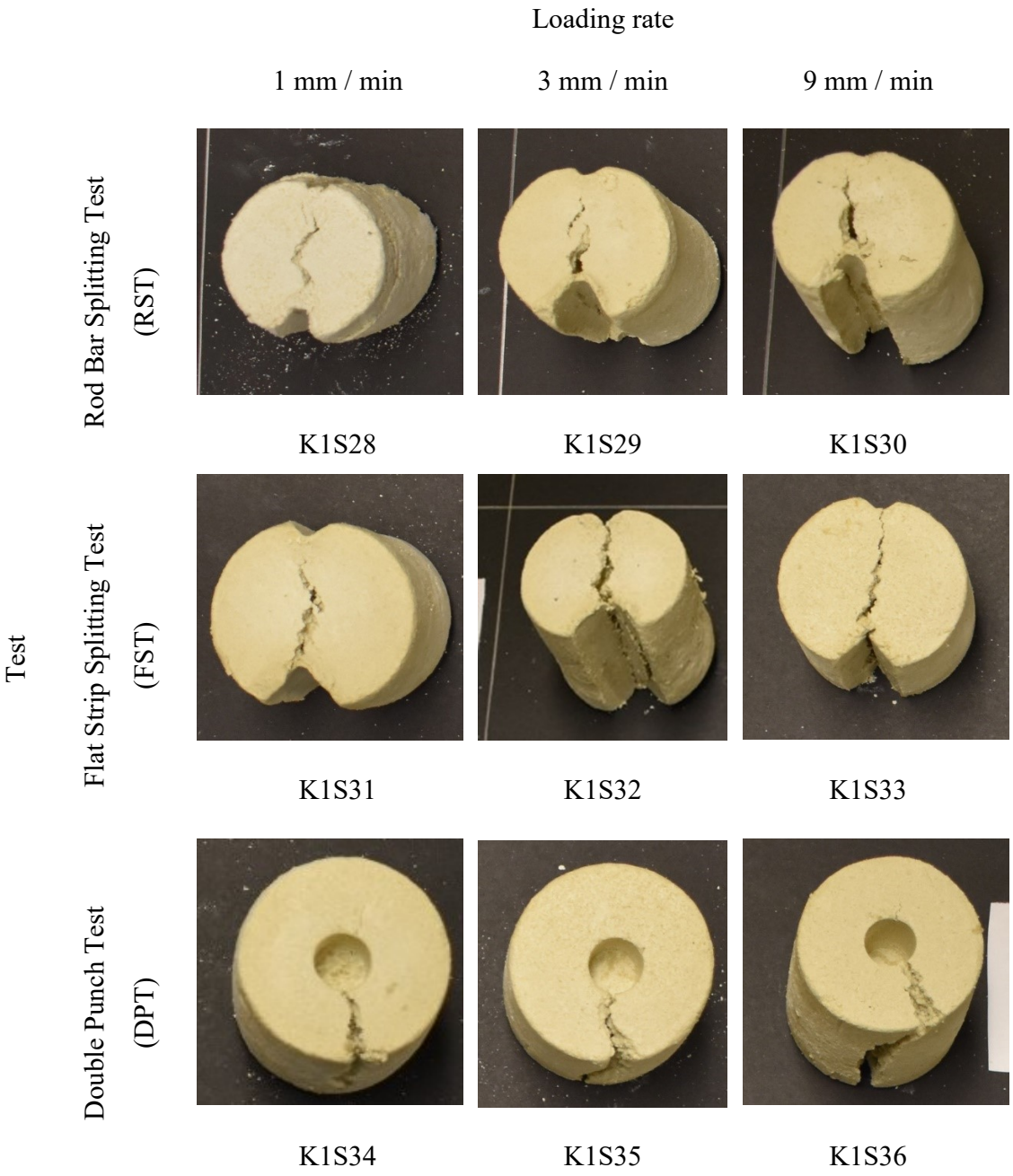

Figure B 39 Post-failure pictures of tested kaolinite-sand samples (T= - 2 °C, Salinity= 1 g/L).

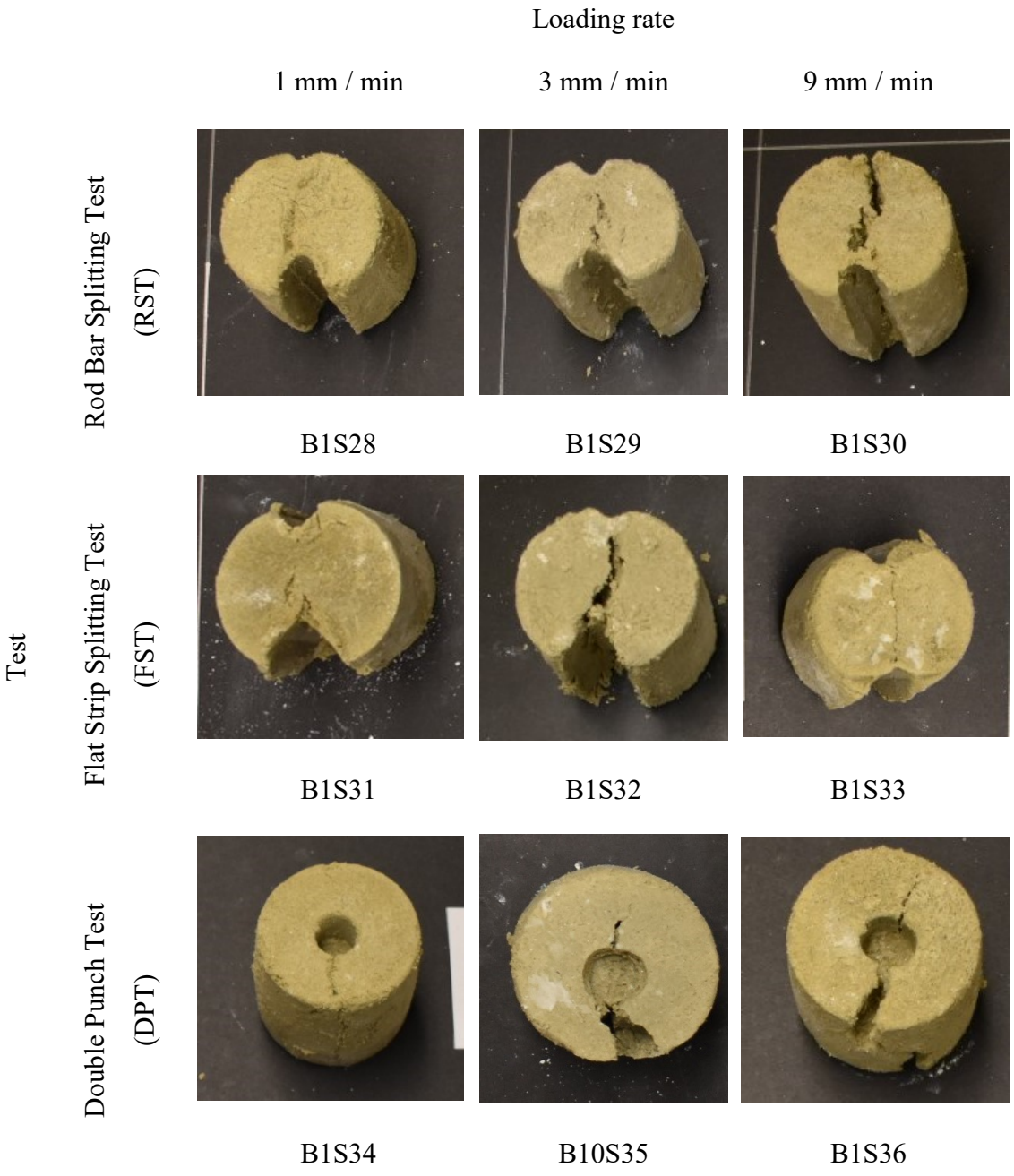

Figure B 40 Post-failure pictures of tested bentonite-sand samples (T= - 2 °C, Salinity= 1 g/L).

`

Table B 4 Details of tensile strength tested groups at -0.5°C.

Group	Samples	Test	Salinity	Loading rate
K-22	K1S46-K1S48	RST	1 g/L	1, 3, and 9 mm/min
K-23	K1S49-K1S51	FST	1 g/L	1, 3, and 9 mm/min
K-24	K1S52-K1S54	DPT	1 g/L	1, 3, and 9 mm/min
B-22	B1S46-B1S48	RST	1 g/L	1, 3, and 9 mm/min
B-23	B1S49-B1S51	FST	1 g/L	1, 3, and 9 mm/min
B-24	B1S52-B1S54	DPT	1 g/L	1, 3, and 9 mm/min

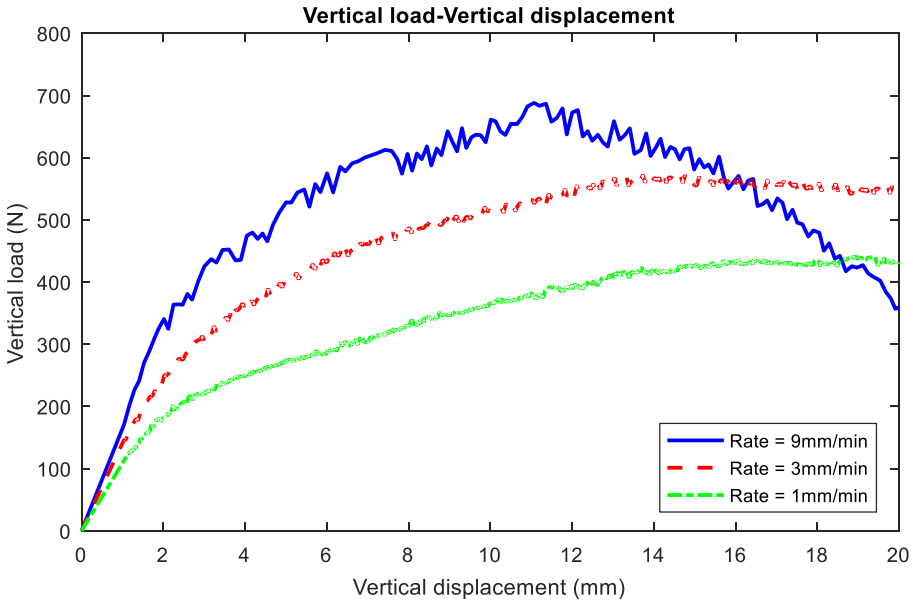

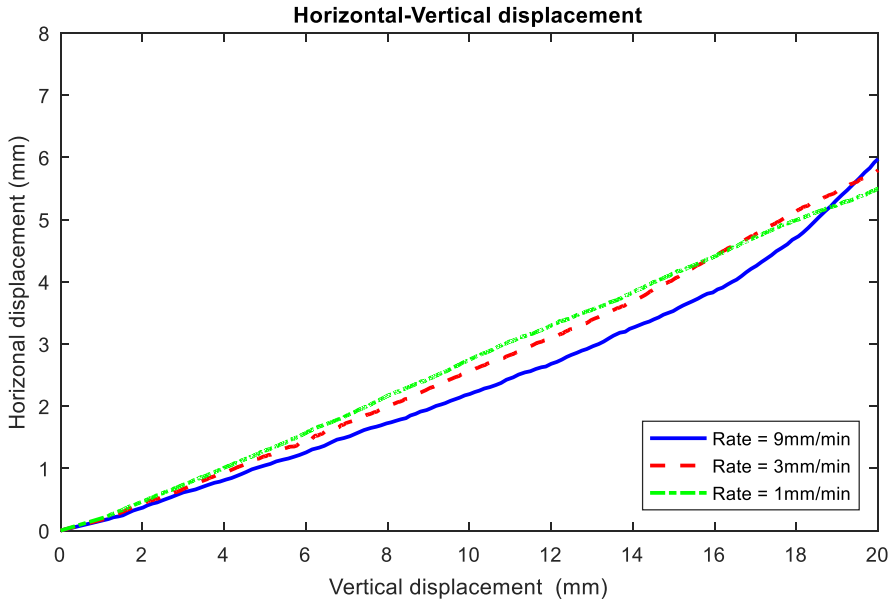

Figure B 41 Results of tensile strength tests performed on group K-22 (Loading approach= RST, T= - 0.5 °C, Salinity= 1 g/L).

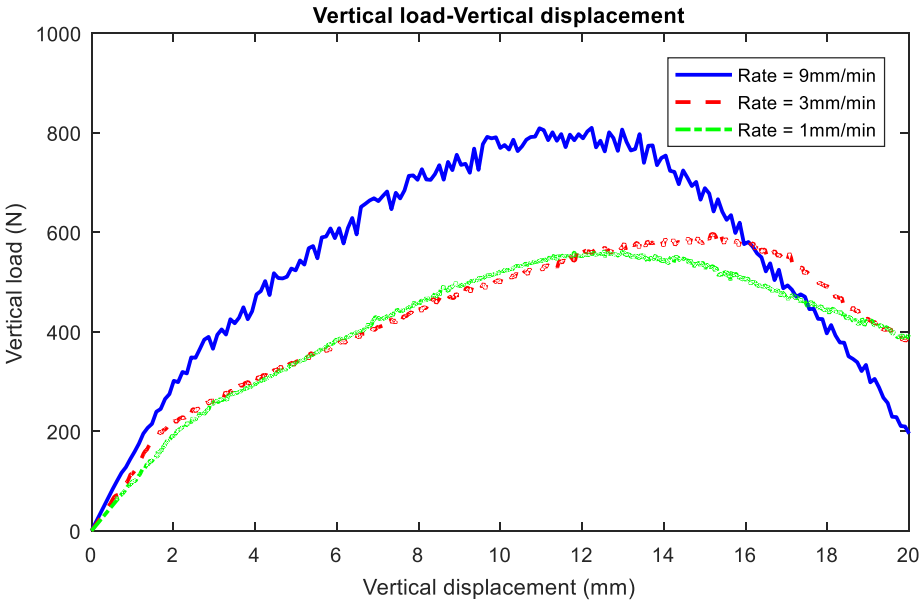

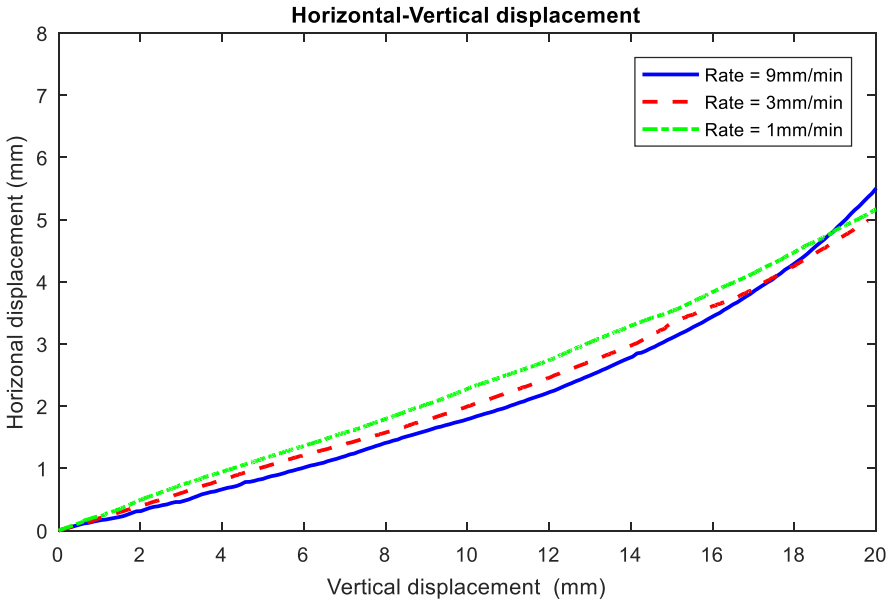

Figure B 42 Results of tensile strength tests performed on group K-23 (Loading approach= FST, T= - 0.5 °C, Salinity= 1 g/L).

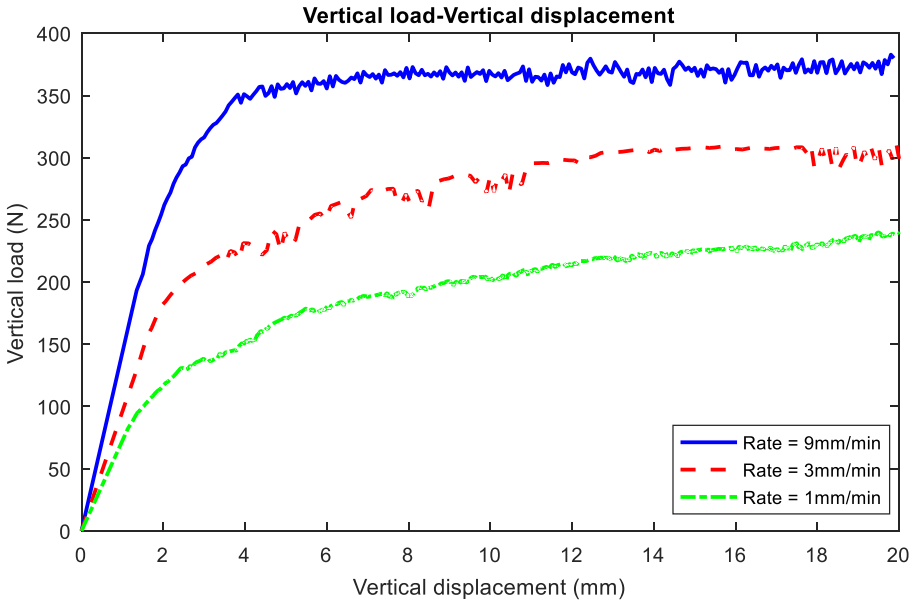

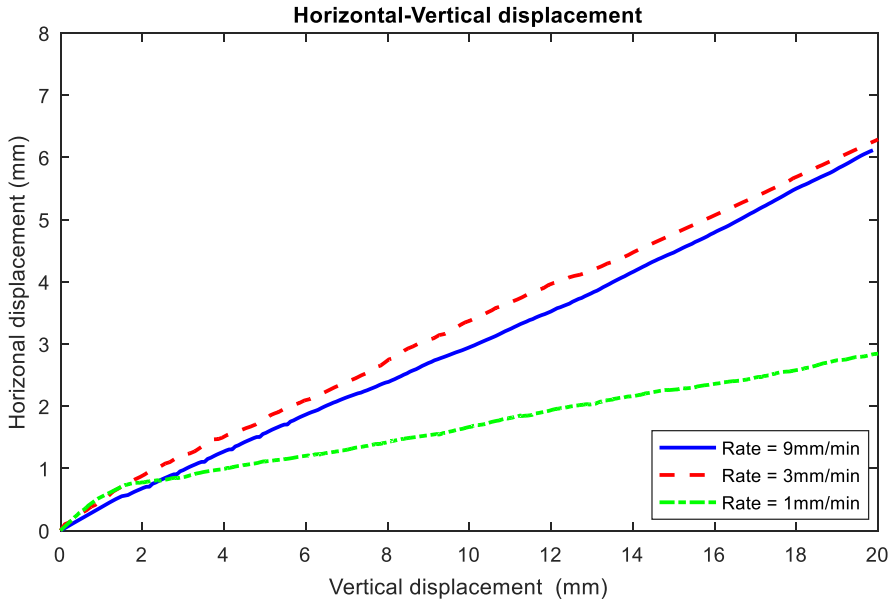

Figure B 43 Results of tensile strength tests performed on group K-24 (Loading approach= DPT, T= - 0.5 °C, Salinity= 1 g/L).

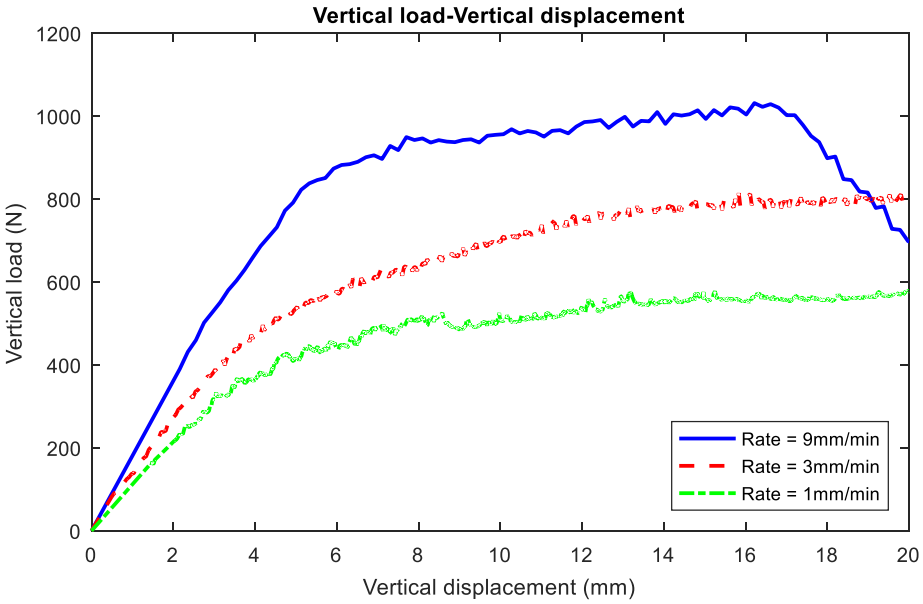

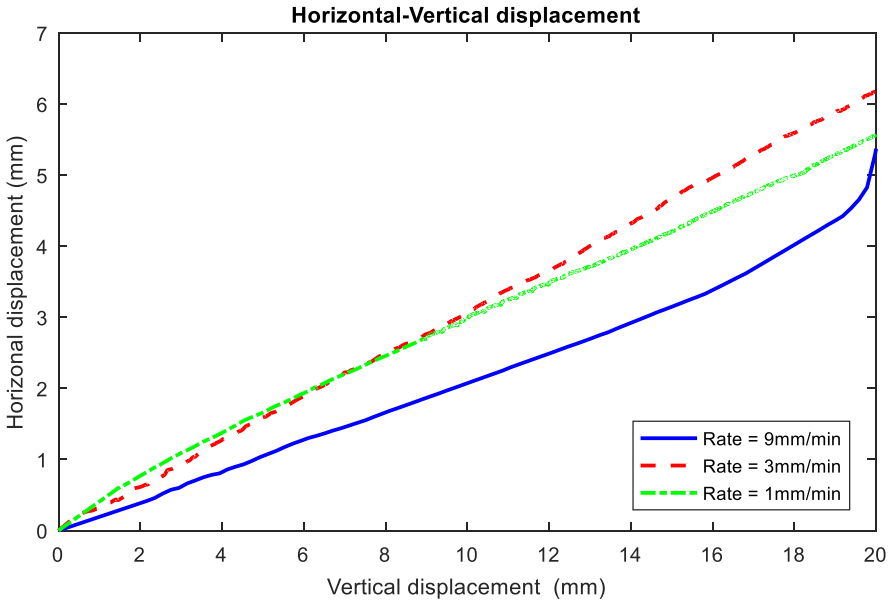

Figure B 44 Results of tensile strength tests performed on group B-22 (Loading approach= RST, T= - 0.5 °C, Salinity= 1 g/L).

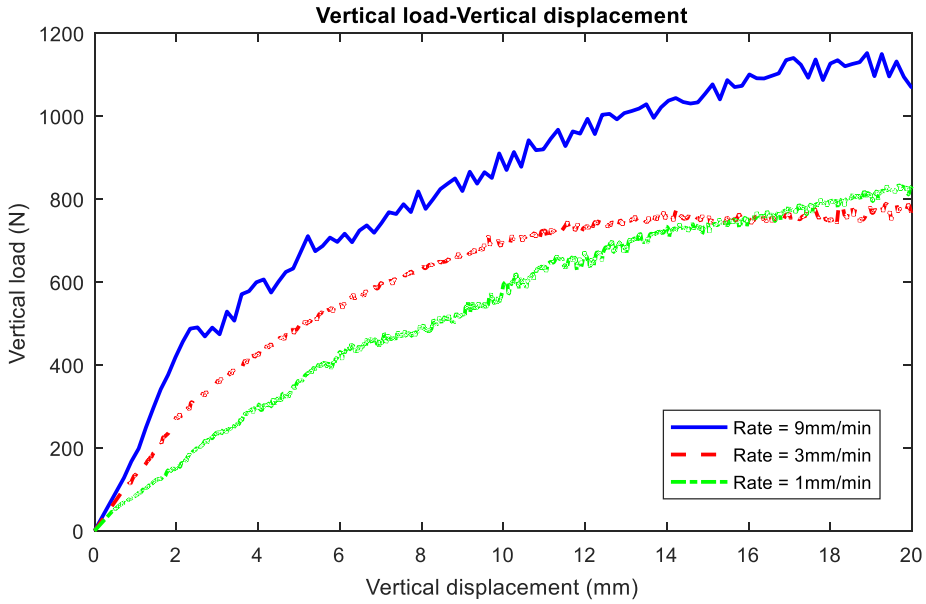

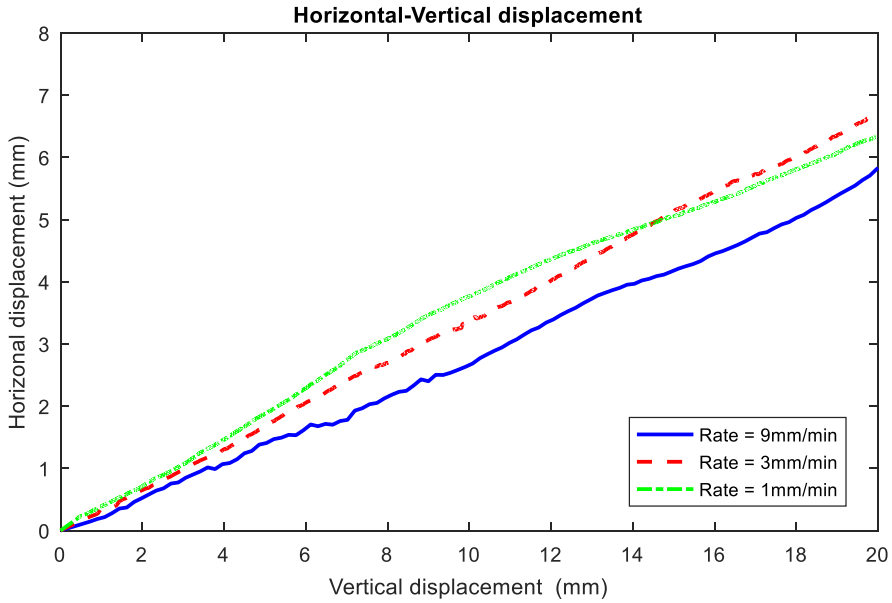

Figure B 45 Results of tensile strength tests performed on group B-23 (Loading approach= FST, T= - 0.5 °C, Salinity= 1 g/L).

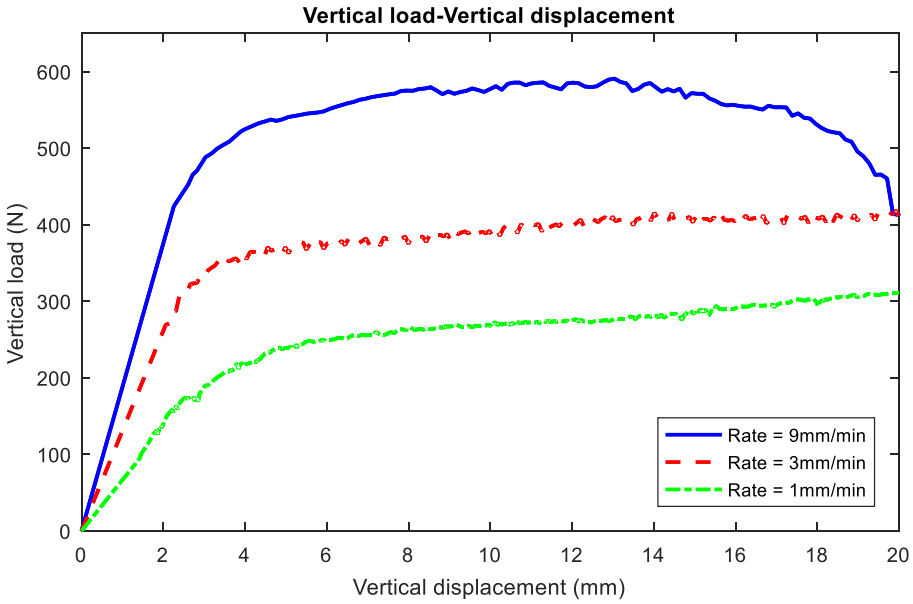

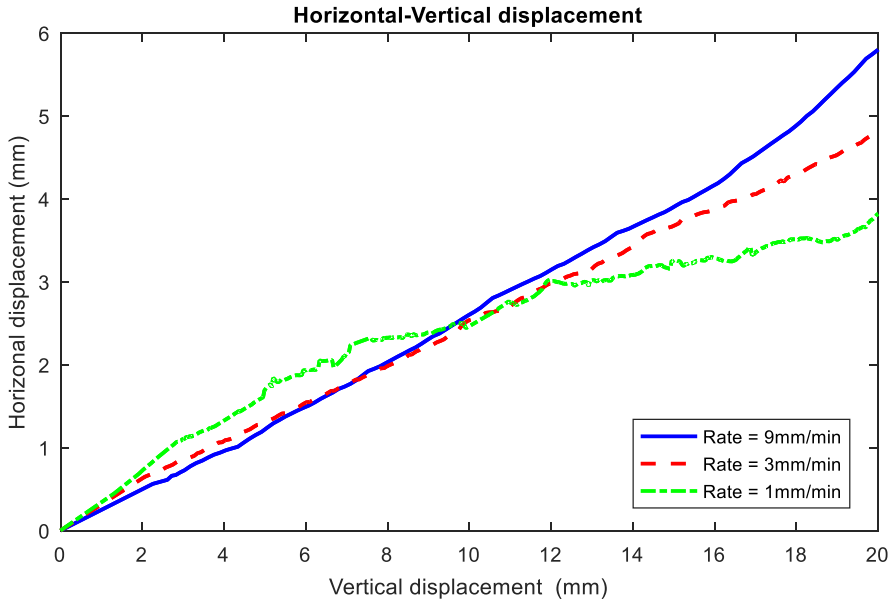

Figure B 46 Results of tensile strength tests performed on group B-24 (Loading approach= DPT, T= - 0.5 °C, Salinity= 1 g/L).

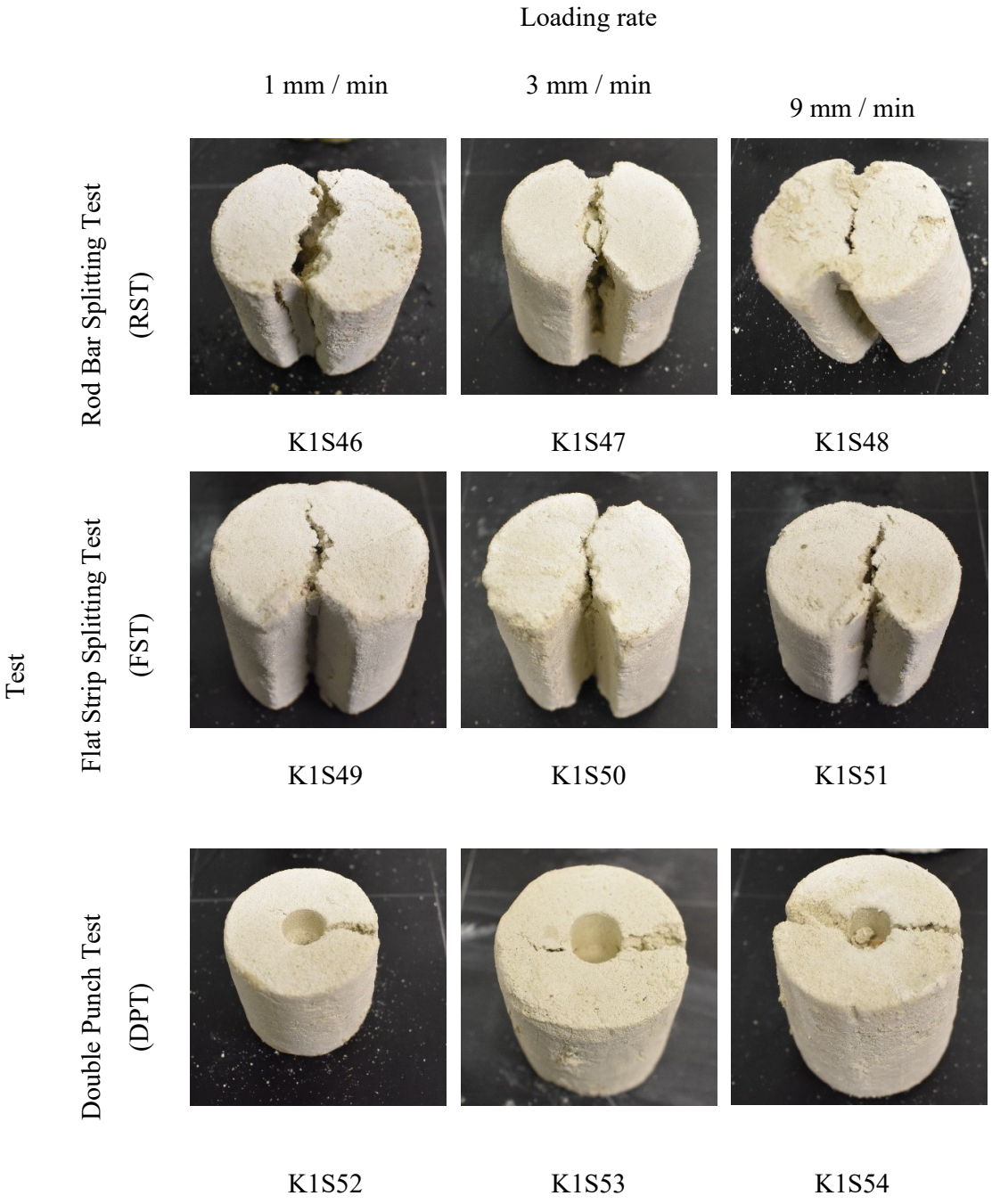

Figure B 47 Post-failure pictures of tested kaolinite-sand samples (T= - 0.5 °C, Salinity= 1 g/L).

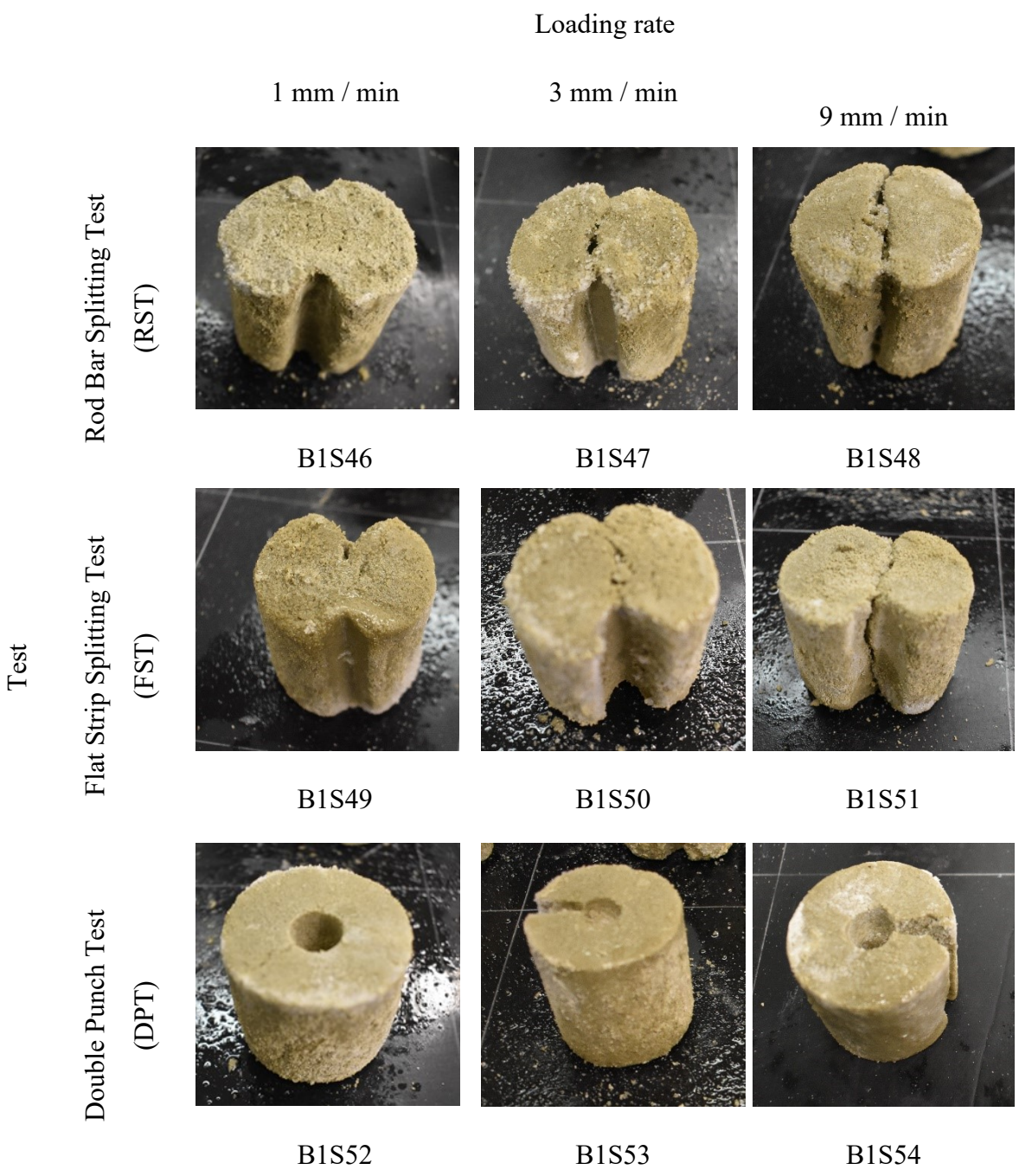

Figure B 48 Post-failure pictures of tested bentonite-sand samples (T= - 0.5 °C, Salinity= 1 g/L).

`

Table B 5 Details of tensile strength tested groups at 0°C.

Group	Samples	Test	Salinity	Loading rate
K-25	K1S55-K1S57	RST	1 g/L	1, 3, and 9 mm/min
K-26	K1S58-K1S60	FST	1 g/L	1, 3, and 9 mm/min
K-27	K1S61-K1S63	DPT	1 g/L	1, 3, and 9 mm/min
B-25	B1S55-B1S57	RST	1 g/L	1, 3, and 9 mm/min
B-26	B1S58-B1S60	FST	1 g/L	1, 3, and 9 mm/min
B-27	B1S61-B1S63	DPT	1 g/L	1, 3, and 9 mm/min

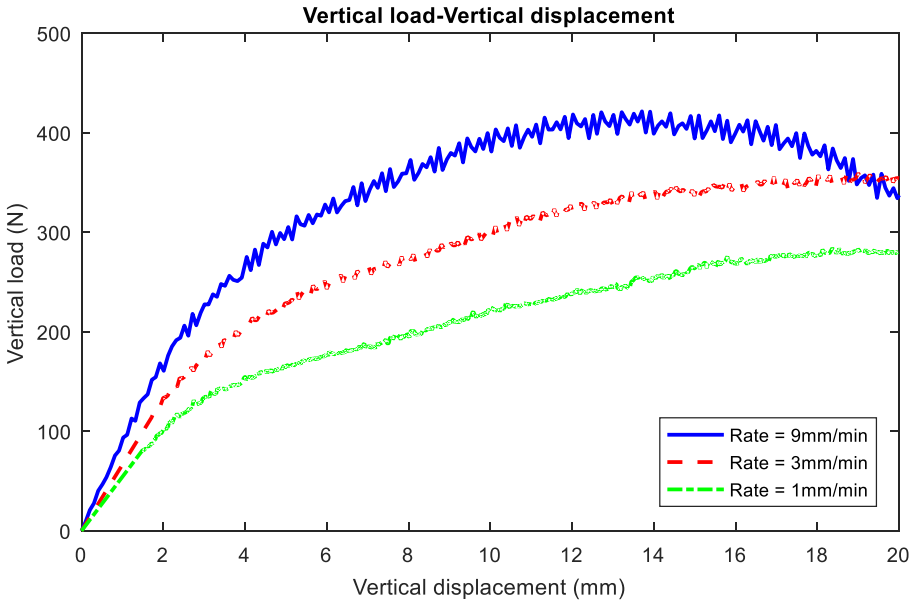

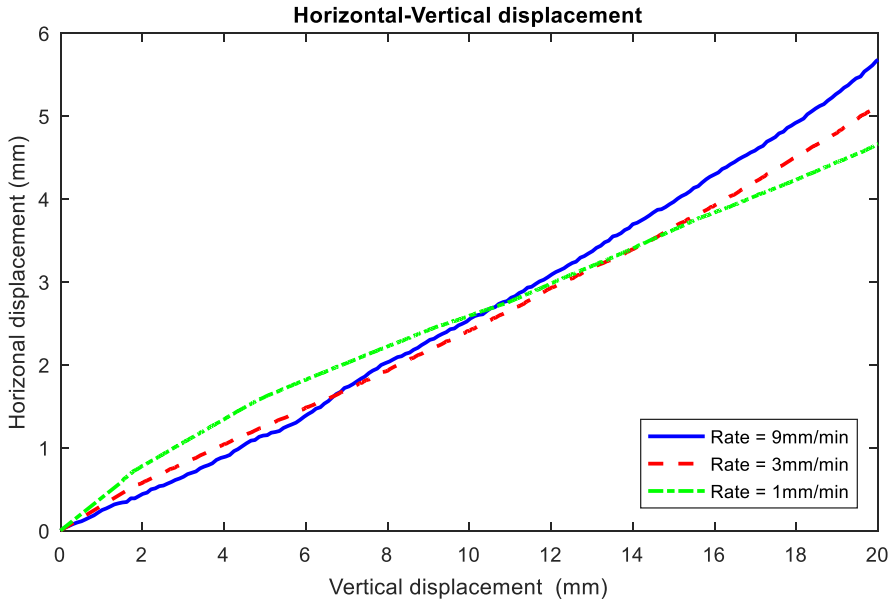

Figure B 49 Results of tensile strength tests performed on group K-25 (Loading approach= RST, T= 0 °C, Salinity= 1 g/L).

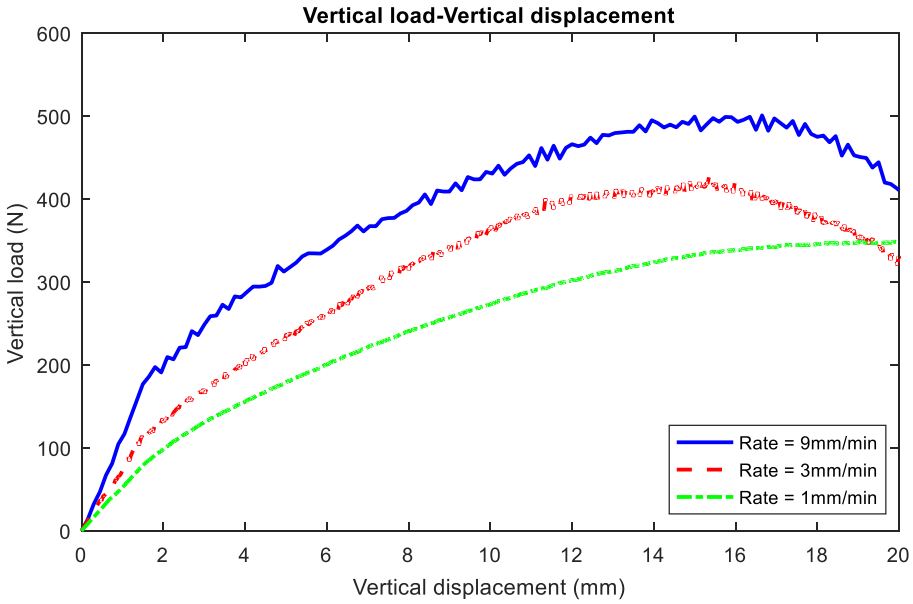

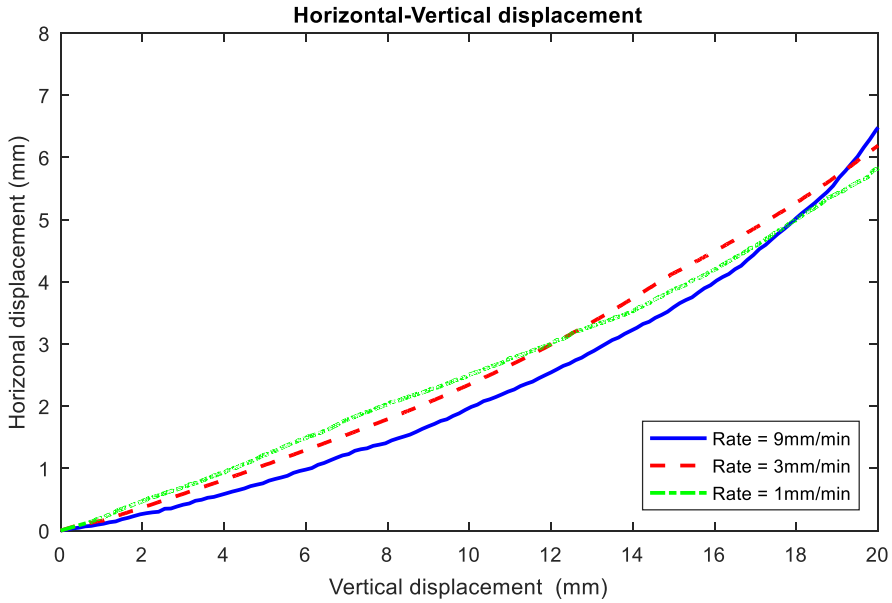

Figure B 50 Results of tensile strength tests performed on group K-26 (Loading approach= FST, T= 0 °C, Salinity= 1 g/L).

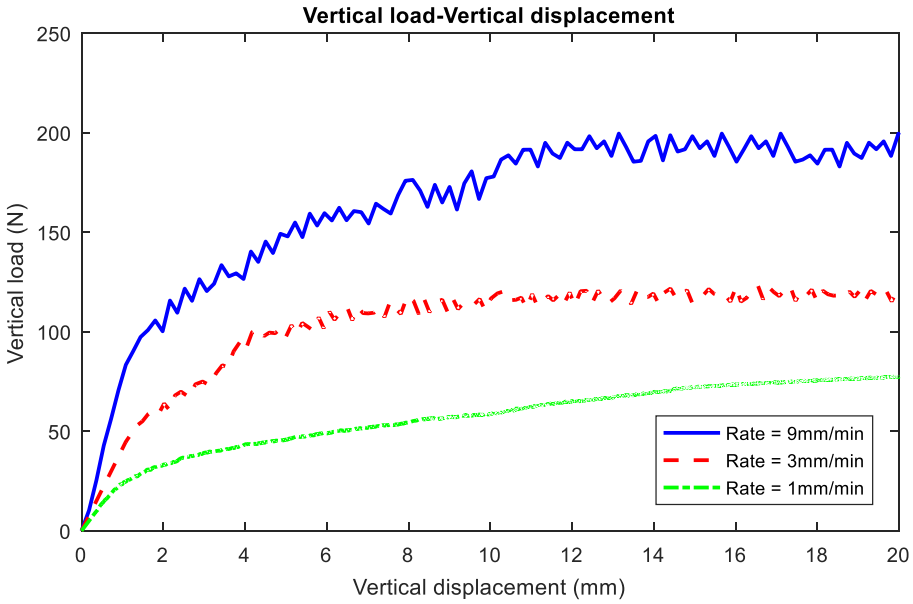

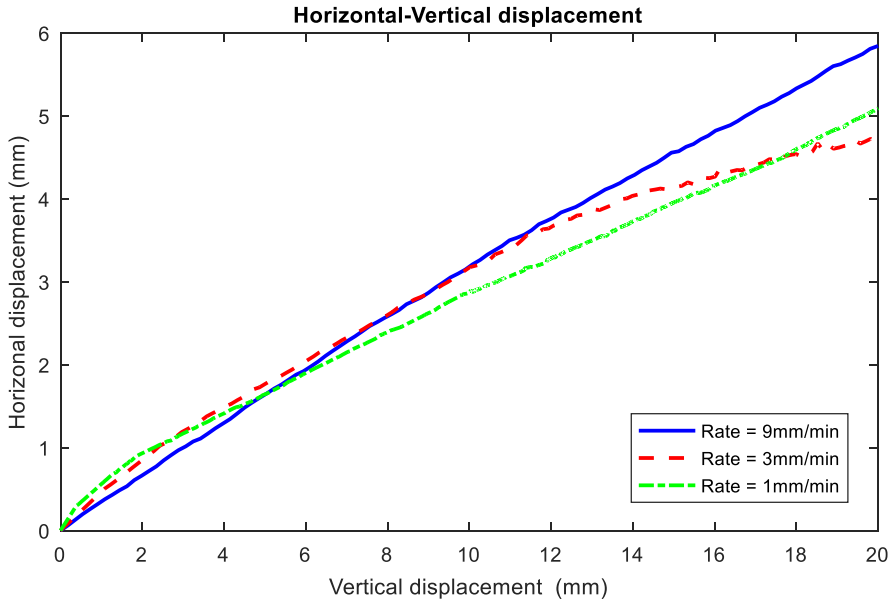

Figure B 51 Results of tensile strength tests performed on group K-27 (Loading approach= DPT, T= 0 °C, Salinity= 1 g/L).

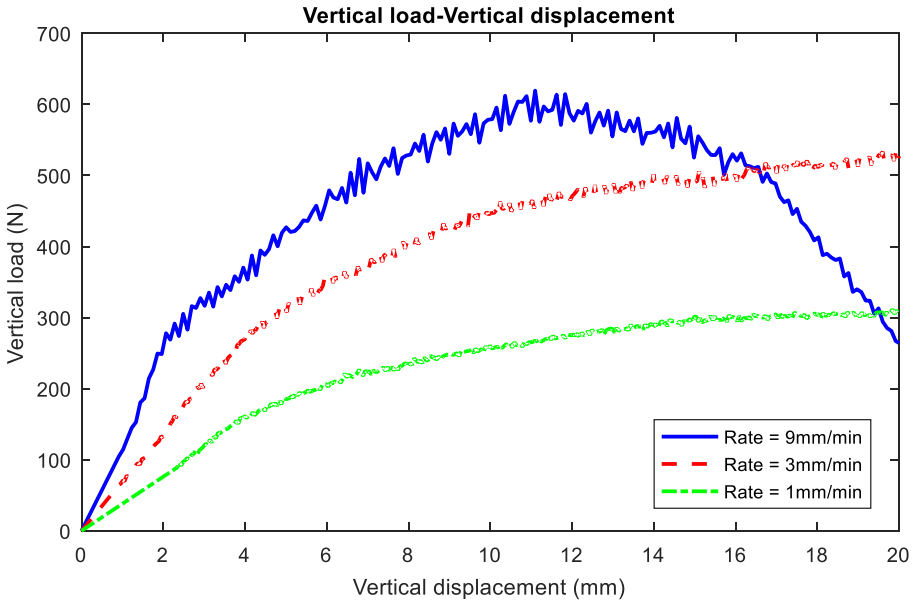

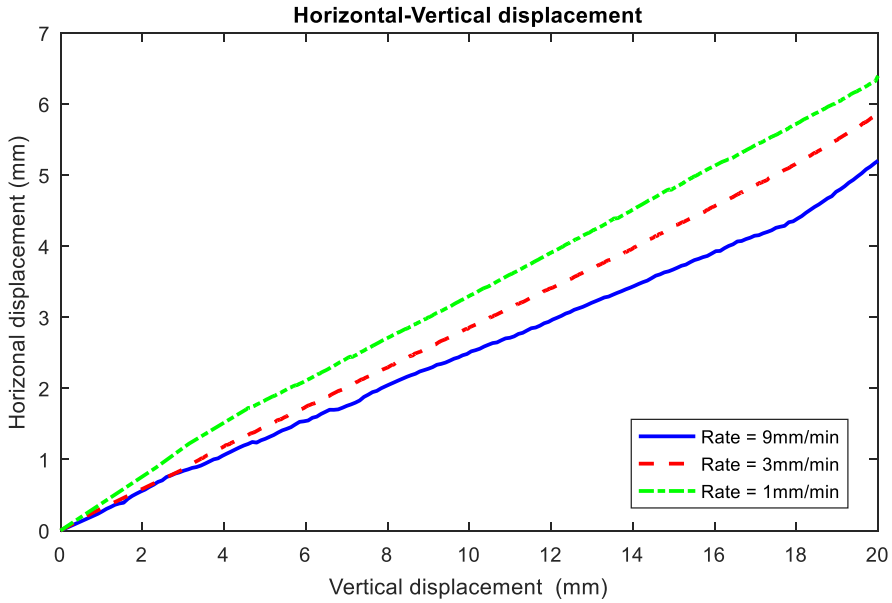

Figure B 52 Results of tensile strength tests performed on group B-25 (Loading approach= RST, T= 0 °C, Salinity= 1 g/L).

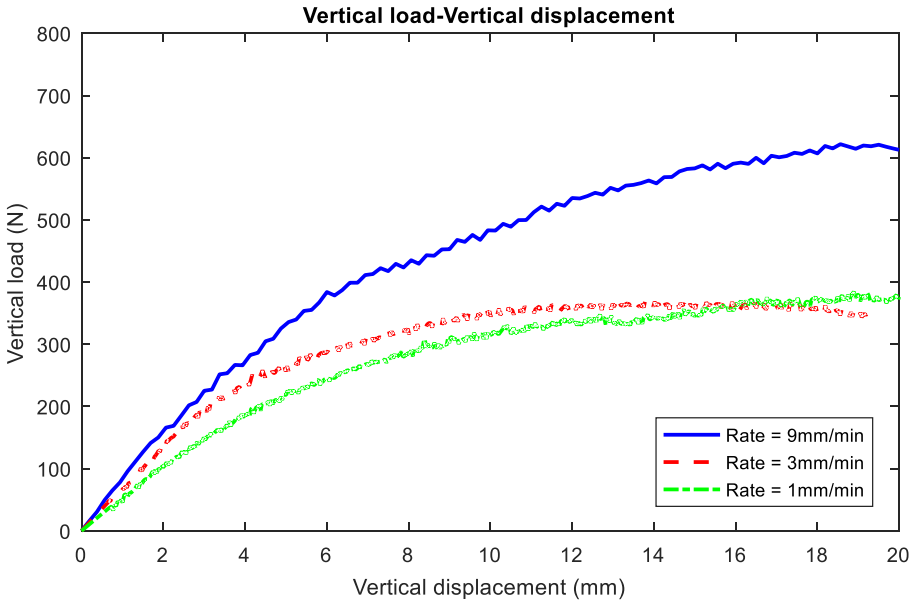

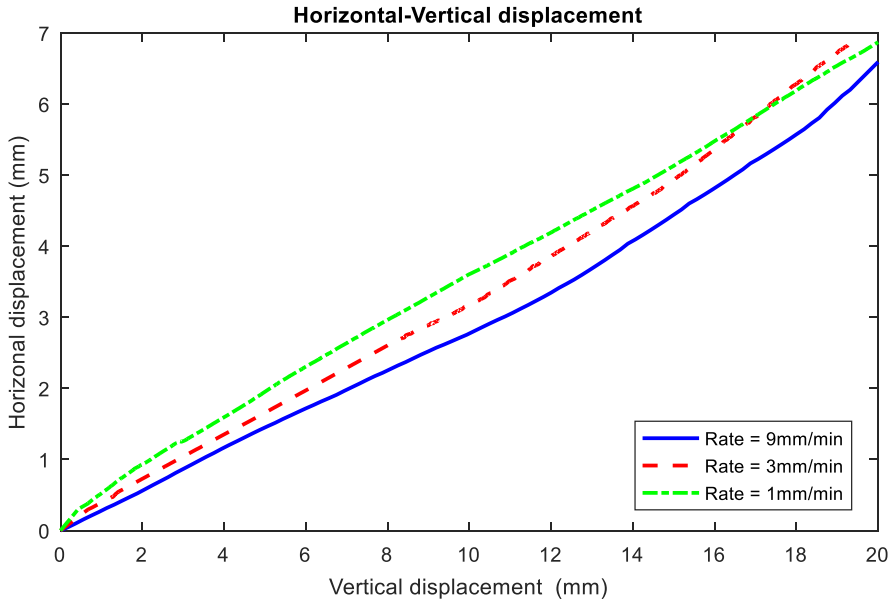

Figure B 53 Results of tensile strength tests performed on group B-26 (Loading approach= FST, T= 0 °C, Salinity= 1 g/L).

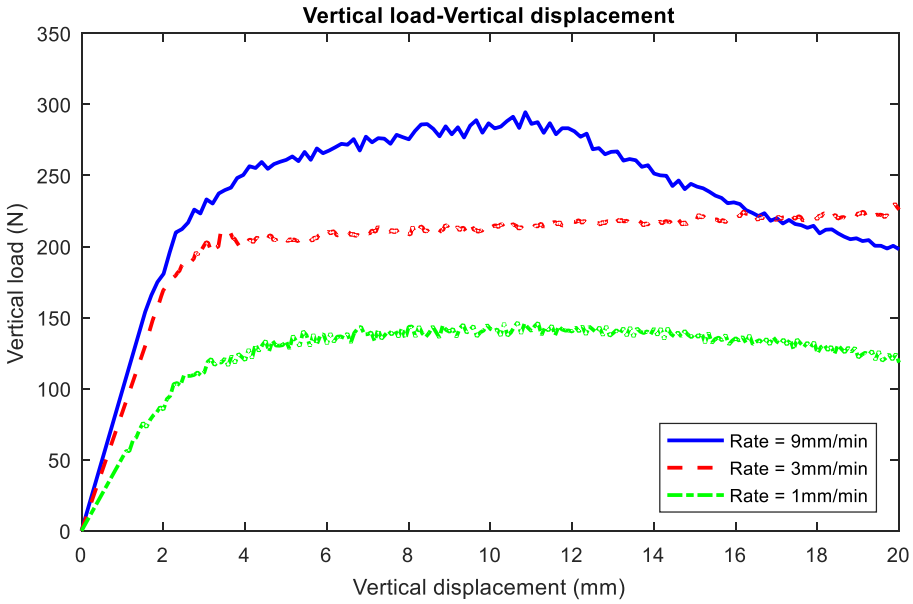

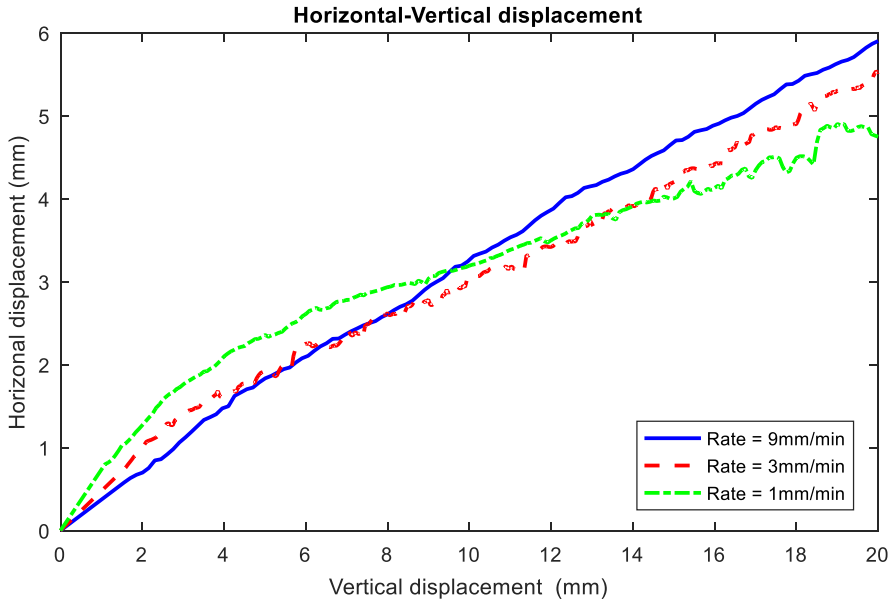

Figure B 54 Results of tensile strength tests performed on group B-27 (Loading approach= DPT, T= 0 °C, Salinity= 1 g/L).

`

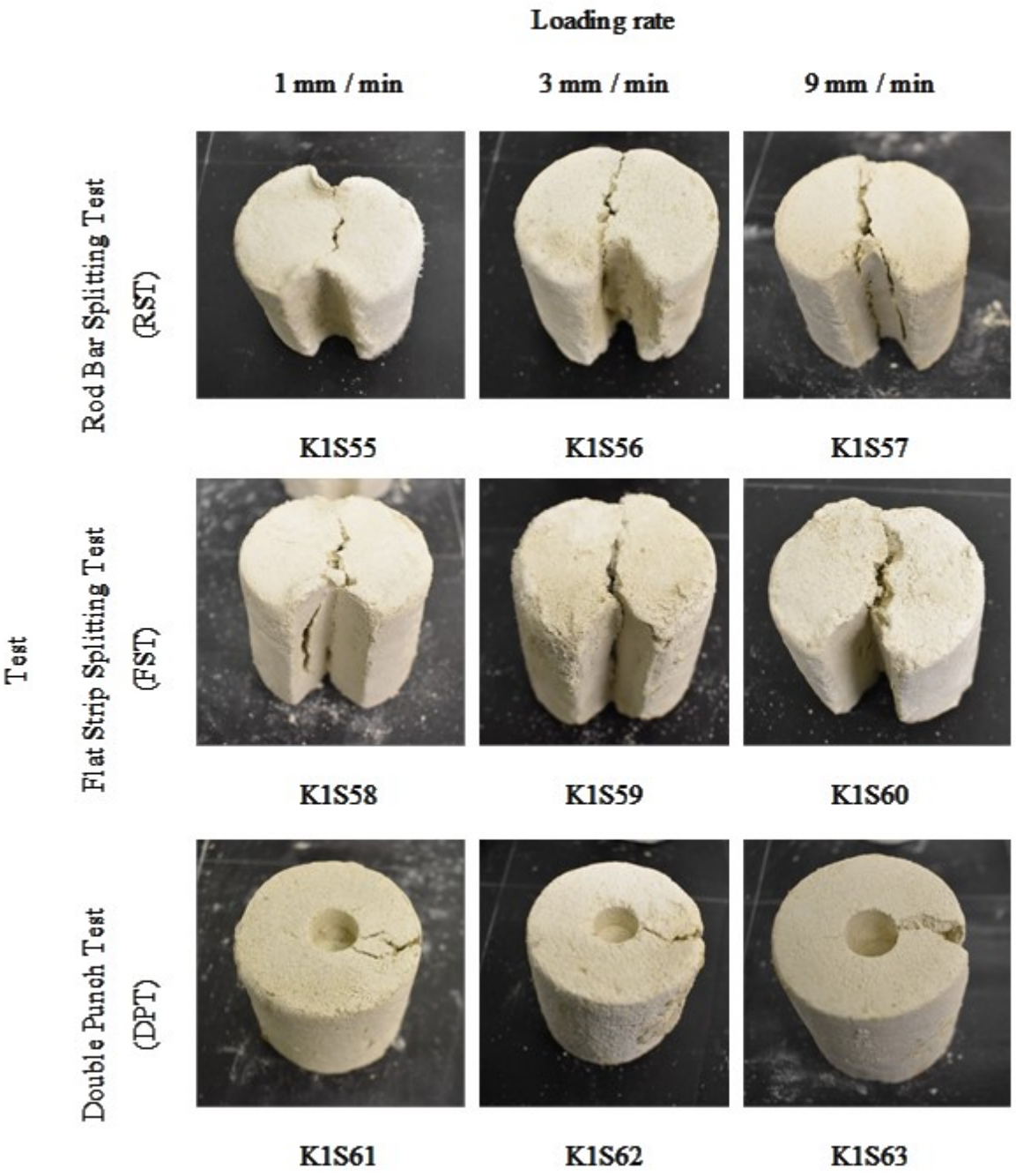

Figure B 55 Post-failure pictures of tested kaolinite-sand samples (T= 0 °C, Salinity= 1 g/L).

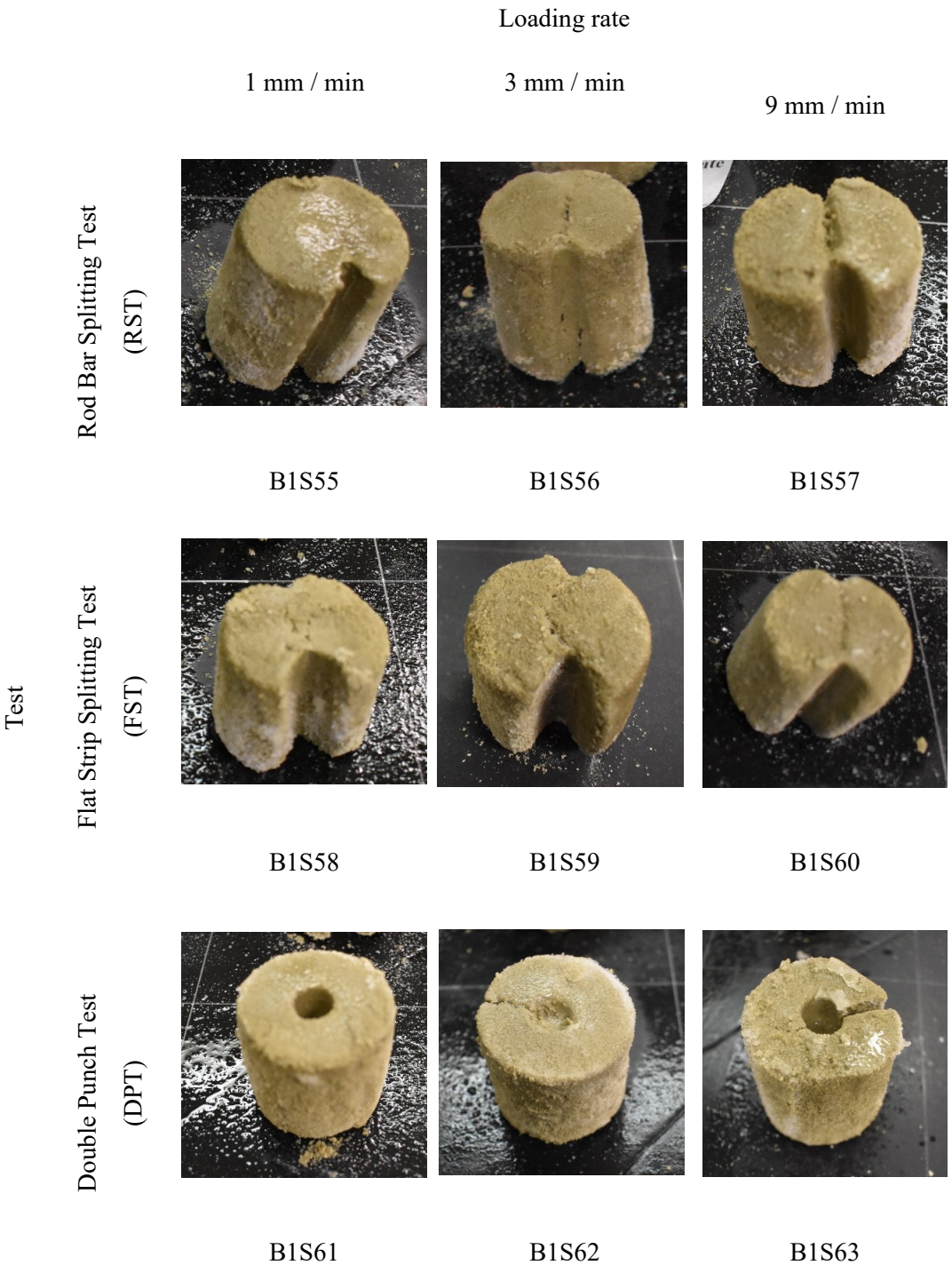

Figure B 56 Post-failure pictures of tested bentonite-sand samples (T= 0 °C, Salinity= 1 g/L).

B 2 Uniaxial compressive strength test results

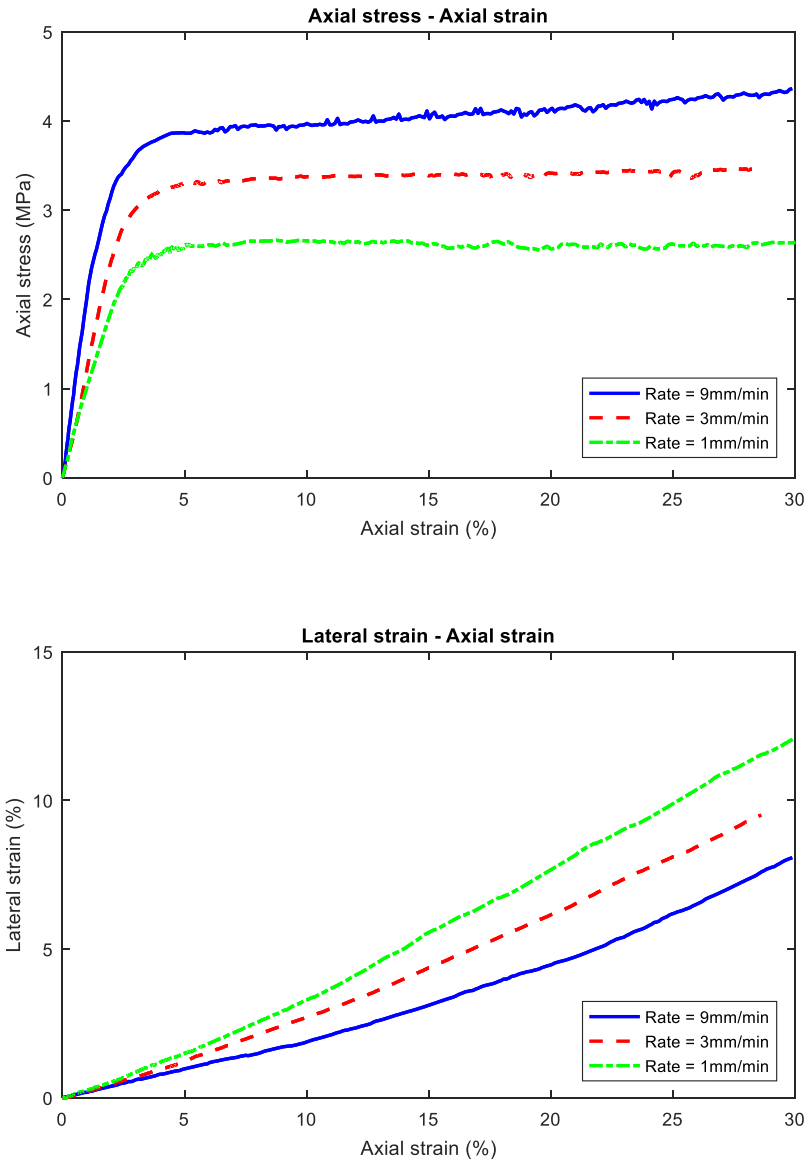

Figure B 57 Results of UCS tests performed on group KC-02 (T= - 10 °C, Laboratory= BEPL).

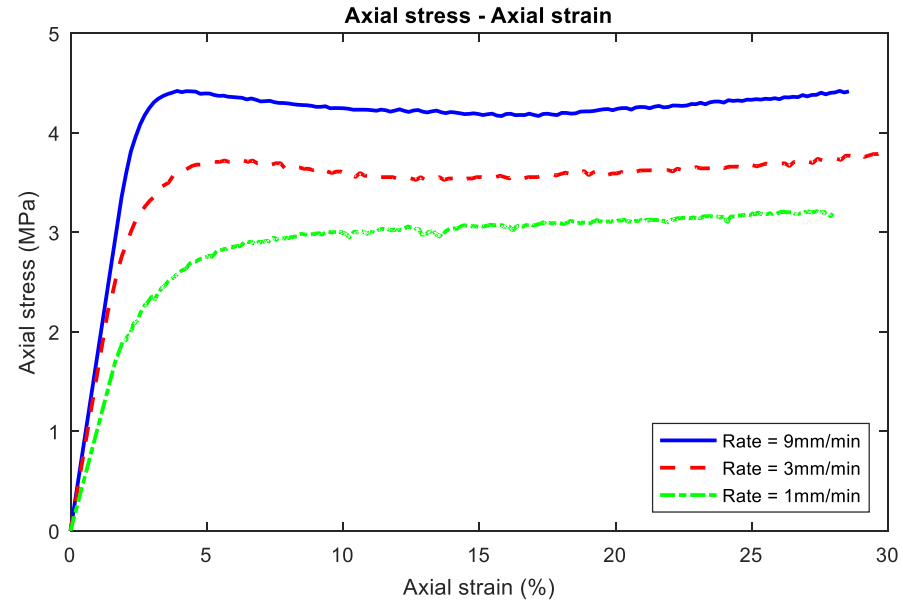

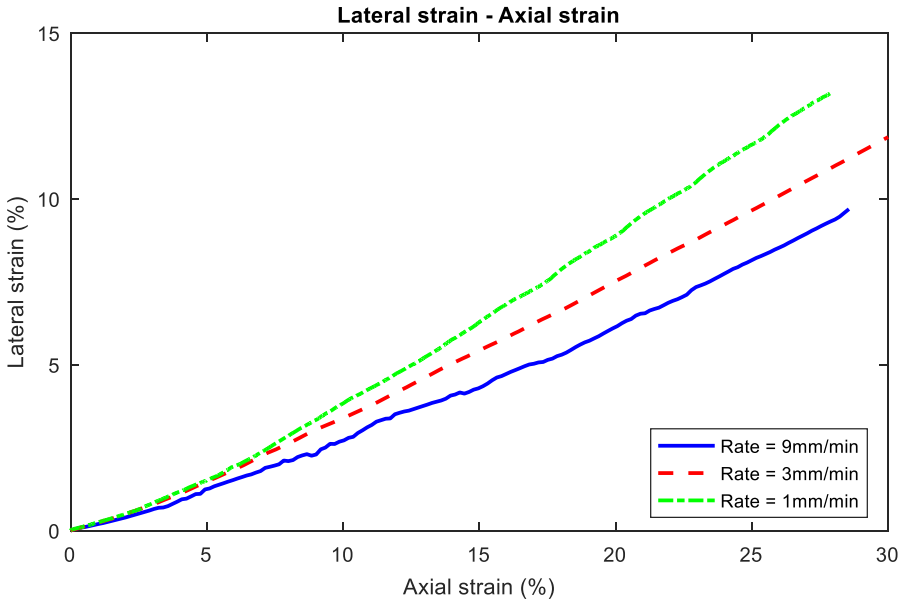

Figure B 58 Results of UCS tests performed on group BC-02 (T= - 10 °C, Laboratory= BEPL).

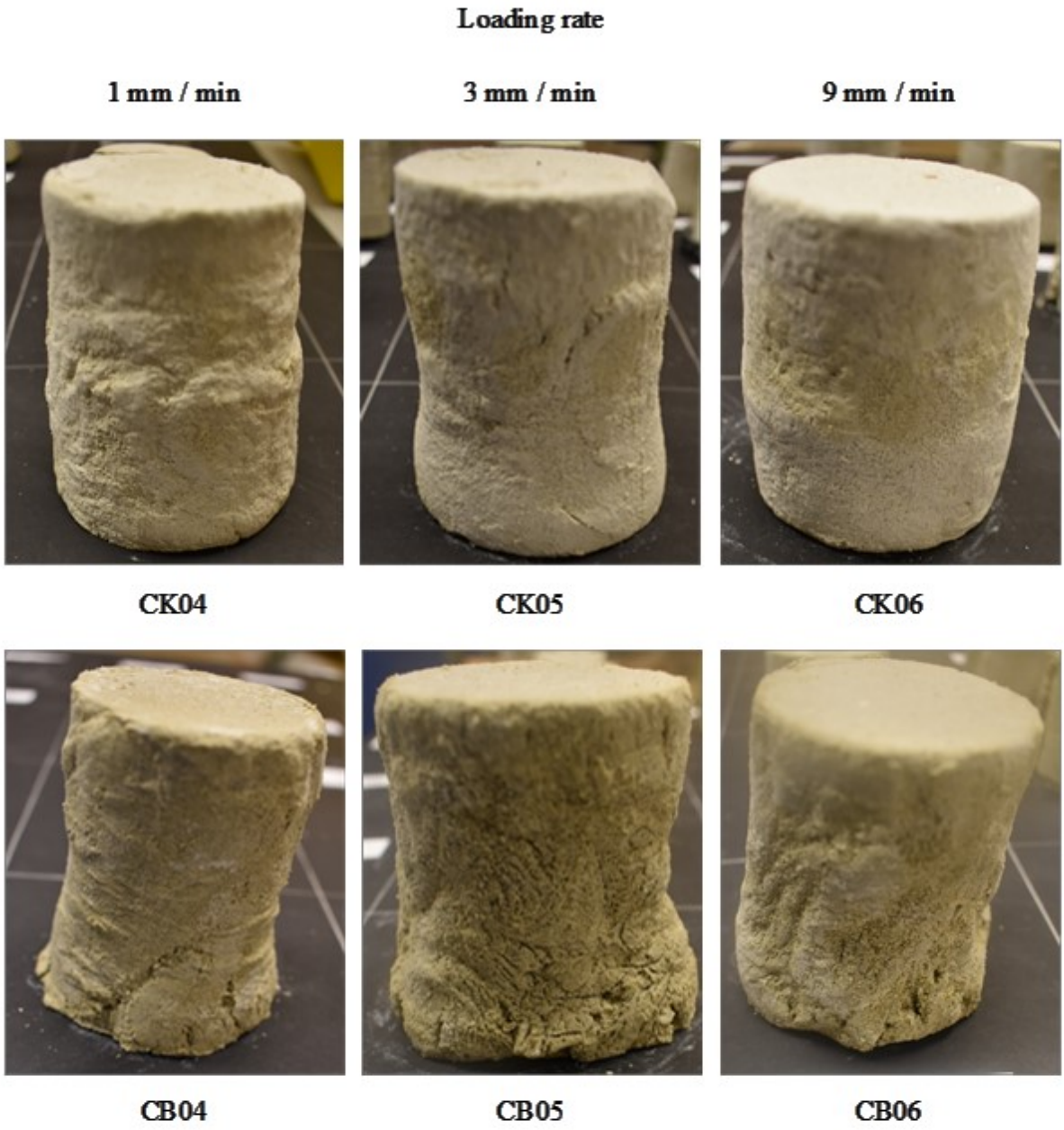

Figure B 59 Post-failure pictures of UCS tested samples (T= - 10 °C, Laboratory= BEPL).

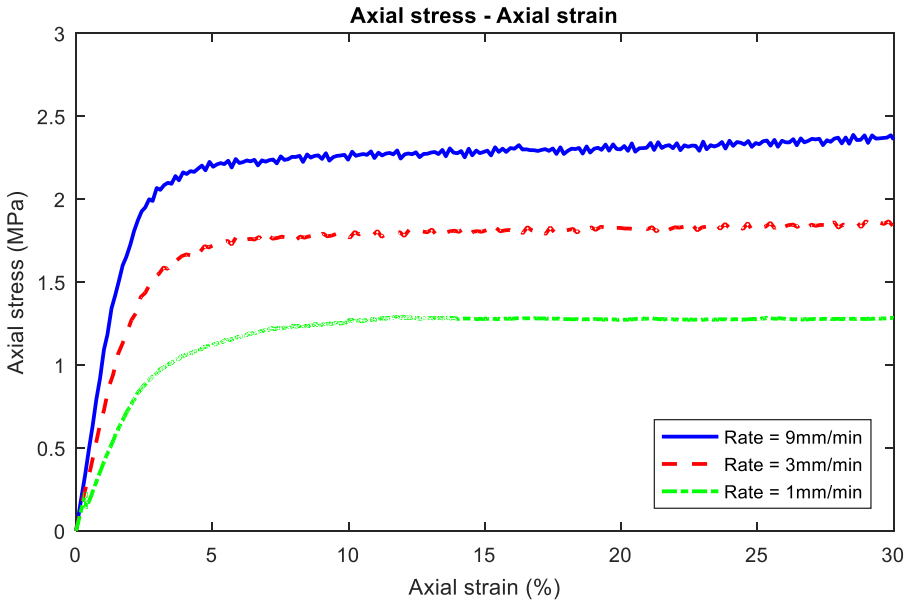

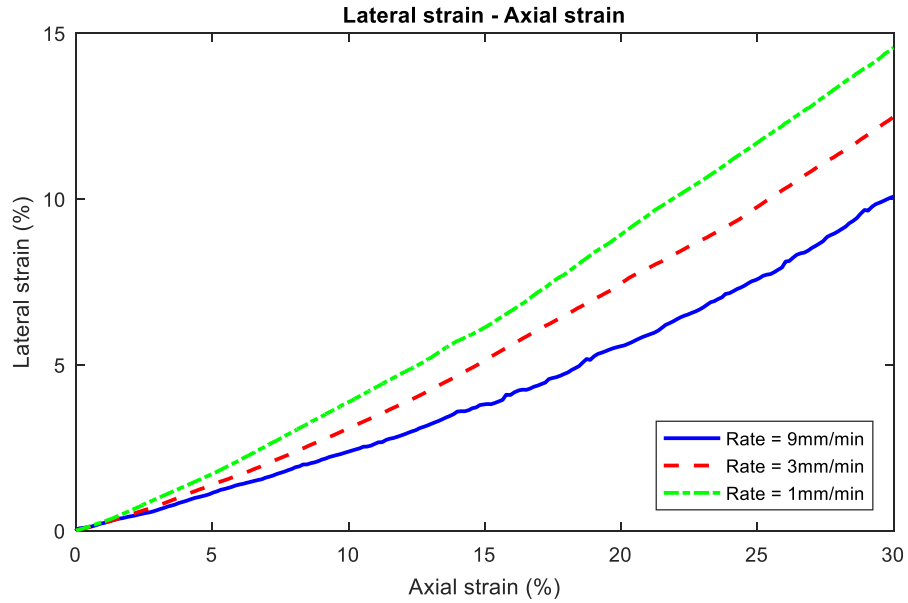

Figure B 60 Results of UCS tests performed on group KC-03 (T= - 5 °C, Laboratory= BEPL).

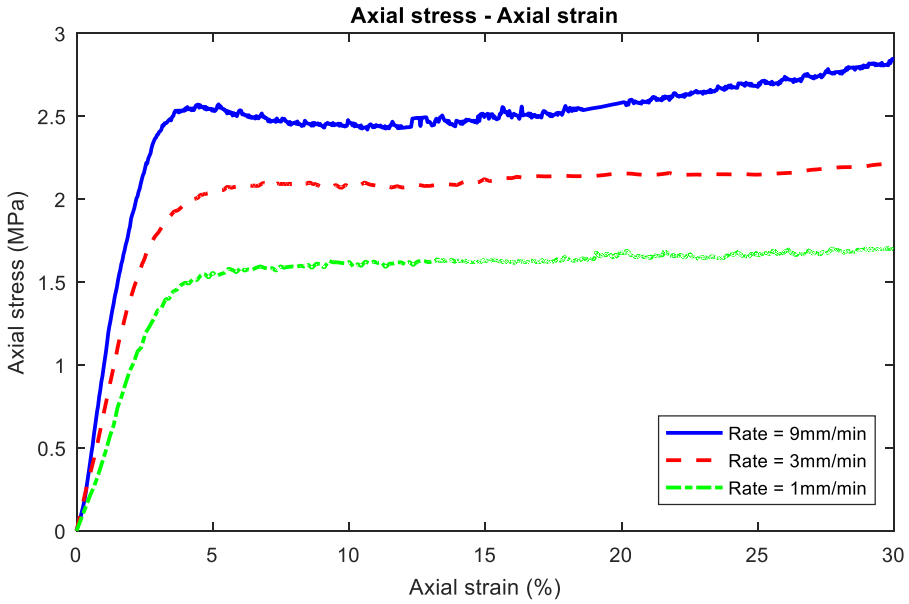

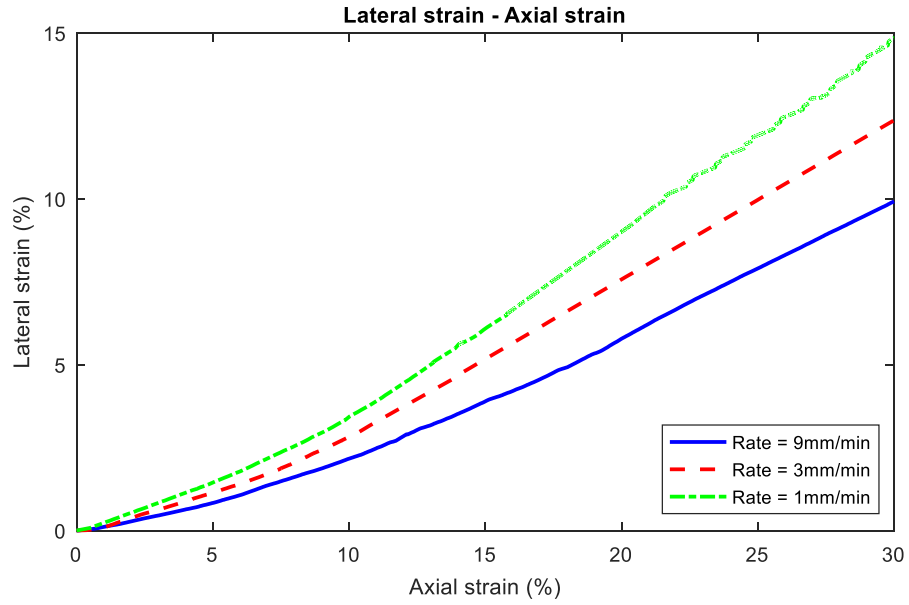

Figure B 61 Results of UCS tests performed on group BC-03 (T= - 5 °C, Laboratory= BEPL).

Figure B 62 Post-failure pictures of UCS tested samples (T= - 5 °C, Laboratory = BEPL).

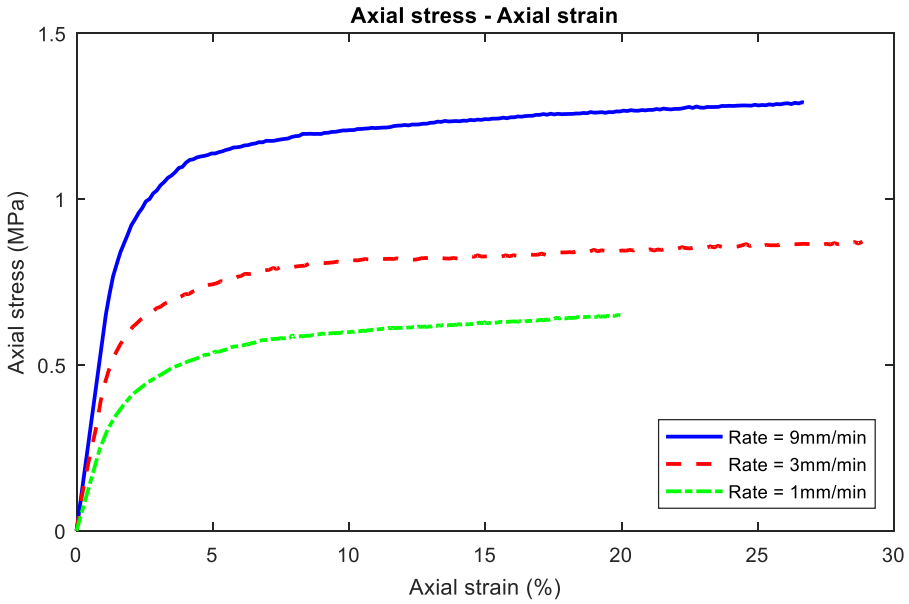

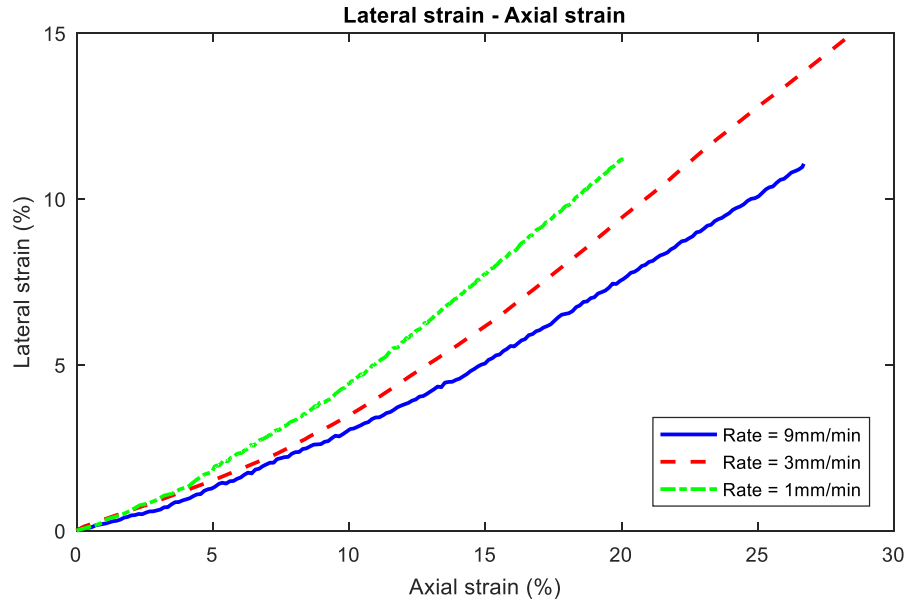

Figure B 63 Results of UCS tests performed on group KC-04 (T= - 2 °C, Laboratory= BEPL).

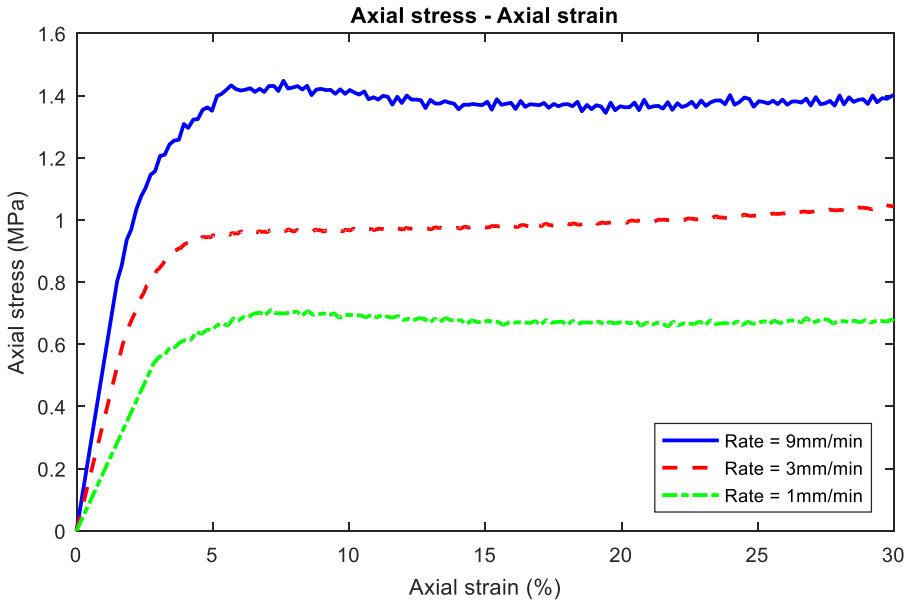

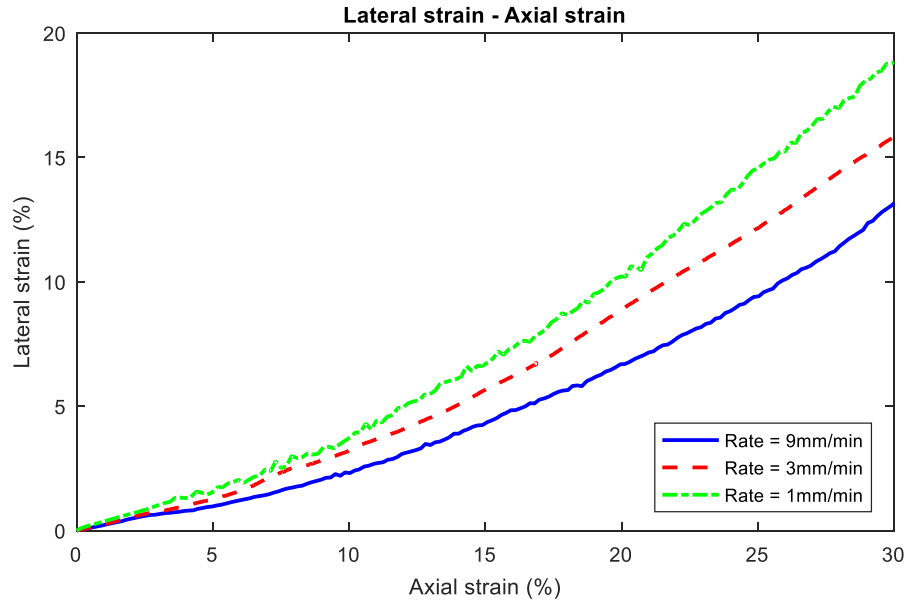

Figure B 64 Results of UCS tests performed on group BC-04 (T= - 2 °C, Laboratory= BEPL).

`

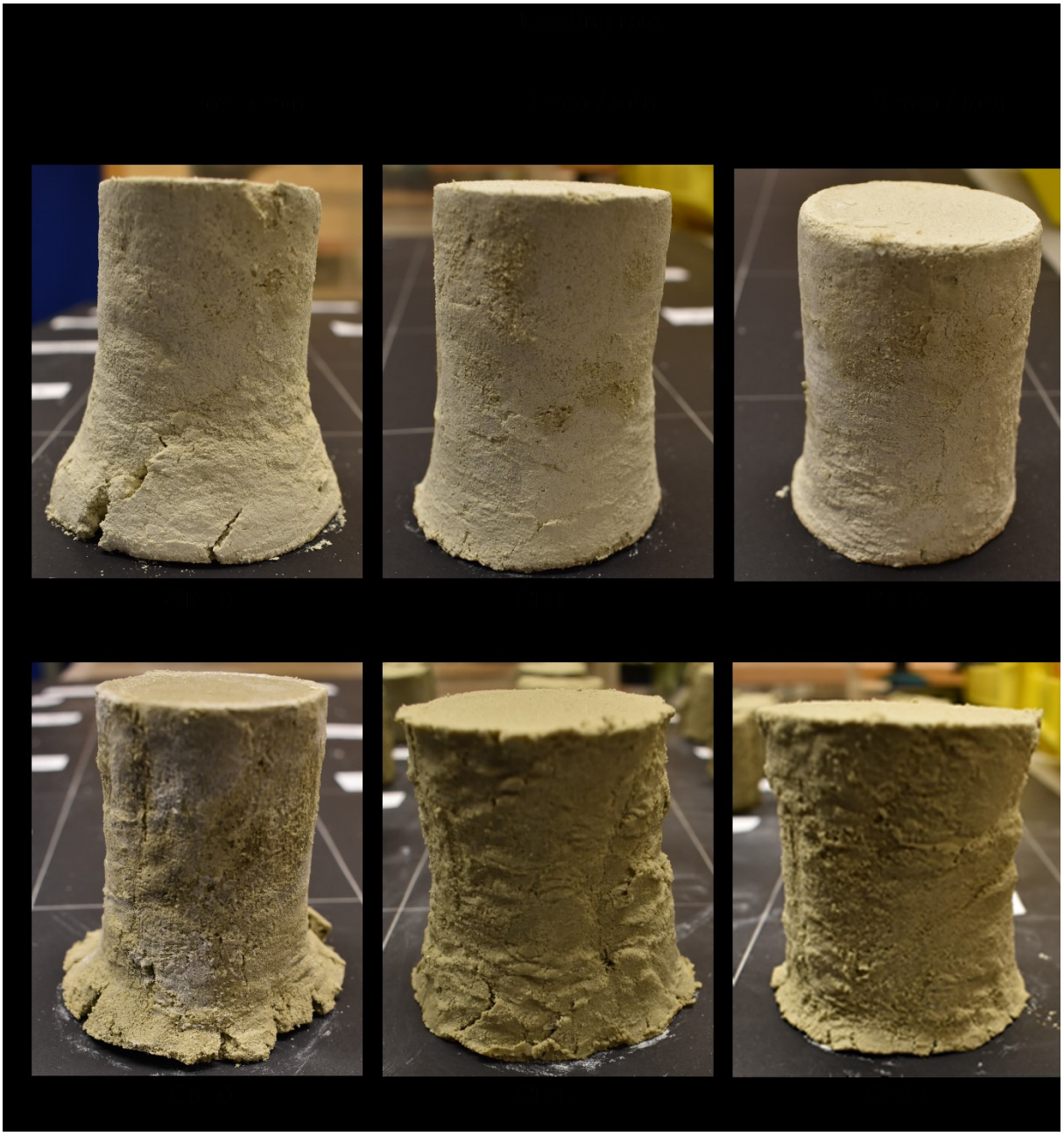

Figure B 65 Post-failure pictures of UCS tested samples (T= - 2 °C, Laboratory = BEPL).

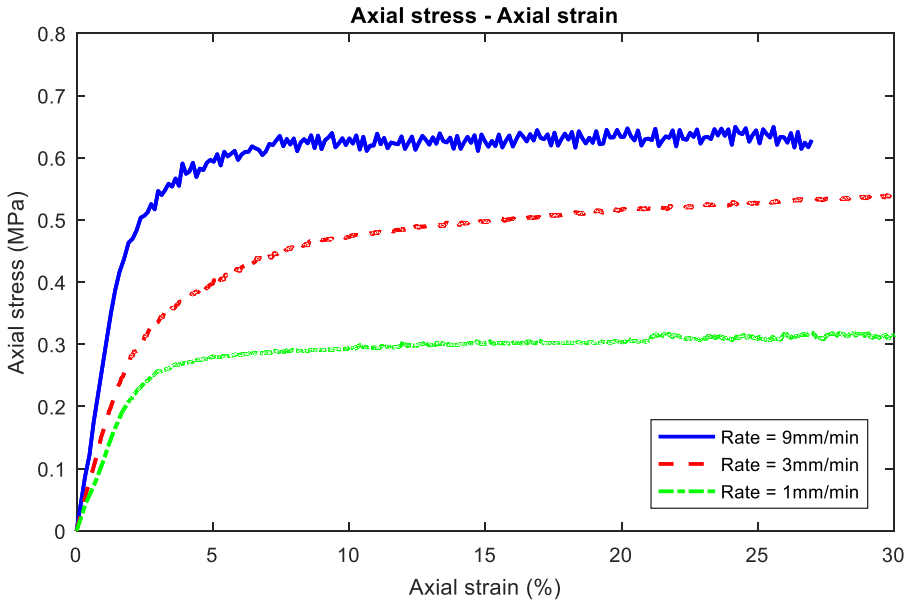

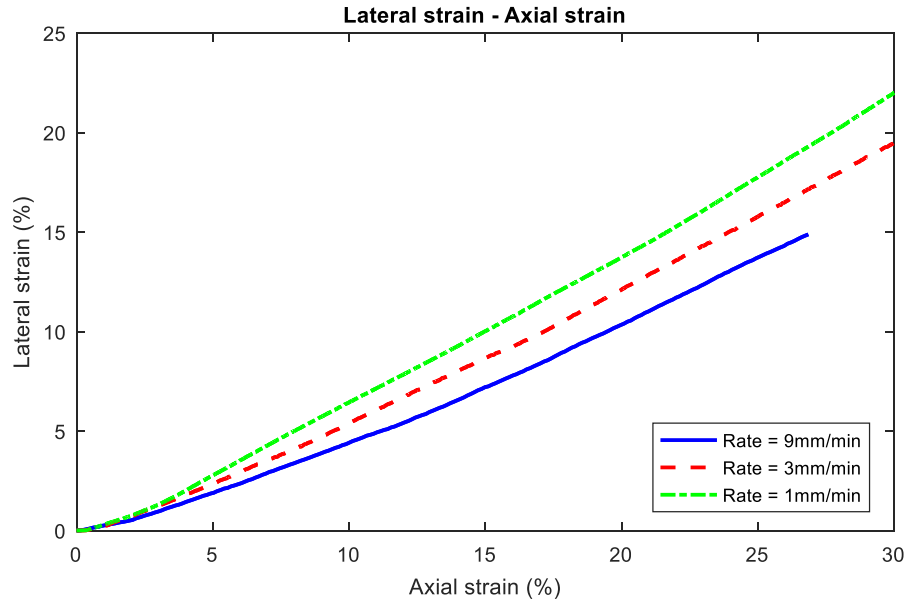

Figure B 66 Results of UCS tests performed on group KC-06 (T= - 0.5 °C, Laboratory= BEPL).

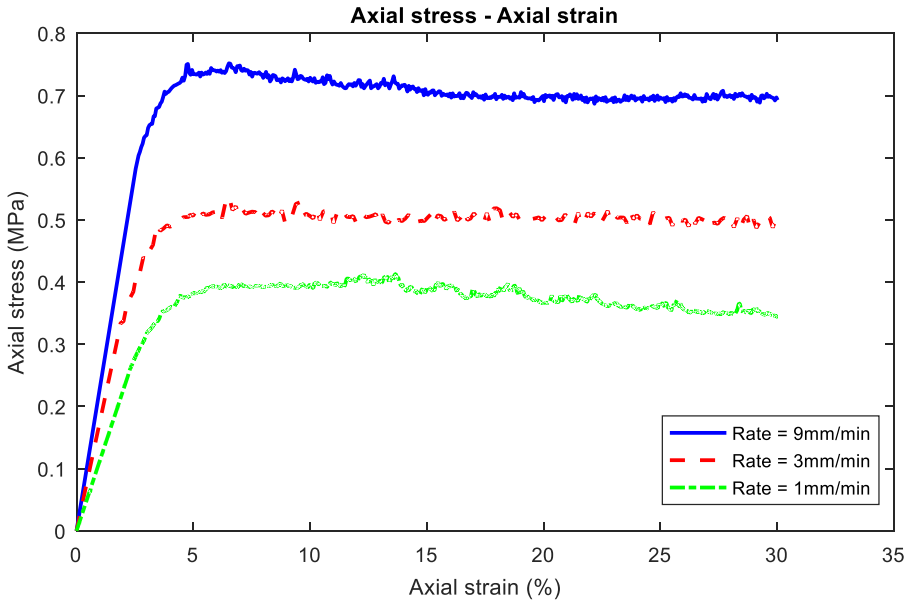

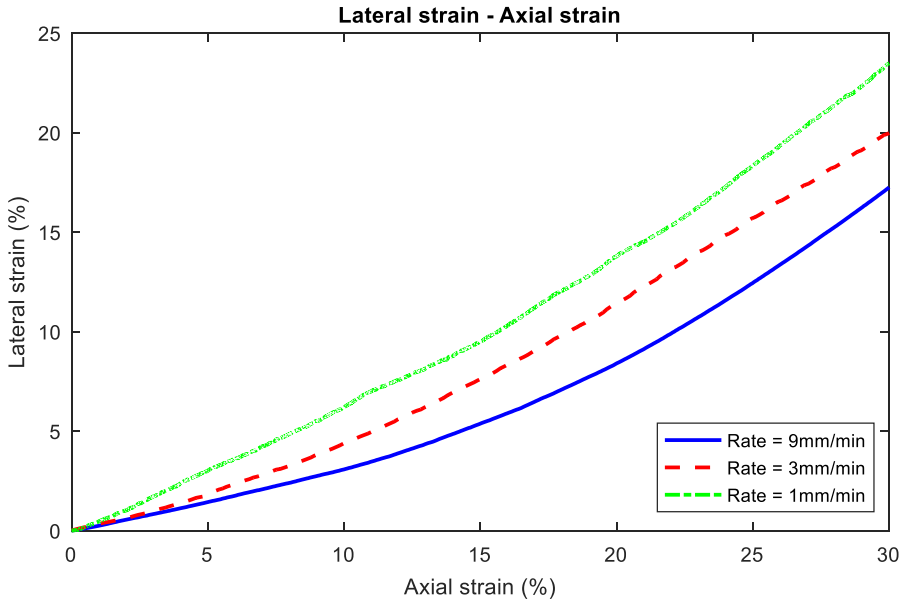

Figure B 67 Results of UCS tests performed on group BC-06 (T= - 0.5 °C, Laboratory= BEPL).

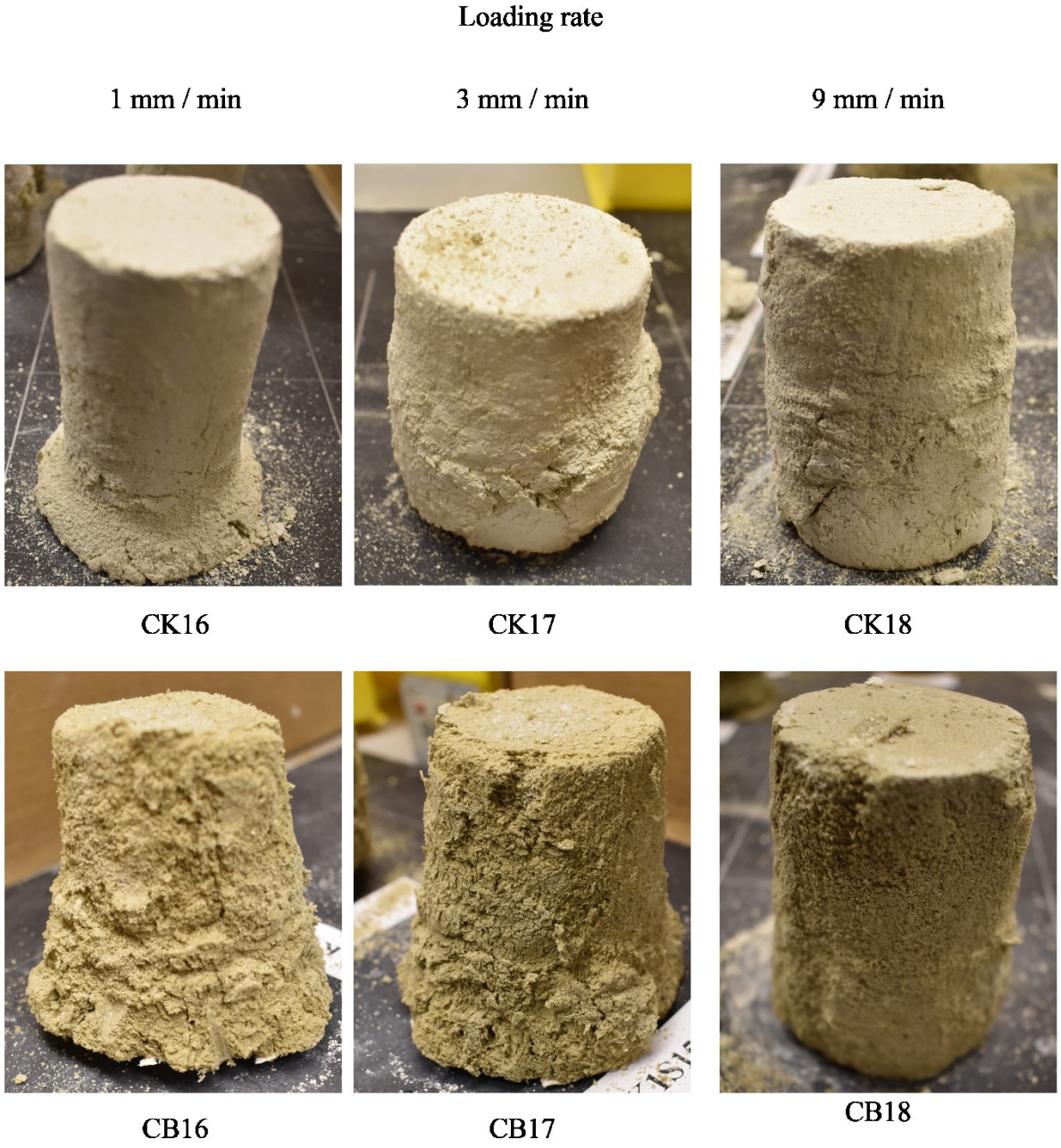

Figure B 68 Post-failure pictures of UCS tested samples (T= - 0.5 °C, Laboratory= BEPL).

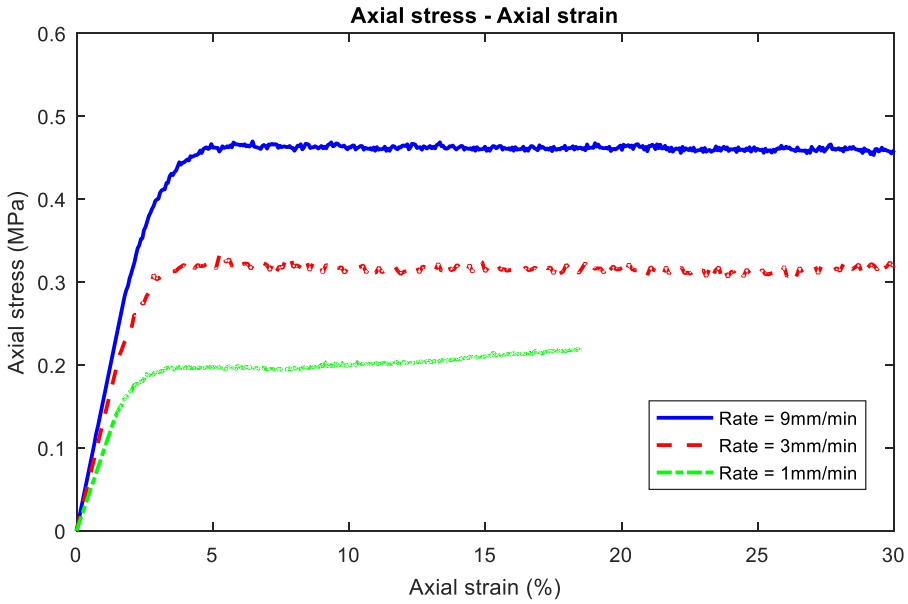

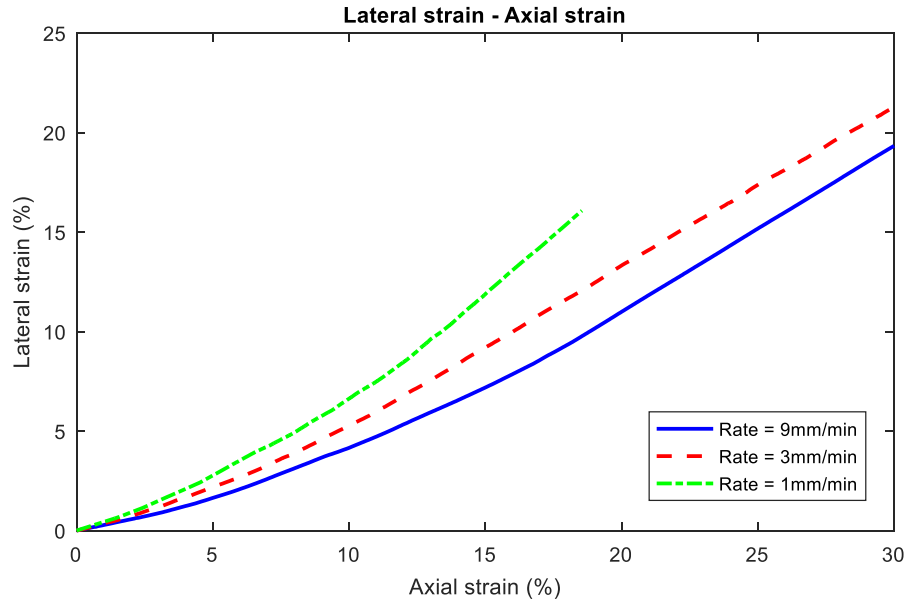

Figure B 69 Results of UCS tests performed on group KC-07 (T= 0 °C, Laboratory= BEPL).

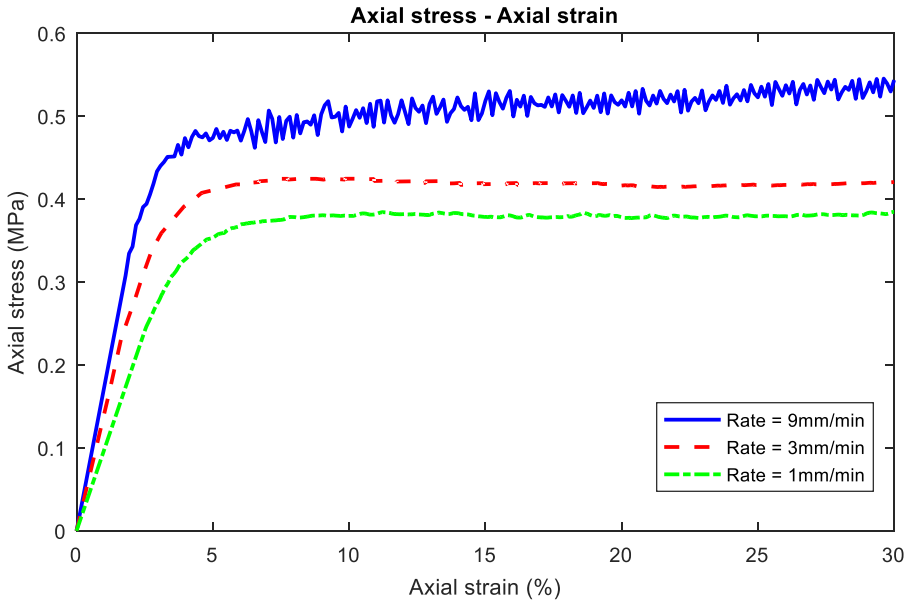

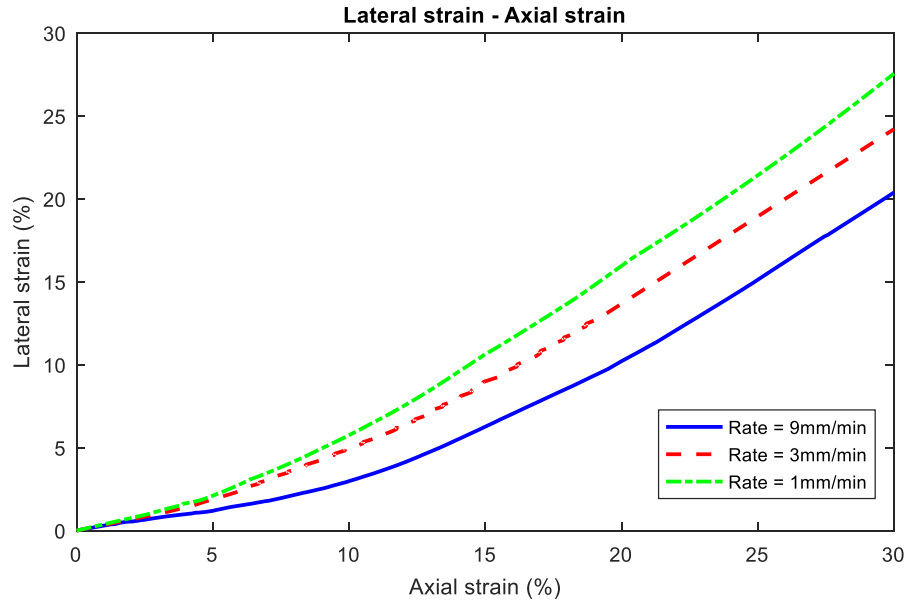

Figure B 70 Results of UCS tests performed on group BC-07 (T= 0 °C, Laboratory= BEPL).

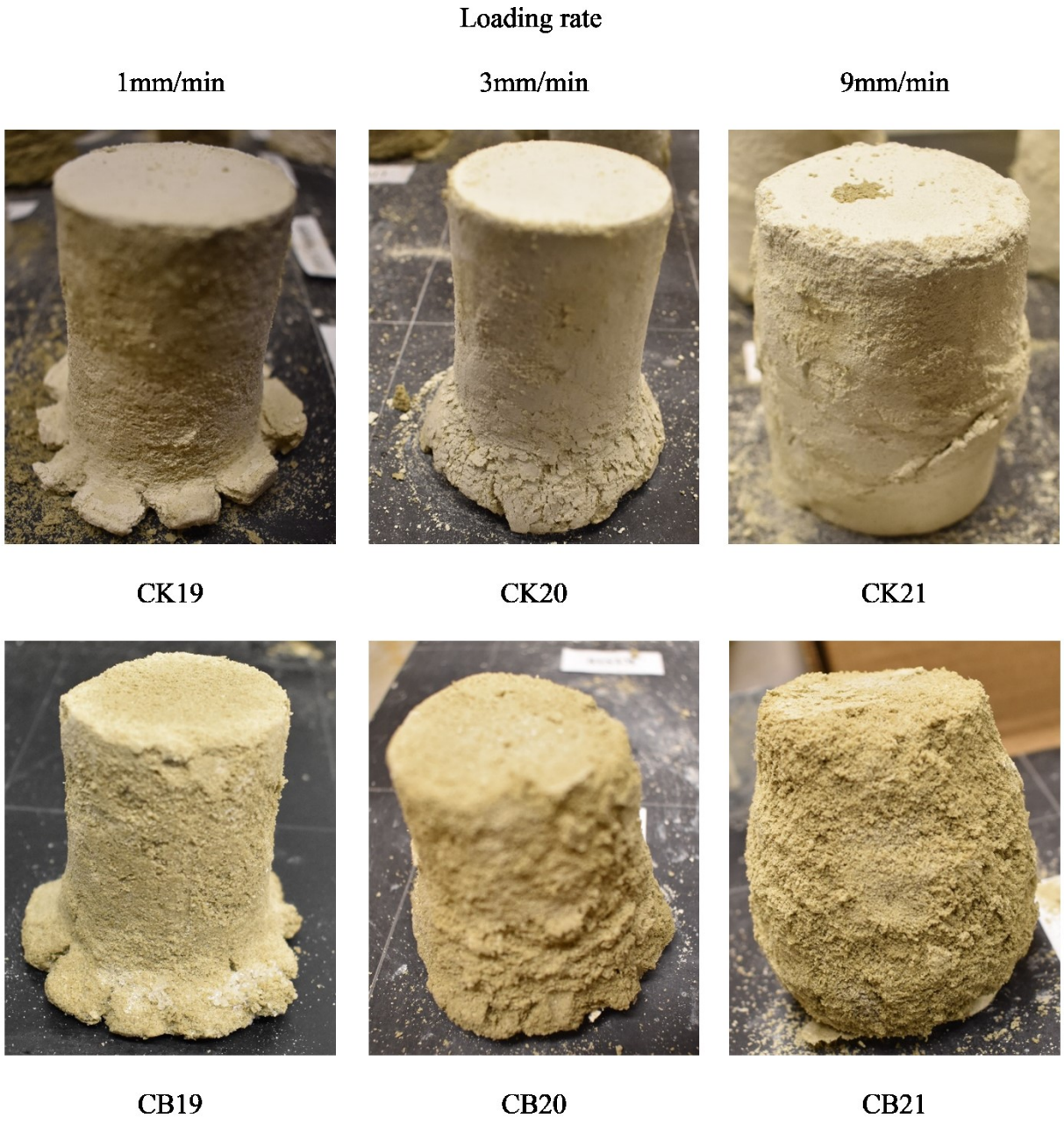

Figure B 71 Post-failure pictures of UCS tested samples (T= 0 °C, Laboratory= BEPL).

B 3 Stress relaxation test results

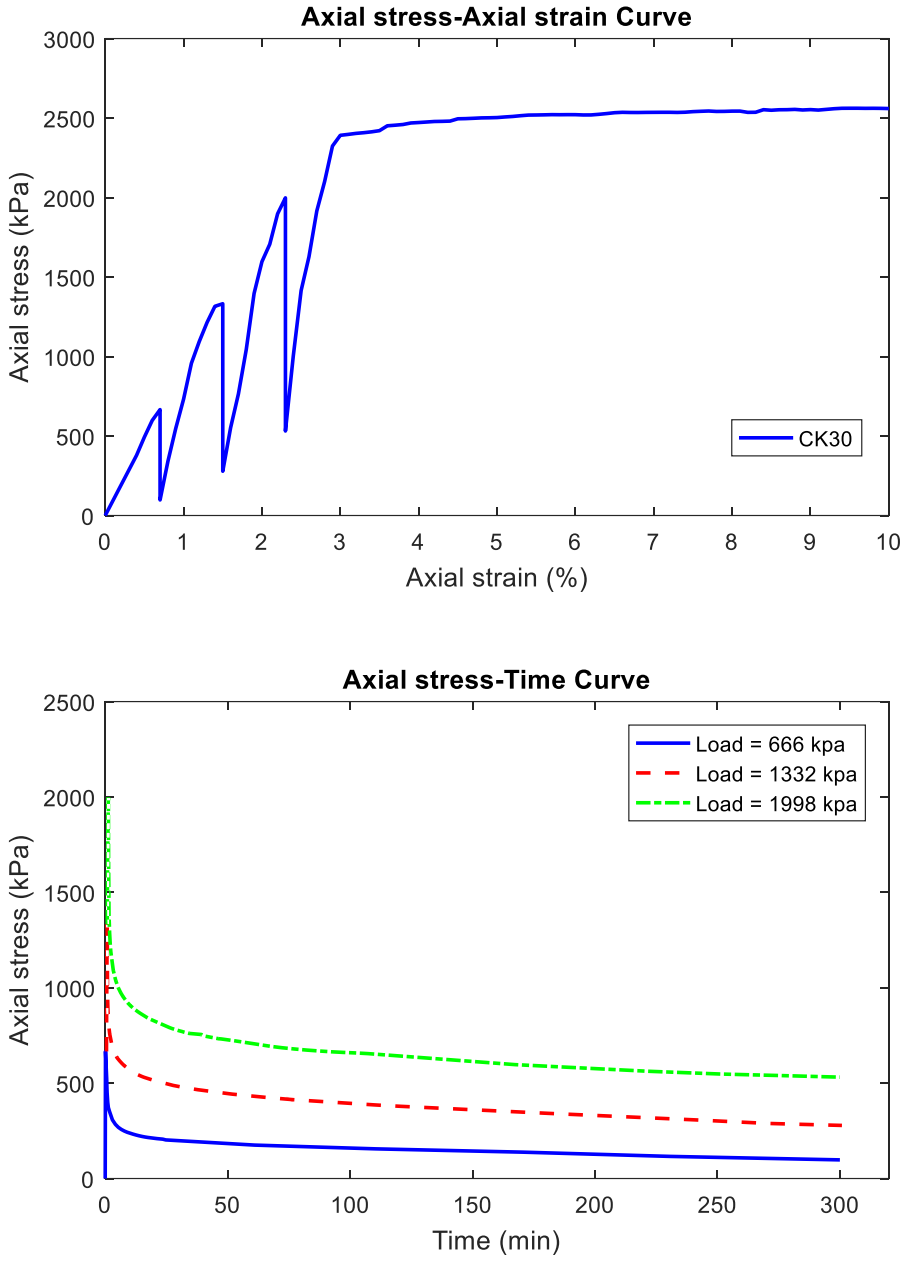

Figure B 72 Results of the stress relaxation test performed on sample CK30 (T= - 10 °C and Loading rate= 1 mm/min).

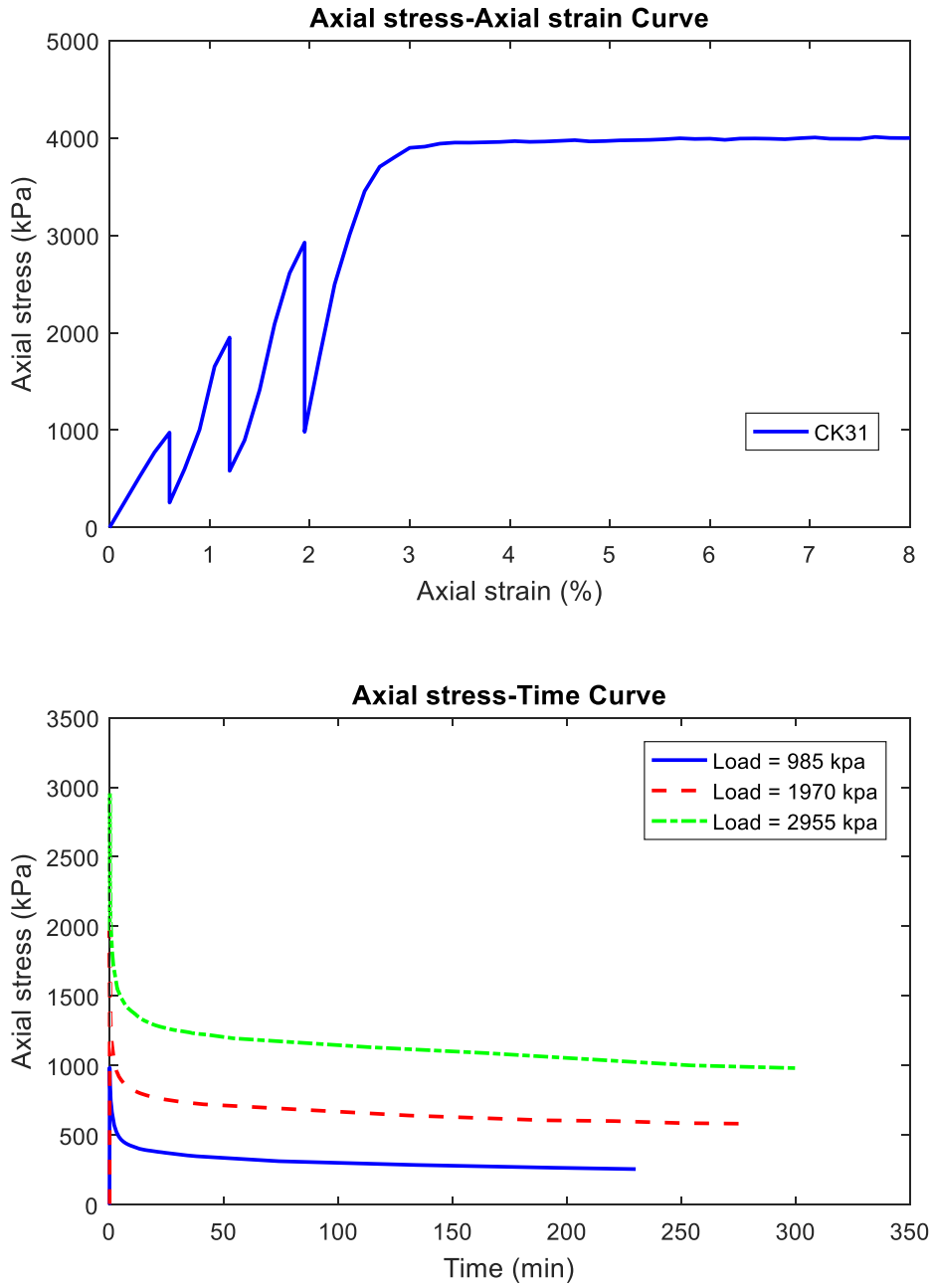

Figure B 73 Results of the stress relaxation test performed on sample CK31 (T= - 10 °C and Loading rate= 9 mm/min).

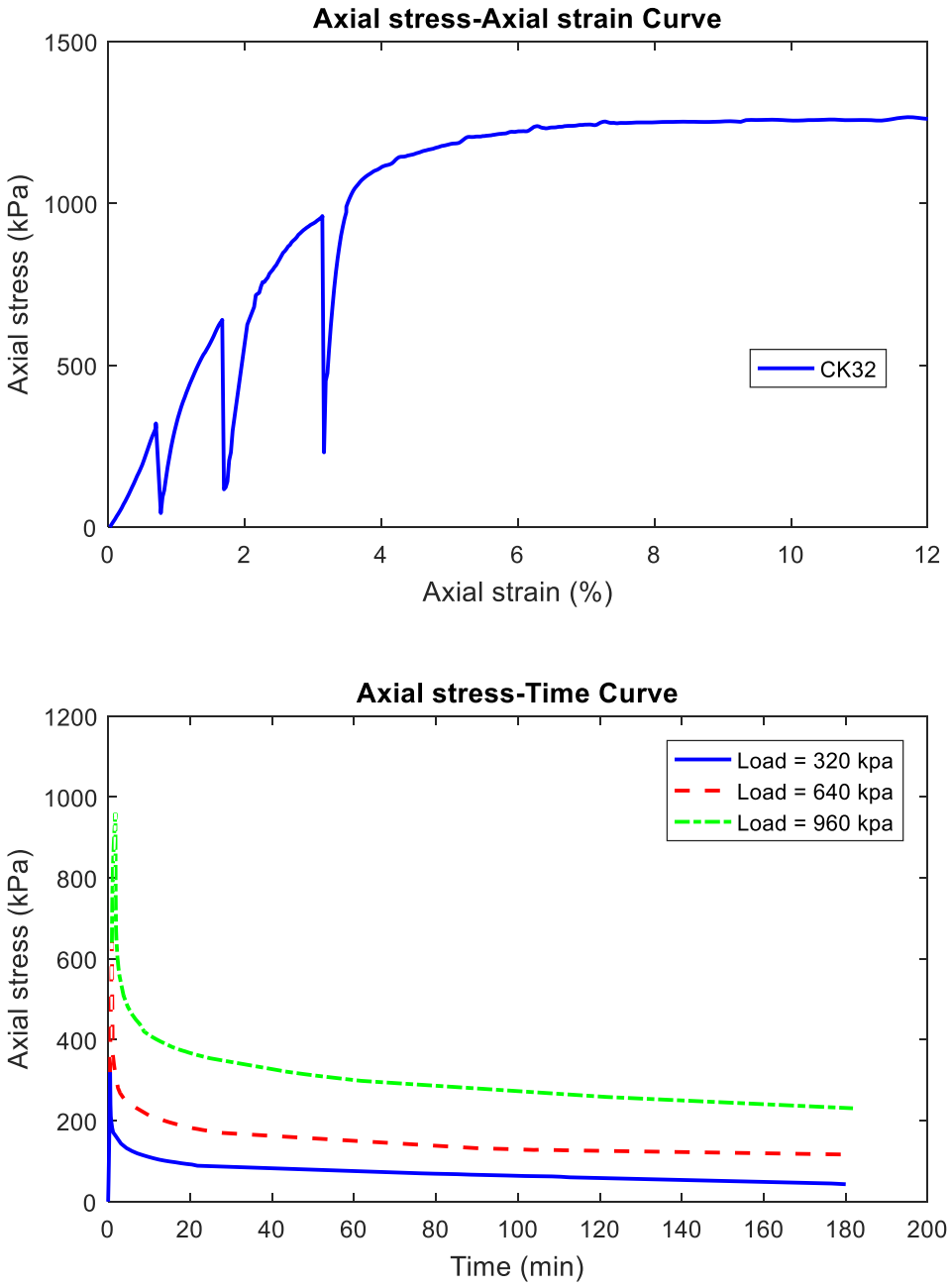

Figure B 74 Results of the stress relaxation test performed on sample CK32 (T= - 5 °C and Loading rate= 1 mm/min).

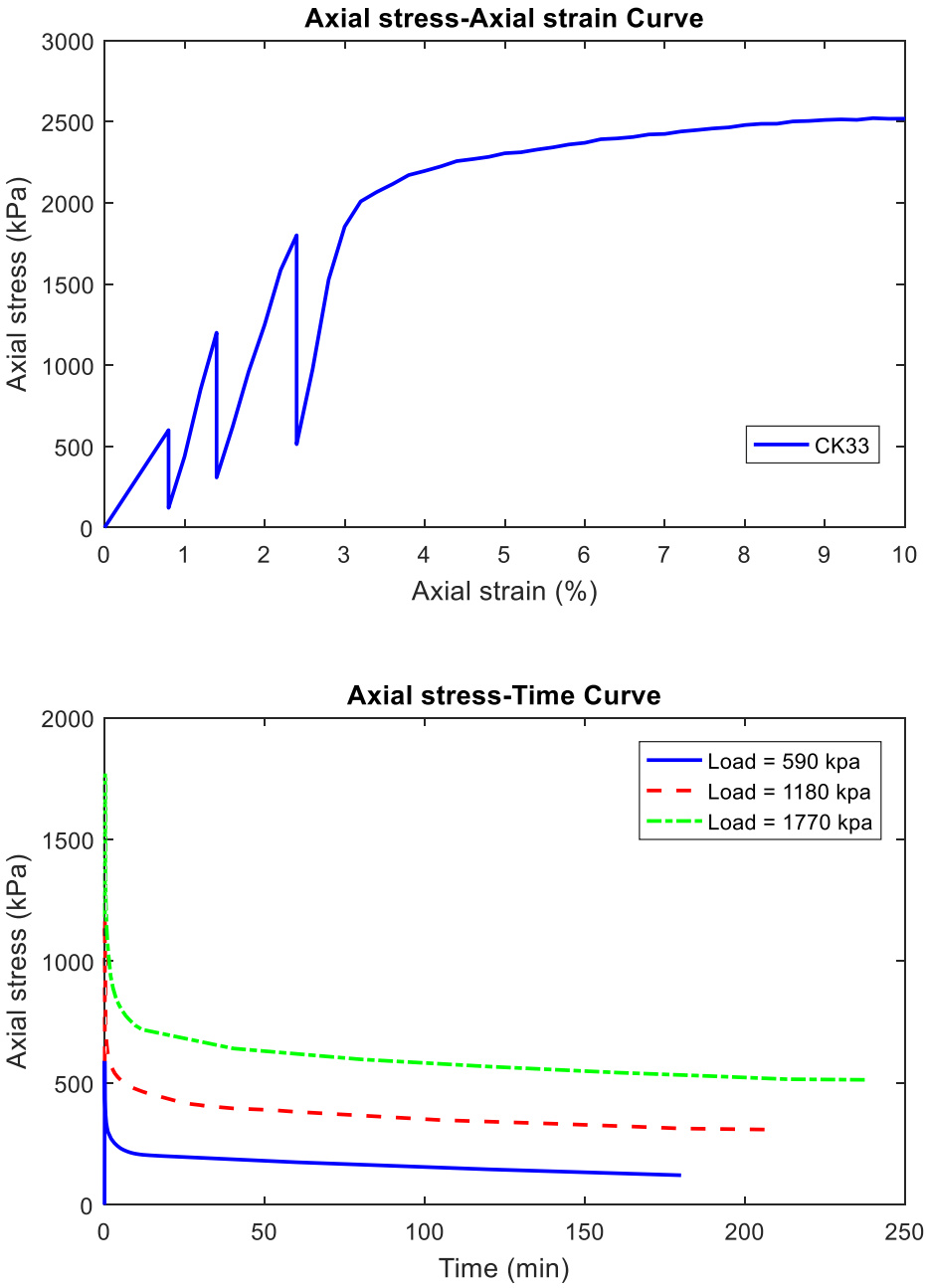

Figure B 75 Results of the stress relaxation test performed on sample CK33 (T= - 5 °C and Loading rate= 9 mm/min).

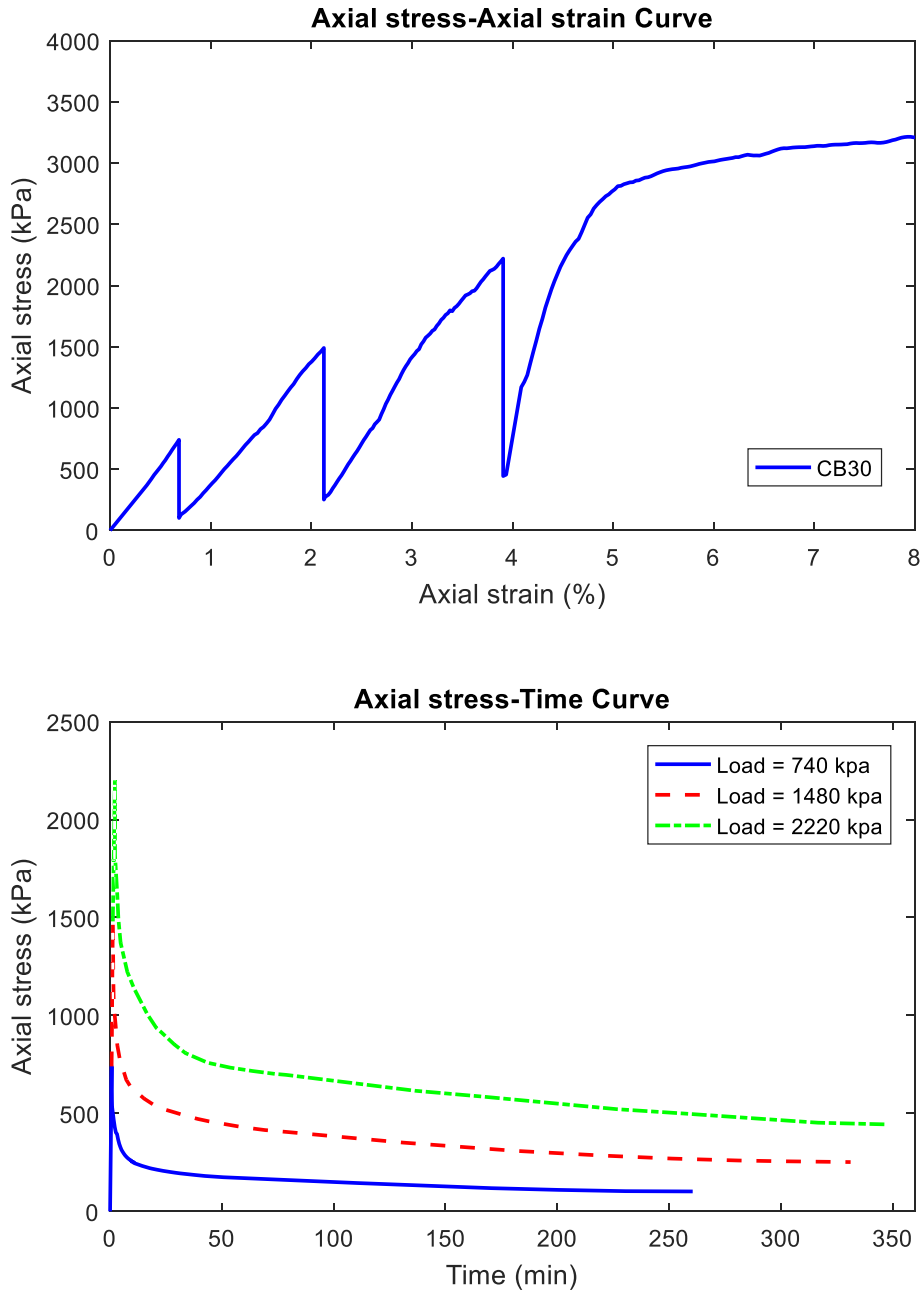

Figure B 76 Results of the stress relaxation test performed on sample CB30 (T= - 10 °C and Loading rate= 1 mm/min).

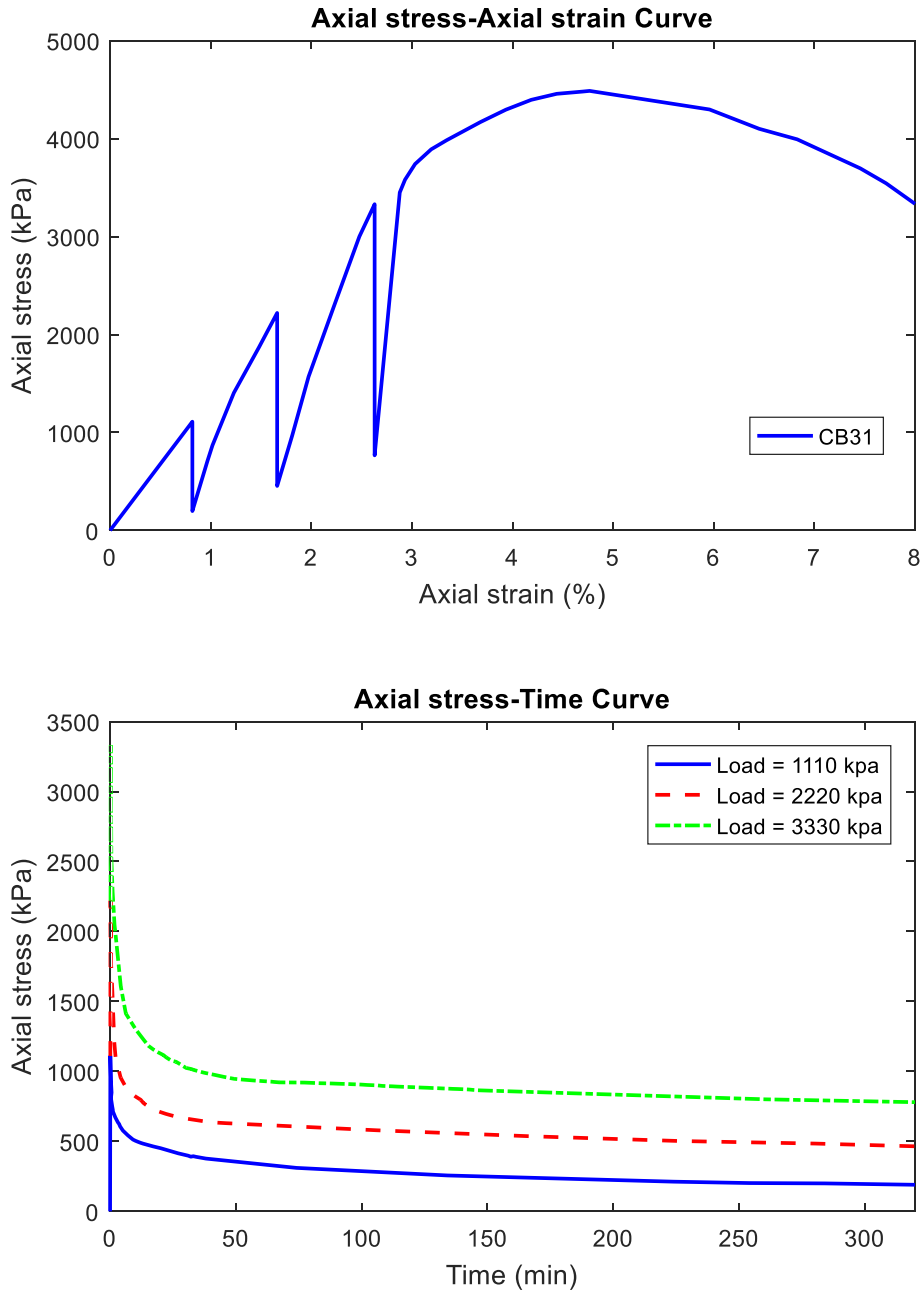

Figure B 77 Results of the stress relaxation test performed on sample CB31 (T= - 10 °C and Loading rate= 9 mm/min).

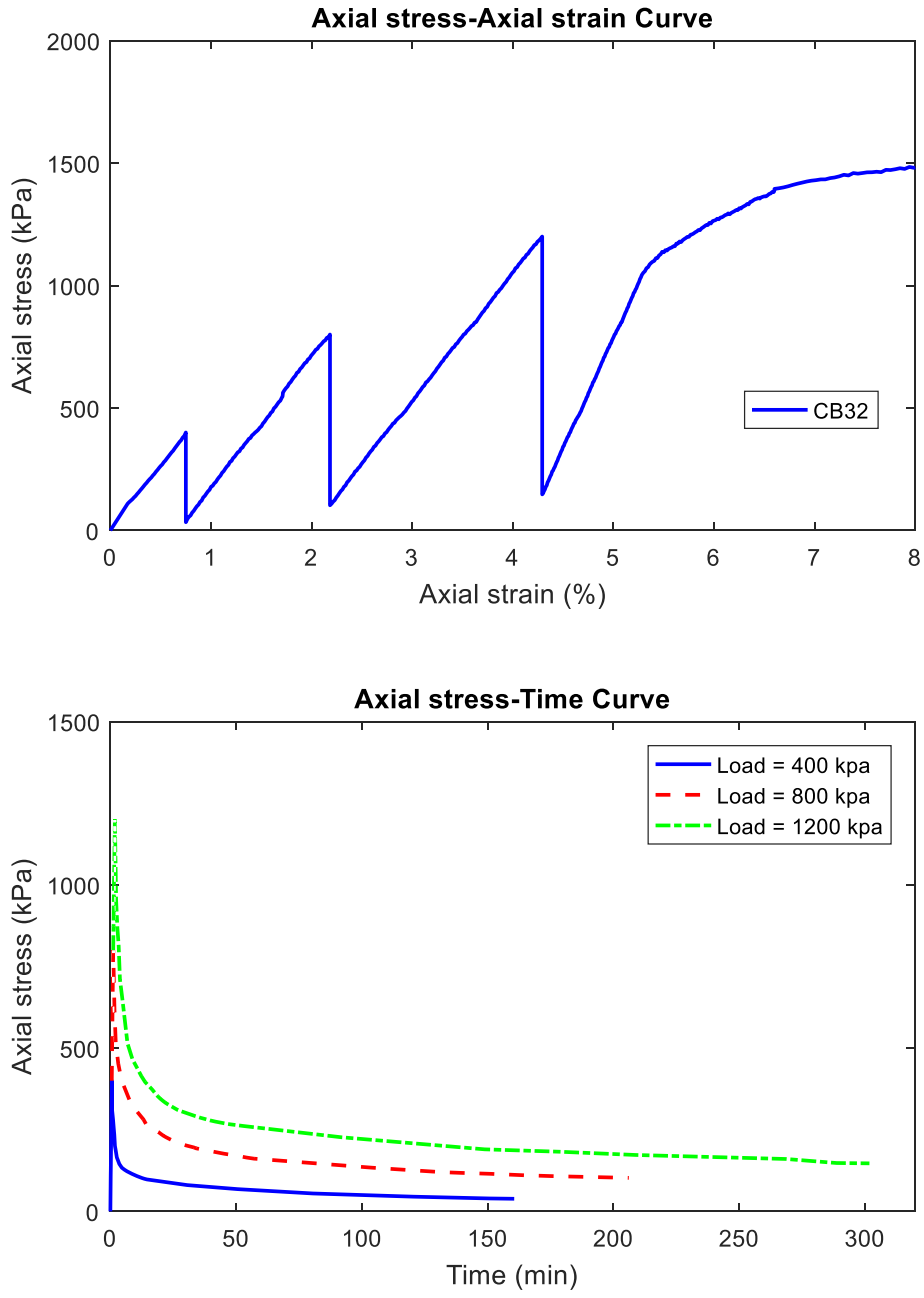

Figure B 78 Results of the stress relaxation test performed on sample CB32 (T= - 5 °C and Loading rate= 1 mm/min).

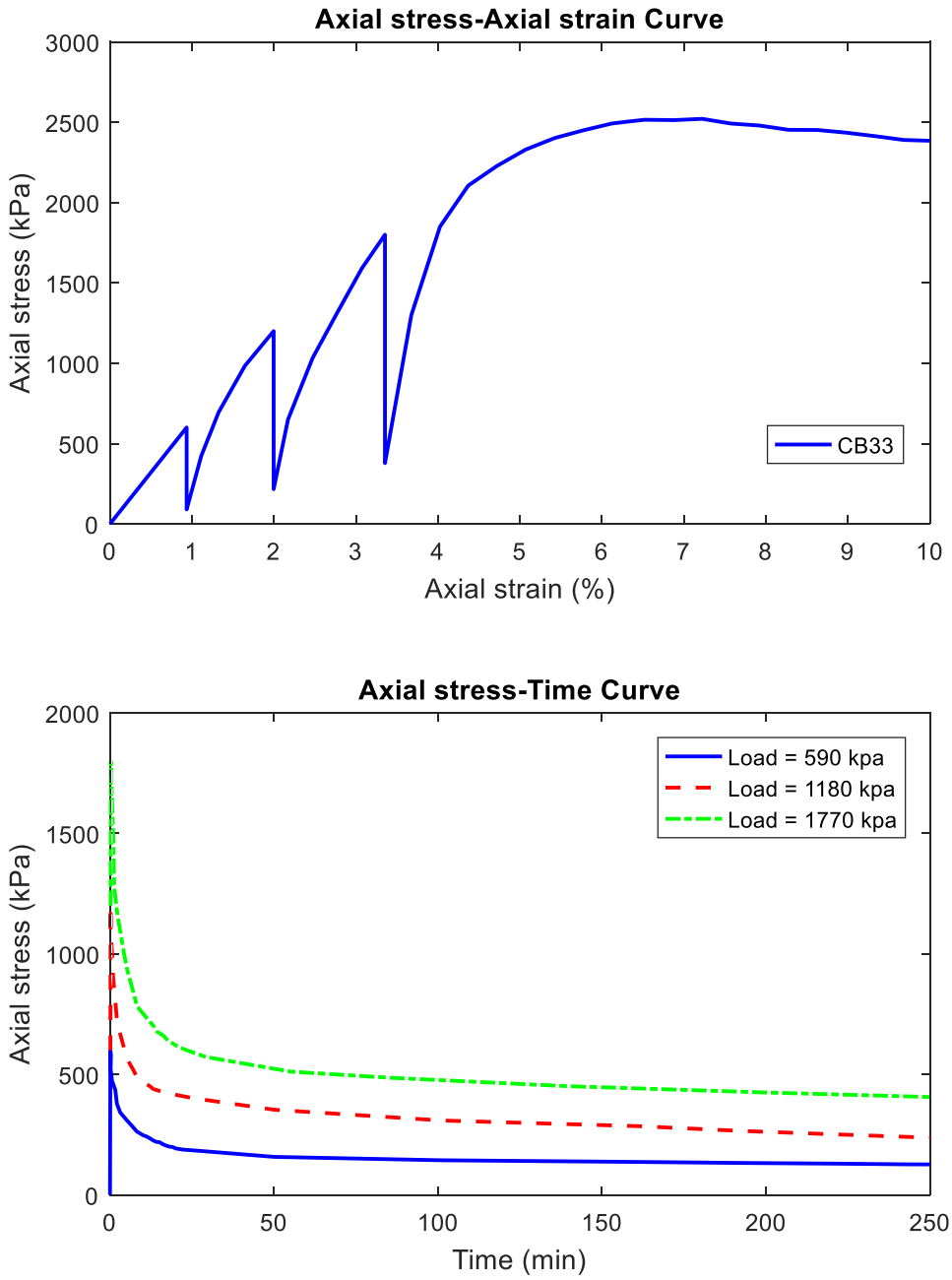

Figure B 79 Results of the stress relaxation test performed on sample CB33 (T= - 5 °C and Loading rate= 9 mm/min).

`

APPENDIX C

TECHNICAL DATA OF MATERIALS USED

TECHNICAL DATA

Granusil®
MINERAL FILLERS

FEATURES AND BENEFITS

ST. CANUT, QUEBEC

GRANUSIL® Mineral Fillers are produced from high purity industrial quartz sands for a wide variety of industrial and contractor mixed applications which need a reliable silica contribution or require a chemically inert structural filler. Consistently uniform grain shapes and particle size distributions offer excellent placement, compaction and mechanical properties. High silica content combined with low level soluble ions, alkalis and alkaline oxides provide non-reactive service in most corrosive and exposed environments.

These durable monocrystalline structures resist abrasion in high traffic-excessive wear applications and provide the stability formulators seek in high solids emulsions, elastomerics, cemented and modified cementitious systems. GRANUSIL® is the preferred structural component in systems ranging from polymerized floor overlays to artificial sports turf.

All GRANUSIL® grades are processed and sized under rigid SPC and UNIMIN QIP℠ statistical and quality assurance programs. The result is chemical purity and consistently uniform particle size distributions for predictable performance in either manufactured or site-prepared products.

PARTICLE SIZE ANALYSIS AND PROPERTIES

Mean Values. These Do Not Represent A Specification.

	Mesh Size ASTM	Mesh Size Microns	4095	4020	4010	7030	8000
	12	1.70mm	---	---	---	---	---
	16	1.18mm	---	---	---	---	---
	20	850	1.3	---	---	---	---
Typical Mean %	30	600	34.9	0.7	0.5	---	---
Retained on	40	425	58.7	15.7	14.0	---	0.2
Individual Sieves	50	300	4.2	36.9	36.8	7.0	1.0
	70	212	0.7	29.3	28.3	39.2	6.2
	100	150	0.2	12.7	13.5	30.3	7.4
	140	106	---	3.6	4.6	13.5	14.2
	200	75	---	0.7	1.5	6.5	16.0
	270	53	---	---	---	---	10.3
	325	45	---	---	---	---	2.0
	PAN	PAN	---	0.4	0.8	3.5	42.7
Prior Grade Designation			4075				

Grain Shape	Subround	Visual
Hardness (Mohs)	7.0	Moh's Scale
Moisture Content (%)	<0.1	ASTM C-566
Specific Gravity (g/cm^3)	2.65	ASTM C-128
Bulk Density, loose (lb/ft^3)	92-95	ASTM C-29
Bulk Density, compacted (lb/ft^3)	98-100	ASTM C-29

TECHNICAL DATA

Granusil

CHEMICAL ANALYSIS

Mean Values. These Do Not Represent A Specification.

Mean Percent by Weight

		4095	4020	4010	7030	8000
Silicon Dioxide	(SiO_2)	99.61	99.48	99.43	99.17	95.98
Iron Oxide	(Fe_2O_3)	0.04	0.04	0.05	0.06	0.25
Aluminum Oxide	(Al_2O_3)	0.13	0.19	0.20	0.27	1.55
Calcium Oxide	(CaO)	0.05	0.07	0.08	0.21	0.83
Titanium Dioxide	(TiO_2)	0.02	0.02	0.02	0.03	0.01
Magnesium Oxide	(MgO)	0.01	0.02	0.02	0.03	0.03
Potassium Oxide	(K_2O)	0.03	0.05	0.05	0.06	0.06
Sodium Oxide	(Na_2O)	tr	tr	tr	tr	0.01
Loss on Ignition	(L.O.I.)	0.11	0.15	0.23	0.23	0.21

ORDERING INFORMATION

Shipping Point: ST. CANUT, QUEBEC, CANADA
ORIGINATING CARRIER: QUEBEC – GATINEAU RAILWAY (QGRY)

Availability: BAG AND BULK
TRUCK AND RAIL

UNIMIN

FOR PRODUCT INFORMATION AND CUSTOMER SERVICE:
U.S. and CANADA 800-243-9004 • FAX 800-243-9005
WORLDWIDE 416-626-1500 • FAX 416-626-1855

UNIMIN CANADA LTD.

Silica Sands • Ground Silica • Feldspar • Ball Clay • Kaolin • Nepheline Syenite • High Purity Quartz • Olivine • Microcrystalline Silica • Bentonite Clay • Dolomite

GRADE NUMBERS INDICATE RELATIVE VALUES OR RESULTS. THEY ARE NOT A SPECIFICATION OR WARRANTY OF PERFORMANCE.

HEALTH HAZARD WARNING: Prolonged inhalation of dust associated with the materials described in this data sheet can cause delayed lung injury including Silicosis, a progressive, disabling and sometimes fatal lung disease. IARC has determined that crystalline silica, inhaled from occupational sources, can cause cancer in humans. Risk of injury is dependent on the duration and level of exposure. Follow OSHA or other relevant safety and health standards for the form of crystalline silica called Quartz. Current material safety data sheets, containing safety information, are available and should be consulted before usage.

Notice: While information contained herein is correct to the best of our knowledge, Unimin Corporation hereby disclaims any warranties as to the accuracy of the same. Recommendations or suggestions are made without guarantee or representation as to result, since conditions of usage are beyond our control. All materials are sold to Unimin Corporation standard terms and conditions of sale and the condition that buyer shall make his own tests to determine the suitability of such product for buyer's purpose. No statement contained herein shall be construed as a recommendation to infringe any patent.

Silica/Silica Containing

GRANUSIL® is a registered trademark of UNIMIN Corporation or its subsidiaries. All rights reserved.

St. Canut – GRANUSIL-2 (06/07)

Figure B 1 Technical data of silica sand 7030

`

APPENDIX D

SAMPLE PREPARATION REPORT

`

Sample preparation Report No. (__)

Batch ID: _ _ _

Date of Preparation: _ _ / _ _ / _ _

1. Mixing Measurements

1.1 Mix Design

	Bentonite	Sand 30/70	Water
Planned	500	500	1150
Absorption			
Corrected			
Actual			

1.2 Water Content

Location	Can No.	Can Wt. (gm)	Wet Wt. (gm)	Dry wt. (gm)	W (%)
Mixer (1)					
Mixer (2)					
1st Cylinder					
2nd Cylinder					
3rd Cylinder					
				Average	
				Range	

2. Consolidation Measurements

2.1 Water Content

Location	Can No.	Can wt. (gm)	Moist wt. (gm)	Dry wt. (gm)	Wc (%)
1st Cylinder					
Top of					
Middle of					
Bottom of					
2nd Cylinder					
Top of					
Middle of					
Bottom of					
3rd Cylinder					
Top of					
Middle of					
Bottom of					

`

Sample Preparation Report No. ( )

Batch ID: _ _ _

Date of Preparation: _ _ / _ _ / _ _

2.2 Density after Consolidation

Location	Sample ID	Weight (gm)	Height (mm)	Volume(cm^3) $V=\pi\ 2.5^2\ H$	Density (gm/cm^3)
1st Cylinder					
Top sample					
Bottom sample					
2nd Cylinder					
Top sample					
Bottom sample					
3rd Cylinder					
Top sample					
Bottom sample					

2.3 Consolidation Readings:

Initial Time (IT): _ _ : _ _

Initial Reading (IR): mm

Initial Height (IH): mm

Serial	Date	Time	Elapsed Time (min)	Reading (mm)	ΔH (mm) ΔH = IR -R	Height H (mm) H = IH -ΔH
1	_ _ / _ _ / _ _	_ _ : _ _	1			
2	_ _ / _ _ / _ _	_ _ : _ _	2			
3	_ _ / _ _ / _ _	_ _ : _ _	4			
4	_ _ / _ _ / _ _	_ _ : _ _	8			
5	_ _ / _ _ / _ _	_ _ : _ _	15			
6	_ _ / _ _ / _ _	_ _ : _ _	30			
7	_ _ / _ _ / _ _	_ _ : _ _	60			
8	_ _ / _ _ / _ _	_ _ : _ _	120			
9	_ _ / _ _ / _ _	_ _ : _ _	240			
10	_ _ / _ _ / _ _	_ _ : _ _	480			
11	_ _ / _ _ / _ _	_ _ : _ _	1440			
12	_ _ / _ _ / _ _	_ _ : _ _	2880			

Page (_ _/ _ _)

`

Sample Preparation Report No. (__)

Batch ID: _ _ _

Date of Preparation: _ _ / _ _ / _ _

2.3 Consolidation Chart

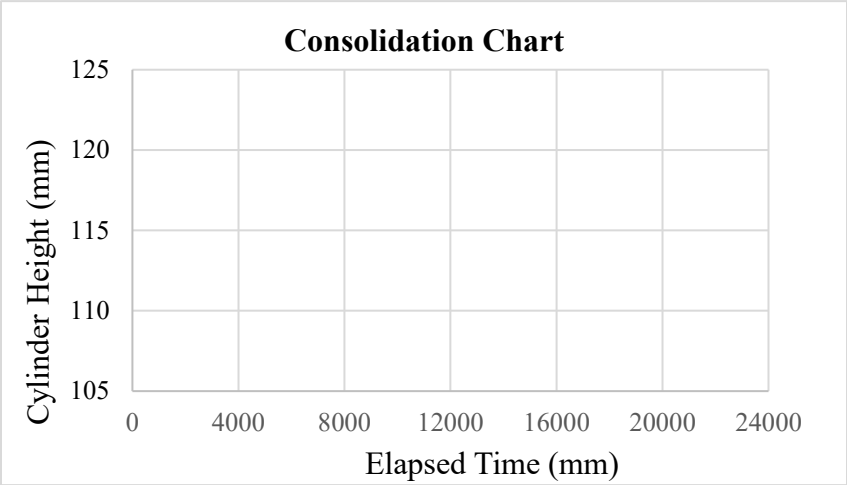

3. Frozen samples Measurements:

Location	Diameter (mm)	Height (mm)	Weight (gm)
1st Cylinder			
Top Sample (Before Freezing)			
Top Sample (After Freezing)			
Bottom Sample (Before Freezing)			
Bottom Sample (After Freezing)			
2nd Cylinder			
Top Sample (Before Freezing)			
Top Sample (After Freezing)			
Bottom Sample (Before Freezing)			
Bottom Sample (After Freezing)			
3rd Cylinder			
Top Sample (Before Freezing)			
Top Sample (After Freezing)			
Bottom Sample (Before Freezing)			
Bottom Sample (After Freezing)			

Page (_ _/ _ _)

Figure C 1 Sample preparation report